27 copies

NASA CONTRACTOR
REPORT

CR-61169

~~GPO PRICE~~

~~OFSTI PRICE(S)~~

CR-61169

DESIGN OF A LOAD-RELIEF CONTROL SYSTEM

FINAL TECHNICAL REPORT

Prepared under Contract No. NAS 8-20155 by

L. D. Edinger, G. B. Skelton, C. R. Stone,
M. D. Ward, and G. D. White
HONEWELL, INC.

N67-27304

FACILITY FORM 602

(ACCESSION NUMBER)	(THRU)
423 (PAGES)	1 (CODE)
NASA-CR-61169 (NASA CR OR TMX OR AD NUMBER)	10 (CATEGORY)

For

NASA-GEORGE C. MARSHALL SPACE FLIGHT CENTER
Huntsville, Alabama

April 21, 1967

CR-61169

DESIGN OF A LOAD-RELIEF CONTROL SYSTEM
(Final Technical Report)

(Report Dated May 9, 1966)

Prepared under Contract No. NAS 8-20155 by

L. D. Edinger, G. B. Skelton, C. R. Stone,
M. D. Ward, and G. D. White

HONEYWELL, INC.

For

Aero-Astrodynamics Laboratory

NASA-GEORGE C. MARSHALL SPACE FLIGHT CENTER

FOREWORD

This report fulfills the final reporting requirement for the development of a design procedure for missile boost-phase control performed under National Aeronautics and Space Administration Contract NAS8-20155.

The program was initiated by the Aero-Astrodynamics Laboratory of National Aeronautics and Space Administration, George C. Marshall Space Flight Center. The research upon which this report is based was carried out by the Systems and Research Division of Honeywell Inc. Dr. Grant B. Skelton of Honeywell was principal investigator for the program. Mr. Robert C. Lewis and Mr. Billy G. Davis of the Aero-Astrodynamics Laboratory were the program's contracting officer representatives. The study began on 1 May 1965 and terminated on 1 May 1966.

The research program at Honeywell was under the supervision of Dr. E. R. Rang. Mr. C. R. Stone did the physical modeling work reported, and Mr. M. D. Ward did all of the digital computer computation. The simulation studies were done by Mr. L. D. Edinger and Mr. G. D. White of the Aeronautical Division of Honeywell Inc., under the direction of Mr. J. C. Larson. Acknowledgements are made to Mr. D. Lukes of S&RD for a proof of the existence of system impulse responses, and to Mr. D. Carlson of Aero Division for simulation of quadratic estimators.

TABLE OF CONTENTS

		Page
SECTION I	INTRODUCTION AND SUMMARY	1
SECTION II	MODELS	9
	Missile Model	9
	Wind Model	17
	Data	17
	Assumptions	19
	Filter	20
	Wind Loads	28
	The Anomaly	28
	Modification of the Bending-Moment Rate Expression	31
	More Accurate Expressions	33
	State Equations	41
SECTION III	THE STOCHASTIC PROBLEM	42
	Formulation	42
	Mission Success	43
	An Upper Bound for the Likelihood of Failure	45
	Basic Assumptions	46
	State Equations	46
	Statement of the Problem	48
	Scope of the Formulation	49
	Quadratic Equivalence	49
	Notation	50
	Existence of S(t), R(t)	52
	Taylor's Series Expansion	53
	Minimization	55
	Assertion of Quadratic Equivalence	55
	The Iteration Procedure	57
	The Quadratic Problem	59
	Problem Division	60
	The Kalman Deterministic Problem	63
	The Stochastic Problem	65
	State Estimation	67
	Combining the Results	69

TABLE OF CONTENTS (Continued)

		Page
SECTION IV	DIGITAL RESULTS	70
	Iteration Details	71
	Q-Matrix Sensitivity	71
	Direct Iteration	77
	Example Controllers Designed	78
	The Simplest Case	79
	The Gimbal Actuator	83
	Estimators	85
	Numerical Evaluations	92
	Controller Descriptions	92
	Evaluations	93
SECTION V	SIMULATION RESULTS	99
	Nominal Load Relief Controller	101
	Description of System	101
	Case I Estimator	104
	Case II Estimator	104
	Performance Results	106
	Parameter Variations	114
	Simplification of the Load-Relief Controller	116
	Description of Nominal Controller with Realistic Sensing	117
	Possibilities for Simplification	119
	Analysis of Simplifications to Load-Relief Controller	120
	Performance Evaluation of Simplified System	125
	Comparison Studies	128
	Description of Minimax Controller	128
	Description of Conventional Controller	132
	Performance Comparison with Load Relief Controller	136
	Stability	139
	Conclusions	140

TABLE OF CONTENTS (Continued)

		Page
SECTION VI	CONCLUSIONS AND RECOMMENDATIONS	142
	Results	142
	Significant Results	142
	Less Significant Results	143
	Good Luck Results	143
	Very Minor Results	144
	Physical Insight	144
	Recommendations for Future Work	145
	Mathematical Recommendations	145
	Convergence	146
	Doubts	146
	Physical Problems	146
	Final Comments	147
REFERENCES		148
APPENDIX A	COEFFICIENTS	
APPENDIX B	WIND FILTER DETERMINATION	
APPENDIX C	DISTRIBUTED AERODYNAMIC (TRANSVERSE) STRIP FORCES FOR A LAUNCH VEHICLE	
APPENDIX D	VECTOR DIFFERENTIAL EQUATIONS	
APPENDIX E	THE UPPER-BOUND J*	
APPENDIX F	TAYLOR'S SERIES MOMENT EXPANSION	
APPENDIX G	DIFFERENCE EQUATIONS	
APPENDIX H	PARTIAL DERIVATIVES OF J*	
APPENDIX J	CONTROL GAINS AND RESPONSE MOMENTS	
APPENDIX K	GAINS AND ESTIMATOR ERRORS	
APPENDIX L	RESPONSE COVARIANCES	

TABLE OF CONTENTS (Continued)

Page

APPENDIX M ANALOG SIMULATION

APPENDIX N ANALOG RESPONSE TRACINGS

APPENDIX O ROOT LOCI PLOTS

LIST OF ILLUSTRATIONS

Figure		Page
2-1	Missile Model Configuration	10
2-2	Tail Section Configuration	13
2-3	Wind Filter	21
2-4	Computed and Given Wind Covariance versus Altitude - 0-km Reference	24
2-5	Computed and Given Wind Covariance versus Altitude - 10-km Reference	24
2-6	Computed and Given Wind Covariance versus Altitude - 20-km Reference	25
2-7	Computed and Given Wind Covariance versus Altitude - 30-km Reference	25
2-8	Approximation of $\partial \dot{I}_b / \partial \omega$	32
2-9	Approximation of $\partial \dot{I}_b / \partial v_\omega$	32
2-10	Representative Sample of Step Side Forces versus Vehicle Length, r	36
2-11	Representative Sample of Step Pitching Moments versus Vehicle Length, r	36
2-12	Representative Sample of Step Bending Moments versus Vehicle Length, r	36
2-13	Wind-Force Response to Step Angle-of-Attack with Approximate Wind Load Filters	40
3-1	Iteration Procedure	58
4-1	Simplest Controller Schematic	80
4-2	Case I Estimator	88
4-3	Control With Wind Estimation	88
4-4	Case II Estimator	89
4-5	Bending Likelihood Densities for Various Controllers	98

LIST OF ILLUSTRATIONS (Continued)

Figure		Page
5-1	Nominal Load-Relief Control System Block Diagram	102
5-2	Mean Wind and NASA Wind versus Time	102
5-3	Case I Kalman Estimator	105
5-4	Case II Kalman Estimator	105
5-5	Comparison of Hybrid and Digital Simulation Results - Drift versus Time	108
5-6	Comparison of Hybrid and Digital Simulation Results - Drift Rate versus Time	108
5-7	Comparison of Hybrid and Digital Simulation Results - Bending Moment versus Time	108
5-8	M'_α versus Time	110
5-9	M'_β versus Time	110
5-10	Nominal Load-Relief Controller with Realistic Sensing	118
5-11	Modification of Gimbal Displacement Feedback	122
5-12	Simplified Load-Relief Controller with Realistic Sensing	126
5-13	Minimax Controller	129
5-14	Minimax Control Gains	129
5-15	Conventional Controller	132

LIST OF TABLES

Table		Page
4-1	Numerical Evaluations - Likelihoods	94
4-2	Numerical Evaluations - Bending	95
4-3	Numerical Evaluations - Terminal Responses	96
5-1	Comparison of the Maximum Bending Moment for Various Estimators with Random Wind Disturbance	112
5-2	Comparison of Maximum Bending Moment for Various Estimators with Sissenwine Wind Disturbances	113
5-3	Maximum Bending Moments Experienced with Parameter Variations for Load-Relief Controller	115
5-4	Performance Comparisons Between the Nominal Load-Relief System and the Simplified Load-Relief System	127
5-5	Minimum Performance Results	131
5-6	Conventional Controller Performance Summary	134
5-7	Performance Comparisons - Sissenwine Winds	137-139

SECTION I
INTRODUCTION AND SUMMARY

The subject of this study is the control of a launch booster disturbed by winds. The booster control problem is caused by wind-induced bending, rotations, and translations. The booster is controlled by gimbaling part of its thrust, and the control problem is to design a gimbal controller so that gimbal motions will compensate for the undesired wind effects. A good controller would both maintain bending moments within ultimate strength limits throughout the flight and produce small terminal translation and rotation errors.

The objective of this study was to develop a load-relief controller design technique. The objective was met by formulating the load-relief problem as a stochastic minimization problem. The incident winds and corresponding booster responses were described as random processes, and an event of mission failure was defined. The event of failure is that one or more responses of concern will fall outside preselected limits at burnout or during the flight. The stochastic problem was to minimize an upper bound on the likelihood of occurrence of this event.

The stochastic problem was formulated in a manner that permitted its solution by application of known optimization theories. Its solution yields a linear, finite-time controller with time-varying gains. The design procedure consists of solving this problem and simplifying the resulting optimum controller.

The missile model employed as a study vehicle was NASA-MSFC's "Model Vehicle No. 2" (Ref. 1). The missile was assumed rigid, and its deviations from a nominal (no wind) trajectory were assumed to be linear functions of wind and gimbal inputs. The vehicle was assumed to fly for 150 seconds, launch to first-stage burnout, and the goal of control was to achieve final errors within the following limits:

- Drift $|z(150)|$ < 3000 meters
- Drift rate $|\dot{z}(150)|$ < 40 meters/sec
- Side force on upper stages $|\dot{\phi}(150) + 0.388\,\alpha(150)|$ < 0.0453 rad/sec

where z is drift, $\dot{z}$ drift rate, $\dot{\phi}$ attitude rate, and α angle of attack. The constraints on the controller throughout the flight were to maintain a bending moment of

$$|I_b(33,t)| < 2.25 \times 10^6 \text{ kilopon-meters (kp-m)}$$

$$|\beta(t)| < 5 \text{ degrees}$$

where $I_b(33, t)$ is the bending moment at a fuselage station 33 meters from the tail, and β is the engine gimbal angle.

Several controllers were designed for this missile by the design procedure developed in the study. The various controllers differed in the responses sensed and fed back. It was shown in digital and analog-simulation evaluations that these controllers were very good load-relief controllers, that they were not parameter sensitive, that they could be successfully simplified, and that they were generally superior to controllers designed by frozen-point methods.

The design method has several advantages over conventional, frozen-point design techniques. The stochastic formulation incorporates in the design the stochastic nature of the incident winds, the time-varying booster dynamics, the finite-time nature of the control problem, the terminal translation and rotation constraints, and the in-flight actuator and bending constraints. The formulation does not include design constraints on parameter insensitivity and controller simplicity; no convenient way for including them was found. Simplification and insensitivity questions were settled by conventional, trial-and-error simulation testing.

The evaluations by digital and analog simulation made evident what are perhaps the most significant advantages of the design procedure. The digital results made the difficult-to-control aspects of the control problem readily evident. In the "Model Vehicle No. 2" problem all response constraints in the early and late portions of the flight were easily met; the control problem was to control bending in the high dynamic pressure region by controlling angle of attack. The analog-simulation evaluations showed that the optimum controller could be simplified without severe performance degradation by replacing most of the time-varying gains by constants. The simplifications took full advantage of the digital results showing what to control and how to control it optimally.

Technical descriptions of the load-relief problem, the design procedure, and the procedure evaluations are presented in Sections II, III, IV, and V of the report. Section VI contains summarizing comments, conclusions, and recommendations. Most of the detail derivations and graphical results are presented in appendices.

Section II contains a derivation of the mathematical description of the wind-missile system. The missile equations of motion are derived there, and an apparent anomaly in the bending moment equation is discussed in some detail. The incident wind is assumed Gaussian, and it is expressed as the sum of a deterministic (mean) time function and the output of a finite-order, time-varying linear filter driven by white noise. The missile and wind filter derivations permit describing the wind-missile system by vector differential equations of the form

$$\begin{aligned} \dot{x}(t) &= F(t)\, x(t) + G_1(t)\, u(t) + G_2(t)\, \bar{v}_\omega(t) + G_3(t)\, \eta_1(t) \\ r(t) &= H_1(t)\, x(t) + D_1(t)\, u(t) + D_2(t)\, \bar{v}_\omega(t) \\ m(t) &= H_2(t)\, x(t) + \eta_2(t)\,, \end{aligned} \tag{1.1}$$

where

$r(t)$ = missile response deviations from ideal (no-wind) trajectory

$m(t)$ = measured responses (sensor outputs)

$\bar{v}_\omega(t)$ = mean incident wind

$u(t)$ = control input to gimbal actuator

$\eta_1(t)$ = Gaussian white noise input to wind filter

$\eta_2(t)$ = Gaussian white message (sensor) noise

$x(t)$ = state vector.

The reader interested only in the stochastic formulation can skip Section II and not miss any essential notions.

The statement and solution of the stochastic formulation of the load-relief problem are presented in Section III. The mathematics are based on the following six results:

- Frequency of Occurrence (Rice, Ref. 2) - Let $r(t)$ be a (one-dimensional) Gaussian, zero-mean, stationary random process of the parameter t (time). Let γ be a positive constant, and let $\mathcal{a}$ be the event that

$$|r(t)| = \gamma$$

$$\frac{d}{dt}|r(t)| > 0$$

[$\mathcal{a}$ is the event that $|r(t)|$ intersects γ with positive slope; i.e., it is the event that $|r(t)|$ will exceed γ]. Then, according to Rice's derivation, the average number of occasions $E[N(\mathcal{a})]$ that the event $\mathcal{a}$ occurs in $[O, T]$ is

$$E[N(a)] = \int_0^T \frac{1}{\pi} \frac{\sigma_{\dot{r}}}{\sigma_r} e^{-\frac{1}{2}\left(\frac{\gamma}{\sigma_r}\right)^2} dt$$

where $\sigma_{\dot{r}}$ and σ_r are the standard deviations of $\frac{dr}{dt}$ and r respectively.

This result was extended in the study to include non-zero mean, non-stationary random processes. In the formulation r(t) and γ represented the bending moment and its limit, and the gimbal angle and its limit.

- <u>Upper-Bound J^*</u> - Let J^* be the sum

$$J^* = \sum_{i=1}^{m} P(\bar{a}_i) + \sum_{i=m+1}^{n} E[N(a_i)] \tag{1.2}$$

where $P(\bar{a}_i)$ is the likelihood that the ith response exceeds its terminal limit

$$|r_i(T)| > \gamma_i$$

and $E[N(a_j)]$ is the expected number of occasions that the jth response exceeds its limit γ_j in the course of the booster flight. Assuming there are m responses whose terminal behavior is to be constrained and n-m responses whose in-flight behavior is to be constrained, it is shown that J^* is an upper bound on the likelihood that one or more responses of interest exceeds its limit:

$$J^* \geq \text{(the likelihood of mission failure)}$$

No analytical expression for the likelihood of mission failure is known. The above result is significant in that an analytical expression for the upper-bound J^* can be written if the responses r(t) are Gaussian. The expression for J^* is a functional of first and second response moments (means and covariances), and it leads to the following assertion.

- Quadratic Equivalence - The linear controller minimizing J^* also minimizes a quadratic functional of the first and second response moments.

The restriction of linear control assures that the responses r(t) are Gaussian and the above analytical expression for the upper-bound J^* is valid. The equivalent quadratic functional is derived by expanding J^* in a Taylor's series and examining the coefficients of its first variation.

The thought behind establishing this equivalence is: Direct minimization of J^* is difficult; but, since J^* is monotone in the response moments in the neighborhood of the optimum, why not minimize the moments themselves? This can be easily done with the three results for quadratic problems given below.

- Estimation (Kalman, Ref. 3, 4), (Bryson, Ref. 5) - Given the system (1. 1), find the conditional state expectation

$$E\{x(t) \mid m(o,t),\ u(o,t)\}$$

This is the expected value of the state given present and past output measurements m(t) and past control inputs u(t). The authors referenced have completely resolved this problem.

- Deterministic Control (Kalman, Ref. 6) - Given the system (1.1) where all inputs are zero ($\eta_1 = \eta_2 = \bar{v}_\omega = 0$), find the control input u(t) which minimizes the response quadratic

$$J^{**} = r(T)' \, Q(T) \, r(T) + \int_0^T r(t)' \, Q(t) \, r(t) \, dt \tag{1.3}$$

Kalman solved this problem, derived the existence and uniqueness conditions, and showed that the control u(t) was of the form

$$u(t) = K(t) \, x(t)$$

where the gains K(t) could be derived from the backwards solution of a matrix Riccati equation.

This result was modified in the study to include the case where the deterministic input $\bar{v}_\omega(t)$ was non-zero.

- Separability (Tou, Ref. 7) - Given the system (1.1) where the deterministic input $\bar{v}_\omega$ is zero, the control u(t) minimizing the expected value of the quadratic J^{**} is

$$u(t) = K(t) \, E\left\{x(t) \mid m(o,t), \; u(o,t)\right\}$$

where K(t) is the solution to the deterministic problem.

This result permits separation of the stochastic quadratic problem into an estimation problem and a deterministic control problem. Tou proved this result for systems described by difference equations; it was assumed true in the study for systems described by differential equations.

These results were combined in the study to provide a general solution to the minimization of a quadratic functional of the response moments.

These six results permitted reducing the load-relief problem to a problem of choosing quadratic weights [the Q(t) coefficients in Equation (1.3)]. An iteration procedure for making these choices was devised and successfully run. The procedure, based on the quadratic equivalence result, involved iterating until initially chosen weights were equal to the coefficients of the first variation of the J^* produced by the quadratic optimum controller.

Section IV contains the results of digital evaluations of three controllers designed by the methods of Section III. Section V contains analog evaluations of those controllers and competitive minimax and conventional controllers. The main results of these evaluations were noted above.

The main conclusion reached in Section VI is that the stochastic problem treated in Section III is a valuable design tool. The formulation handles high-order system representations, it treats many aspects of the design problem, and it produces a very good load-relief controller. Recommendations for future study mentioned in Section VI include treating higher-order system representations, adding realistic sensing, including the nominal pitch program in the formulation, and examining the sensitivity of controller performance to Gaussianess and wind-force assumptions.

SECTION II
MODELS

The differential equations describing the missile, the wind random process, and the wind loads on the missile are presented in this section.

MISSILE MODEL

The missile employed as a study vehicle was NASA-MSFC's "Model Vehicle No. 2". The vehicle was assumed to be rigid, and fuel-slosh and engine-inertia effects were ignored. Control of only one axis was considered.

The missile response-perturbation equations were obtained (by NASA) by writing the missile equations in terms of a coordinate system moving along the nominal (no-wind) vehicle trajectory. These equations were then expanded in Taylor's series about the nominal trajectory, and the higher-order and insignificant first-order terms were dropped.

The configuration is shown in Figure 2-1. The linearized response perturbation equations are:

- Drift: $$m\ddot{z} = (F-X)\phi + R\beta + \int_0^{x_N} \frac{d\tau}{d\alpha}\,\alpha\,dx \qquad (2.1)$$

- Pitch: $$I_{xx}\ddot{\phi} = -Rx_{cg}\,\beta + \int_0^{x_N} \frac{d\tau}{d\alpha}\,(x - x_{cg})\,\alpha\,dx \qquad (2.2)$$

where:

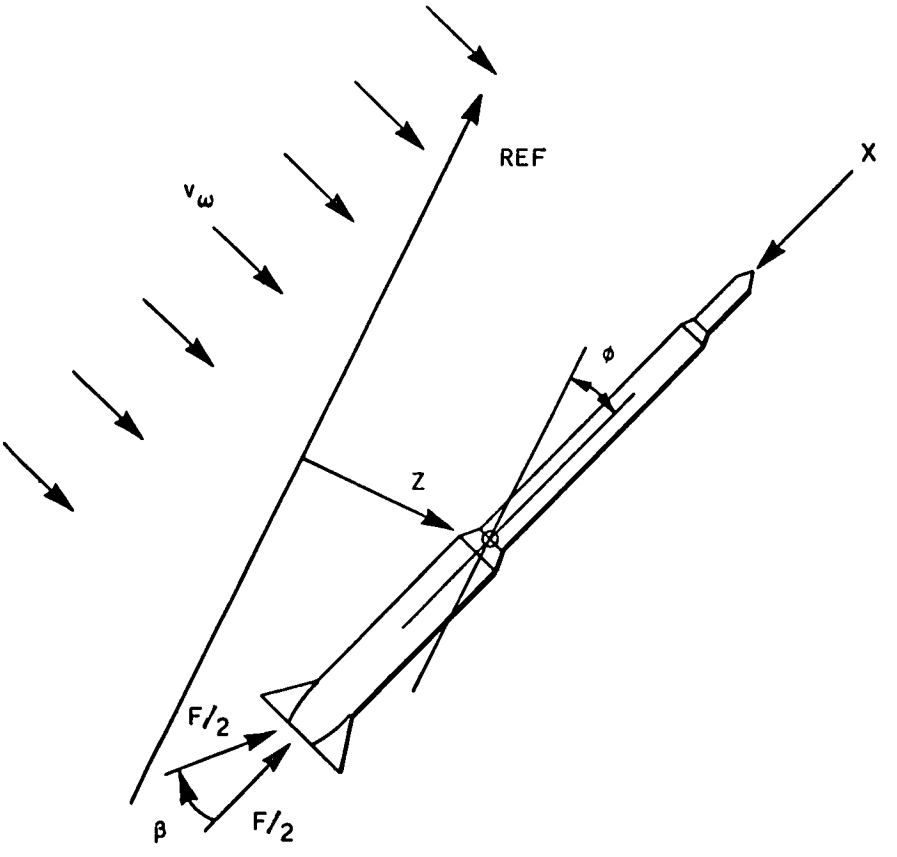

Figure 2-1. Missile Model Configuration

m = vehicle mass

I_{xx} = pitch moment of inertia

X = drag

R = controlled thrust

z = drift orthogonal to nominal trajectory

ϕ = attitude deviation from the nominal trajectory

x_{cg} = distance from tail to booster center of gravity

x_N = length of booster, tail to nose

$\frac{d\tau}{d\alpha}$ = side force on missile per unit length per unit angle-of-attack

$$\alpha(x,t) = \phi(t) + \frac{v_\omega(x,t) - \dot{z}(t) - [x - x_{cg}(t)]\,\dot{\phi}(t)}{V(t)} \tag{2.3}$$

= angle of attack at a station x meters from the vehicle tail

$v_\omega(x,t)$ = wind component orthogonal to missile at a station x meters from the tail

$V(t)$ = vehicle nominal velocity

$\beta(t)$ = gimbal angle

The derivation of the per-unit-side-load term $\frac{d\tilde{t}}{d\alpha}$ is discussed in the subsection on wind loads.

The bending moment at a point x_o meters from the vehicle tail can be obtained from the equations of motion for a rear section of the vehicle x_o meters long. These are:

- Drift: $$m_T\,[\,\ddot{z} + (x_T - x_{cg})\,\ddot{\phi}\,] = R\beta + F_s + \int_o^{x_o} \frac{d\tilde{t}}{d\alpha}\,\alpha\,dx \qquad (2.4)$$

- Pitch: $$I_T\,\ddot{\phi} = -Rx_T\beta + \int_o^{x_o} \frac{d\tau}{d\alpha}\,(x - x_T)\,\alpha\,dx + I_b + F_s\,(x_o - x_T) \qquad (2.5)$$

where:

m_T = mass of section

I_T = pitch moment of inertia of section

x_T = center of gravity of section measured from the tail

F_s = shear force at x_o

I_b = bending moment at x_o

The configuration of the tail section is shown in Figure 2-2.

By defining

$$\gamma_1 = \frac{I_T + (x - x_T)\,(x_{cg} - x_T)\,m_T}{I_{xx}} \qquad (2.6)$$

$$\gamma_2 = (x - x_T)\,\frac{m_T}{m} - x_{cg}\,\gamma_1 \qquad (2.7)$$

solving for the bending moment I_b produces

$$I_b = (x_o - \gamma_2)\,R\beta + \int_o^{x_o} \frac{d\tau}{d\alpha}\,(x_o - x)\,\alpha\,dx + \int_o^{x_N} \frac{d\tilde{t}}{d\alpha}\,(\gamma_1 x - \gamma_2)\alpha\,d\alpha \qquad (2.8)$$

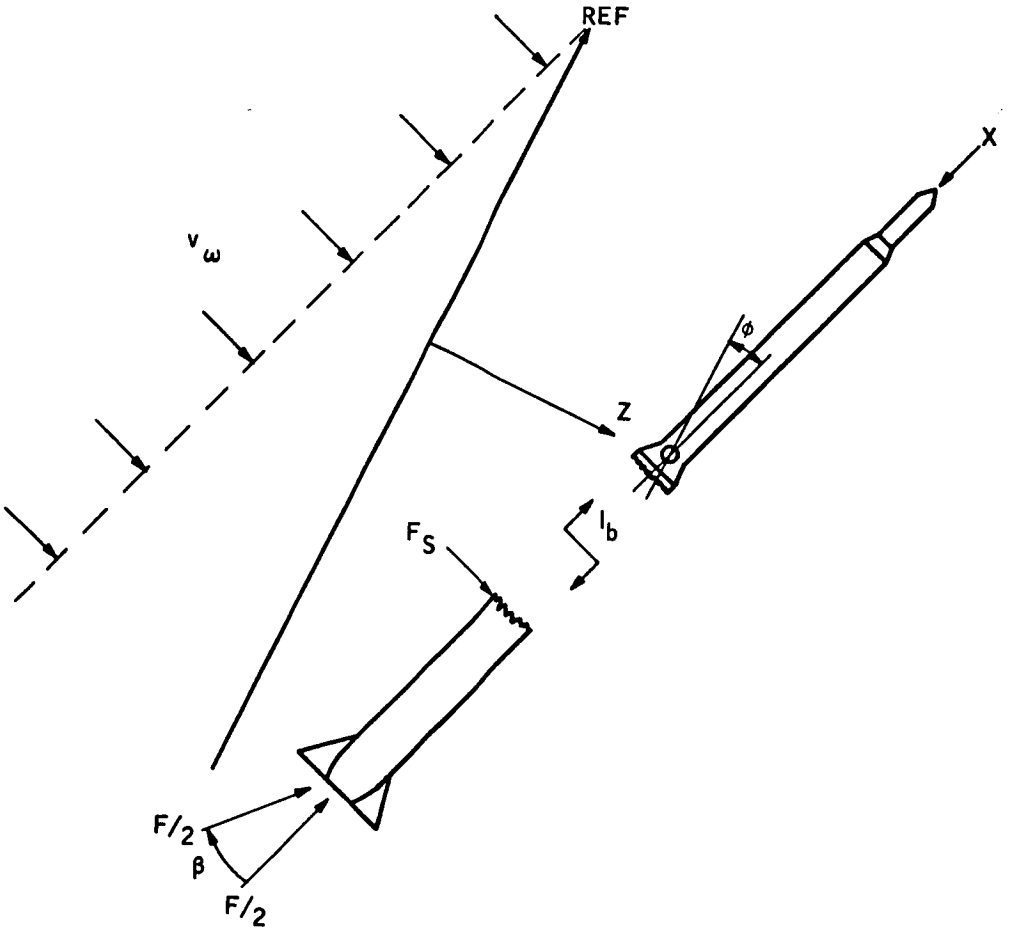

Figure 2-2. Tail Section Configuration

By defining

$$N = \int_o^{x_N} \frac{d\tau}{d\alpha}\, dx \tag{2.9}$$

$$N\ell cp = \int_o^{x_N} \frac{d\tilde{t}}{d\alpha}\, (x - x_{cg})\, dx$$

$$M_\beta{}' = R\ [x_o - \gamma_2]$$

$$M_{\dot\phi} = \int_o^{x_o} \frac{d\tau}{d\alpha}\, (x_o - x)\, (x - x_{cg})\, dx + \int_o^{x_N} \frac{d\tilde{t}}{d\alpha}\, (\gamma_1 x - \gamma_2)\, dx$$

$$M_\alpha{}' = \int_o^{x_o} \frac{d\tilde{t}}{d\alpha}\, (x_o - x)\, dx + \int_o^{x_N} \frac{d\tilde{t}}{d\alpha}\, (\gamma_1 x - \gamma_2)\, dx$$

$$T_{\dot\phi} = \int_o^{x_N} \frac{d\tau}{d\alpha}\, (x - x_{cg})^2\, dx$$

the equations reduce to

$$m\ddot{z} = R\beta + N(\phi - \frac{\dot{z}}{V}) - \dot{\phi}\, \frac{N\ell cp}{V} + \int_o^{x_N} \frac{v_\omega}{V}\, \frac{d\tilde{t}}{d\alpha}\, dx + (F - X)\, \phi \tag{2.10}$$

$$I_{xx}\ddot{\phi} = x_{cg} R\beta + N\ell cp\, (\phi - \frac{\dot{z}}{V}) - \dot{\phi}\, \frac{T_{\dot\phi}}{V} + \int_o^{x_N} \frac{v_\omega}{V}\, \frac{d\tau}{d\alpha}\, (x - x_{cg})\, dx$$

$$I_b = M_\beta{}'\beta + M_\alpha{}'(\phi - \frac{\dot{z}}{V}) - \frac{M_{\dot\phi}}{V}\, \dot{\phi} + \int_o^{x_N} \frac{v_\omega}{V}\, \frac{d\tilde{t}}{d\alpha}\, [(x - x_o)\, u_{-1}\, (x - x_o)$$

$$+ \gamma_1 x - \gamma_2]\, dx$$

The gimbal actuator equation assumed was

$$\dot{\beta} = -14.6\beta + 14.6u \tag{2.11}$$

where u = control input.

(It will be shown in a later section that the results are independent of the constants in this equation. Any first-order actuator equation

$$\dot{\beta} = a_1\beta + a_2 u$$

can be substituted for the above.)

An expression for $\dot{I}_b$, the bending-moment rate, is required in the evaluation of the expected number of occasions of exceeding the bending limit. By ignoring $\frac{d}{dt}V(t)$ and defining

$$R_\beta = M_{\dot{\beta}}' - 14.6\, M_\beta' - \frac{M_\alpha'}{V}\frac{R}{m} + \frac{M_{\dot{\phi}}}{V}\frac{Rx_{cg}}{I_{xx}} \tag{2.12}$$

$$R_{\dot{\phi}} = M_{\dot{\alpha}}' - M_\alpha' \frac{N}{mV} - \frac{M_\phi}{V}\frac{N\ell cp}{I_{xx}}$$

$$R_{\dot{\phi}} = M_\alpha'\left(1 + \frac{N\ell cp}{mV^2}\right) + \frac{M_{\dot{\phi}}T_{\dot{\phi}}}{I_{xx}V^2} - \frac{M_{\dot{\phi}}}{V},$$

the bending-moment rate equation is

$$\dot{I}_b = R_\beta\beta + R_{\dot{\phi}}(\phi - \frac{\dot{z}}{V}) + 14.6\, M_\beta' u + R_{\dot{\phi}}\dot{\phi} + \frac{d}{dt}\int_0^{x_N} \frac{v_\omega}{V}\frac{d\tau}{d\alpha}\,[(x-x_o)u_{-1}(x-x_o)$$

$$+ \gamma_1 x - \gamma_2]\,dx - \int_0^{x_N} \frac{v_\omega}{V}\frac{d\tilde{t}}{d\alpha}\left[\frac{M_\alpha'}{mV} + \frac{M_{\dot{\phi}}}{I_{xx}V}(x-x_{cg})\right] dx \tag{2.13}$$

In the "Model Vehicle No. 2" data package these equations were simplified by assuming that local angle-of-attack effects along the fuselage could be ignored. This amounts to replacing

$$\int_0^{x_N} \frac{d\tau}{d\alpha}\,\alpha\,dx \quad \text{by} \quad N(\phi + \frac{v_\omega - \dot{z}}{V}), \tag{2.14}$$

$$\int_0^{x_N} \frac{d\tau}{d\alpha}\,(x-x_{cg})\,\alpha\,dx \text{ by } N\ell cp\,(\phi + \frac{v_\omega - \dot{z}}{V}),$$

$$\int_0^{x_o} \frac{d\tau}{d\alpha}\,\alpha\,dx \quad \text{by} \quad (\phi + \frac{v_\omega - \dot{z}}{V}) \int_0^{x_o} \frac{d\tau}{d\alpha}\,dx,$$

and

$$\int_0^{x_o} \frac{d\tau}{d\alpha}\,(x-x_T)\,\alpha\,dx \text{ by } (\phi + \frac{v_\omega - \dot{z}}{V}) \int_0^{x_o} \frac{d\tau}{d\alpha}\,(x-x_T)\,dx$$

This ignores the $\dot{\phi}$ contribution to angle to attack and is equivalent to assuming that the wind over the entire vehicle length is the same as the wind at the center of gravity. The above equations were reduced to

$$\ddot{z} = \frac{R}{m}\beta + \frac{F - X}{m}\phi + \frac{N}{m}(\phi + \frac{v_\omega - \dot{z}}{V}) \tag{2.15}$$

$$\ddot{\phi} = \frac{-x_{cg}R}{m}\beta + \frac{N\ell cp}{m}(\phi + \frac{v_\omega - \dot{z}}{V})$$

$$L_b = M_\alpha'(\phi + \frac{v_\omega - \dot{z}}{V}) + M_\beta'\beta$$

$$\dot{I}_b = (\dot{M}_\beta' - 14.6 M_\beta' - \frac{M_\alpha'}{V}\frac{R}{m})\beta + 14.6 M_\beta' u$$

$$+ (\dot{M}_\alpha' - M_\alpha' \frac{N}{mV})(\phi + \frac{v_\omega - \dot{z}}{V}) - \frac{M_\alpha'}{V}\phi + \frac{M_\alpha'}{V}\dot{v}_\omega$$

The various coefficients in these equations are graphed in Appendix A, Figures A-1 through A-28.

The $\dot{I}_b$ equation had to be approximated with a simpler equation for the analyses. The reasoning and approximations employed are discussed in the subsection on wind loads.

WIND MODEL

Calculation of first and second response moments (means and covariances) requires knowledge of the means and correlations of the incident wind $v_\omega(t)$. Means and correlations of horizontal winds as a function of altitude have been published (Vaughan, Ref. 8). Convenient use of that data requires the construction of a "wind filter". The construction of the filter employed in the study is discussed in this subsection.

Data

Vaughan's wind data were obtained by tracking the vertical ascent of balloons. Horizontal displacement and time of observation were recorded at altitude intervals of 1 kilometer. The displacement increments divided by the time increments gave average horizontal wind-velocities over each interval. The velocity data from various ascents were then averaged and correlated for various geographic locations and months of the year. The published averages for Patrick Air Force Base for the month of March were employed in the study. The averages were given at discrete altitudes h_i, $i = 0, \ldots 30$:

$h_o = o$

$h_1 = 1$ kilometer altitude

.
.
.

$h_i = i$ kilometers altitude

The averages included:

$\bar{v}_{NS}(h_i)$, the mean north-south wind velocity

$\bar{v}_{EM}(h_i)$, the mean east-west wind velocity

$\sigma_{NS}(h_i)$, the standard deviation of north-south wind velocity

$\sigma_{EW}(h_i)$, the standard deviation of east-west wind velocity

$\rho_{NS-EW}(h_i)$, the correlation coefficient of north-south and east-west winds

$\rho_{NS}(h_i, h_j)$, the correlation coefficient of north-south winds at each altitude pair

$\rho_{EW}(h_i, h_j)$, the correlation coefficient of east-west winds at each altitute pair

The data also included the number of observations included in each average.

The data did not include correlations of east-west and north-south winds at all altitude pairs. Data to 30 kilometers altitude were presented.

Since the data were based on observations made at 1-kilometer altitude intervals, it does not include high (spatial) frequency wind-velocity variations. To be precise, the Vaughan data cannot be interpolated between the 1-kilometer intervals without assuming that the highest spatial frequency component in the wind velocity is less than 1/2 cycle per kilometer. There is no basis for such an assumption, and the inherent inaccuracies of the 1-kilometer sampling intervals must be tolerated.

Assumptions

Use of this data in the booster problem requires assumptions of statistical regularity and time constancy, and construction of a vertical wind component.

The statistical-regularity assumption is that if the balloon experiments were repeated in the future, nearly the same averages would result. This is a necessary and reasonable assumption. Without it, it would be impossible to infer anything about future winds.

The time constancy assumption is that, over a time interval corresponding to the ascent time of a balloon, the wind at a point in space is nearly constant. This assumption has been experimentally verified by comparing the winds calculated from balloons released at one-hour intervals (Lenhard, et al, Ref. 9). A booster rises much faster than a balloon, and the assumption permits expressing the winds encountered by the booster as functions of time rather than altitude.

The veritical wind construction is required because a booster does not always fly vertically, and calculation of response moments therefore requires knowledge of the horizontal and vertical distributions of both horizontal and vertical winds. The only wind data available are the vertical distributions of horizontal winds. To use this data, it is assumed that the wind component orthogonal to the booster fuselage at a point in space is equal to the horizontal component of the wind at that point as determined from the Vaughan data.

There is no data to test this assumption, but it is felt that the response moments calculated with it will not differ significantly from those that would be obtained if all of the various distributions were known and were included in the moment formulae.

Filter

The Vaughan data as given is inconveniently expressed for the calculation of response moments and for the design of a booster controller. The most efficient method for obtaining response moments involves constructing a linear filter, white-noise driven, whose output statistics approximate the given wind statistics. Expressing the data in the form of a filter is also essential to the optimization method used to design the control system.

The problem of constructing a linear filter with given output moments has been solved for stationary random processes and for some processes derived from stationary processes. It has not been solved for general nonstationary processes, and examination of Vaughan's data shows that the wind random process is not stationary.

Lacking a general approach to filter construction, the only recourse in the study was to assume a form for the wind filter, compute its response moments, and adjust filter parameters for a best fit of the given data. There was no basis for selecting one filter form over another other than quality of fit, and filter form had to be determined on a trial and error basis.

The general form of the filters considered is shown in Figure 2-3. The east-west and north-south wind components were taken to be

$$v_{EW}(h) = \bar{v}_{EW}(h) + \sigma_{EW}(h)\,\omega_1(h)$$

$$v_{NS}(h) = \bar{v}_{NS}(h) + \sigma_{NS}(h)\,[\lambda(h)\omega_1(h) + \sqrt{1-\lambda(h)^2}\;\omega_2(h)]$$

where h is altitude, and ω_1 (h) and ω_2 (h) are the unity standard-deviation outputs of stationary (in altitude) linear filters driven by independent white noise sources; $\lambda(h)$ is the correlation coefficient $\rho_{EW-NS}(h)$. This choice of a general filter form automatically ensures the proper output means

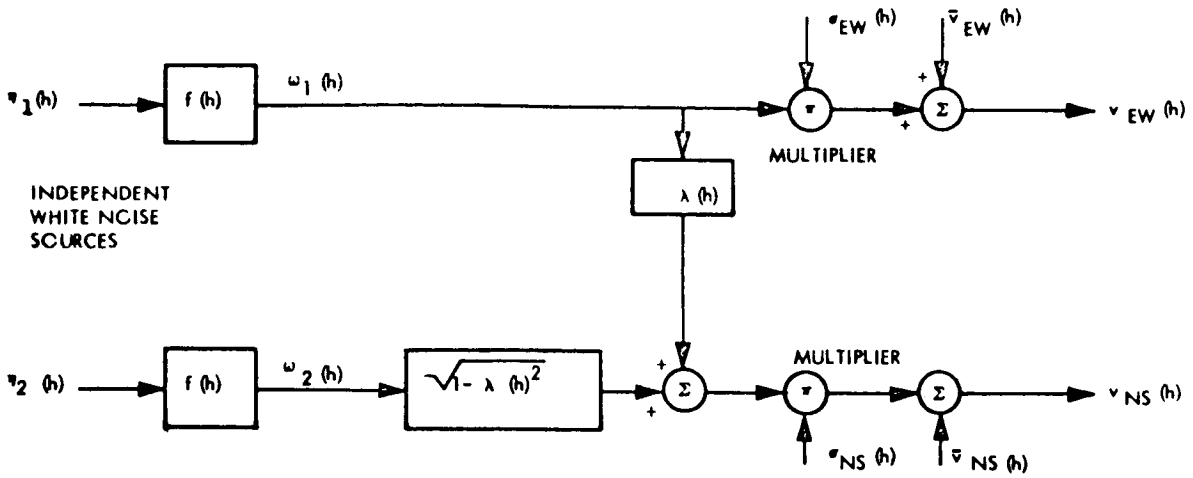

Figure 2-3. Wind Filter

$$\left\{ E \left[\left| v_{EW}(h) - \bar{v}_{EW}(h) \right|^2 \right] \right\}^{1/2} = \sigma_{EW}(h)$$

$$\left\{ E \left| v_{NS}(h) - \bar{v}_{EW}(h) \right|^2 \right\}^{1/2} = \sigma_{NS}(h)$$

and east-west · north-south interlevel correlation coefficients

$$\frac{E\left\{ \left[v_{EW}(h) - \bar{v}_{EW}(h) \right] \left[v_{NS}(h) - \bar{v}_{NS}(h) \right] \right\}}{\sigma_{EW}(h)\, \sigma_{NS}(h)} = \lambda(h) = \rho_{EW-NS}(h)$$

The f(h) impulse responses were chosen to fit the given interlevel correlation coefficients. Since the interlevel correlations of east-west · north-south winds were not know, the f(h) were chosen to fit only the east-west · east-west interlevel correlations and the north-south · north-south interlevel correlations.

The east-west · east-west and north-south · north-south covariances to be approximated were

$$E\left\{\left[v_{EW}(h_i) - \bar{v}_{EW}(h_j) - v_{EW}(h_j)\right]\right\} = \rho_{EW}(h_i, h_j)\ \sigma_{EW}(h_i)\,\sigma_{EW}(h_j)$$

$$\approx E\left\{\left[\omega_1(h_i)\ \omega_1(h_j)\right]\right\}\ \sigma_{EW}(h_i)\ \sigma_{EW}(h_j)$$

$$E\left\{\left[v_{NS}(h_i) - \bar{v}_{NS}(h_i)\right]\left[v_{NS}(h_j) - \bar{v}_{NS}(h_j)\right]\right\} = \rho_{NS}(h_i, h_j)\,\sigma_{NS}(h_i)\,\sigma_{NS}(h_j)$$

$$\approx \lambda(h_i)\,\lambda(h_j)\,E\left\{\left[\omega_1(h_i)\ \omega_1(h_j)\right] + \left[\sqrt{1 - \lambda(h_i)^2\,(1 - \lambda(h_j)^2}\right]\right\}$$

$$E\left\{\left[\omega_2(h_i)\ \omega_2(h_j)\right]\right\}\ \sigma_{NS}(h_i)\,\sigma_{NS}(h_i).$$

Two correlation functions were tried, an exponential function

$$E\left\{\left[\omega_1(h_i)\ \omega_1(h_j)\right]\right\} = E\left\{\left[\omega_2(h_i)\ \omega_2(h_j)\right]\right\} = \exp\left(\frac{|h_i - h_j|}{L}\right)$$

and an exponential-cosine function

$$E\left\{\left[\omega_1(h_i)\ \omega_1(h_j)\right]\right\} = E\left\{\left[\omega_2(h_i)\ \omega_2(h_j)\right]\right\}$$

$$= (\cos a_2\ |h_i - h_j| + a_3 \sin a_2\ |h_i - h_j|)\ \exp(-a_1\ |h_i - h_j|)$$

The criterion for quality-of-fit employed was the sum over all data points of the squares of the differences between the actual and computed covariances, weighted by the number of observations of each data point. The "cost" of a poor fit was then

$$J = \sum_{i=0}^{29} \sum_{j=i+1}^{30} C_{ij} \min(N_i, N_j)$$

where N_i = the number of observations of wind velocities at altitude h_i, and

$$C_{ij} = \left\{\rho_{EW}(h_i, h_j) - E\left\{\left[\omega_1(h_i)\ \omega_1(h_j)\right]^2\right\}\right. \sigma_{EW}(h_i)^2\ \sigma_{EW}(h_j)^2$$

$$+ \left\{\rho_{NS}(h_i, h_j) - \left[\lambda(h_i)\ \lambda(h_j) + \sqrt{1-\lambda(h_i)^2\,(1-\lambda(h_j)^2}\right]\ E\left\{\left[\omega_1(h_i)\ \omega_1(h_j)\right]\right\}\right.$$

$$\sigma_{NS}(h_i)^2\ \sigma_{NS}(h_j)^2$$

The parameters L in the exponential autocorrelation and a_1, a_2, a_3 in the exponential-cosine autocorrelation were chosen to minimize J.

The exponential autocorrelation was tried first and discarded, as it gave too poor a fit. The exponential-cosine coefficients a_1, a_2, a_3 were determined with a digital computer by minimizing J with a standard gradient-minimization procedure. The procedure is described in Appendix B.

The gradient search for the minimizing coefficients was terminated when successive iterations produced values agreeing to two significant digits. The values determined were

$$a_1 = 0.95 \cdot 10^{-4}\ \text{meters}^{-1}$$

$$a_2 = 0.735 \cdot 10^{-4}\ \text{meters}^{-1}$$

$$a_3 = -0.91 \cdot 10^{-8}$$

Plots of the original east-west covariances, the computed east-west covariances, and the corresponding number of data observations for four reference altitudes are presented in Figures 2-4 through 2-7. (These are the correlations of the wind at the reference altitude and the abscissa altitudes.) It is seen that the

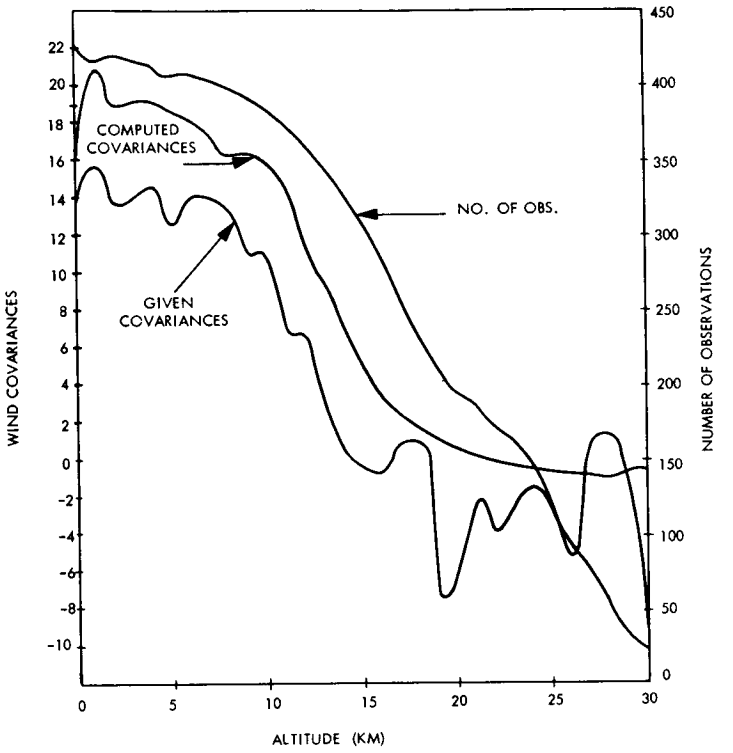

Figure 2-4

Computed and Given Wind Covariance versus Altitude - 0-km Reference

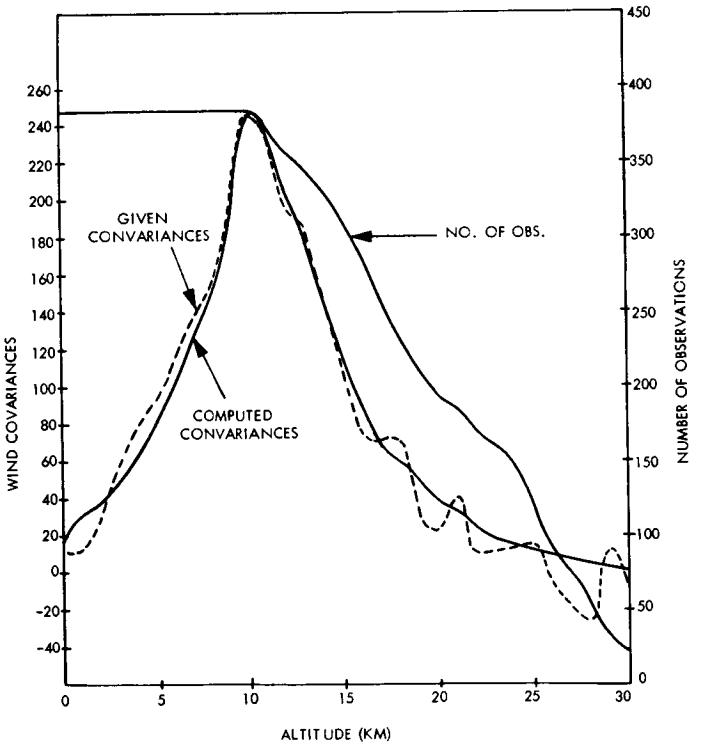

Figure 2-5

Computed and Given Wind Covariance versus Altitude - 10-km Reference

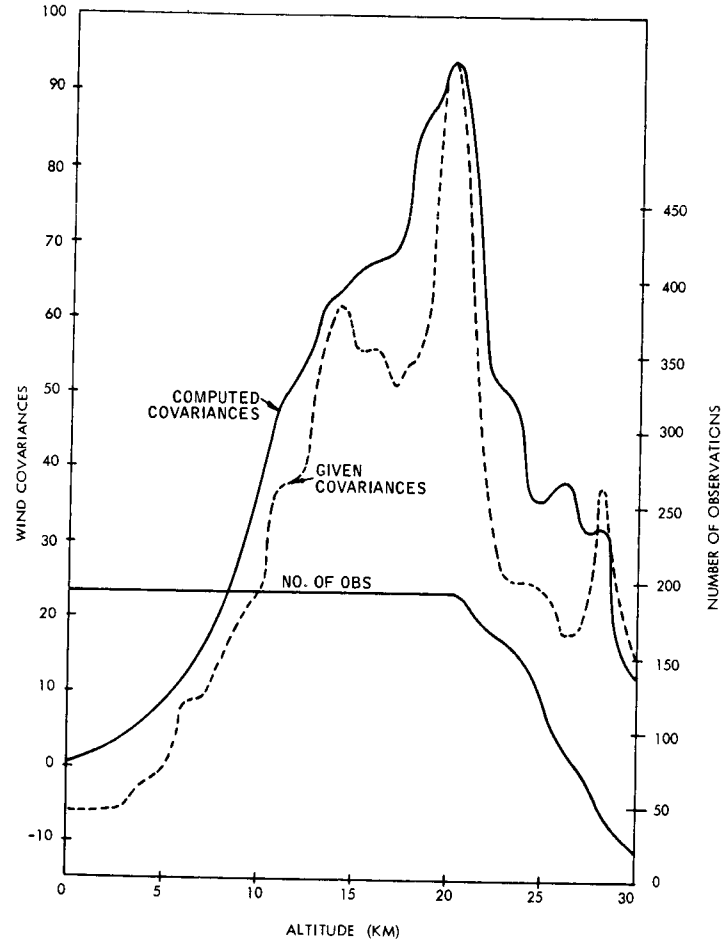

Figure 2-6

Computed and Given Wind Covariance versus Altitude - 20-km Reference

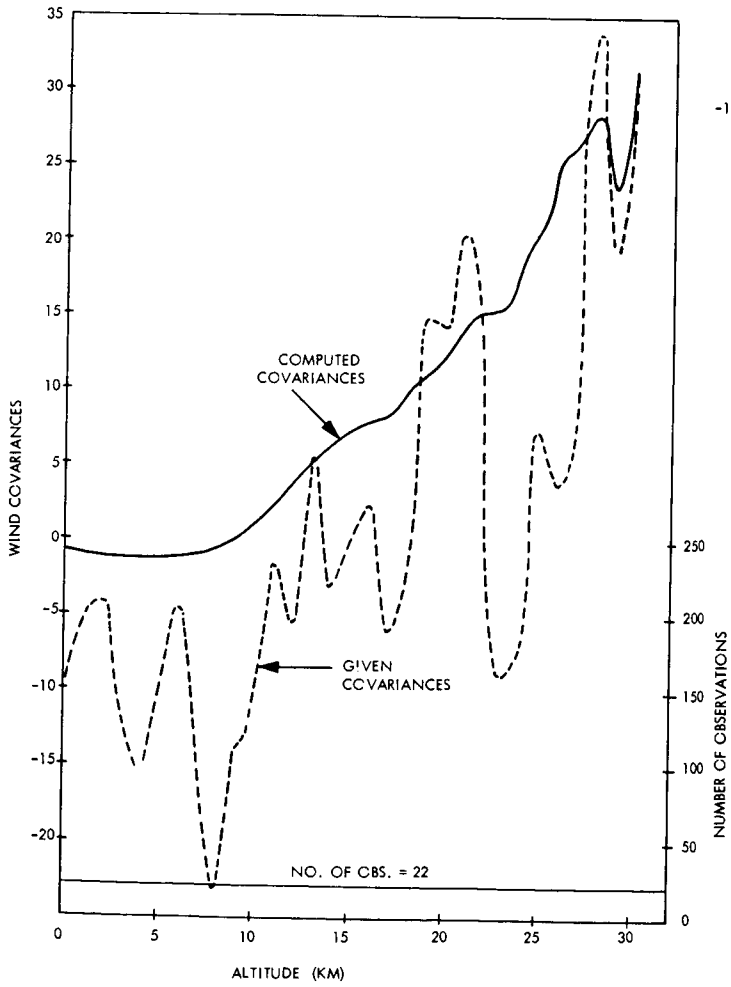

Figure 2-7

Computed and Given Wind Covariance versus Altitude - 30-km Reference

given covariance data is somewhat scattershot, especially where the covariances are based on few observations. The exponential-cosine filter approximates the data fairly well.

It was felt that attempts to better fit the given covariances with a higher-order stationary filter, or with any other filter, would not be worthwhile. The original data was too irregular, and the exponential-cosine filter was probably as close to reality as the given data was.

The last task in constructing the wind filter was to find a filter with the given exponential-cosine output autocorrelation. This was straightforward. The details of the derivation are presented in Appendix B. The resulting impulse response f(h) of Figure 2-3 is

$$f(h) = \frac{\sqrt{a_1 - a_2 a_3}}{a_2} \left[(a_0 - a_1)^2 + a_2^2)^{\frac{1}{2}} e^{-a_1 h} \sin (a_2 h + \psi) u_{-1}(h) \right]$$

where

$$a_0 = \sqrt{\frac{(a_1 + a_2 a_3)(a_1^2 + a_2^2)}{a_1 - a_2 a_3}}$$

$$\psi = \tan^{-1} \left(\frac{a_2}{a_0 - a_1} \right)$$

As shown in Appendix B, the filter f(h) is equivalent to a second-order system described by the vector differential equations

$$\frac{d}{dh} \begin{bmatrix} \omega(h) \\ x(h) \end{bmatrix} = \begin{bmatrix} 0 & c_3 \\ -c_5 & -c_4 \end{bmatrix} \begin{bmatrix} \omega(h) \\ x(h) \end{bmatrix} + \begin{bmatrix} c_1 \\ c_2 \end{bmatrix} \eta(h)$$

where $\eta(h)$ is white noise

$$E\left\{\left[\eta(h_1)\ \eta(h_2)\right]\right\} = \delta(h_2 - h_1)$$

and

$$c_1 = \sqrt{2(a_1 - a_2 a_3)}$$

$$c_2 = \sqrt{2(a_1 + a_2 a_3)(a_1^2 + a_2^2) - 2a_1 c_1}$$

$$c_3 = 1$$

$$c_4 = 2a_1$$

$$c_5 = (a_1^2 + a_2^2)$$

Since the Vaughan data extended only to 30-kilometer altitude and the booster flies to twice that altitude, it was necessary to arbitrarily extend the Vaughan mean wind and wind standard deviations to 60-kilometer. The two moments were smoothed to zero-burnout values. The resulting east-west mean and standard deviations are shown in Appendix A.

The above filter is expressed in terms of altitude h

$$h(t) = \int_0^t \dot{h}(t)dt$$

where $\dot{h}(t)$ is the vertical component of booster velocity. The booster differential equations are expressed in terms of time rather than altitude. It is shown in Appendix B that the above filter equations can be rewritten as

$$\frac{d}{dt}\begin{bmatrix}\omega(t)\\ x(t)\end{bmatrix} = \begin{bmatrix}0 & \dot{h}c_3\\ -\dot{h}c_5 & -\dot{h}c_4\end{bmatrix}\begin{bmatrix}\omega(t)\\ x(t)\end{bmatrix} + \begin{bmatrix}\dot{h}c_1\\ \dot{h}c_2\end{bmatrix}\eta(t)$$

where

$$E\left\{\eta(t_1)\ \eta(t_2)\right\} = \delta(t_2 - t_1)$$

This completes the discussion of the wind model.

WIND LOADS

There is an anomaly in the bending-moment-rate expression previously derived. A modified bending-moment-rate expression was substituted for it in the analyses, and a start towards resolving the anomly was made.

The Anomaly

The bending-moment-rate expression previously developed was

$$\dot{I}_b = \left(\dot{M}_\beta' - 14.5M_\beta' - \frac{M_\alpha'}{V}\ \frac{R}{m}\right)\beta + 14.6M_\beta'\,u - \frac{M_\alpha'}{V}\ \dot{\phi}$$

$$+ \left(\dot{M}_\alpha' - \frac{M_\alpha' N}{mV}\right)\left(\phi + \frac{v_\omega - \dot{z}}{V}\right) + \frac{M_\alpha'}{V}\ \dot{v}_\omega$$

Substituting the wind filter equations

$$v_\omega = \bar{v}_\omega + \sigma_{v_\omega}\omega$$

$$v_\omega = \dot{\bar{v}}_\omega + \dot{\sigma}_{v_\omega}\omega + \sigma_{v_\omega}(\dot{h}c_3 x + \sqrt{\dot{h}c_1}\eta)$$

into this expression produces

$$\dot{I}_b = (\dot{M}_\beta' - 14.6M_\beta' - \frac{M_\alpha'}{V}\frac{R}{m})\beta + 14.6M_\beta' u - \frac{M_\alpha'}{V}\dot{\phi}$$

$$+ \left(\dot{M}_\alpha' - M_\alpha'\frac{N}{mV}\right)\left(\phi + \frac{\bar{v}_\omega - \dot{z}}{V}\right) + \frac{M_\alpha'}{V}\dot{\bar{v}}_\omega$$

$$+ \left[(\dot{M}_\alpha' - M_\alpha')\frac{N}{mV}\frac{\sigma_{v_\omega}}{V} + \frac{M_\alpha'}{V}\dot{\sigma}_{v_\omega}\right]\omega + \frac{M_\alpha'}{V}\sigma_{v_\omega}\dot{h}c_3 x$$

$$+ \frac{M_\alpha'}{V}\sigma_{v_\omega}\dot{h}c_1\eta$$

Hence, with that wind filter, both the wind shear $\dot{v}_\omega$ and the bending-moment-rate $\dot{I}_b$ contain a white noise term $\eta(t)$. Since the standard deviation of white noise is infinite, the standard deviations of both the wind-shear and the bending-moment-rate are infinite. This is nonsensical.

The anomaly is due to two approximations. Wind shear in nature does not have an infinite standard deviation, and, although the above wind filter approximates the wind fairly well, it poorly approximates wind shear.

The second approximation is the implied assumption that the wind is constant over vehicle length. This approximation, a reasonable one when calculating

attitudes and drifts, ignores the averaging of the instantaneous winds over the vehicle length. That is, the side load due to wind is better approximated by

$$\int_{o}^{x_N} \frac{d\tau}{d\alpha} \frac{v_\omega}{V} dx$$

then by

$$N' \frac{v_\omega}{V}$$

The effect of this approximation is to make the force and moment expressions unrealistically sensitive to instantaneous wind-amplitude variations.

The problem caused by these approximations could be defined away by constructing a wind filter with the property that the computed wind shear did not contain white noise. This is an unsatisfactory solution. There is no wind shear data with which to construct such a model, and the form of the wind filter would have to be chosen arbitrarily. If the performance of the controlled booster were sensitive to wind shear, it would be sensitive to arbitrarily chosen parameters, and the calculated performance measures would have little meaning.

The issue, then, is whether or not booster performance is sensitive to wind shear. The only way to test this would be to replace the constant wind approximations with the more accurate integral expressions. Various wind filter forms, with approximately the same wind statistics but widely differing wind shear statistics, could then be employed as wind generators. By comparing the results obtained with the various filters we could determine, within our ability to calculate wind forces, whether or not booster performance was sensitive to wind shear.

Unfortunately, time limitations forced us to choose between resolving this question and studying other issues pertinent to the optimum load-relief controller. Development of a controller design technique was considered to be the principal

purpose of the contract. It was decided therefore to emphasize the latter, and the question of whether or not booster performance is sensitive to wind shears was not resolved.

Modification of the Bending-Moment Rate Expression

It was necessary to modify the above bending-moment rate expression to obtain a vehicle model for study of the controller design technique. Three gross changes were made. The angle-of-attack coefficient

$$(\dot{M}_\alpha{}' - M_\alpha{}' \frac{N}{mV})$$

and the ω (wind state) coefficient

$$(\dot{M}_\alpha{}' - M_\alpha{}' \frac{N}{mV}) \frac{\sigma_{v_\omega}}{V} + \frac{M_\alpha{}'}{V} \dot{\sigma}_{v_\omega}$$

both of which exhibited severe variations in the high-dynamic-pressure portion of the flight, were arbitrarily smoothed. The smoothed coefficients are shown in Figure 2-8 and 2-9. In addition, the white noise contribution to the bending-moment rate was set to zero.

The bending-moment-rate expression is used to evaluate the expected number of occasions that the bending-moment limit is exceeded in the flight. The above modifications were made to get a reasonably-behaved expectation, and the computed expectations are therefore in error. The controller was chosen, in part, to minimize the expectation, and the computed controller-gains probably differ from what would result if more accurate wind-force expressions were employed. The simulation tests, fortunately, were not affected by the modifications, as bending-moment responses could be obtained without calculating bending-moment rates.

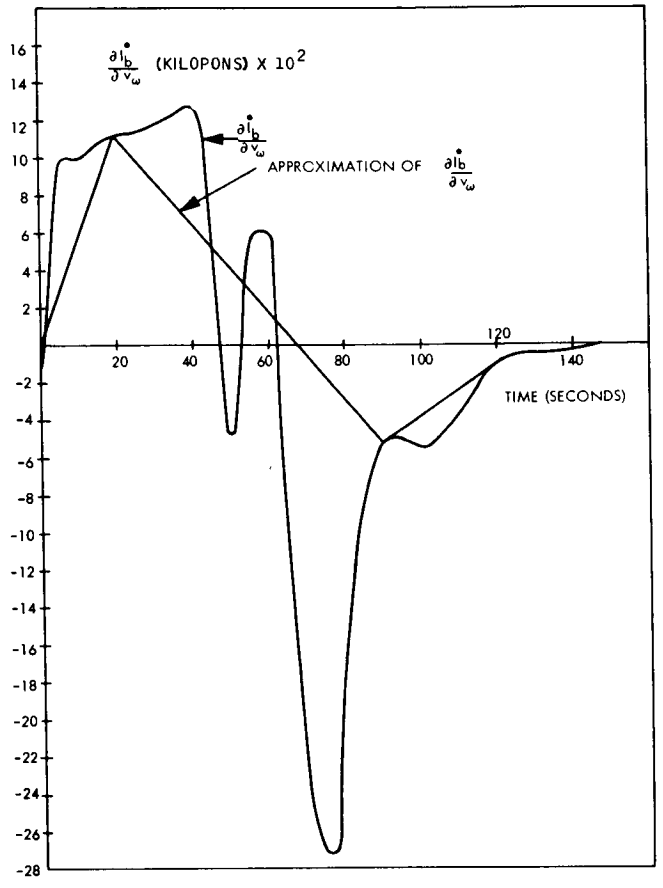

Figure 2-8
Approximation of $\partial \dot{I}_b / \partial \bar{v}_\omega$

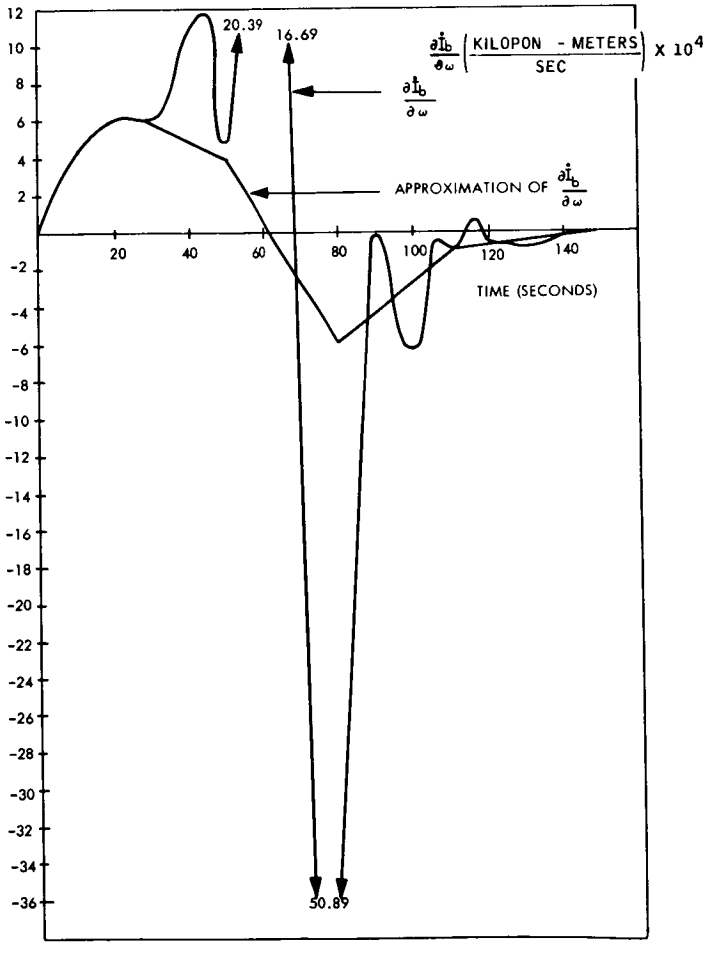

Figure 2-9
Approximation of $\partial \dot{I}_b / \partial \omega$

More Accurate Expressions

A start towards resolving the wind-shear question was made. It was assumed that an optimal controller would not be sensitive to plant-parameter variations. This assumption, which requires verification, permits introducing approximations that simplify the plant model.

The existence of a side-force-density derivative was assumed. Its value was estimated by simple aerodyanmic theories, and the side-force density ($\frac{d\tau}{d\alpha}(x,t)$ = side force at body station x per-unit length per unit angle-of-attack) and the pitching moment and bending moment densities

$$(x - x_{cg}) \frac{d\tau}{d\alpha}(x,t) \qquad \text{(pitching moment)}$$

$$\left[(x - x_o)u_{-1}(x - x_0) + \gamma_1 x - \gamma_2 \right] \frac{d\tau}{d\alpha}(x,t) \qquad \text{(bending moment)}$$

were calculated. The integrals

$$\int_o^{x_n} \frac{v_\omega}{V} \text{(density)}dx$$

were then approximated by finite-order filters, and a computer program to calculate the optimum controller was written.

The derivation of the $\frac{d\tau}{d\alpha}$ density is presented in Appendix C.

The $\frac{d\tau}{d\alpha}$ density computed with the aerodynamic theories presented there did not, when integrated, agree exactly with the N, $N\ell cp$, $M_\alpha{}'$ data presented in the "Model Vehicle No. 2" data package. To enforce agreement, the aerodynamic density was multiplied by the ratios of the given data over the derived data. Letting $\frac{d\tau_o}{d\alpha}$ be the aerodynamic density, the resulting drift density was

$$\frac{d\tau_1}{d\alpha} = \frac{d\tau_o}{d\alpha}\left[\frac{N}{\int_o^{x_n} \frac{d\tau_o}{d\alpha}\,dx}\right]$$

the pitching density was

$$(x - x_{cg})\frac{d\tau_2}{d\alpha} = (x - x_{cg})\frac{d\tau_o}{d\alpha}\left[\frac{N\ell cp}{\int_o^{x_n} (x - x_{cg})\frac{d\tau_o}{d\alpha}\,dx}\right]$$

and the bending moment density was

$$\left[(x - x_o)\,u_{-1}(x - x_o) + \gamma_1 x - \gamma_2\right]\frac{d\tau_2}{d\alpha} = \left[(x - x_o)\,u_{-1}(x - x_o) + \gamma_1 x - \gamma_2\right]\frac{d\tau_o}{d\alpha}$$

$$\left[\frac{M_\alpha{}'}{\int_o^{x_n}\left[\left((x - x_o)\,u_{-1}(x - x_o) + \gamma_1 x - \gamma_2\right)\frac{d\tau_o}{d\alpha}\right]dx}\right]$$

Plots of the side force, pitching moment, and bending moment due to a step angle-of-attack are presented in Figures 2-10, 2-11 and 2-12. It is evident that the major portions of the forces and moments are due to the side loads on the booster tail fins, and that the tail-fin effects are rather abrupt. This brought up the question of developing a computationally feasible approximation to the above densities.

This question was not completely resolved. The most accurate formulations, involving a sampled delay line of $\frac{x_n}{v}$ seconds, were rejected as requiring too large an increase of the order of the difference equations describing the system. Approximation of the $\frac{d\tilde{t}}{d\alpha}$ weighting function with simpler functions was rejected as inaccurate, as the $\frac{d\tilde{t}}{d\alpha}$ function contains "spikes" at the various frustrums and the tail fins.

After considerable casting about, we concluded that we would be unable to generate a computationally feasible, accurate approximation of the wind loads in the time available. We decided to settle for less -- for an inaccurate formulation we could defend as being superior to the expressions presently employed.

The approximation employed is based on the following rationale:

- The wind undoubtedly has lower high-frequency components than the above wind model would indicate:

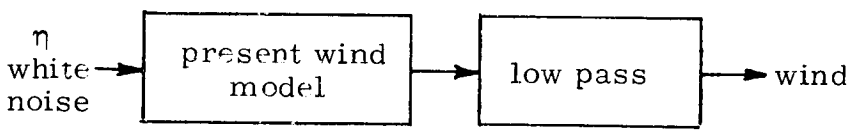

Since the wind data was based on 1000-meter samples, it does not contain small-wavelength components, and there is no way of assessing what the high-frequency spectra should be.

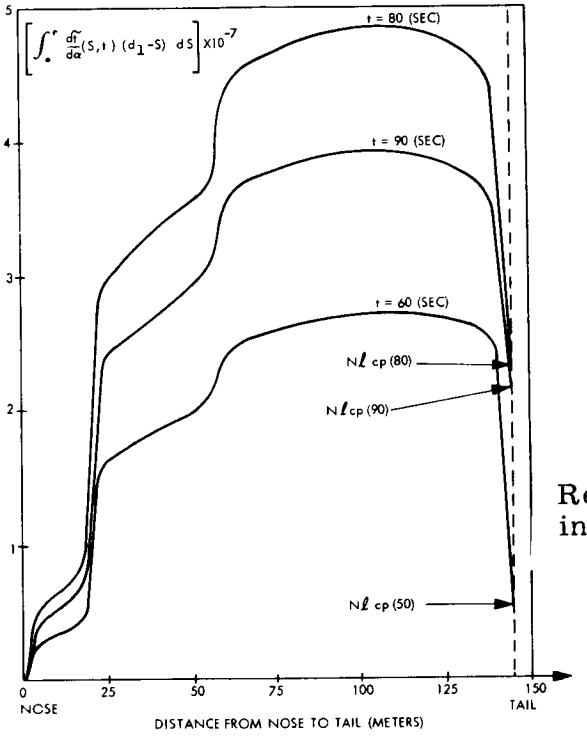

Figure 2-10

Representative Sample of Step Side Forces versus Vehicle Length, r

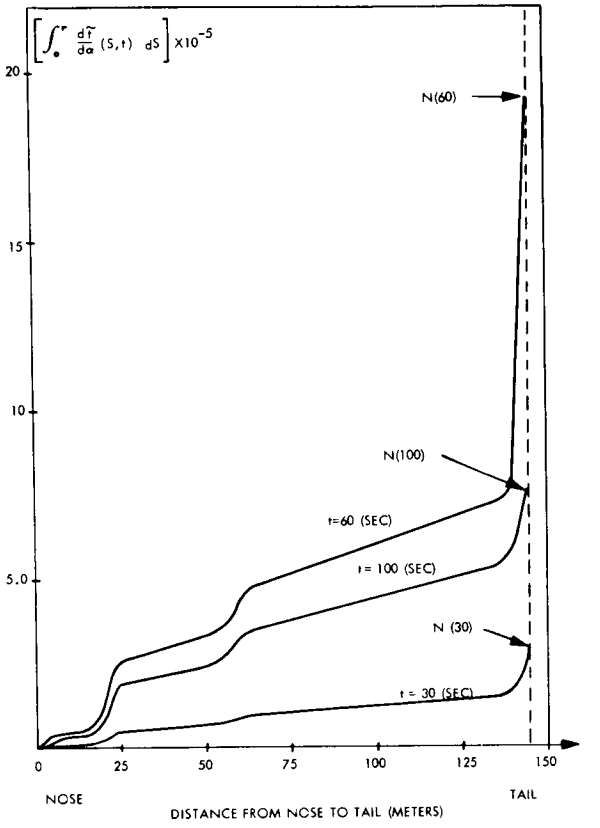

Figure 2-11

Representative Sample of Step Pitching Moments versus Vehicle Length, r

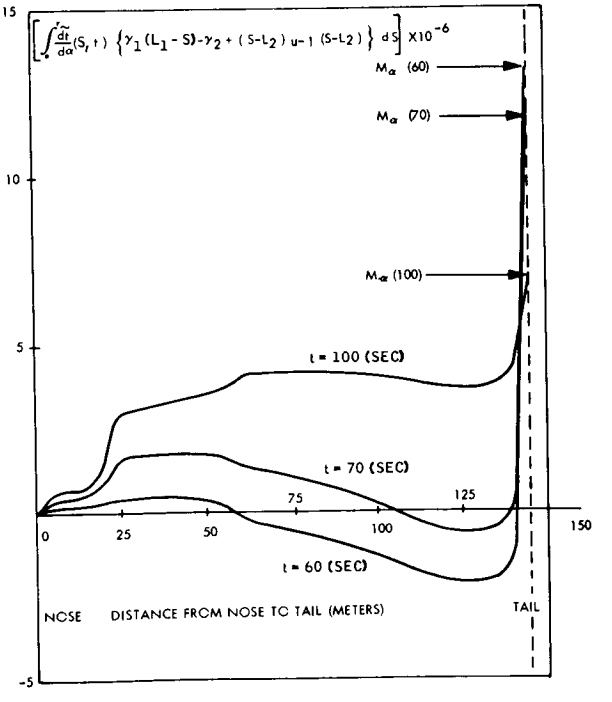

Figure 2-12

Representative Sample of Step Bending Moments versus Vehicle Length, r

- The effect of the above low-pass would be to smooth the wind and thereby reduce the emphasis of the wind loads on the "spikes" of the $\frac{\tilde{d}t}{d\alpha}$ load density. Again, how much is not known.

- The time required to pass a point in space is somewhat less than the time constants of the vehicle drift and pitch responses. The wind load integrals

$$\int_0^{x_n} v_\omega (x, t) \frac{\tilde{dt}}{d\alpha} (x, t)\, dx$$

$$\int_0^{x_n} v_\omega (x, t) \frac{\tilde{dt}}{d\alpha} (x, t) \; (x - x_{cg})\, dx$$

can therefore be safely approximated by replacing $\frac{\tilde{dt}}{d\alpha}$ and $\frac{\tilde{dt}}{d\alpha}(x - x_{cg})$ by smooth functions of somewhat the same shape, providing the integrals of these functions over vehicle length have the values N and $N\ell cp$.

- The contributions of v_ω to the bending-moment and bending-moment-rate equations are employed only to estimate these quantities and are not used as force terms. Smoother functions approximating the integrands that are larger at all locations than the present integrands would serve as well for this purpose and could be considered "worst-case" approximations.

The approximation employed, based on this rationale, involved the impulse responses of a first-order filter and a second-order Pade′-type filter. Let $r = x_n - y$ (distance measured from the nose), and let $h_1(r)$ and $h_2(t)$ be the inverse transforms

$$h_1(r) = \frac{1}{2\pi j} \int_{-j\infty}^{+j\infty} e^{sr} \frac{1}{sX_1 + 1} \, ds$$

$$h_2(r) = \frac{1}{2\pi j} \int_{-j\infty}^{+j\infty} e^{sr} \frac{-\frac{5}{6}X_2 s + 1}{\frac{1}{6}X_2^2 s^2 + \frac{2}{3}X_2 s + 1} \, ds$$

The approximations replaced

$$\frac{\widetilde{dt}}{d\alpha}(r, t) \text{ by } N(t) \left[a_1(t)\, h_1(r) + a_2(t)\, h_2(r)\right]$$

$$(x_n - r - x_{cg}) \frac{\widetilde{dt}}{d\alpha}(r, t) \text{ by } N(t) \left[a_3(t)\, h_1(r) - a_4(t)\, h_2(r)\right]$$

$$(x - x_n - r)\, u_{-1}(r - x_n + x + \gamma_1 (x_n - r) - \gamma_2) \frac{\widetilde{dt}}{d\alpha}(r, t) \text{ by}$$

$$M_\alpha' \left[a_5(t)\, h_1(r) + a_6(t)\, h_2(r)\right]$$

where $a_1(t), \ldots a_6(t)$ are slowly varying functions of time. The X_1, X_2, a(t) coefficients were chosen to reasonably approximate the distribution of loads, and X_1, X_2, a_1, a_2, a_5, a_6 were chosen to be

$$X_1 = 80/3$$

$$X_2 = 100$$

$$a_1(t) = 1/2$$

$$a_2(t) = 1/2$$

$$a_5(t) = 1/3 + 2/3 \frac{t}{150}$$

$$a_6(t) = 2/3 - 1/3 \frac{t}{150}$$

The a_3, a_4 coefficients were chosen to match the peak and final step angle-of-attack responses of the filters and the pitching moment

$$a_3(t) - a_4(t) = \ell cp(t) \quad \text{(final value)}$$

$$a_3(t) - 0.3a_4(t) = \frac{\frac{MAX}{y}\left[\int_0^y (x_n - r - x_{cg}) \frac{d\tau_2}{d\alpha}(r,t)\, dr\right]}{N(t)}$$

The filter step responses and their approximations to the drift, pitch, and bending responses are shown in Figure 2-13.

In state vector notation, the impulse responses correspond to the equations

$$\dot{x}_1(t) = -\frac{V}{x_1} x_1(t) + \frac{v_\omega(t)}{x_1}$$

$$\begin{bmatrix} \dot{x}_2(t) \\ \dot{x}_3(t) \end{bmatrix} = \begin{bmatrix} \frac{-4V}{X_2} & \frac{-6V}{X_2} \\ \frac{V}{X_2} & 0 \end{bmatrix} \begin{bmatrix} x_2(t) \\ x_3(t) \end{bmatrix} + \begin{bmatrix} \frac{-5}{X_2} \\ \frac{1}{X_2} \end{bmatrix} v_\omega(t)$$

where $v_\omega(t)$ is the wind at the vehicle nose. The angle-of-attack loads are then:

- Side force:

$$(\phi - \frac{\dot{z}}{v}) N - \frac{\dot{\phi}}{v} N\ell cp + N(a_1 x_1 + a_2 x_2)$$

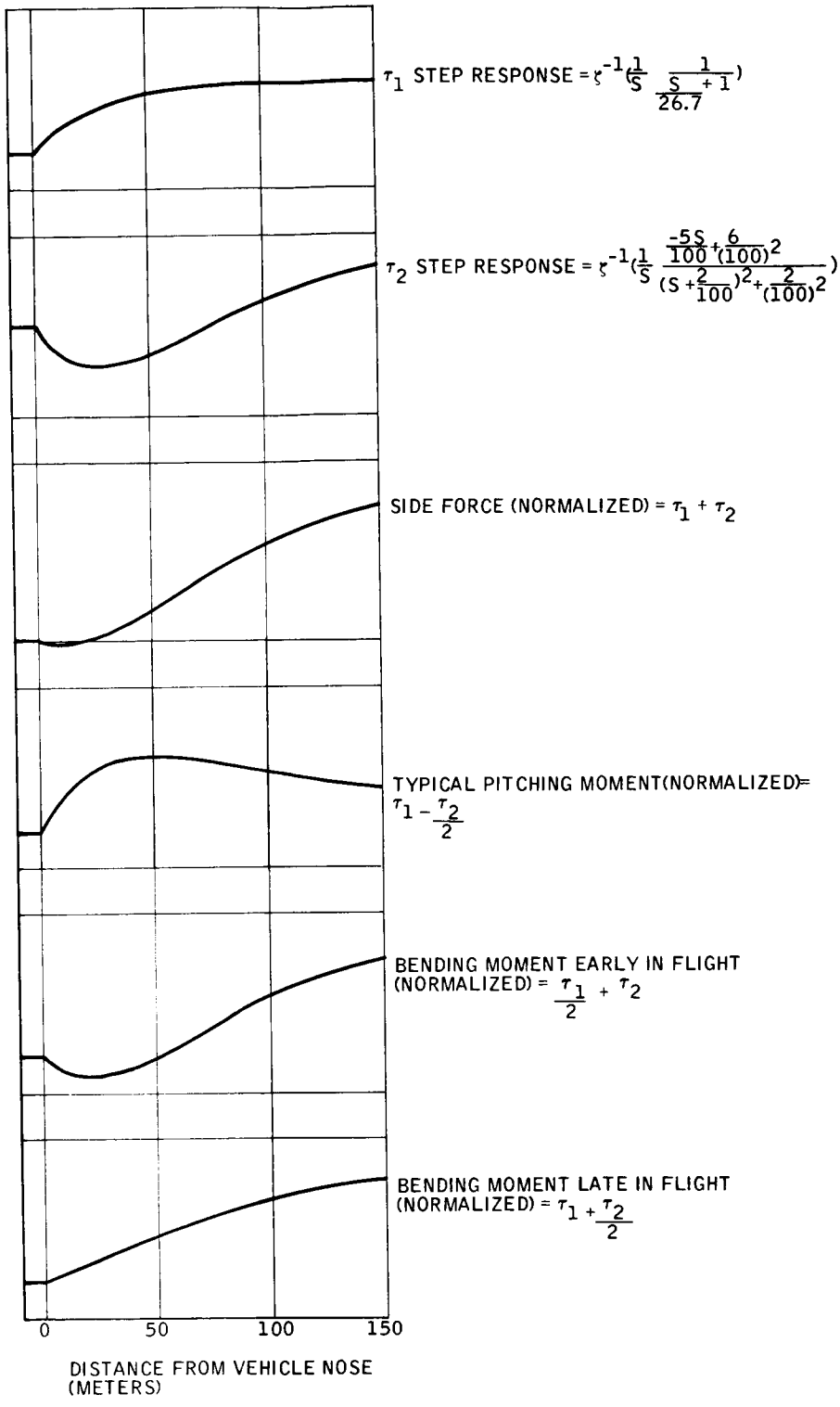

Figure 2-13. Wind-Force Response to Step Angle-of-Attack with Approximate Wind Load Filters

- Pitch moment:

$$(\phi - \frac{\dot{z}}{v}) N\ell cp - \frac{\dot{\phi}}{v} T_{\dot{\phi}} + N(a_3 x_1 - a_4 x_2)$$

- Bending moment:

$$(\phi - \frac{\dot{z}}{v}) M_{\alpha}' - \frac{\dot{\phi}}{v} M_{\alpha}' (a_5 x_1 + a_6 x_2)$$

The angle-of-attack contribution to the bending-moment rate, after dropping $\dot{v}$, $\dot{a}_5$, $\dot{a}_6$ terms as negligible, is

$$(\ddot{\phi} - \frac{\dot{z}}{v}) M_{\alpha}' + (\phi - \frac{\dot{z}}{v}) \dot{M}_{\alpha}' - \frac{\ddot{\phi}}{v} M_{\dot{\phi}} - \frac{\dot{\phi}}{v} \dot{M}_{\alpha}' (a_5 x_1 + a_6 x_2)$$

$$+ M_{\alpha}' a_5 (\frac{-v}{X_1} x_1 + \frac{v_{\omega}}{X_1}) + M_{\alpha}' a_6 (\frac{-4v}{X_2} x_2 - \frac{6v}{X_2} x_3 - \frac{5v_{\omega}}{X_2})$$

STATE EQUATIONS

The quadratic theory discussed in Section III requires that the vehicle and wind-filter equations be written as first-order vector differential equations of the form

$$x(t) = F(t)\, x(t) + G_1(t)\, u(t) + G_2(t)\, \eta(t) + G_3(t)\, \overline{v}_{\omega}(t)$$

$$r(t) = H_1(t)\, x(t) + D_1(t)\, u(t) + D_2(t)\, \overline{v}_{\omega}(t)$$

The above vehicle equations are expressed in this form in Appendix D. Both the constant-wind and the $\frac{d\tau}{d\alpha}$ approximation cases are presented.

SECTION III
THE STOCHASTIC PROBLEM

The definition and solution of the stochastic formulation of the load-relief problem are presented in this section. The formulation of the load-relief problem as a stochastic minimization problem is discussed in the first subsection, and the equivalent quadratic method for its solution is presented in the second. The last subsection contains a discussion of the form of the solution and the equations which define it.

FORMULATION

The load-relief problem is essentially a problem of keeping missile responses within prescribed limits. Some of these constraints, such as stress limits and actuator-travel limits, must be met throughout the booster flight. Others, such as translation-error limits, need be met only at the terminal (burnout) time.

The problem is seen both as a statistics problem and an optimization problem. It is a statistics problem because the winds to be encountered on a particular flight will not be known at the time the load-relief controller is designed. However, the set of possibly-occurring winds can be described as a random process, and the corresponding missile responses can therefore be described as random processes. Meaningful statistical measures of controller quality are standard deviations of terminal-response, mean miss distance, and peak-stress standard deviations. Perhaps the most appealing of such measures is the percentage of possibly-occurring winds for which all of the response constraints would be met. Maximization of this measure is the basis of the formulation below.

The design problem is an optimization problem; choosing any quality measure implies that the design procedure should maximize (or minimize) it.

These notions are the motives for formulating the load-relief problem as a stochastic optimization problem. The particular formulation described below was chosen because it could be solved.

Mission Success

The above percentage-of-winds for which the response constraints would be met can be defined in the following manner:

Let $t = 0$ be the time of missile lift-off and $t = T$ be the booster burnout time. Let $r_i(t)$, $i = 1, \ldots m$, be the deviations from ideal (no-wind) values of the m booster responses whose behaviors are to be constrained at the burnout time T. Let $r_i(t)$, $i = m+1, \ldots n$, be the deviations from ideal of the n-m booster responses whose excursions are to be constrained throughout the flight. Let γ_i, $i = 1, \ldots n$, be finite positive constants and let a_i, $i = 1, \ldots m$, denote the event

$$|r_i(T)| < \gamma_i \tag{3.1}$$

and $\bar{a}_i$ the event

$$|r_i(T)| \geq \gamma_i \tag{3.2}$$

The events a_i, $i = 1, \ldots m$, are the events that the m responses $r_i(t)$, $i = 1, \ldots m$, fall within their limits at burnout.

Let $b_i(j)$ denote the event that the two conditions

$$\begin{aligned} &|r_i(t)| = \gamma_i \\ &\frac{d}{dt} |r_i(t)| > 0 \end{aligned} \tag{3.3}$$

are met exactly j times in the interval $[0, T]$. This is the event that response $r_i(t)$ exceeds its bound γ_i exactly j times in the course of the flight.

The idea of controlling the booster is to have the events $a_1, a_2, \ldots a_m, b_{m+1}, (0), \ldots b_n(0)$ occur. Therefore, define

$$\left\{\begin{array}{l}\text{The event of}\\ \text{mission success}\end{array}\right\} = \left\{\begin{array}{l}\text{The event that all of the events}\\ a_1, a_2, \ldots a_m, b_{m+1}(0), \ldots b_n(0) \text{ occur}\end{array}\right\} \tag{3.4}$$

Mission success is then the event that all terminal and in-flight constraints are met.

The above definitions apply to a single missile flight. Restated, they apply to the missile's responses to a particular wind input. Given a wind input, the flight is a success if the vehicle's responses to that input fall within the constraints.

The percentage of possibly-occurring winds for which mission success occurs is the percentage for which all of the events $a_1, \ldots b_n(0)$ occur. This is by definition the joint probability

$$P\left[a_1, \ldots b_n(0)\right] \tag{3.5}$$

Defining mission failure to be the event that one or more of the events $\bar{a}_i$, or the events $b_i(j)$, $j > 0$, occur, the probability of mission failure is the difference J

$$J = 1 - P\left[a_1, \ldots b_n(0)\right]. \tag{3.6}$$

Maximization of $P\left[a_1, \ldots b_n(0)\right]$, or what is the same thing, minimization of the failure-likelihood J, is a meaningful basis for a control design procedure.

An Upper Bound for the Likelihood of Failure

Unfortunately no analytical expression for the likelihood of mission success is known, even for Gaussian processes. However, a useful upper bound on the failure-likelihood J can be constructed:

Let $E\left\{N_i\right\}$ be the expected number of occasions that the response $r_i(t)$ exceeds its limit in the interval $\left[0, T\right]$. Then,

$$E\left\{N_i\right\} = \sum_{j=0}^{\infty} j\, P\left[b_i(j)\right] \tag{3.7}$$

where $P\left[b_i(j)\right]$ is the probability that event $b_i(j)$ occurs. Let $P(\bar{a}_i)$ be the probability that event $\bar{a}_i$ occurs (a_i does not occur), and let J^* be the sum

$$J^* = \sum_{i=1}^{m} P(a_i) + \sum_{i=m+1}^{n} E\left\{N_i\right\}. \tag{3.8}$$

It is shown in Appendix E that, for general (not necessarily Gaussian) random processes, J^* satisfies

$$J^* \geq J \tag{3.9}$$

That is, J^* is an upper bound for J. If J^* can be made sufficiently small by proper choice of a controller, J will be smaller, and the controller will be a "good" controller. In what follows, J^* is regarded as the "cost of control", and the goal of control will be minimization of this cost.

Analytical expressions for the probabilities $P(\bar{a}_i)$ and the expectations $E\left\{N_i\right\}$ are derived in Appendix E under the assumption that the responses $r_i(t)$ are non-stationary Gaussian processes. Expressions for them for general (non-Gaussian) processes are not known.

Basic Assumptions

It is known (Davenport and Root, Ref. 10) that linear transformations of Gaussian processes are Gaussian processes. Therefore if it is assumed that (a) the incident wind is Gaussian, (b) the missile's response perturbations are linear transformations of wind and gimbal inputs, and (c) the restriction that the gimbal controller is a linear controller is imposed, the responses $r_i(t)$ will be Gaussian processes.

These assumptions are made in this formulation to permit writing an analytical expression for J^*.

State Equations

The Gaussianess and linearity assumptions above are fundamental to the description of the missile's responses as random processes. Convenient minimization of J^* requires several additional assumptions. They are convenient in that they permit applying Kalman's results, via the quadratic equivalence described in the next subsection, to the J^* minimization.

It is assumed that the missile's response perturbations can be accurately approximated by finite-order vector equations of the form

$$\begin{aligned} \dot{x}_v(t) &= F_v(t)\, x(t) + G_{1v}(t)\, u(t) + G_{2v}(t)\, v_\omega(t) \\ r_v(t) &= H_v(t)\, x(t) + D_{1v}(t)\, u(t) + D_{2v}(t)\, v_\omega(t) \end{aligned} \tag{3.10}$$

where the coefficients in the matrices F_v, G_{1v}, G_{2v}, H_{1v}, D_{1v}, D_{2v} are known functions of time. In this notation

$x_v(t)$ = vehicle state vector $(z, \dot{z}, \phi, \dot{\phi}, \beta)$

$r_v(t)$ = vector of responses to be controlled

$u(t)$ = control input to gimbal actuator

$v_\omega(t)$ = wind input

It is further assumed that the vehicle responses sensed (by accelerometers, gyros, etc.) can be approximated by the sums

$$m_v(t) = H_{2v}(t)\, x(t) + D_{3v}(t)\, v_\omega(t) + \eta_2(t) \tag{3.11}$$

where the coefficients of H_{2v} and D_{3v} are known, and

$m_v(t)$ = vector of sensed responses

$\eta_2(t)$ = Gaussian white sensor noise

$$E\,[\eta_2(t)\, \eta_2(t_1)'\,] = W_2(t)\, \delta(t_1 - t) \tag{3.12}$$

It is assumed in addition that the wind input $v_\omega(t)$ can be approximated by the sum of a deterministic (mean) time function and the output of a finite-order linear filter driven by white noise

$$\begin{aligned} v_\omega(t) &= \bar{v}_\omega(t) + H_\omega(t)\, x_\omega(t) \\ \dot{x}_\omega(t) &= F_\omega(t)\, x_\omega(t) + G_\omega(t)\, \eta_1(t) \;, \end{aligned} \tag{3.13}$$

where the coefficients of H_ω, F_ω, G_ω are known time functions and

$\bar{v}_\omega(t)$ = $E[\,v_\omega(t)]$ = mean wind

$x_\omega(t)$ = state of wind filter

$\eta_1(t)$ = Gaussian white noise input to the wind filter

$$E[\eta_1(t)\ \eta_1(t_1)'] = W_1(t)\ \delta(t_1 - t)\,. \tag{3.14}$$

These assumptions were implied in the development of the model equations presented in Section II.

The controller determining $u(t)$ was required to be linear; $u(t)$ is then a linear transformation of present and past measurements $m_v(t)$

$$u(t) = L[t, m(0,t)]\,. \tag{3.15}$$

To avoid having to introduce measure theory notions, L is required to be of the form

$$u(t) = K(t)\, m_v(t) + \int_0^t A(t,\tau)\, m_v(\tau)\, d\tau \tag{3.16}$$

and the coefficients of K, A, F_v, G_{1v}, G_{2v}, H_{1v}, D_{1v}, D_{2v}, H_{2v}, D_{3v}, W_1, W_2, H_v, F_v, G_v, $\bar{v}_v$ are all taken to be piecewise continuous functions of their arguments.

Statement of the Problem

The to-be-controlled system is defined by Equations (3.10) through (3.14), the class of admissible controllers by (3.15) and (3.16), and the cost-of-control by (3.8). Within this framework the stochastic optimization problem is:

Given the system Equations, (3.10) through (3.14), find the linear transformation L, Equations (3.15) and (3.16), that minimizes the cost-of-control J^*, Equation (3.8).

Scope of the Formulation

This problem is intended to be the basis of a load-relief controller design procedure. Before proceeding to its solution, it is appropriate to comment on the aspects of the design problem it encompasses.

The formulation incorporates into the design the stochastic nature of the incident winds, the time-varying booster dynamics, the finite-time nature of the control problem, the terminal translation and rotation constraints, and the in-flight actuator and stress constraints. It defines an optimum linear controller, and it provides a quality measure for evaluating any linear controller.

The formulation does not include design constraints on parameter insensitivity and controller simplicity. The parameter sensitivity problem is that the coefficients of the system equations are not precisely known in practice, and a good controller should control well all possibly occurring parameter values. The simplicity constraint is the familiar argument that the simpler a controller, the more reliable it will be, and the number of amplifiers, summers, wires, etc., in a controller should be considered in the controller selection. Insensitivity and simplicity were not included in the formulation because no convenient means for including them was found. Questions on these constraints must be settled by other methods.

QUADRATIC EQUIVALENCE

In the previous subsection, the load-relief problem was cast as a stochastic optimization problem. The stochastic problem was to minimize an upper bound on the likelihood that one or more booster responses would fall outside preselected limits.

In this subsection an iterative procedure for finding the linear controller which minimizes the upper-bound J^* is developed. The procedure is based on an assertion of quadratic equivalence.

The assertion states that the linear controller minimizing J^* also minimizes a quadratic functional of the first and second response moments (i.e., means and covariances). The coefficients of that quadratic functional are the partial derivatives of J^* with respect to the response moments, evaluated with the moments produced by the optimum controller.

The assertion suggests the iteration procedure. In the procedure, quadratic weights are initially chosen, and the resulting quadratic functional is minimized by application of the known solution of the quadratic problem. The response moments calculated with the quadratic-optimum controller are then used to compute the partial derivatives of the upper-bound J^*. This process is repeated until the initially chosen coefficients and the derived partial derivatives are approximately equal.

This approach to the minimization of J^* is computationally convenient. The maximum principle for this problem is cumbersome, and employment of it, gradient techniques, or other variational techniques would entail extensive digital evaluation of complex mathematical expressions. The iterative search for the equivalent quadratic functional is direct, and the solution to the quadratic problem is straightforward and computationally reasonable.

In the discussion, the iteration procedure and the quadratic equivalence theorem are developed from Taylor's series expansions of J^* and a quadratic functional.

Notation

The most convenient notation for the exposition is that of mean-product matrices, covariance matrices, and the trace of matrix products.

Define the vector of mean responses $\bar{r}(t)$ as

$$r_i(t) = E[r_i(t)] \quad , \tag{3.17}$$

and the matrix of mean-response-products $R(t)$ as

$$R(t) = \bar{r}(t)\bar{r}(t)' \tag{3.18}$$

where the prime (′) superscript indicates a transpose. Define the response covariance matrix $S(t)$ as

$$S(t) = E\left\{[r(t) - \bar{r}(t)][r(t) - \bar{r}(t)]'\right\} \tag{3.19}$$

The matrices $R(t)$, $S(t)$ are then positive indefinite and symmetric. The ij^{th} term of $R(t)$ is the mean-response-product

$$R_{ij}(t) = \bar{r}_i(t)\,\bar{r}_j(t)$$

and the ij^{th} term of $S(t)$ is the covariance

$$S_{ij}(t) = E\left\{[r_i(t) - \bar{r}_i(t)][r_j(t) - \bar{r}_j(t)]\right\}$$

It is shown in Appendix E that the terminal likelihood $P(\bar{a}_i)$ and in-flight expectations $E(N_i)$ making up the upper-bound J^* are functionals only of response means and covariances. By replacing the mean responses by the square root of the means squared, J^* can be written in the general form

$$J^* = f_1[S(T), R(T)] + \int_0^T f_2[S(t), R(t)]\, dt \tag{3.20}$$

Define the trace TR of a square matrix to be the sum of its diagonal components. The functionals $TR[V(t)R(t)]$ and $TR[Q(t)S(t)]$ are then the quadratic forms

$$TR[V(t)\,R(t)] = \sum_{i=1}^{n}\sum_{i=1}^{n} V_{ij}(t)R_{ji}(t)$$

$$= \sum_{i=1}^{n}\sum_{j=1}^{n} \bar{r}_i(t)V_{ij}(t)\bar{r}_j(t)$$

$$= \bar{r}(t)'V(t)\bar{r}(t)$$

$$TR[Q(t)S(t)] = \sum_{i=1}^{n}\sum_{i=1}^{n} Q_{ij}(t)S_{ji}(t)$$

$$= \sum_{i=1}^{n}\sum_{j=1}^{n} E\left\{[r_i(t) - \bar{r}_i(t)]\;Q_{ij}(t)\,[r_j(t) - \bar{r}_j(t)]\right\}$$

$$= E\left\{[r(t) - \bar{r}(t)]'\,Q(t)\,[r(t) - \bar{r}(t)]\right\}$$

The quadratic form J^{**}, where

$$J^{**} = TR\left\{Q(T)S(T) + V(T)R(T) + \int_0^T [Q(t)S(t) + V(t)R(t)]\;dt\right\} \tag{3.21}$$

then contains all of the mean-response-products and covariances contained in the upper-bound functional J^*.

<u>Existence of S(t), R(t)</u>

It is shown in Appendix F that the matrices S(t), R(t) exist (do not have infinite coefficients) when the control law

$$u(t) = L[t, m(0,t)] \tag{3.22}$$

is of the form defined by Equation (3.16).

Taylor's Series Expansion

The existence of S(t) and R(t) permits their expansion in Taylor's series about a variation in the control law. Let the control law be of the form

$$u(t) = L_o[t, m(0, t)] + \epsilon L_1[t, m(0, t)] \tag{3.23}$$

where L_o and L_1 are of the form defined by Equation (3.16), and ϵ is a real constant lying in the range (-1, +1). It is shown in Appendix F that S(t) and R(t) may be expanded in the finite Taylor's series

$$\begin{aligned} S(t) &= S_o(t) + \epsilon S_1(t) + \epsilon^2 S_2(t, \epsilon) \\ R(t) &= R_o(t) + \epsilon R_1(t) + \epsilon^2 R_2(t, \epsilon) \end{aligned} \tag{3.24}$$

where

(a) $S_o(t)$ are the covariance and response product matrices obtained with ϵ set to zero (i.e., they are dependent only on L_o)

(b) the matrices $S_1(t)$, $R_1(t)$ are dependent on L_o and L_1 but are independent of ϵ

(c) the coefficients of $S_2(t, \epsilon)$, $R_2(t, \epsilon)$ are dependent on L_o, L_1 and ϵ, but are bounded above and below for ϵ lying in (-1, 1)

If it is assumed that the functions $f_1[S(T), R(T)]$, $f_2[S(t), R(t)]$ making up J^* possess continuous second derivatives in the neighborhood of S_o, R_o, J^* may be expanded to

$$J^* = J_o^* + \epsilon J_1^* + \epsilon^2 J_2^* (\epsilon) \tag{3.25}$$

where

$$J_o^* = f_1[S_o(T), R_o(T)] + \int_o^T f_2[S_o(t), R_o(t)]\, dt \tag{3.26}$$

and

$$\begin{aligned} J_1^* = {} & TR\left[\left(\frac{\partial f_1}{\partial S}\bigg|_{\substack{S_o(T)\\R_o(T)}}\right) S_1(T) + \left(\frac{\partial f_1}{\partial R}\bigg|_{\substack{S_o(T)\\R_o(T)}}\right) R_1(T)\right] \\ & + \int_o^T TR\left[\left(\frac{\partial f_2}{\partial S}\bigg|_{\substack{S_o(t)\\R_o(t)}}\right) S_1(t) + \left(\frac{\partial f_2}{\partial R}\bigg|_{\substack{S_o(t)\\R_o(t)}}\right) R_1(t)\right] dt \end{aligned} \tag{3.27}$$

the quadratic functional J^{**} similarily expands to

$$J^{**} = J_o^{**} + \epsilon J_1^{**} + \epsilon^2 J_2^{**} (\epsilon) \tag{3.28}$$

where

$$J_i^{**} = TR\left\{Q(T)S_i(T) + V(T)R_i(T) + \int_o^T [Q(t)S_i(t) + V(t)R_i(t)]\, dt\right\} \tag{3.29}$$

In both of these expansions, the first variations J_1^*, J_1^{**} are independent of the value chosen for ϵ, and the second variations J_2^*, J_2^{**} are bounded for ϵ in the range $(-1, +1)$.

Minimization

If it is assumed that for any ϵ in the range (-1, +1) the controller $L_o + \epsilon L_1$ is an admissible controller, then, if L_o is the control law minimizing the upper-bound J^*, the first variation J_1^* of J^* is identically zero. If it were not zero, one could always choose ϵ sufficiently small so that the first variation would dominate the remaining term of the expansion

$$\left|\epsilon J_1^*\right| > \left|\epsilon^2 J_2^*\right| \tag{3.30}$$

In which case, choosing the sign of ϵ opposite to that of J_1^* would produce a J^* less than the minimum J_o^*. In addition, the second variation J_2^* is positive semidefinite

$$J_2^* \geq 0 \tag{3.31}$$

if L_o is the optimum control law. If it were not (if it were negative), any choice of ϵ would produce a J^* less than the minimum J_o^*.

Assertion of Quadratic Equivalence

If the Q, V matrices of the quadratic functional J^{**} are chosen to be the partial derivatives

$$\begin{aligned} Q(T) &= \left.\frac{\partial f_1}{\partial S}\right|_{\substack{S_o(T) \\ R_o(T)}} \\ V(T) &= \left.\frac{\partial f_1}{\partial R}\right|_{\substack{S_o(T) \\ R_o(T)}} \end{aligned} \tag{3.32}$$

$$Q(t) = \left.\frac{\partial f_2}{\partial S}\right|_{\substack{S_o(t)\\R_o(t)}}$$

(3.32 cont'd)

$$V(t) = \left.\frac{\partial f_2}{\partial R}\right|_{\substack{S_o(t)\\R_o(t)}},$$

then the first variations of J^{**} and the upper-bound J^* are identical

$$J_1^{**} = J_1^* \tag{3.33}$$

If L_o is the control law minimizing J^*, it follows that

$$J_1^{**} = J_1^* = 0 \tag{3.34}$$

This is a necessary condition for the minimization of the quadratic J^{**}, and it suggests the following assertion:

The linear controller L_o minimizing the upper-bound J^* also minimizes the quadratic functional J^{**} defined by Equations (3.21) and (3.32).

This assertion is the basis of the optimization technique described below. It is not stated as a theorem because doing so would require showing that the upper-bound J^* has a minimum, that the minimized J^* has continuous first and second derivatives with respect to the matrices $S(t)$, $R(t)$, and that definitions (3.32) imply that sufficiency conditions for the minimization of J^{**} are met. It was assumed in the study that J^* has a minimum, and that the iteration procedure described below would converge to it.

Examination of partial derivatives of the terminal likelihoods $P(\bar{a}_i)$ and in-flight expectations $E(N_i)$ reveals that the derivative conditions on J^* would be met if the determinants of $R(t)$ and $S(t)$ satisfied

$$\begin{aligned} 0 < \mathrm{DET}\,[S(t)] &< \infty \text{ for } t \in (0, T) \\ \mathrm{DET}[R(t)] &< \infty \text{ for } t \in (0, T) \end{aligned} \tag{3.35}$$

It is known from quadratic theory that the quadratic J^{**} can be minimized if the matrices

$$\left.\begin{matrix} Q(t) \\ V(t) \end{matrix}\right\} \text{ are positive semidefinite for } t \in (0, T) \tag{3.36}$$

$$\left.\begin{matrix} D_{1V}(t)\,'Q(t)D_{1V}(t) \\ D_{1V}(t)\;V(t)D_{1V}(t) \end{matrix}\right\} \text{ are positive definite for } t \in (0, T)$$

[The matrix $D_{1V}(t)$ is the contribution of the control to the response $r(t)$, Equation (3.10).] It was found that the values of $S(t)$, $R(t)$ produced by the iteration satisfied (3.35) and that, in the neighborhood of the optimum controller, the matrices $\partial f/\partial S$, $\partial f/\partial R$ satisfied (3.36).

The Iteration Procedure

The above assertion suggests the following iteration technique:

(a) Choose values for $Q(t)$, $V(t)$

(b) Find the controller minimizing J^{**} by application of the quadratic theory

(c) Calculate the response products R(t) and covariances S(t) obtained with the quadratic-optimum controller

(d) Calculate the matrices $\partial f/\partial S$, $\partial f/\partial R$ and compare with the Q, V matrice initially chosen

(e) Rechoose Q, V and repeat (b), (c) and (d) until the derived partial derivatives satisfy Equations (3. 32). The choice of new Q, V matrices can be made by gradient, Newton-Raphson, or other standard iteration techniques.

The procedure is shown schematically in Figure 3-1.

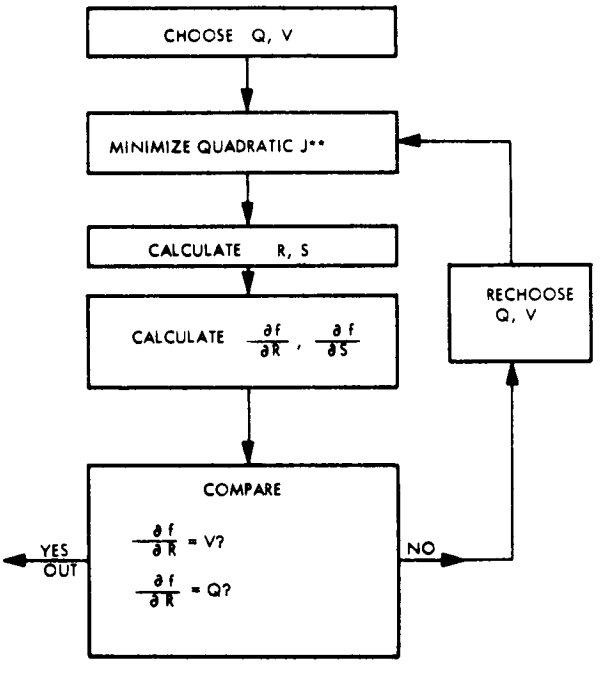

Figure 3-1. Iteration Procedure

This approach to minimizing J^* requires, in theory, continuing the iteration process until Equations (3.32) are satisfied at every time instant t in the flight interval (0, T). Matching all of the functions $\partial f/\partial S_{ij}(t)$, $\partial f/\partial R_{ij}(t)$ over the entire flight is a difficult task, and it would seem that the above iteration implies a great deal of labor.

Fortunately this was not the case in the examples considered in the study. Whether or not the above procedure would be computationally reasonable for other load-relief problems is not known. In this study the insensitivity of the R, S matrices to variations in the Q, V matrices greatly simplified the iteration requirements. The simplifications are discussed in detail in Section IV under the heading "Q Matrix Sensitivity".

THE QUADRATIC PROBLEM

The iterative procedure described in the previous subsection converts the minimization of the upper-bound J^* to minimization of the quadratic functional J^{**} defined in Equation (3.21). The determination of the controller minimizing the quadratic J^{**} is discussed in this subsection.

There is a problem of brevity in discussing the minimization of J^{**}. The results on which the minimization is based are scattered throughout the technical literature, and inclusion of all of the significant theorems of those publications in one discussion is a project equivalent to writing a textbook. The discussion below is in the nature of a summary. The reader is asked to return to the works referenced for detailed derivations of the results.

In the study, J^{**} was minimized by following the digital optimization procedures presented by Tou (Ref. 7). Tou formulated the quadratic problem as a difference equation problem, and he derived the optimum controller by

applying the techniques of "dynamic programming". The difference-equation approach he employed is particularly well suited for digital computation of the quadratic optimum controller.[1]

The algebra and notations of the difference-equation - dynamic programming approach are cumbersome and tend to obscure the central issues of the quadratic theory. The quadratic problem is discussed as a differential-equations problem in the following. It is shown that the minimization of J^{**} can be separated into a deterministic problem and a stochastic problem, and that the solutions of these two problems can be combined to form the optimum controller. The difference-equation equivalents of the Riccati equations defining the solution are presented in Appendix G.

Problem Division

The J^{**} minimization problem can be divided into the control of the mean response $\bar{r}(t)$ and the control of the response deviation from the mean, $r(t) - \bar{r}(t)$. The original problem was:

Given the linear system

$$\begin{aligned} \dot{x}(t) &= F(t)\, x(t) + G_1(t)\, u(t) + G_2(t)\, \eta_1(t) + G_3(t)\, \bar{v}_\omega(t) \\ r(t) &= H_1(t)\, x(t) + D_1(t)\, u(t) + D_2(t)\, \bar{v}_\omega(t) \\ m(t) &= H_2(t)\, x(t) + \eta_2(t)\,, \end{aligned} \tag{3.37}$$

[1] Unfortunately, Tou did not pay too much attention to existence theorems. In particular, he inverted matrices without showing that the inverses existed. It can be shown that all of his results are valid if it is assumed that the difference equation equivalents of the conditions expressed by (3.36) are true.

where η_1, η_2 are white Gaussian processes

$$
\begin{aligned}
E[\eta_1(t)\,\eta_1(t_1)'] &= W_1(t)\,\delta(t - t_1) \\
E[\eta_2(t)\,\eta_2(t_1)'] &= W_2(t)\,\delta(t - t_1) \\
E[\eta_1(t)\,\eta_2(t_1)'] &= W_3(t)\,\delta(t - t_1)\ ,
\end{aligned}
\tag{3.38}
$$

the initial state covariance is known, and $\bar{v}_\omega(t)$ is the known (deterministic) mean wind. Find the linear transformation of present and past measured outputs $m(t)$

$$
u(t) = L[t,\ m(o,t)] \tag{3.39}
$$

that minimizes the quadratic J^{**}

$$
\begin{aligned}
J^{**} = {} & E\left\{[r(T) - \bar{r}(T)]'\,Q(T)\,[r(T) - \bar{r}(T)]\right\} + \bar{r}(T)'\,V(T)\,\bar{r}(T) \\
& + \int_0^T \left\{E\left[\left(r(t) - \bar{r}(t)\right)'\,Q(t)\left(r(t) - \bar{r}(t)\right)\right] + \bar{r}(t)'V(t)\,\bar{r}(t)\right\} dt
\end{aligned}
\tag{3.40}
$$

where $\bar{r}(t)$ is the mean response.

The expression $r(t)$ is the response of (3.37) when the inputs $\eta_1(t)$, $\eta_2(t)$ are zero. By defining $\bar{x}$, $\bar{m}$, $\bar{u}$ to be mean responses, and

$$
\begin{aligned}
x^* &= x - \bar{x} \\
m^* &= m - \bar{m} \\
u^* &= u - \bar{u} \\
r^* &= r - \bar{r}\ ,
\end{aligned}
\tag{3.41}
$$

there results the two sets of system equations

$$\dot{\bar{x}}(t) = F(t)\,\bar{x}(t) + G_1(t)\,\bar{u}(t) + G_3(t)\,\bar{v}_\omega(t)$$

$$\bar{r}(t) = H_1(t)\,\bar{x}(t) + D_1(t)\,\bar{u}(t) + D_2(t)\,\bar{v}_\omega(t) \qquad (3.42)$$

$$\bar{m}(t) = H_1(t)\,\bar{x}(t)$$

and

$$x^*(t) = F(t)\,x^*(t) + G_1(t)\,u^*(t) + G_2(t)\,\eta_1(t)$$

$$r^*(t) = H_1(t)\,x^*(t) + D_1(t)\,u^*(t) \qquad (3.43)$$

$$m^*(t) = H_2(t)\,x^*(t) + \eta_2(t)$$

The cost J^{**} becomes

$$J^{**} = [\,\bar{r}(T)'\,V(T)\,\bar{r}(T) + \int_0^T \bar{r}(t)'\,V(t)\,\bar{r}(t)\,dt]$$

$$+ E[\,r^*(T)'\,Q(T)\,r^*(T) + \int_0^T r^*(t)'\,Q(t)\,r^*(t)\,dt] \qquad (3.44)$$

Since u^* in (3.43) does not in any way affect $\bar{r}$ in (3.42), and u in (3.42) does not in any way affect r^* in (3.43), the controls $\bar{u}$ and u^* may be designed separately to minimize their respective contributions to J^{**}.

The Kalman Deterministic Problem (Ref. 6)

The mean control $\bar{u}$ will be determined first. Given (3.42), the functional $J_{\bar{r}}^{**}$, where

$$J_{\bar{r}}^{**} = \bar{r}(T)' V(T) \bar{r}(t) + \int_0^T \bar{r}(t)' V(t) \bar{r}(t) \, dt \tag{3.45}$$

is to be minimized.

Examination of the responses whose terminal behavior is to be controlled (drift, drift rate, etc.) reveals that the equations for those responses do not contain the final control u(T). Since Q(t), V(t) are chosen so that the quadratic J^{**} contains only those covariances and means appearing in the upper-bound J^{*}, it can therefore be assumed that the contribution of $\bar{u}(T)$ to $\bar{r}(T)' V(T) \bar{r}(T)$ is zero. That is,

$$V(T) \, D_1(T) = 0$$

The above problem is then a Bolza variational problem (Bliss, Ref. 11). By writing

$$J_{\bar{r}}^{**} = G_1 \, \bar{x}(T) + \int_0^T G_2 \; \bar{x}(t) \;, \bar{u}(t), t \quad dt \tag{3.46}$$

The Hamiltonian for the problem is

$$H = G_2 + \lambda' \dot{\bar{x}} \tag{3.47}$$

and the control $\bar{u}(t)$ is defined by the equations

$$\frac{\partial H}{\partial \bar{u}(t)} = 0$$

$$\frac{\partial H}{\partial \bar{x}(t)} = -\dot{\lambda}(t) \tag{3.48}$$

$$\frac{\partial G_1}{\partial \bar{x}(T)} = \lambda(T).$$

With

$$H = [H_1(t)\bar{x}(t) + D_1(t)\bar{u}(t) + D_2(t)\bar{v}_\omega(t)]' V(t) [H_1(t)\bar{x}(t) + D_1(t)\bar{u}(t) + D_2(t)\bar{v}_\omega(t)] + \lambda(t)'[F(t)\bar{x}(t) + G_1(t)\bar{u}(t) + G_3(t)\bar{v}_\omega(t)] \tag{3.49}$$

then

$$\frac{\partial H}{\partial x(t)} = -\dot{\lambda}(t) = F(t)'\lambda(t) + 2H_1(t)' V(t)[H_1(t)\bar{x}(t) + D_1(t)\bar{u}(t) + D_2(t)\bar{v}_\omega(t)]$$

$$\frac{\partial G_1}{\partial x(T)} = \lambda(T) = 2H_1(T)'V(T)[H_1(T)'\bar{x}(T) + D_2(T)\bar{v}_\omega(T)]$$

$$\frac{\partial H}{\partial \bar{u}(t)} = 0 = G_1(t)'\lambda(t) + 2D_1(t)'V(t)[H_1(t)\bar{x}(t) + D_1(t)\bar{u}(t) + D_2(t)\bar{v}_\omega(t)]$$

By making the additional substitutions (as in Ref. 6)

$$\lambda(t) = 2[P_V(t)\bar{x}(t) + g(t)]$$

$$\bar{u}(t) = K_V(t)\bar{x}(t) + f_V(t), \tag{3.50}$$

and assuming that the inverse $[D_1(t)'V(t)D_1(t)]^{-1}$ exists for $t \in [0, T)$, there results the familiar Riccati end conditions

$$P_V(T) = H_1(T)' V(T) H_1(T)$$
$$g(T) = H_1(T)' V(T) D_2(T)\bar{v}_\omega(T), \tag{3.51}$$

the backwards differential equations

$$\begin{aligned} -\dot{P}_V(t) &= F(t)' P_V(t) + P_V(t)F(t) + H_1(t)' V(t)H_1(t) \\ &- [P_V(t)G_1(t) + H_1(t)'V(t)D_1(t)] [D_1(t)' V(t)D_1(t)]^{-1} \\ &. [G_1(t)'P_V(t) + D_1(t)'V(t)H_1(t)] \end{aligned} \tag{3.52}$$

$$\begin{aligned} -\dot{g}(t) &= F(t)' g(t) + [P_V(t)G_2(t) + H_1(t)' V(t)D_2(t)] \bar{v}_\omega(t) \\ &- [P_V(t)G_1(t) + H_1(t)' V(t)D_1(t)][D_1(t)' V(t)D_1(t)]^{-1}[G_1(t)'g(t) \\ &+ D_1(t)' V(t)D_2(t)\bar{v}_\omega(t)], \end{aligned}$$

and the controller equations

$$K_V(t) = -[D_1(t)' V(t) D_1(t)^{-1}[G_1(t)' P_V(t)' P_V(t) + D_1(t)' V(t) H_1(t)]$$
$$f_V(t) = -[D_1(t)' V(t) D_1(t)]^{-1} [G_1(t)' g(t) + D_1(t)' V(t) D_2(t) \bar{v}_\omega(t)] \tag{3.53}$$

These three sets of equations completely define the mean control $\bar{u}(t)$.

The Stochastic Problem

Given the system equations, (3.43), it remains to find the controller

$$u^*(t) = L(t, m^*[o, t])$$

minimizing the quadratic $J_{r^*}^{**}$

$$J_{r^*}^{**} = E[\, r^*(T)\,' Q(T)\, r^*(T) + \int_0^T r^*(t)\,' Q(t)\, r^*(t)\, dt] \tag{3.54}$$

Let $x^*(t)$ be the sum

$$x^*(t) = x_1(t) + \tilde{x}(t) \tag{3.55}$$

where $x_1(t)$ is defined by the orthogonality condition

$$E[\, x_1(t)\,' \tilde{x}(t) \mid m^*(o,t),\ u^*(o,t)] = 0 \tag{3.56}$$

This is the expected value of the product $x_1(t)\,' \tilde{x}(t)$, given present and past output measurements $m^*(t)$ and past inputs $u^*(t)$. Let $K_Q(t)$ be the set of gains defined by (3.51), (3.52) and (3.53) when V(t) is replaced by Q(t). It is asserted that the controller $L\left(t,\ m^*(0,t)\right)$ minimizing the quadratic $J_{r^*}^{**}$ is

$$u^*(t) = K_Q(t)\, x_1(t)$$

That is, the optimum control input $u^*(t)$ is the product of the state estimate $x_1(t)$ defined by the orthogonality relation (3.56), and the gains $K_Q(t)$ defined by the Riccati equations, (3.51), (3.52) and (3.53).

This assertion is known at the "separability property". It permits separating the $J_{r^*}^{**}$ minimization into two problems:

- The determination of the state estimate $x_1(t)$
- The determination of the controller gains $K_Q(t)$ that would be employed if the entire state $x^*(t)$ could be measured, and the system inputs $\eta_1(t)$ were known

The assertion, if true, considerably simplifies the minimization of $J_{r^*}^{**}$. The assertion has been proved by Tou (Ref. 7) for a difference equation formulation of the quadratic problem. Tou's equations for the optimum discrete controller converge, when the sampling interval is reduced to zero, to a continuous controller of the form $K_Q(t)\ x_1(t)$. To the writers' knowledge, the assertion has not been proved or disproved for a continuous-time formulation. The convergence of Tou's controller to the above is considered strong evidence that the assertion is true, and it was assumed true in the study.

State Estimation

The state estimate $x_1(t)$ must be generated to complete the controller design. The problem of generating state estimates $x_1(t)$ satisfying the orthogonality (3.56) has been completely resolved. In Kalman (Ref. 3) it was known that the orthogonality condition (3.56) implied that, with $x^*(t)$ Gaussian, $x_1(t)$ is the conditional expectation

$$x_1(t) = E\left\{x^*(t) \mid m^*[o,t],\ u^*[o,t]\right\} \tag{3.54}$$

It was further shown that $x_1(t)$ could be generated by a linear transformation of $m^*(t)$ and $u^*(t)$

$$x_1(t) = L^*\left\{t, m^*[o,t],\ u[o,t]\right\} \tag{3.55}$$

In Reference 3, Kalman found the appropriate linear transformation L^* for the case where

$$\text{rank}\ [W_2(t)] = \dim\ [m^*(t)]$$

$$W_3(t) = 0$$

That is, every non-zero linear transformation of $m^*(t)$ contains white noise, and the inputs $\eta_1(t)$ $\eta_2(t)$ in (3.43) are uncorrelated. In Reference 4, Kalman removed the latter restriction ($W_3 = 0$).

Bryson (Ref. 5) showed that all of the cases in which not all output measurements were noisy

$$\text{rank}\,[W_2(t)] < \dim\,[m^*(t)]$$

could be reduced to the latter Kalman formulation. The paper contained successive treatments of all occurring special cases, and it is difficult to summarize its content in one or two paragraphs. In part, Bryson reduced the dimension of the estimation problem by finding all of the states (or state projections) whose present values could be ascertained from linear transformations of the current output $m^*(t)$ and its derivatives $d^j m^*(t)/dt^j$.

Assuming the (Bryson-reduced) system is of the form (3.43), Kalman's solution showed that $x_1(t)$ could be generated from the linear system

$$\dot{x}_1(t) = [F(t) - L(t)\,H_2(t)]\,x_1(t) + L(t)\,m^*(t) \tag{3.56}$$

where L(t) is the solution of the forwards Riccati equation

$$\begin{aligned}\dot{P}_\eta(t) = {} & F(t)\,P_\eta(t) + P_\eta(t)\,F(t)' + G_2(t)\,W_1(t)\,G_2(t)' \\ & - \left[P_\eta(t)\,H_2(t)' + G_1(t)\,W_3(t)\right] W_2(t)^{-1} \left[W_3(t)'\,G_1(t) + H_2(t)\,P_\eta(t)\right]\end{aligned} \tag{3.57}$$

Then

$$L(t) = (P_\eta(t)\,H_2(t)' + G_1(t)\,W_3(t)\;\;W_2(t)^{-1}$$

where the initial conditions are

$$P_\eta(o) = \text{cov}\,[x^*(o)\,x^*(o)'] \tag{3.58}$$

Combining the Results

The optimum control is the sum of the deterministic and stochastic solutions

$$
\begin{aligned}
u(t) &= \bar{u}(t) + u^{*}(t) \\
&= K_V(t)\,\bar{x}(t) + f_V(t) + K_Q(t)\,x_1(t) \\
&= K_Q(t)\,[\,x_1(t) + \bar{x}(t)\,] + [\,K_V(t) - K_Q(t)\,]\,\bar{x}(t) + f_V(t) \\
&= K_Q(t)\,\hat{x}(t) + f(t)
\end{aligned}
\tag{3.59}
$$

where f(t) is the deterministic input

$$
f(t) = [\,K_V(t) - K_Q(t)\,]\,\bar{x}(t) + f_V(t) \tag{3.60}
$$

and $\hat{x}(t)$ is the conditional state expectation

$$
\hat{x}(t) = x_1(t) + \bar{x}(t) = E[\,x(t) \mid m(o,t),\ u(o,t),\ \bar{v}_\omega(o,t)\,] \tag{3.61}
$$

SECTION IV
DIGITAL RESULTS

The digital results obtained in the course of the study are presented in this subsection.

Digital results were obtained only for the seventh-order, constant-angle-of-attack, rigid "Model Vehicle No. 2" missile described in Section II. The missile was assumed to fly for 150 seconds, from launch to burnout, and the response deviation limits considered were:

- Final drift $|z(150)| < 3000$ meters
- Final drift rate $|\dot{z}(150)| < 40$ meters/sec
- Final angle-of-attack $|\dot{\phi}(150) + 0.388\,\alpha(150)| < 0.0453$ rad/sec
- In-flight gimbal angle $|\beta(t)| < 5$ degrees
- In-flight bending moment $|I_b(t)| < 2.25 \cdot 10^6$ kilopon-meters.

The angle-of-attack limit is actually a limit on the angle-of-attack side forces on the upper stages at burnout. The bending moment limit refers to the bending moment at a station 33 meters from the vehicle tail; $M_\alpha{}'$ and $M_\beta{}'$, as functions of position along the missile fuselage, both peak in the neighborhood of the 33-meter station at all time instants in the flight.

Significant details of the quadratic-equivalence iteration technique employed in the minimization of the upper-bound J^* are presented in the first subsection. The example controllers designed by the technique are then discussed. The section concludes with presentation of the digital evaluations of those controllers, a simplified version of one of the controllers, and a competitive minimax controller.

ITERATION DETAILS

This subsection contains discussions of several simplifications of the equivalent-quadratic iteration technique and of the "direct iteration" method employed to close the iteration loop.

Q-Matrix Sensitivity

The iteration procedure for minimizing the upper-bound J^* requires:

- Choosing quadratic coefficients Q, V
- Finding the quadratic-optimum controller
- Finding the response means and covariances
- Finding the partial derivatives $\frac{\partial f}{\partial R}$, $\frac{\partial f}{\partial S}$
- Rechoosing the Q, V matrices and repeating the iteration

Upon running through this procedure several times, it became evident that certain properties of the mean response and response covariances greatly simplified the iteration process.

It was found that the response covariances and means were considerably smaller that the imposed response limits. The bending-moment standard deviation peaked to about one-fourth its limit in the high-dynamic-pressure (max-q) region of the flight. The final standard deviations of drift, drift rate, and angle of attack ran one-tenth or less their respective limits. The gimbal-angle standard deviation ran one-tenth or less its 5-degree limit throughout the flight. The various mean responses were very small, generally about one-tenth their respective standard deviations.

It was found, in addition, that the response means and covariances and the controller gains were relatively insensitive to changes in the Q, V matrices.

The terminal coefficients Q(T), V(T) had virtually no affect on the means, covariances, and gains in the high-dynamic-pressure portion of the flight (around 80 seconds, or 70 seconds back from burnout). Large (10:1) variations in the Q's during the flight produced small (2:1 or less) variations in the bending-moment and bending-moment-rate standard deviations in the max-q region.

The terminal Q(T), V(T) values did, however, have a great effect on the terminal response means and covariances. Variations of the ratios of the bending-moment and bending-moment-rate coefficients significantly affected the ratios of the corresponding response covariances.

These response levels and sensitivities had a considerable effect on the upper-bound J^* and on its derivatives $\partial f/\partial R$, $\partial f/\partial S$. The equations defining J^* are derived in Appendix F. The equations for the derivatives $\partial f/\partial R$, $\partial f/\partial S$, are presented in Appendix H. Examination of these expressions reveals that they all contain exponential multipliers of the (Gaussian density) form

$$e^{-1/2\left(\frac{\gamma \pm \bar{r}}{\sigma}\right)^2}$$

where γ is the response limit, $\bar{r}$ is the mean response, and σ is the response standard deviation. Since

$$\bar{r} << \gamma$$

$$\sigma << \gamma$$

these exponentials took very small values. Further, reasonable variations in the mean responses had virtually no effect on the exponentials

$$\frac{\frac{\partial}{\partial \bar{r}}\left(e^{-1/2\left(\frac{\gamma \pm \bar{r}}{\sigma}\right)^2}\right)}{e^{-1/2\left(\frac{\gamma \pm \bar{r}}{\sigma}\right)^2}} \approx 0$$

but small variations in the standard deviations had very large effects

$$\frac{\frac{\partial}{\partial \bar{r}}\left(e^{-1/2\left(\frac{\gamma \pm \bar{r}}{\sigma}\right)^2}\right)}{e^{-1/2\left(\frac{\gamma \pm \bar{r}}{\sigma}\right)^2}} >> 1$$

In summary, it was found that:

(a) Large variations in the V-matrix produced small variations in the mean responses (and in the control deterministic input) and almost indetectable variations in the upper-bound J^*.

(b) The likelihoods of exceeding the terminal-drift, drift-rate, and angle-of-attack limits were sensitive to the terminal Q(T) values. However, values were easily chosen so that the contributions of these likelihoods to the upper-bound J^* were considerably smaller (by at least four orders of magnitude) than that of the bending-moment expectations.

(c) The expected number of occasions that the gimbal angle exceeded its limit could be made at least four orders of magnitude less than the bending-moment expectation with virtually no effect on the latter.

(d) The expected number of occasions that the bending moment exceeded its limit was by far the largest term in the upper-bound J^*.

(e) The bending-moment and bending-moment-rate covariances peaked in the high-dynamic-pressure portion of the flight. The large values in this region dictated the values of the bending-moment expectation and the upper-bound J^*.

(f) Varying the Q-matrix had little effect on the bending covariance amplitudes in the high-dynamic-pressure region of the flight. These variations did, however, have a significant effect on the ratios of bending-moment covariances to bending-moment-rate covariances.

(g) The value of the bending-moment expectation, the value of J^*, and the values of the derivatives $\partial f/\partial S$ were very sensitive to small variations in the bending-moment and bending-moment-rate covariances in the max-q region.

These properties of the response means and covariances suggested that the iteration procedure for minimizing the upper-bound J^* could be considerably simplified as follows:

(1) Since J^* was virtually independent of the values assigned to the coefficients V(t), it was decided to set

$$V(t) = Q(t)$$

This assignment produced reasonable mean responses, and it reduced the number of Riccati equations involved in each iteration from three to two (one each for the deterministic input, the stochastic gains K_Q, and the state estimator; the first of these was deleted). No attempt to match V(t) to $\partial f/\partial R$ was made.

(2) Since J^* was virtually independent of the terminal values of Q(T), once small terminal liklihoods were produced, no further variations of Q(T) were made. No attempt to match Q(T) to $\partial f_1/\partial S(T)$ was made.

(3) Since J^* was virtually independent of the gimbal coefficients in Q(t), once small gimbal responses were produced, no further variations of these coefficients were made. No attempt to match these Q(t) coefficients to their corresponding $\partial f_2/\partial S(t)$ derivatives was made.

(4) Since J^* was virtually independent of the bending-moment and bending-moment-rate covariances in the early and late portions of the flight (low-dynamic-pressure portions), no attempt to minimize these covariances was made.

These simplifications permitted focusing the iteration procedure on reducing the bending covariances in the high-dynamic-pressure region of the flight.

Two engineering rationale were added to the above observations to produce a fifth simplification. These were that:

(h) The coefficients in the vehicle equations are not precisely known in practice. Therefore, attempts to reduce bending covariances by 10 percent or less are a waste of time, as the errors in these covariances are at least that large.

(i) Little faith can be placed in the bending-moment-rate responses. As discussed in Section II, the bending-moment-rate equation is artificial, over-simplified, and of doubtful validity. Therefore, attempts to achieve anything smaller than gross reductions of the rate covariances are unwarranted.

These rationale, combined with the strong sensitivity of J^* and the derivatives $\partial f_2/\partial S(t)$ to small changes in the bending covariances, suggested the simplification:

(5) The iteration process could be terminated when it had converged to the extent that further iterations produced small changes in the bending covariances in the high-dynamic-pressure region of the flight. That is, the iteration termination was based on covariance convergence rather that convergence of J^* and its derivatives $\partial f/\partial S$.

A sixth simplification that was never experimentally justified was employed:

(6) The Q-matrix coefficients in the course of the flight [in the region [O,T), not including the terminal Q(T) values] were made constants,

$$Q(t_1) = Q(t_2) \text{ for } t_1,\ t_2 \neq T.$$

This latter simplification amounts to assuming that variations in the Q-matrix before and after the max-q region would not have large effects on the max-q bending covariances. This assumption was never tested.

It was not tested for reasons of convenience. The constant Q's, with the Q coefficients determined from the max-q $\partial f/\partial Q$ derivatives, were used to start the iteration procedure. The upper-bounds J^* produced with the constant Q's were of the order of 10^{-6}, and the resulting controllers were obviously good controllers. The analog-simulation tests described in Section V were getting underway about this time, and they required a firm commitment as to the controller to be evaluated. It was decided to retain the constant Q's and investigate the estimation and bending-moment anomaly problems, rather than to continue iteration tests. Time-varying Q-tests were formulated and programmed, but each time they were to be run there was always something else more important to be tested.

In retrospect, not testing the assumption was an error.

None the less, the assumption is thought to be true. The various bending covariances are reasonably flat-topped (nearly constant) across the max-q region, indicating that the Q's over that region should be nearly constant. Further, it is known from the terminal Q(T)-variations that the effects of Q-variations in the Riccati equation damp out quickly. The control gains in the max-q region would then not be much affected by Q-variations before and after max-q, and the system covariances at max-q should therefore not be much affected. The bending-moment-rate covariance should be least affected since its value is largely determined by high-frequency wind-rate terms.

Needless to say, these six simplifications greatly reduced the iteration computation times.

Direct Iteration

In the discussion of the iteration procedure in Section III, it was stated that new values for the Q, V matrices could be chosen after each iteration by gradient, Newton-Raphson, or other iterative techniques. A crude but simple "direct iteration" procedure was employed in the study.

Letting Q_i be the Q values at the ith iteration and $\partial f^i / \partial S$ be the derivatives produced by those Q's, the direct iteration procedure, choose new Q values with the algorithm

$$Q_{i+1}(t) = \lambda Q_i(t) + (1-\lambda) \frac{\partial f^i}{\partial S(t)}$$

where $0 < \lambda < 1$. All of the above observations and all of the numerical results presented below were obtained with this algorithm.

The successful employment of this algorithm was due mostly to the monotonicity of the derivatives and the effects of varying Q. Increasing the quadratic weight on a particular response decreased that response covariance at the expense of other response covariances. The derivatives $\partial f / \partial S$ are monotone in the covariances in the neighborhood of the optimum. Thus if a Q coefficient was too low, the corresponding covariance and derivative $\partial f / \partial S$ were too high, and the direct iteration algorithm chose a higher Q coefficient to reduce the covariance and the derivative.

This one-one relationship of the Q's and $\partial f / \partial S$ derivatives, the emphasis on the bending covariances in the high-dynamic-pressure region of the flight, and the obviation of final convergence, together made the equivalent quadratic iteration procedure an efficient procedure for minimizing the upper-bound J^*.

EXAMPLE CONTROLLERS DESIGNED

This subsection contains discussions of the load-relief controllers designed in the study. A total of five controllers were designed by the methods of Section III. Three of these controllers were evaluated, but a lack of time prevented evaluation of the other two.

The first four of the five controllers were designed for the seventh-order, constant-angle-of-attack, "Model Vehicle No. 2" described in Section II. The fifth was designed for the tenth-order "Model Vehicle No. 2" also described in Section II. This fifth model included a third-order approximation to the local angle-of-attack effects along the booster fuselage. Since there was time only to debug the tenth-order programs, no evaluations of this controller were made, and there are no results on it to discuss.

The four controllers designed for the constant-angle-of-attack missile model differed only in the responses assumed physically measurable:

- In the Simplest Case, it was assumed that all four booster states z, $\dot{z}$, ϕ, $\dot{\phi}$, the gimbal state β, and the two wind-filter states ω, x could be measured.
- In Case I, it was assumed that z, $\dot{z}$, ϕ, $\dot{\phi}$, and β could be measured and that the wind input $v_\omega(t)$ could be measured.
- In Case II, it was assumed that z, $\dot{z}$, ϕ, $\dot{\phi}$, and β could be measured and the wind input $v_\omega(t)$ could be measured but the measurement was noisy.
- In Case III, it was assumed that ϕ, $\dot{\phi}$, β and an accelerometer output $\ddot{z}$ could be measured, but the $\ddot{z}$ measurement was noisy.

The Simplest Case controller was considered because it permitted examination of the control aspects of the load-relief problem without the complicating effects of incomplete state measurement. The Case I and Case II controllers were studied to determine the performance degradation produced by poor wind measurement. The Case III controller was intended to approximate realistic sensing; unfortunately a lack of time precluded evaluation of its performance.

The Simplest Case

In this example all of the states of the system were assumed measurable. The optimum controller took the form

$$u(t) = f(t) + K_z(t)\, z(t) + K_{\dot{z}}(t)\, \dot{z}(t) + K_\phi(t)\, \phi(t) + K_{\dot{\phi}}(t)\, \dot{\phi}(t)$$

$$+ K_\beta(t)\, \beta(t) + K_\omega(t)\, \omega(t) + K_x(t)\, x(t)$$

The seven gains and the deterministic input for this controller are presented in Appendix J, Figures J-1 through J-8. The mean responses and several of the response covariances obtained with the controller are graphed in Figures J-9 through J-22 of that appendix. A schematic of the controller is shown in Figure 4-1.

The behavior of the controller can be deduced from the graphs in Appendix J. The controller is essentially a wind canceller, a bending damper, and a dead-beat, final-time controller. The deterministic input f(t) tries to cancel the effects of the deterministic (mean) wind input $\bar{v}_\omega(t)$. The feedforward input $K_\omega(t)\, \omega(t) + K_x(t)\, x(t)$ from the wind filter tries to cancel the effects of the wind deviations from the mean wind. The feedback input $K_\beta(t)\, \beta(t) + K_{\dot{z}}(t)\, \dot{z}(t) + K_z(t)\, z(t) + K_{\dot{\phi}}(t)\, \dot{\phi}(t) + K_\phi(t)\, \phi(t)$ damps the effects of the wind not perfectly cancelled by the feedforward input.

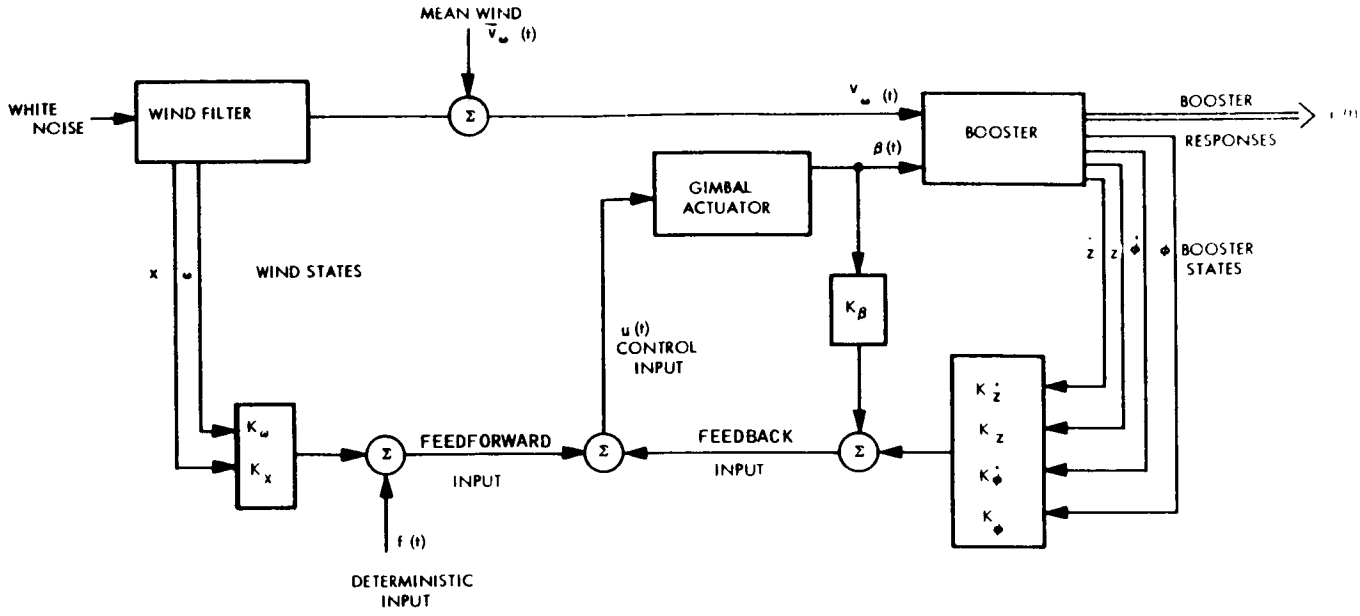

Figure 4-1. Simplest Controller Schematic

In the last 5 seconds of the booster flight, the five feedback gains K_β, $K_{\dot{z}}$, K_z, $K_{\dot{\phi}}$, K_ϕ are chosen to force nearly dead-beat (zero) final values for drift, drift rate, and angle of attack (the responses whose terminal behavior are to be controlled). That the controller well accomplished this is evidenced by the sharp drop in these response covariances at the terminal time. The price paid for the dead-beat characteristic is large bending at the end of the flight, as evidenced by the peaking of the bending covariances there (the bending standard-deviation there is well below the bending-moment limit). The sharp variations in the control gains at the end of the flight are due to the change of emphasis from bending control to dead-beat control; the variations are typical of those produced in linear dead-beat control problems.

In the first 145 seconds of the 150-second booster flight, the controller is essentially a bending controller. Little control emphasis is placed on drift, drift-rate, and local angle-of-attack responses, as these are easily controlled in the final 5 seconds of the flight. Gimbal control is not a problem; as pointed out below, gimbal control is an essential part of bending control.

Examination of the expression for the expected number of occasions that the bending limit is exceeded over the flight (Appendix E) reveals that the expectation is monotone in both the bending moment I_b and the bending moment rate $\dot{I}_b$. That is, the controller should simultaneously minimize both of these responses to successfully control bending. The equations for these responses are

$$I_b = M_{\alpha'}\alpha + B_{\beta'}\beta$$

$$\dot{I}_b = \dot{M}_{\alpha'}\alpha + \dot{M}_{\beta'}\beta + M_{\alpha'}\dot{\alpha} + M_{\beta'}\dot{\beta}$$

Thus, control of bending requires control of angle of attack, gimbal angle, and their time derivatives.

Both of these bending terms could be made zero by cancellation if the control input u(t) could be chosen so that β and $\dot{\beta}$ simultanously would satisfy

$$\beta = -\frac{M_{\alpha'}}{M_{\beta'}}\alpha$$

$$\dot{\beta} = -\frac{M_{\alpha'}}{M_{\beta'}}\dot{\alpha} - \left(\frac{\dot{M}_{\alpha'}}{M_{\beta'}} - \frac{\dot{M}_{\beta'}}{M_{\beta'}}\frac{M_{\alpha'}}{M_{\beta'}}\right)\alpha$$

The control input cannot be so chosen, however, because of the booster dynamics. The wind $v_\omega(t)$ enters the angle-of-attack α directly

$$\alpha = \phi + \frac{v_\omega - \dot{z}}{V}$$

but ϕ and $\dot{z}$ require, respectively, double and single integrations of β. Further, the effects of v_ω on ϕ and $\dot{z}$ cannot simultanously be cancelled by the effects of β because the center of pressure is not at the booster tail

$$\frac{R/m}{-x_{cg}\ R/I_{xx}} \neq \frac{N/m}{\ell cp\ N/I_{xx}}$$

and one cannot pick a β to simultaneously cancel the contributions of v_ω to the accelerations $\ddot{\phi}$, $\ddot{z}$. Finally, because $M_{\beta'} > M_{\alpha'} > 0$, cancellation would require choosing β of the opposite sign to α; but, with

$$\frac{\partial \ddot{\phi}}{\partial \beta} = -x_{cg}\ R/I_{xx} < 0$$

$$\frac{\partial \ddot{z}}{\partial \beta} = R/m > 0$$

this sign of β would tend to increase α by increasing $\phi - \frac{\dot{z}}{V}$.

Without a perfect cancellation ability, the best that can be done with the feedback gains K_β, K_z, $K_{\dot{z}}$, K_ϕ, $K_{\dot{\phi}}$ is to reduce the ϕ, $\dot{z}$ contributions to α and $\dot{\alpha}$ by damping angle of attack. Because

$$M_{\beta'} > M_{\alpha'} > |\dot{M}_{\alpha'}| >> |\dot{M}_{\beta'}|$$

the gimbal-angle β and rate $\dot{\beta}$ contributions to I_b, $\dot{I}_b$ are larger than the α and $\dot{\alpha}$ contributions, and the feedback control is therefore a low-frequency damper. If the reverse were true

$$M_{\beta'} < M_{\alpha'}$$

one could afford larger β and $\dot{\beta}$ signals, and the resulting damper would be high-frequency (tight, high bandwidth, fast response, etc.).

The deterministic input f(t) cancels the effects of the mean wind $\bar{v}_\omega(t)$ to some extent. The feedforward input $K_\omega(t)\ \omega(t) + K_x(t)\ x(t)$ similarly cancels the effects of the (random) wind deviation from the mean. The cancellation emphasis is placed on minimizing the bending-moment I_b rather than the rate $\dot{I}_b$, as reducing the former will reduce the upper-bound J* more than would reducing the latter

$$\frac{\partial f}{\partial(\dot{I}_b{}^2)} < \frac{\partial f}{\partial(I_b{}^2)}$$

In summary, the feedforward inputs cancel the effects of the wind inputs on bending as best possible. The feedback loop slowly damps the effects of the wind inputs not perfectly cancelled. The feedback loop is an angle-of-attack damper because it cannot be a perfect canceller. It is a low-frequency damper because large or rapid gimbal motions are more expensive in bending than are large or rapid angle-of-attack variations.

Since the expected number of occasions of exceeding the gimbal limit of 5 degrees is also reduced by simultanously reducing β and $\dot{\beta}$, good bending control automatically implies good gimbal control. In this problem the bending restriction was much more severe than the gimbal restriction, and the latter could be ignored with no ill effect.

(We feel a little guilty about the above explanation of the physical behavior of the optimum controller. The explanation is based on the optimization results, and it is no engineering feat to explain results already obtained. It was not perceived before the stochastic problem was solved that the controller would behave in the above manner. The saving grace of the situation is that it is an argument for optimization theory; the theory, in this case, provided insight into the physical nature of the control problem.)

The Gimbal Actuator

It was stated in Section II that the results of the optimization would not be changed if the first-order gimbal actuator

$$\dot{\beta} = -14.6\beta + 14.6u$$

were replaced by any first-order actuator

$$\mathring{\beta} = -a_1\beta + a_2 u$$

This result is due to the fact that the control input u(t) does not appear explicitly in the upper-bound J* but enters J* through the dependence of the bending and gimbal expectations on the gimbal rate $\mathring{\beta}$.

With the above control law, $\mathring{\beta}$ is

$$\mathring{\beta} = -14.6\beta + 14.6\ (K_\beta\beta + f + K \circ x)$$

$$= (14.6K_\beta - 14.6)\ \beta + 14.6\ [f(t) + K \circ x]$$

where $K \circ x$ is shorthand for

$$K \circ x = K_{\mathring{z}}\mathring{z} + K_z z + K_{\mathring{\phi}}\mathring{\phi} + K_\phi\phi + K_\omega\omega + K_x x$$

If the $\mathring{\beta} = -a_1\beta + a_2 u$ actuator were employed, the resulting $\dot{\beta}$ would be of the same form

$$\mathring{\beta} = -a_1\beta + a_2\ (K_{\beta*}\beta + f^* + K^* \circ x)$$

$$= (a_2K_{\beta*} - a_1)\ \beta + a_2\ (f^* + K^* \circ x)$$

The two gimbal rates $\mathring{\beta}$ are equal if

$$f^* = \frac{14.6}{a_2}\ f$$

and

$$K^* = \frac{14.6}{a_2}\ K$$

for K_z, $K_{\dot{z}}$, K_ϕ, $K_{\dot{\phi}}$, K_ω, K_x, and

$$K_{\beta *} = \frac{14.6}{a_2} K_\beta + \frac{a_1 - 14.6}{a_2}$$

Since the control u(t) was chosen to minimize a functional of $\dot{\beta}$, the gains and deterministic input that would result from any first-order actuator can be obtained from the present results via the above transformations.

Estimators

In the above "simplest case" it was assumed that the four booster states z, $\dot{z}$, ϕ, $\dot{\phi}$, the gimbal state β, and the two wind-filter states ω, x could all be physically measured. In practice, of course, they cannot. The following examples were introduced to assess the performance degradation implied by incomplete state measurement.

The wind $v_\omega(t)$ in nature is not generated by a second-order filter, and physical measurement of the fictitious wind states ω, x is obviously impossible. It is conceivable, however, that measurement of the wind amplitude $v_\omega(t)$ might some day be possible. The first two estimators treat this case.

Case I Estimator -- In this example it was assumed that all of the vehicle states β, z, $\dot{z}$, ϕ, $\dot{\phi}$ could be measured, and the wind input $v_\omega(t)$ could be measured. Estimates of the two wind-filter states ω, x had to be generated.

The wind-filter equations derived in Section II are

$$v_\omega(t) = \bar{v}_\omega(t) + \sigma_\omega(t)\,\omega(t)$$

$$\begin{bmatrix} \dot{\omega}(t) \\ \dot{x}(t) \end{bmatrix} = \begin{bmatrix} 0 & -c_3\dot{h} \\ -c_5\dot{h} & -c_4\dot{h} \end{bmatrix} \begin{bmatrix} \omega(t) \\ x(t) \end{bmatrix} + \begin{bmatrix} c_1\sqrt{\dot{h}} \\ c_2\sqrt{\dot{h}} \end{bmatrix} \eta_1(t)$$

when η_1 (t) is white noise. Since the mean wind $\bar{v}_\omega)t)$ was known, the wind-filter state $\omega(t)$ was obtained from

$$\omega(t) = \frac{v_\omega(t) - \bar{v}_\omega(t)}{\sigma_\omega(t)}$$

It was assumed that this signal could be differentiated but that differentiation introduced noise $\eta_2(t)$. The measured signal was then

$$m(t) = \dot{\omega}(t) + \eta_2(t) = -c_3\dot{h}\,x(t) + c_1\sqrt{\dot{h}}\,\eta_1(t) + \eta_2(t)$$

By letting

$$x(t) = x_1(t) + x_2(t)$$

where $x_1(t)$ was the known portion of $x(t)$

$$\dot{x}_1(t) = -c_5\dot{h}\,\omega(t) - c_4\dot{h}\,x_1(t)$$

it remained to estimate $x_2(t)$

$$\dot{x}_2(t) = -c_4\dot{h}\,x_2(t) + c_2\sqrt{\dot{h}}\,\eta_1(t)$$

given

$$m(t) + c_3\dot{h}\,x_1(t) = -c_3\dot{h}\,x_2(t) + c_1\dot{h}\,\eta_1(t) + \eta_2(t)$$

This is the form of the Kalman filter problem discussed in Section III. The solution is the estimate $\hat{x}_2(t)$

$$\dot{\hat{x}}_2(t) = (-c_4\dot{h} + Lc_3\dot{h})\,\hat{x}_2 + L\,[\,m(t) + c_3\dot{h}\,x_1(t)]$$

By adding the known $x_1(t)$ to this, the complete filter is

$$\dot{\hat{x}}(t) = (-c_4\dot{h} + Lc_3\dot{h})\,\hat{x}(t) + L[\,\dot{\omega}(t) + \eta_2(t)\,] - c_5\dot{h}\,\dot{\omega}(t)$$

The complete estimator is shown in Figure 4-2, and the resulting controller is shown in Figure 4-3.

Two levels of differention noise were considered

$$\frac{E\left\{\omega^2\right\}}{W_2} = 10$$

and

$$\frac{E\left\{\omega^2\right\}}{W_2} = 1$$

where

$$E\left\{\eta_2(t)\ \eta_2(t_1)\right\} = W_2\delta\,(t-t_1)$$

The gains L and mean-square measurement errors $E\left\{[x(t) - x(t)]^2\right\}$ for the two cases are shown in Appendix K, Figures K-1 and K-2. It is seen there that the effects of an increased signal-to-noise ratio are lower mean-square measurement errors and higher gains L.

<u>Case II Estimator</u> -- This example is very similar to the above. the only difference being that the measured wind $v_\omega(t)$ was assumed noisy

$$m(t) = v_\omega(t) + \eta_2(t)$$

where $\eta_2(t)$ is white noise. The estimator for this case takes the form

$$\begin{bmatrix} \dot{\omega}(t) \\ \\ \dot{\hat{x}}(t) \end{bmatrix} = \begin{bmatrix} 0 & -c_3\dot{h} \\ \\ -c_5\dot{h} & -c_4\dot{h} \end{bmatrix} \begin{bmatrix} \omega \\ \\ x \end{bmatrix} + \begin{bmatrix} L_\omega \\ \\ L_x \end{bmatrix} \left[-\omega + \frac{1}{\sigma_\omega}\left(v_\omega - \bar{v}_\omega + \eta_2\right) \right]$$

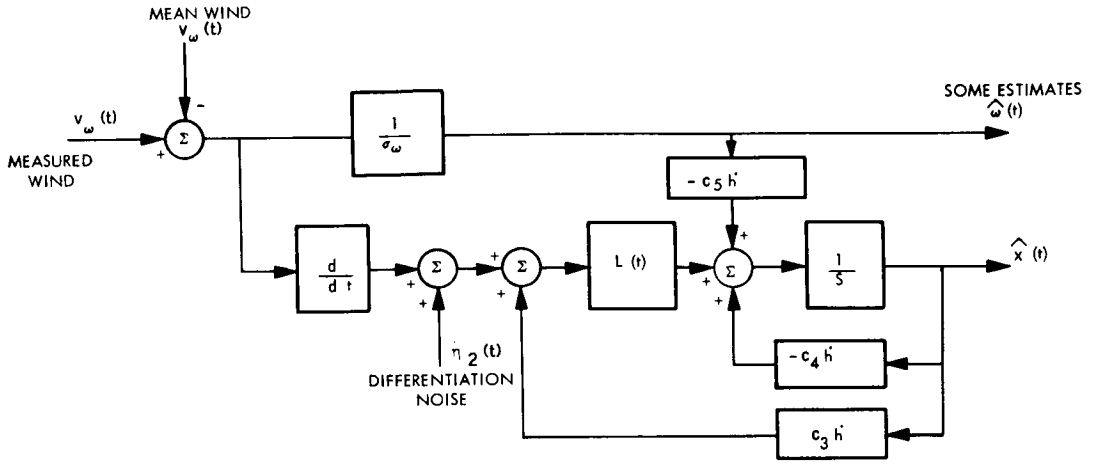

Figure 4-2. Case I Estimator

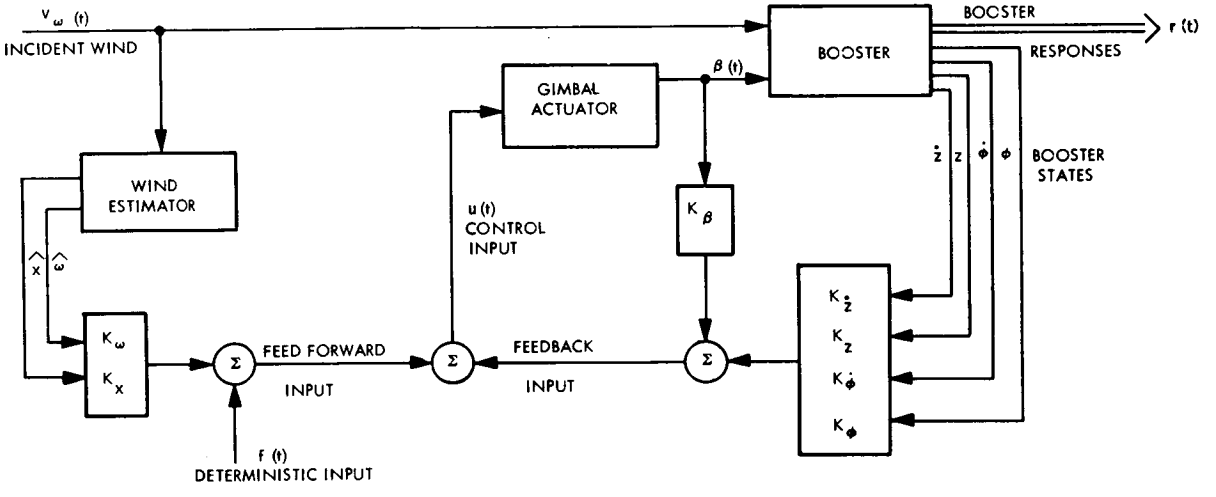

Figure 4-3. Control With Wind Estimation

The estimator is shown in Figure 4-4. The controller employing this estimator is of the same form as that for the Case I Estimator shown in Figure 4-3.

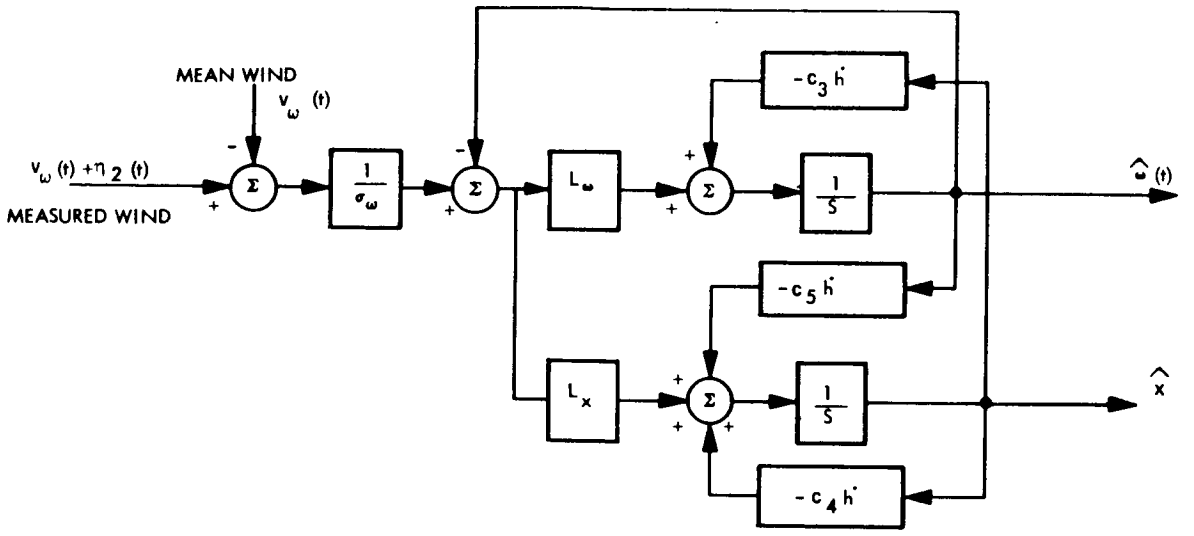

Figure 4-4. Case II Estimator

This estimator was introduced, in contrast to the Case I Estimator above, to make evident the performance degradation implied by a noisy wind measurement. Two noise levels were considered:

$$\frac{E\left\{(v_\omega - \bar{v}_\omega)^2\right\}}{W_2} = 10$$

and

$$\frac{E\left\{(v_\omega - \bar{v}_\omega)^2\right\}}{W_2} = 1$$

where

$$E\left\{\eta_2(t)\ \eta_2(t_1)\right\} = W_2 \delta\,(t-t_1).$$

The resulting gains L_ω, L_x are shown in Appendix K, Figure K-3, and the corresponding error covariances $E\left\{(\omega-\hat{\omega})^2\right\}$ and $E\left\{(x-\hat{x})^2\right\}$ are presented in Figure K-4. Again, the effects of an increased signal-to-noise ratio are lower errors and higher gains.

Case III Estimator -- This example was intended to approximate physical reality. It was assumed that ϕ, $\dot{\phi}$, and β could be measured, and a noisy drift-accelerometer signal was available

$$m(t) = \ddot{z}(t) + \eta_2(t)$$

where

$$E[\eta_2(t)\ \eta_2(t_1)] = 0.04\ \delta(t-t_1)\ (m/sec^2)^2$$

Unfortunately, there was not time to evaluate the performance of this estimator.

The drift equation is

$$\ddot{z}(t) = \frac{R}{m}\beta + \frac{N}{m}\left[\phi + \frac{v_\omega - z}{V}\right] + \frac{F-X}{m}\phi$$

By letting z(t) be

$$z(t) = z_1(t) + z_2(t)$$

where $z_1(t)$ is the known portion of the drift

$$\ddot{z}_1(t) = \frac{R}{m}\beta + \frac{N}{m}\left[\phi - \frac{\dot{z}_1}{V}\right] + \frac{F-X}{m}\phi + \frac{N}{mV}\bar{v}_\omega$$

the problem was to estimate ω, x, z_2, and $\dot{z}_2$ where the measured signal is

$$m(t) - \frac{R}{m}\beta - \frac{N}{m}\left[\phi - \frac{\dot{z}_1}{V}\right] - \frac{F-X}{m}\phi - \frac{N}{mV}\bar{v}_\omega$$

and the to-be-estimated states satisfy

$$\begin{bmatrix} \ddot{z}_2 \\ \dot{z}_2 \\ \dot{\omega} \\ \dot{x} \end{bmatrix} = \begin{bmatrix} \frac{-N}{mV} & 0 & \frac{N\sigma_\omega}{mV} & 0 \\ 1 & 0 & 0 & 0 \\ 0 & 0 & 0 & -c_3\dot{h} \\ 0 & 0 & -c_5\dot{h} & -c_4\dot{h} \end{bmatrix} \begin{bmatrix} \dot{z}_2 \\ z_2 \\ \omega \\ x \end{bmatrix} + \begin{bmatrix} 0 \\ 0 \\ c_1\sqrt{\dot{h}} \\ c_2\sqrt{\dot{h}} \end{bmatrix} \eta_1(t)$$

The resulting estimator, after adding the known z_1, $\dot{z}_1$, is

$$\ddot{\begin{bmatrix} \dot{\hat{z}} \\ \dot{\hat{z}} \\ \dot{\hat{\omega}} \\ \dot{\hat{x}} \end{bmatrix}} = \begin{bmatrix} (-1+L_{\dot{z}})\frac{N}{mV} & 0 & (1-L_{\dot{z}})\frac{N\sigma_\omega}{mV} & 0 \\ 1+L_z\frac{N}{mV} & 0 & -L_z\frac{N\sigma_\omega}{mV} & 0 \\ L_\omega\frac{N}{mV} & 0 & -L_\omega\frac{N\sigma_\omega}{mV} & -c_3\dot{h} \\ L_x\frac{N}{mV} & 0 & -c_5\dot{h} - L_x\frac{N\sigma_\omega}{mV} & -c_4\dot{h} \end{bmatrix} \begin{bmatrix} \dot{\hat{z}} \\ \hat{z} \\ \hat{\omega} \\ \hat{x} \end{bmatrix} +$$

$$+ \begin{bmatrix} L_z \\ L_{\dot{z}} \\ L_x \\ L_\omega \end{bmatrix} (\ddot{z} + \eta_2) + \begin{bmatrix} -L_z \\ 1-L_{\dot{z}} \\ -L_x \\ -L_\omega \end{bmatrix} \left[\left(\frac{F-X}{m} + \frac{N'}{m} \right) \phi + \frac{R}{m}\beta + \frac{N}{mV}\bar{v}_\omega \right]$$

The gains and error covariances for this estimator are shown in Appendix K, Figures K-5 and K-6.

NUMERICAL EVALUATIONS

Six controllers were evaluated numerically by computing their response moments and upper-bound measures. Their evaluations are presented in this subsection.

Controller Descriptions

The controllers evaluated were:

(1) Simplest Case - This is the controller described above. All vehicle and wind-filter state components were measured.

(2) Case I - This controller employed the Case I estimator described above and the "simplest case" control gains. All vehicle state components plus the wind $v_\omega(t)$ were measured. Only the $x(t)$ wind-filter state was estimated. The 10:1 signal-to-noise ratio estimator was evaluated. This controller was evaluated to ascertain the degradation produced by incomplete wind knowledge.

(3) Case II - The Case II controller employed the 10: 1 signal-to-noise ratio Case II estimator described above and the "simplest case" control gains. All vehicle states were measured, a noisy wind measurement was made, and the two wind-filter states $\omega(t)$ and $x(t)$ were estimated. This controller was evaluated as a contrast to the above controllers.

(4) $K_\omega = K_x = 0$ - This controller is the same as the ideal, simplest case controller except that the feedforward gains $K_\omega(t)$ and $K_x(t)$ were set equal to zero. The first controller above employs perfect wind measurement and the second and third employ imperfect wind measurement. This controller employs zero wind measurement.

(5) Simplified - This is a "constant-gain" approximation of the Case I controller above. It was developed by engineering cut-and-try methods in the analog-simulation studies; its development is described in Section V. The gains K_β, K_ϕ, and $K_{\dot{\phi}}$ were made constants, K_x and K_z were set equal to zero, K_ω and the deterministic input were left unchanged, and $K_{\dot{z}}$ was replaced by a piecewise constant time function. This controller was evaluated to determine whether the optimum load-relief controller could be successfully simplified.

(6) Minimax - The minimax controller was developed under contract NAS8-11206 and it is described in detail by Graham (Ref. 12). The minimax design procedure is a frozen-point technique and its basic objective is to minimize the maximum possible response excursions. It was evaluated as a comparison to the stochastic formulation employed in this study. Unfortunately gain values for this controller were available only through the max-q region, so its terminal behavior and response likelihoods could not be evaluated.

Evaluations

The response covariances of the six controllers are presented in Appendix L, Figures L-1 through L-20. The significant features of the covariances and their resulting likelihoods are tabulated in Tables 4-1, 4-2, and 4-3.

The likelihoods and expectations making up the upper-bound J* are presented in Table 4-1. It is readily seen that meeting the gimbal and terminal constraints is not a problem. The bending expectations are the only significant contributors to the upper-bounds J* for all five controllers.

Table 4-1. Numerical Evaluations - Likelihoods

Controller	J^*	$E\{N_{I_b}\}$	$E\{N_\beta\}$	$P(\|z\|)$	$P(\|\dot{z}\|)$	$P(\|\dot{\phi} + 0.388\alpha\|)$
Simplest Case	0.283×10^{-6}	0.283×10^{-6}	0*	0*	0*	0*
Case I	0.574×10^{-6}	0.574×10^{-6}	0*	0*	0*	0*
Case II	0.704×10^{-5}	0.704×10^{-5}	0*	0*	0*	0*
$K_\omega = K_x = 0$	0.602×10^{-2}	0.602×10^{-2}	0.128×10^{-45}	0*	0*	0*
Simplified	0.173×10^{-1}	0.173×10^{-1}	0.912×10^{-36}	0.224×10^{-5}	0*	0*

J^* = upper bound on likelihood that one or more booster responses would exceed its prescribed limit

$E\{N_{I_b}\}$ = expected number of occasions that the bending moment limit is exceeded in the flight

$E\{N_\beta\}$ = expected number of occasions that the gimbal angle limit is exceeded in the flight

$P(|z|)$ = probability that $|z(150)| > 3000$ meters

$P(|\dot{z}|)$ = probability that $|\dot{z}(150)| > 40$ meters/sec

$P(|\dot{\phi} + 0.388\alpha|)$ = probability that $|\dot{\phi}(150) + 0.388\alpha(150)| > 0.0453$ rad/sec

*The number is less than 10^{-46}.

Table 4-2. Numerical Evaluations - Bending

Controller	σ_{I_b} peak	$\sigma_{\dot{I}_b}$ peak	$T(I_b^2) > 10^{11}$	$T(\dot{I}_b^2) > 10^{10}$	$\bar{I}_b$ peak
Simplest Case	0.434×10^6	1.15×10^5	20*	10*	0.538×10^5
Case I	0.446×10^6	1.14×10^5	30*	10*	0.538×10^5
Case II	0.481×10^6	1.41×10^5	25*	15*	0.538×10^5
$K_\omega = K_x = 0$	0.756×10^6	0.61×10^5	50*	0*	0.538×10^5
Simplified	0.56×10^6	1.48×10^5	35*	20*	5.9×10^5
Minimax	1.57×10^6	2.37×10^5	**	**	**

σ_{I_b} peak = peak bending-moment standard-deviation

$\sigma_{\dot{I}_b}$ peak = peak bending-moment-rate standard-deviation

$T(I_b^2) > 10^{11}$ = approximate length of time that $(\sigma_{I_b})^2 > 10^{11}$

$T(\dot{I}_b^2) > 10^{10}$ = approximate length of time that $(\sigma_{\dot{I}_b})^2 > 10^{10}$

$\bar{I}_b$ = peak mean bending-moment

* Numbers to nearest 5 seconds

** No data

Table 4-3. Numerical Evaluations - Terminal Responses

Controller	Drift (meters)			Drift Rate (meters/sec)			$\dot{\phi}+0.388\alpha$ (rad/sec)	
	$\sigma_z$peak	$\sigma_z(140)$	$\sigma_z(150)$	$\sigma_{\dot{z}}$peak	$\sigma_z(140)$	$\sigma_z(150)$	$\sigma_{\phi}*(140)$	$\sigma_{\phi}*(150)$
Simplest Case	343	88	1.08	18.7	16.9	0.014	0.162	0.00006
Case I	312	83	0.85	17.2	15.8	0.012	0.159	0.00240
Case II	262	67	0.69	14.2	12.9	0.009	0.131	0.00076
$K_\omega = K_x = 0$	814	210	2.2	43.5	39.8	0.029	0.400	0.00095
Simplified	655	655	655	11.1	0.22	0.028	0.00016	0.00108

σ peak = peak response standard deviation

$\sigma(140)$ = response standard deviation 10 seconds from burnout

$\sigma(150)$ = response standard deviation at burnout

ϕ^* = $\dot{\phi}+0.388\alpha$

The J* tabulation shows that the price of poor wind measurement is small, but zero wind measurement is expensive. The simplified controller fares worst of all. But the progressive increase in J* in this tabulation is misleading.

The data in Table 4-2 better illustrates the controllers' behaviors. Poorer wind measurement implies two effects:

- The peak bending responses are slightly larger.
- The bending responses are large over longer periods of time.

The second of these effects is considered significant.

The first effect is of some significance, but in an engineering sense the upper-bound criterion weights it too heavily. As discussed above, the J* functional is extremely sensitive to small variations in the bending covariances. This sensitivity is evidenced in the five-orders-of-magnitude difference between the simplified J* and the simplest-case J*. Figure 4-5 presents plots of the bending expectation densities $\frac{\partial}{\partial t} E\left[N_{I_b}\right]$; it is clear from the peaking of these plots that the value of J* is determined almost solely by the peak covariances. The original dynamical description of the missile is too imprecise to warrant reading this much significance into small peak variations.

The control action of the feedforward wind inputs is evidenced by the performance of the $K_\omega = K_x = 0$ controller. Comparing it with the three optimum controllers, the data in Table 4-2 show that the feedforward inputs raise the bending-moment-rate covariances, lower bending-moment covariances and reduce the intervals over which the bending-moment covariances are large. That is, the feedforward inputs pay a rate price to lower amplitudes. Both J* and the width of the bending-moment covariance peak show that this is a good bargain. It is concluded that including feedforward inputs purchases a significant improvement in the load-relief controller's performance.

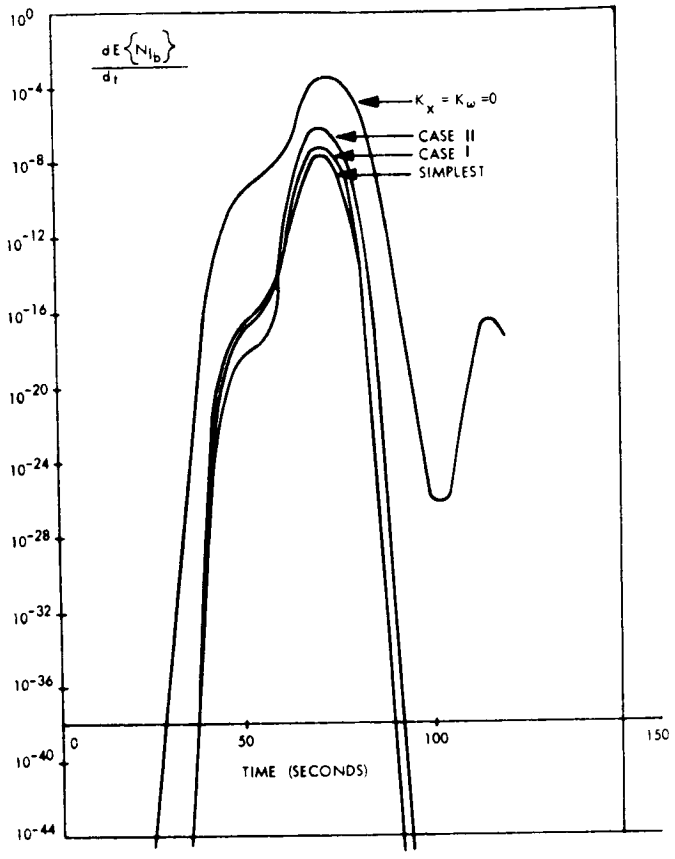

Figure 4-5.

Bending Likelihood Densities for Various Controllers

Comparing the simplified controller's bending covariances with those of the three optimum controllers, it is evident that the simplified controller is slightly worse in all categories. It is concluded that the optimum load-relief controller can be successfully simplified.

The minimax bending standard-deviation peak is too close to the 2.25×10^6 bending limit for comfort. Apparently too much weight was given to other booster responses in the max-q region when this particular controller was designed.

The terminal behavior of the first five controllers is evidenced in Table 4-3. The load-relief controller is a fantastic dead-beat terminal controller. It is evident that the large gain variations in the last 5 seconds of flight are not needed. The terminal responses are extremely small, and simpler gain functions producing terminal responses larger by orders of magnitude would be entirely acceptable. The simplified controller's terminal performance demonstrates this.

SECTION V
SIMULATION RESULTS

The load-relief control system defined by the synthesis technique described in the previous sections was thoroughly evaluated on a time-varying flight simulator. The purpose of the evaluation was to demonstrate more fully the performance capability of the controller and to provide an engineering evaluation of the system. The work was performed by the Aerospace Flight Systems group of Honeywell's Aeronautical Division.

The simulation was mechanized on a hybrid analog-digital computer. Rigid-body vehicle equations of motion and data were simulated on the analog computer, and the load-relief controller was simulated on the digital computer. For purposes of comparison, a conventional control system and the minimax control system were also evaluated on the simulator. A complete description of the simulation is presented in Appendix M.

The load-relief controller was evaluated for the nominal wind model and for Sissenwine wind models furnished for the minimax contract (NAS8-11206). Vehicle and controller parameter variations and simplification of system mechanization were investigated to determine the practicality of the controller. Finally, the performance of the load-relief controller was compared with that obtained for a conventional controller and the minimax controller.

The nominal load-relief control system was found to provide superior performance in terms of the performance constraints when compared to the conventional control system and the minimax controller. The load-relief controller demonstrated satisfactory tolerance to ± 20 percent variations in both the vehicle and controller parameters. Further, it was shown that the load-relief control system could be greatly simplified by replacing several of the time-varying gains by constants or piecewise constant approximations. Analysis showed that if the wind angle of attack

could be measured no significant loss in performance would result if the Case I or Case II estimator were replaced by a single time-varying gain. In general the simulation showed that the deterministic input and the feedforward terms were responsible for providing the load-relief capability, while the drift and drift-rate feedbacks assured that the terminal condition constraints would be met. The remaining feedbacks functioned to provide a measure of stability for at least the early portions of the flight.

This section first describes the performance evaluation of the nominal load-relief controller. The nominal system performance for a mean-wind input is compared with that obtained from a pure digital computer simulation. The system performance is then demonstrated for vehicle and parameter variations and for a variety of wind disturbances.

Next, the simplification of the system is described and the change in performance with each successive approximation is pointed out. The performance of the simplified controller is presented and compared with that obtained from the nominal load-relief controller.

The performance of a conventional controller and the minimax controller (defined under NASA contract NAS8-11206) is then presented and compared to that of the load-relief controller.

Finally, the conclusions and recommendations drawn from the simulator evaluation are presented. Appendix M describes the time-varying simulation, and Appendix N contains the simulator time responses.

NOMINAL LOAD RELIEF CONTROLLER

Description of System

The controller, which was designed by the methods described in earlier sections, is referred to as the nominal load-relief controller and is shown in block diagram form in Figure 5-1. As its name implies, the load-relief controller is designed primarily to minimize structural loads (bending moment) in the presence of cross-wind disturbances. The actuator command signal produced by the controller is a linear combination of five feedback and two feedforward signals (with time-varying gains), and an open-loop wind-bias function known as the deterministic input. The two feedforward signals, ω and x, can be obtained from a Kalman estimator.

As in the design of any system, certain assumptions are made at the outset. The assumptions made in the design of the load-relief controller are the following:

- Wind Model - The wind model used in the design of the controller is a random wind composed of a deterministic mean wind plus a stochastic component obtained by passing white noise through a filter. A plot of the mean wind profile is shown in Figure 5-2.
- Ideal Sensing - It was also assumed that any variable required by the controller (e.g., z, $\dot{z}$) was either available from a sensor or could be generated by a Kalman estimator.
- Nominal Trajectory - It was assumed that the vehicle follows a predetermined trajectory. This assumption allows one to make a rather accurate (within 20 percent of actual) estimate of the vehicle parameters over the entire flight. Nominal values of the vehicle parameters as a function of flight time are then used in obtaining the controller gains (as a function of time) and in designing the Kalman estimator to be used with a particular system.

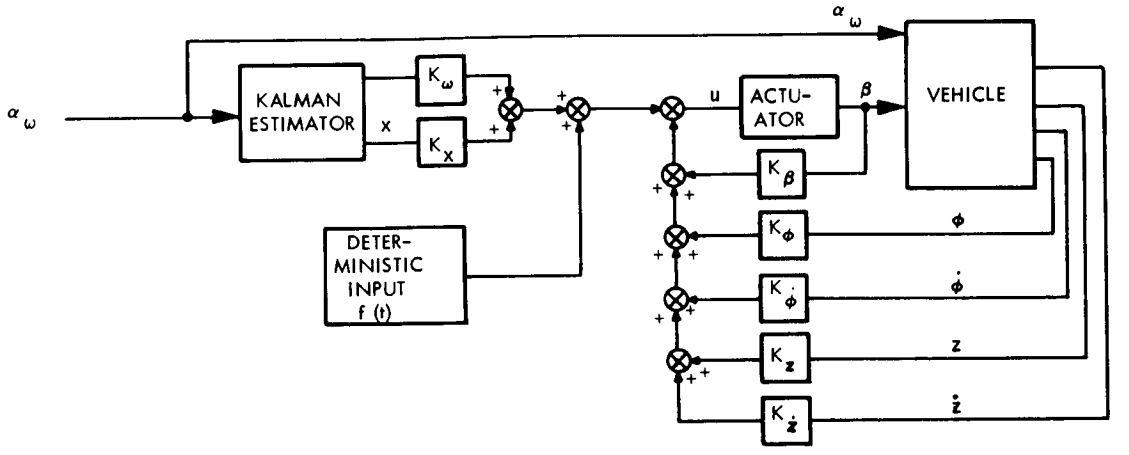

Figure 5-1. Nominal Load-Relief Control System Block Diagram

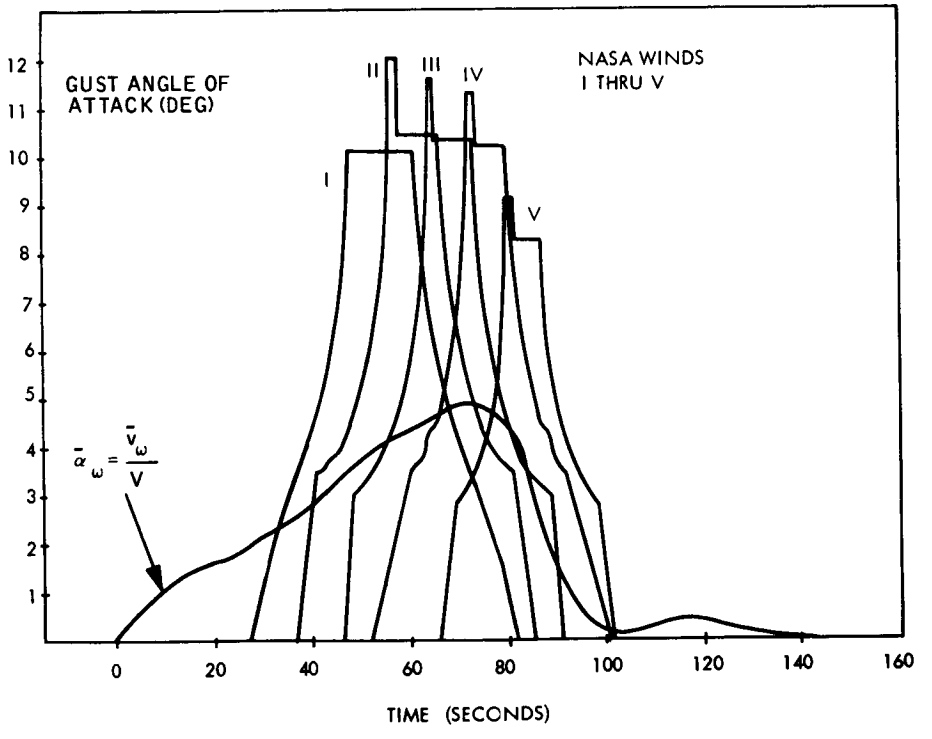

Figure 5-2. Mean Wind and NASA Wind versus Time

An examination of the individual terms of the controller equation is helpful in understanding the operation of the controller and in determining what changes in performance will result when the system is simplified. The controller equation may be expressed in the following form:

$$u = \left[K_{\phi}(t) \;\; K_{\dot{\phi}}(t) \; K_{\beta}(t) \; K_{z}(t) \; K_{\dot{z}}(t) \; K_{\omega}(t) \; K_{x}(t)\right] \begin{bmatrix} \phi(t) \\ \dot{\phi}(t) \\ \beta(t) \\ z(t) \\ \dot{z}(t) \\ \omega(t) \\ x(t) \end{bmatrix} + f(t)$$

Graphs of the time-varying gains and the deterministic input f(t) appear in Appendix N, Figures N-1 through N-8. Analysis has shown that the attitude and attitude-rate feedbacks ϕ and $\dot{\phi}$ and gimbal angle β primarily furnish a measure of stability augmentation for the statically unstable Model Vehicle No. 2. Further, the gimbal-angle feedback β can be shown to alter the frequency response characteristics of the actuator (see the following discussion on "Simplification of the Nominal Load Relief Controller"). Since lateral drift z is a measure of the distance of the vehicle away from a nominal trajectory, feeding back z and $\dot{z}$ provides a steering command to assist in bringing the vehicle within a desired target area at burnout. The feedforward signals obtained from an estimator are a measure of the deviation of the wind magnitude (ω) and rate (x) from the assumed mean wind $\bar{\alpha}_{\omega}$. These signals furnish load-relief capability for random wind disturbances. The deterministic input f(t) is an open-loop command used to combat the assumed mean wind $\bar{v}_{\omega}$. The assumption of a different nominal, or mean wind profile would lead to a different deterministic input. The action of the deterministic input will be more fully discussed under "Performance Results". It should be emphasized that the load-relief controller derives its primary load-relief capabilities from the deterministic input and from the feedforward signals.

It is the function of the estimator to generate signals required by the controller which are not otherwise measurable (i. e., by sensors). Since estimators may be designed to generate many different combinations of controller inputs, the complexity of the estimator will depend upon what information is assumed to be available from sensors. The present discussion will serve to identify the estimators investigated on the hybrid simulator. Discussion of the derivation and operation of the estimators is contained in Sections III and IV.

Case I Estimator

The Case I estimator is a first-order estimator which contains one differentiation. A block diagram of the Case I estimator is shown in Figure 5-3. Input-output information for the system with this estimator is as follows:

- Signals required to be sensed: ϕ, $\dot{\phi}$, β, z, $\dot{z}$, v_ω
- Signals assumed known: $\bar{\alpha}_\omega = \bar{v}_\omega / V$
- Signals generated by estimator: $\hat{x}$, $\hat{\omega}$

Figure N-1 (Appendix N) is a time-response comparison of the estimated $\hat{x}$ and $\hat{\omega}$ signals generated by the Case I estimator and the actual x_A and ω_A signals produced by the stochastic wind generator. A block diagram of the stochastic wind generator is shown in Appendix M, Figure M-1. The excellent agreement of the actual and estimated signals indicates that the Case I estimator works well.

Case II Estimator

The Case II estimator is a second-order estimator which contains no differentiation and is thus more feasible to mechanize. A block diagram of the Case II estimator is shown in Figure 5-4. Input-output information for the system employing the Case II is exactly the same as that for the Case I estimator.

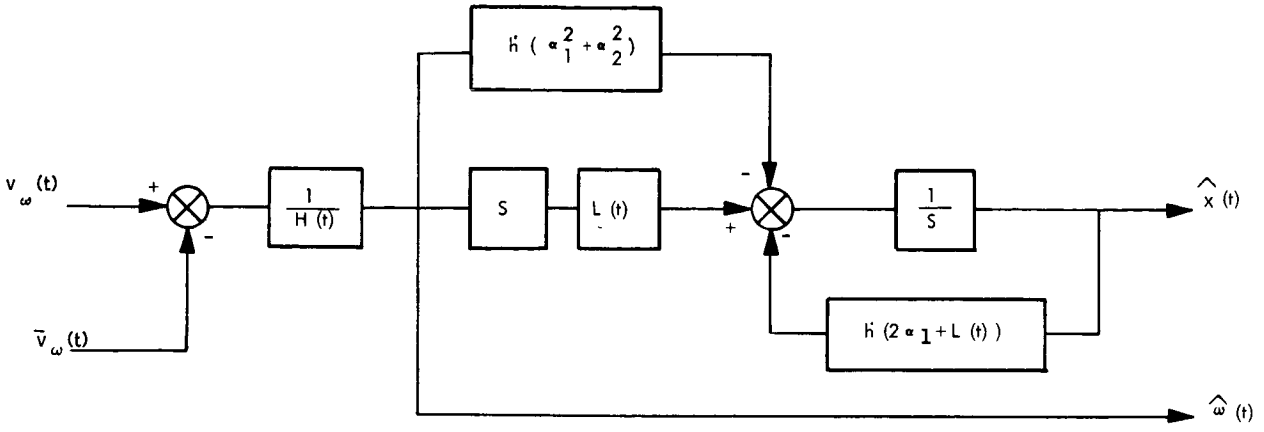

$$\hat{\omega}(t) = \frac{1}{H(t)}\left[\omega(t) - \bar{v}_\omega(t)\right]$$

$$\dot{\hat{x}}(t) = -\dot{h}(2\alpha_1 + L(t))\,x(t) + L(t)\,\dot{\hat{\omega}}(t) - h(\alpha_1^2 + \alpha_2^2)\,\hat{\omega}(t)$$

Figure 5-3. Case I Kalman Estimator

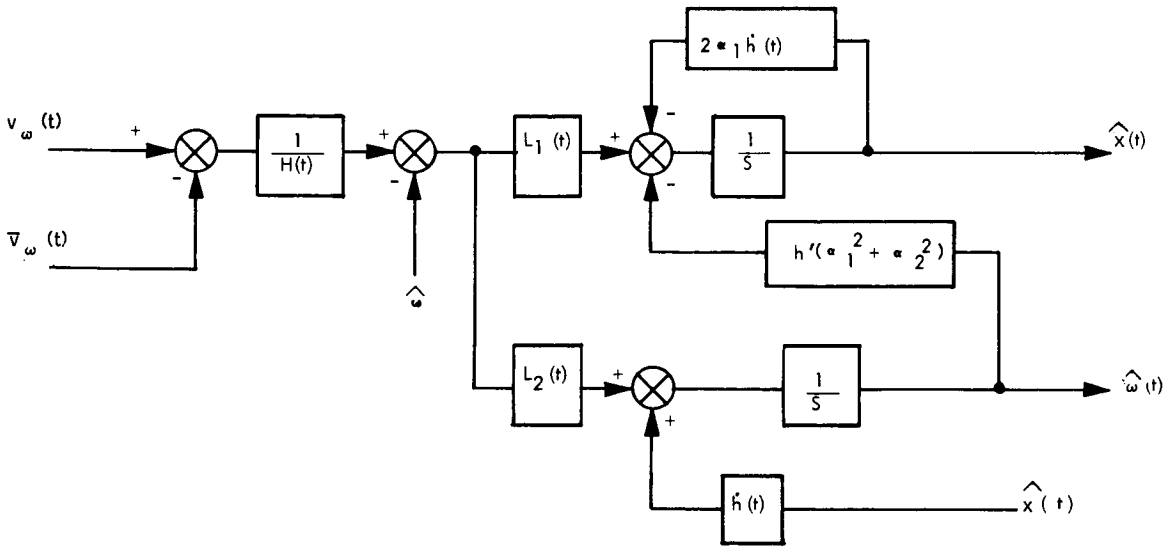

$$\dot{\hat{\omega}} = \dot{h}\hat{x} + L_2\left(\frac{v_\omega - \bar{v}_\omega}{H(t)} - \hat{\omega}\right)$$

$$\dot{\hat{x}} = -2\alpha_1\dot{h}\hat{x} - \dot{h}(\alpha_1^2 + \alpha_2^2)\hat{\omega} + L_1\left(\frac{v_\omega - \bar{v}_\omega}{H(t)} - \hat{\omega}\right)$$

Figure 5-4. Case II Kalman Estimator

A comparison of the actual x_A and ω_A signals and the estimated $\hat{x}$ and $\hat{\omega}$ is also shown for the Case II estimator in Figure N-1. Again the traces of the actual and estimated signals are seen to agree very closely, indicating that the Case II estimator works well.

Performance Results

Performance of the nominal load-relief controller was evaluated for the following requirements:

- Bending moment $|I_b|$ $< 2.25 \times 10^6$ kilopon-meters over entire flight
- Gimbal deflection $|\beta|$ <5 degrees over entire flight
- Lateral drift $|z|$ < 3000 meters at burnout
- Lateral drift rate $|\dot{z}|$ < 40 meters/sec at burnout
- Local angle of attack $|\dot{\phi} + 0.388\,\alpha|$ < 0.0453 rad/sec at burnout

Performance of the load-relief controller (and of the other controllers used for comparison) was investigated for the following types of wind disturbances:

- Random Wind - Design of the load-relief controller was based on the random wind which is composed of a deterministic wind profile plus a stochastic component.
- Mean Wind - This is the deterministic portion of the random wind. The mean wind profile is shown in Figure 5-2.
- Sissenwine Wind Profiles - These deterministic wind profiles were obtained from the data package furnished by NASA. The five Sissenwine wind profiles are all of similar shape but occur at different times in the flight. The individual profiles are denoted by the time at which the peak first occurs and are as follows:

48 seconds
56 seconds
64 seconds
72 seconds
80 seconds

The Sissenwine wind profiles are also included in Figure 5-2.

Because of the complexity of the hybrid simulation, it was desirable to have some means of checking the results. A pure digital simulation was made for this purpose. The deterministic nature of the mean wind made it suitable as the input for these comparison runs.

Performance of the vehicle and load-relief controller for the mean-wind input is shown on the analog computer trace of Figure N-2. The lateral drift and drift rate from the hybrid simulation, as shown in Figure N-2, are plotted with the corresponding variables obtained from the pure digital simulation in Figures 5-5 and 5-6 respectively. The excellent agreement of the results from the two simulations provides a high level of confidence in each.

A similar comparison of the bending moment obtained by the two simulations is shown in Figure 5-7. These results show only an order-of-magnitude agreement for the two simulations. A better agreement between the two simulations could not be obtained because of the presence of a low-level random noise generated in the A/D and D/A converters of the hybrid computer. This low-level noise will not be significant for any disturbance other than the mean wind since the bending moment response due to the other wind inputs will be at least a factor of five larger.

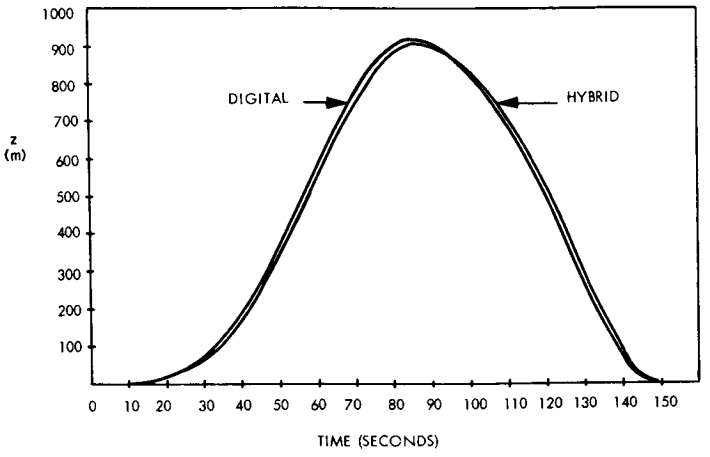

Figure 5-5

Comparison of Hybrid and Digital Simulation Results - Drift versus Time

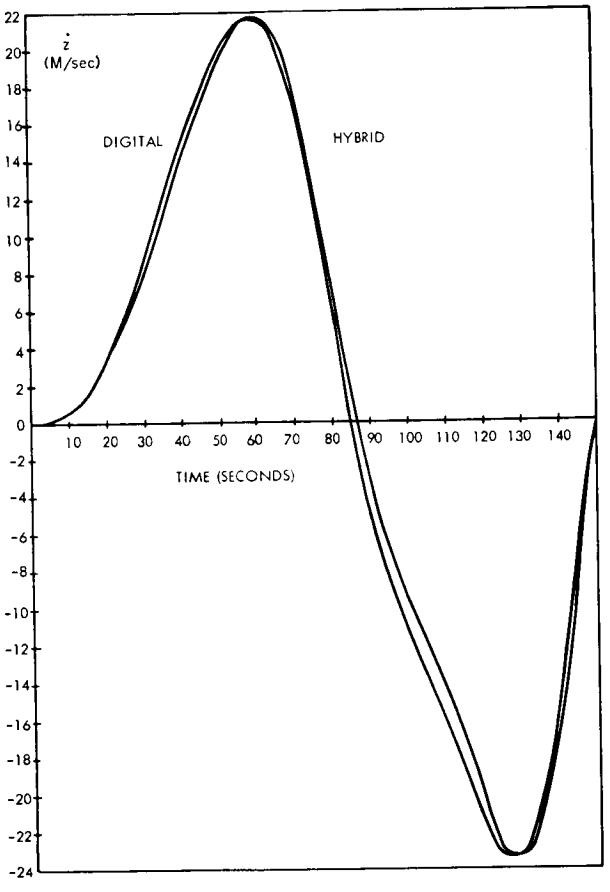

Figure 5-6

Comparison of Hybrid and Digital Simulation Results - Drift Rate versus Time

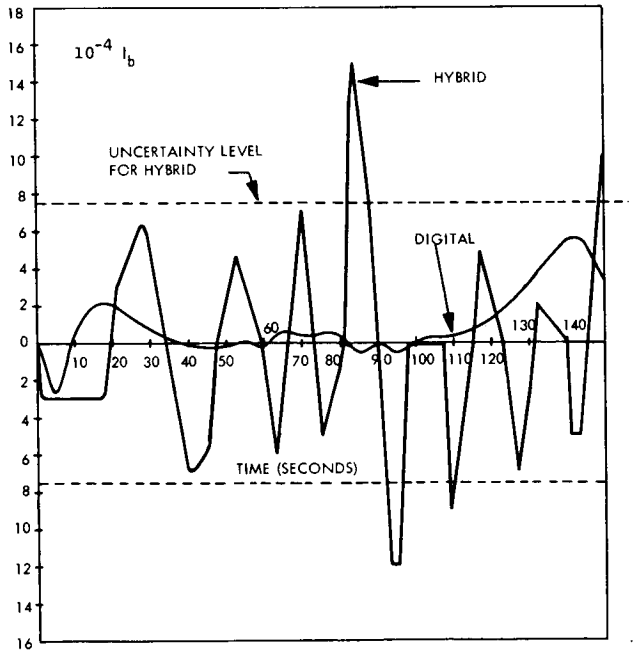

Figure 5-7

Comparison of Hybrid and Digital Simulation Results - Bending Moment versus Time

A more extensive examination of the mean-wind response indicates how the load-relief controller functions to minimize the bending moment. The total bending moment is calculated from the expression

$$I_b = M'_\alpha \alpha + M'_\beta \beta$$

A plot of M'_α in Figure 5-8 shows that the M'_α coefficient is zero at the beginning and end of flight and is a maximum in the middle of the flight. The M'_β coefficient shown in Figure 5-9 is larger than M'_α and peaks up at the end of flight. It is generally true, however, that the values of angle of attack α are at least a factor of 10 higher than the values of gimbal angle β for any given flight. The $M'_\alpha \alpha$ term of the bending-moment expression is then the more significant of the two. The load-relief controller minimizes the bending moment essentially by keeping α small when M'_α is large and allowing α to become large when M'_α is small.

The deterministic input f(t) plays a large part in the reduction of the bending moment. Early in the flight, f(t) commands a positive vehicle attitude with the result that the vehicle flies downwind (positive z). The deterministic input then changes sign, driving angle of attack to zero and then causing the vehicle attitude to become negative. The peak wind occurs while α remains zero resulting in a low bending moment as discussed above. After the max-q condition (at about 80 seconds), the lateral drift and drift feedback gains K_z and $K_{\dot{z}}$ become orders of magnitude larger than their earlier values, driving the lateral drift and drift rate to zero at burnout.

The excellent performance of the load-relief controller for the mean-wind disturbance may be illustrated by comparing the performance results with the performance requirements as follows:

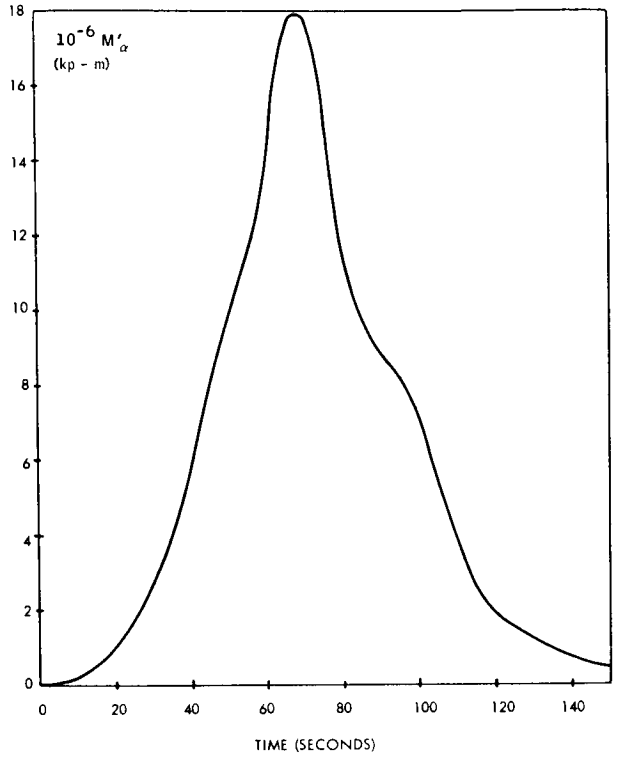

Figure 5-8
M$'_\alpha$ versus Time

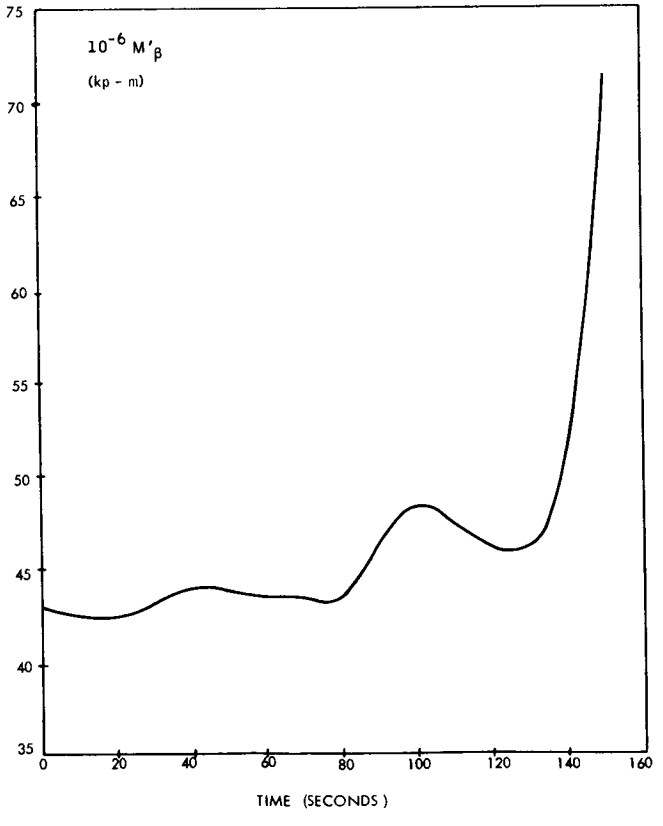

Figure 5-9
M$'_\beta$ versus Time

Performance Requirements		Performance Results	
$\lvert I_b \rvert < 2.25 \times 10^6$ kp-m	$0 \le t \le 150$	$\lvert I_b \rvert \le 0.15 \times 10^6$ kp-m	$0 \le t \le 150$
$\lvert \beta \rvert < 5$ deg	$0 \le t \le 150$	$\lvert \beta \rvert \le 0.1$ deg	$0 \le t \le 150$
$\lvert z \rvert < 3000$ m	$t = 150$	$\lvert z \rvert < 25$ m	$t = 150$
$\lvert \dot{z} \rvert < 40$ m/sec	$t = 150$	$\lvert \dot{z} \rvert < 0.5$ m/sec	$t = 150$
$\lvert \dot{\phi} + 0.388\alpha \rvert < 0.0453$ rad/sec	$t = 150$	$\lvert \dot{\phi} + 0.388\,\alpha \rvert < 0.005$ rad/sec	$t = 150$

All performance results are seen to be well within their required maximum values. Performance results obtained with other wind disturbances all show that the bending moment is the only critical requirement for the system. Attention will thus be focused on the bending moment for the remainder of the responses, and the other four performance requirements may be assumed to be met unless otherwise specified.

Evaluation of system performance for the random wind is made difficult by the very nature of the input. Definite conclusions about the response to the random wind necessitates a statistical average which (in theory) requires an infinite number of responses. The results obtained, however, do present an approximate measure of the performance.

Analog traces of system performance for the random wind for (a) $\hat{x} = \hat{\omega} = 0$ (no estimator), (b) $\hat{x}$ and $\hat{\omega}$ generated by the Case I estimator, and (c) $\hat{x}$ and $\hat{\omega}$ generated by the Case II estimator are shown in Figures N-3, N-4 and N-5, respectively. Three complete flights (0 to 150 seconds) are shown for each condition. The maximum bending moment over each of these flights is indicated in Table 5-1.

Table 5-1. Comparison of the Maximum Bending Moment for Various Estimators With Random-Wind Disturbance

System	$\lvert I_b \rvert_{Max}$ (kp-m)		
	Run No. 1	Run No. 2	Run No. 3
No Estimator	0.65×10^6	0.60×10^6	0.80×10^6
Case I Estimator	0.60×10^6	1.3×10^6	0.9×10^6
Case II Estimator	0.7×10^6	0.55×10^6	0.75×10^6

The following conclusions concerning the system performance for the random-wind disturbance may be drawn:

- The maximum bending moment resulting from the random wind is always higher than that due to the mean wind and generally runs about a factor of five higher.
- It is impossible to ascertain from the results presented whether or not the x and ω feedforward signals from the estimator are effective in reducing the bending moment.

Performance of the vehicle and load-relief controller was investigated for the NASA Sissenwine wind profiles as well as for the mean-and random-wind disturbances. The maximum bending moments which result from the Sissenwine wind disturbances will be significantly larger than those obtained with the mean-wind disturbance for two reasons. First, the Sissenwine wind profiles are much more severe than the mean wind, both in peak magnitude and in rate of increase. Secondly, the deterministic input f(t) was designed to counteract the effect of the mean wind, and, since it remains unchanged, it will be less effective in reducing the bending moment for other wind disturbances.

Results were obtained for the Sissenwine wind disturbances for the cases of (a) no $\hat{\omega}$ and $\hat{x}$ inputs to the controller (i.e., no estimator), (b) $\hat{x}$ and $\hat{\omega}$ signals generated by the Case I estimator, and (c) $\hat{x}$ and $\hat{\omega}$ signals generated by the Case II estimator. In addition, responses were obtained for a simulated angle-of-attack sensor noise of 0.5-degree amplitude on the input signal to the estimators. It was found for all cases that the simulated sensor noise had no effect on system performance. Analog computer traces of the results are shown in Figures N-6 and N-7 for the no estimator system, in Figures N-8 and N-9 for the Case I estimator system, and in Figures N-10 and N-11 for the Case II estimator system. Results are also shown in Figures N-12 and N-13 for the sensor noise added to the Case I estimator input to illustrate the absence of effect on the results.

Table 5-2 presents the maximum bending moment experienced over each of the flights for the Sissenwine wind disturbances.

Table 5-2. Comparison of Maximum Bending Moment for Various Estimators with Sissenwine Wind Disturbances

Wind Disturbance	$\lvert I_b \rvert_{max} \times 10^6$ (kp-m)			
	No Estimator	Case I Estimator		Case II Estimator
		With No Sensor Noise	With 0.5-degree Sensor Noise	
48-sec α_ω	2.2	1.6	1.6	1.4
56-sec α_ω	1.7	2.2	2.2	1.8
64-sec α_ω	2.5	2.6	2.6	2.4
72-sec α_ω	3.1	2.8	2.8	2.6
80-sec α_ω	2.9	1.9	1.9	1.5

From Table 5-2 it is apparent that, for all three system variations, the bending moment did not remain within the required maximum of 2.25×10^6 kp-m for the 64-second and 72-second wind profile disturbances. These are the only cases for which the load-relief control system failed to meet all the performance requirements.

The results presented in Table 5-2 also show that the maximum bending moments which occurred with the Case II estimator in the system are slightly lower for each of the Sissenwine winds than for the Case I estimator. It may also be seen that the amount of reduction in bending moment provided by the estimators, particularly the Case II estimator, is quite significant for the 48-second, 72-second, and 80-second wind profiles. Although the peak bending moments which result from the 56-second and 64-second wind profiles are about the same with or without the estimators, examination of the analog computer traces reveals that the length of time for which the bending moment is a maximum is greatly reduced by the use of the estimators.

In summary, the estimators generally reduce the peak bending moment and always provide a rapid reduction of the bending moment following the peak value.

Parameter Variations

Performance of the nominal load-relief controller was also evaluated for plus and minus 20 percent variations of all vehicle parameters and controller parameters. The deterministic mean wind was used as the disturbance input for all parameter variation cases.

The results of the parameter variations studies are shown in Figure N-14 through N-22.

In general, it can be seen that the system is more sensitive to variations in the controller gains than to variations in the vehicle parameters.

Examination of the results presented indicates again that bending moment is the critical parameter in terms of performance results. The maximum bending moment experienced during the total flight for each parameter variation is given in Table 5-3.

Table 5-3. Maximum Bending Moments Experienced with Parameter Variations for Load-Relief Controller

Controller Parameter Variations	$\lvert I_b \rvert_{max} \times 10^6$ (kp-m)	Vehicle Parameter Variations	$\lvert I_b \rvert_{max} \times 10^6$ (kp-m)
Nominal System	0.15	+20% c_1	0.15
+20% f(t)	0.55	+20% c_1	0.15
-20% f(t)	0.50	+20% c_2	0.15
+20% K_ϕ	0.85		
-20% K_ϕ	0.45	-20% c_2	0.15
+20% $K_{\dot{\phi}}$	0.15	+20% $\frac{F-X}{m}$	0.23
-20% $K_{\dot{\phi}}$	0.20	-20% $\frac{F-X}{m}$	0.80
+20% K_z	0.15	+20% $\frac{N'}{m}$	0.15
-20% K_z	0.25	-20% $\frac{N'}{m}$	0.15
+20% $K_{\dot{z}}$	0.55	+20% $\frac{R'}{m}$	0.10
-20% $K_{\dot{z}}$	0.50	-20% $\frac{R'}{m}$	0.15
+10% K_β	Oscillatory		
+20% K_β	Unstable	+20% V	0.18
-20% K_β	0.55	-20% V	0.30

Special mention should be made of the oscillatory and unstable responses for the +10 and +20 percent variations of gimbal-angle feedback K_β. The gimbal-angle feedback is a positive feedback loop which will cause system instability if the loop gain K_c is raised above 1.0 (K_c is the forward loop gain). Since K_c is 1.0, and the nominal value of K_β is 0.9, a small increase in K_c will cause instability. As shown in the next subsection, the gimbal-angle feedback may be replaced by an appropriate first-order transfer function in the forward loop. With this change, the possibility of instability due to changes in the gimbal-angle feedback is removed.

In many of the parameter-variation flights, the maximum bending moment shown in Table 5-3 occurs within the last few seconds of flight. This is apparently due to an attempt by the controller to null errors which have built up during the flight. (It should be noted that many of the controller gains go through rapid excursions during the last few seconds of flight. See Appendix J, Figures J-1 through J-8.)

Table 5-3 also shows that the maximum bending moment for all the parameter variation cases is well within the required maximum of 2.25×10^6 kp-m. In summary, performance of the load-relief controller is not seriously degraded by variations in the vehicle parameters or controller parameters with the exception of increases in the K_β feedback gain. As indicated, the K_β feedback gain may be replaced by a linear filter which eliminates the system sensitivity to this parameter.

SIMPLIFICATION OF THE LOAD-RELIEF CONTROLLER

The nominal load-relief control system described in the previous subsection is rather complex. It contains several time-varying gains and requires feedback and feedforward signals which are not easily measured. From a practical application standpoint, it is very desirable to reduce the complexity

of the controller as much as possible and to put it into a form whereby the information required by the controller is easily measurable.

This section describes the simplification of the system in the following order:

- The nominal load-relief controller is redefined in terms of the information which would be available from realistic sensors (i.e., rate gyros, accelerometers, etc.). This discussion will illustrate the full complexity of the nominal load-relief controller.
- Possible ways for simplifying the system are discussed.
- The change in performance for each successive step in the process of simplifying the system is presented.
- Finally, the resulting simplified system is described and compared with the nominal load-relief control system on the basis of system complexity and performance.

Description of Nominal Controller with Realistic Sensing

The nominal load-relief controller has been designed with the assumption that all information required by the controller is measurable. In practice, this will not be the case. Consequently, the controller has been modified to make use of state-of-the-art sensing techniques (e.g., rate gyros, accelerometers, etc.). Figure 5-10 is a block diagram of the load-relief controller with realistic sensing. As can be seen from the diagram, a body-mounted normal accelerometer is used to obtain a signal proportional to drift acceleration according to the following equation:

$$\ddot{z} = \ddot{\tau} + \frac{F-X}{m}\phi - \ell_A \ddot{\phi}$$

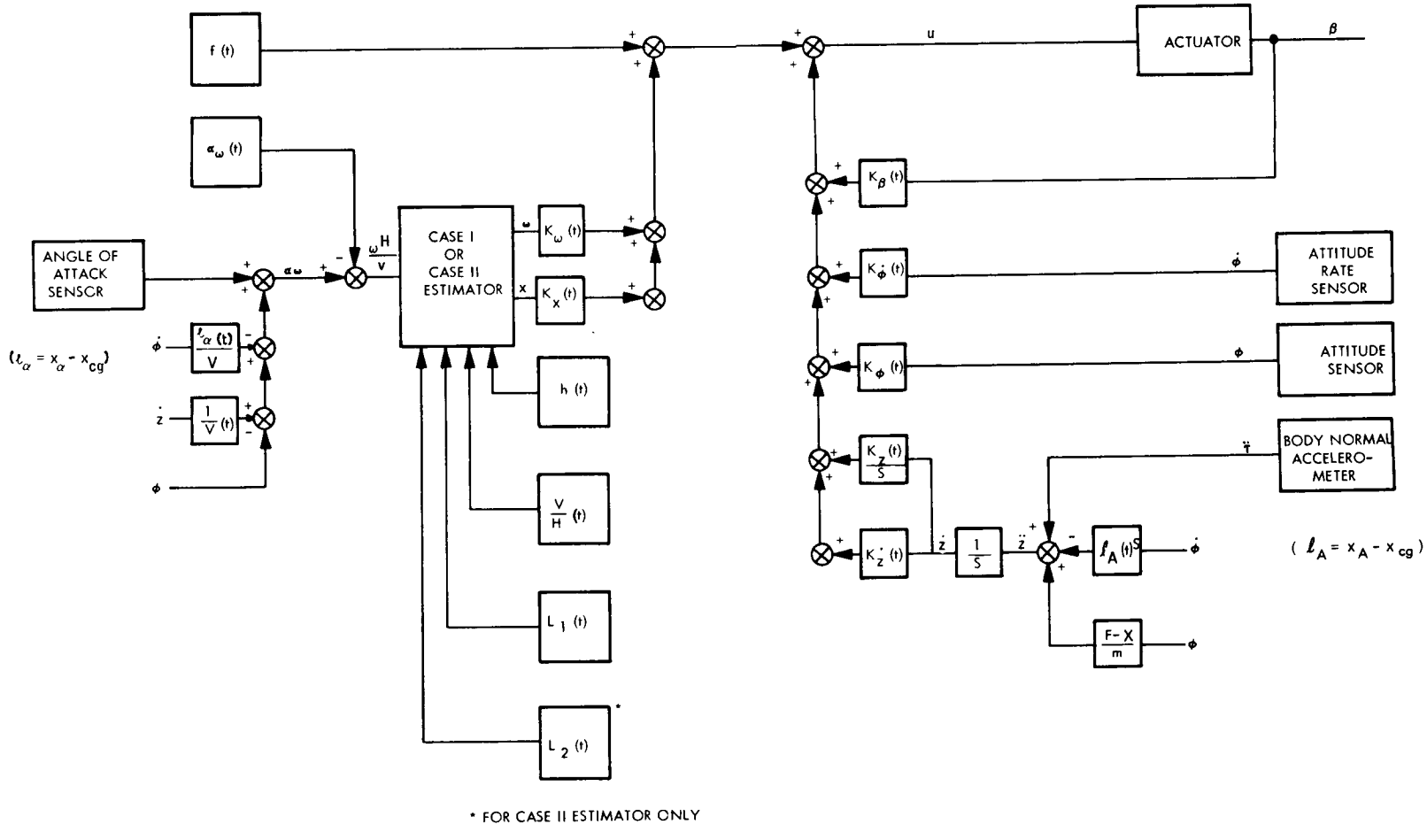

Figure 5-10. Nominal Load-Relief Controller with Realistic Sensing

Drift acceleration is then integrated to provide the drift and drift-rate feedback signals required by the controller. This computation requires that the longitudinal acceleration F-X/m and the accelerometer location with respect to the center of gravity ℓ_A be measured or that estimated values of them be stored as functions of time.

The wind angle-of-attack required for the estimator input (with a first- or second-order estimator assumed) is obtained through the use of an angle-of-attack sensor. The following equation is used in the mechanization to derive the wind angle-of-attack:

$$\alpha_\omega = \alpha_{sensed} - \phi + \frac{\dot{z}}{V} - \frac{\ell_\alpha}{V}\dot{\phi}$$

The drift-rate term can be obtained from the integration of the drift acceleration. The vehicle velocity V and angle-of-attack sensor location with respect to the center of gravity ℓ_α must be computed or estimated as functions of time. With these additional functions of time and a second-order estimator, the nominal load-relief controller becomes overwhelmingly complex. This system utilizes 17 functions of time. Fortunately, as the following discussion will show, this system can be greatly simplified. Since the nominal load-relief controller provides performance well within the design performance constraints, a large degradation in performance due to system simplification can be tolerated.

Possibilities for Simplification

The objective of the simplification process was to reduce the number of time-varying gains and to reduce the number of feedback signals required. The time-varying gains were simplified in one of three ways:

- The function was replaced by a constant value
- The function was set to zero
- The function was replaced by a piecewise constant approximation

Of course, setting a time-dependent gain to zero would eliminate the need for the corresponding feedback.

Since the estimators were, in themselves, relatively complex, it was desirable to determine if they were essential to maintain satisfactory performance. The function of both the Case I and the Case II estimators was primarily to obtain a measure of the wind-rate term, x. The ω term could be obtained without all the complexity required for the estimator. Thus, an evaluation was made to determine the significance of each of the estimator outputs, $\dot{x}$ and $\hat{\omega}$.

Finally, some tests were made to determine to what degree drift acceleration $\ddot{z}$ could be replaced by body-normal accelerations. The question was asked: "Could terms such as the compensation for having the accelerometer at some location other than at the center of gravity (i.e., the $\ell_A \ddot{\phi}$ term) be neglected?".

No attempt was made to simplify the deterministic input f(t). This function could easily be combined with the standard pitch program and thus would not constitute any increase in complexity.

Analysis of Simplifications to Load-Relief Controller

Simplifying the time-varying functions was first approached by taking each function one at a time and replacing it by a constant value. Analog traces of the system response to the mean wind for each of these variations are shown in Figures N-23 and N-24.

The following simplifications were tried one at a time:

- Set $K_{\phi}(t) = 0.035$
- Set $K_{\dot{\phi}}(t) = 0.12\ sec^{-1}$
- Set $K_z(t) = 0$
- Set $K_{\dot{z}}(t) = 1 \times 10^{-4}$ rad/m/sec
- Set $K_{\beta}(t) = 0.90$

These constant values were picked by examining each function and estimating an average value. The drift rate gain $K_{\dot{z}}$ actually takes on both plus and minus values over the flight. However, since a positive value was necessary for the last portion of flight in order to reduce the drift-rate error to zero, only a positive value was considered. As can be seen from Figure N-24, setting $K_{\dot{z}}$ equal to 10^{-4} rad/m/sec resulted in a significant deterioration in performance. All other fixed-gain approximations had only a small effect on system performance.

Figures N-25 and N-26 illustrate the performance of the system with a mean wind input for increasing level of system simplicity. Figure N-25(a) is a nominal system response to the mean wind for purposes of comparison. The following simplifications were evaluated:

- $K_{\beta}(t)$ was found to be nearly constant, equal approximately to 0.9. Thus, it was replaced by an equivalent gain the the forward loop. Since the β feedback was around the actuator, it also changed the dynamics of the actuator. Thus, a lag-lead network was added to the forward loop to account for this change in actuator dynamics. This change is reflected in the simplified block diagrams shown in Figure 5-11.

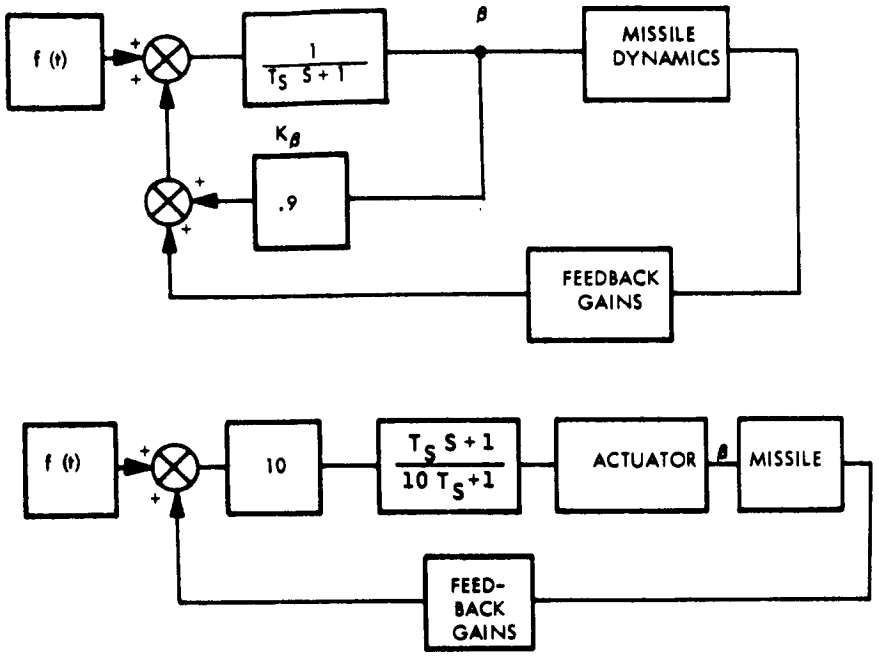

Figure 5-11. Modification of Gimbal Displacement Feedback

System performance with this modification is shown in Figure N-25(b). No significant deterioration in performance was noted.

- $K_{\dot{\phi}}$ (t) was set equal to 0.12 sec^{-1}. Figure N-25(c) shows the results with this added simplification. The over-all performance was not seriously degraded.

- K_{ϕ}(t) was set equal to 0.035. Figure N-26(a) shows the system response with this added simplification. The performance was degraded slightly by this approximation. The effect is most evident at the burnout condition where large pitch rate and bending moment were obtained. However, further simplifications eliminated these undesirable effects.

- $K_z(t)$ was set equal to zero. This simplification alleviated the large excursions of the burnout condition and, of course, resulted in a drift error at burnout. The drift error at burnout was well within the allowable value, however. Responses are shown in Figure N-26(c).

- The drift-rate gain was approximated by the following fixed values:

$$
\begin{aligned}
K_{\dot{z}}(t) &= 0.5 \times 10^{-6} \text{ rad/m/sec} \\
&= 0 \\
&= +0.3 \times 10^{-4} \\
&= -0.3 \times 10^{-4}
\end{aligned}
$$

  These results are shown in Figure N-27.

All these values resulted in a significant deterioration in system performance. These results pointed out the sensitivity of the system performance to the variations in the $K_{\dot{z}}(t)$ gain.

From these variations for the mean-wind response, it was concluded that most all the feedback gains could be replaced by a constant value with the possible exception of the drift-rate gain $K_{\dot{z}}(t)$.

Figures N-28 through N-32 illustrate the analysis results of the feedforward gains $K_x(t)$ and $K_\omega(t)$. Runs were made with and without each of the gains to determine their individual significance. For the analysis, each of the NASA winds were used. The results of the analysis show that the $K_x(t)$ feedforward gain has little or no effect on system performance using the NASA winds. However, the $K_\omega(t)$ feedforward gain does contribute to the reduction of the bending moment. Since it is the primary function of the Case I (or Case II) estimator to generate the x-feedforward, these results indicate that the estimator is not required. In fact, all that is necessary

is to measure the wind angle-of-attack α_ω, subtract out the mean wind $\bar{\alpha}_\omega$, and multiply by a time-varying gain as shown below:

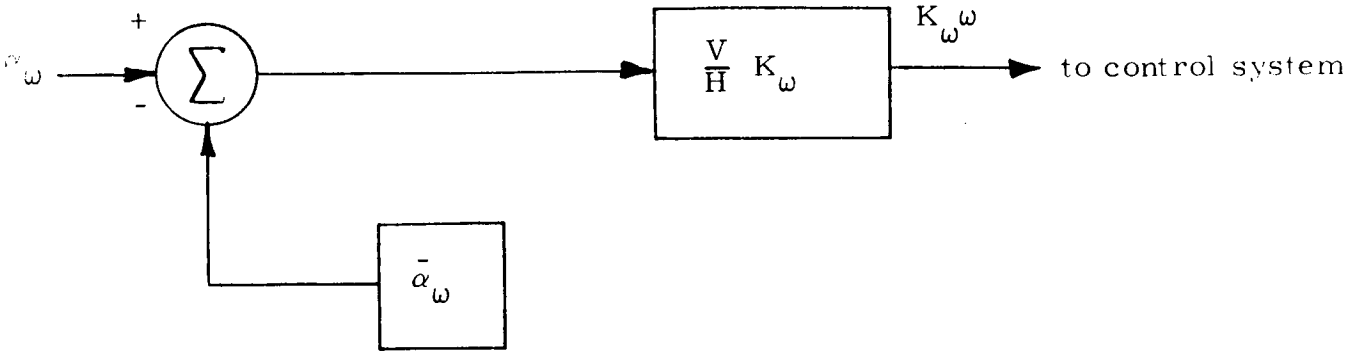

This result greatly simplifies the system since the estimator is no longer required.

The system with the above simplifications has the following control law (retaining $K_{\dot{z}}(t)$):

$$u = 10 \left| \frac{T_s S+1}{10 T_s S+1} \right| \left| f(t) + 0.035\phi + 0.12\dot{\phi} + K_{\dot{z}}(t)\dot{z} + (\alpha_\omega - \bar{\alpha}_\omega) \frac{V}{H} K_\omega \right.$$

Figures N-33 and N-34 illustrate the performance of the system using various piecewise constant approximations to the $K_{\dot{z}}(t)$ gain. The best approximation in terms of resulting performance turned out to be a simple bistable gain approximation. The gain was initially set equal to -0.3×10^{-4} rad/m/sec. At 90 seconds into the flight, the $K_{\dot{z}}(t)$ gain was switched to 0.5×10^{-4} rad/m/sec. An initially negative value reduced the stability of the system, making it easier to turn the vehicle in anticipation of the wind. After the peak winds occurred, the gain was switched to a positive value in an attempt to reduce the drift rate to zero. This configuration resulted in acceptable performance. The time responses (see Figure N-34) showed a large switching transient resulted when the drift-rate gain was switched. In actual practice, the gain would be blended smoothly from the one gain level to the other to avoid this transient.

Generation of drift rate from a body-mounted accelerometer was evaluated to determine if the compensation of the body-acceleration feedback could be simplified. Drift acceleration was obtained from the following equation:

$$\ddot{z} = \ddot{t} + \frac{F-X}{m}\phi - \ell_A\ddot{\phi}$$

Figure N-35 illustrates the effect of eliminating the $\ell_A\ddot{\phi}$ term and the effect of eliminating the $(F-X/m)\phi$ term. The results indicate the $\ell_A\ddot{\phi}$ term can be neglected, but the $(F-X/m)\phi$ term cannot be neglected.

Time did not permit further analysis of system simplification. Additional simplifications in measuring the wind angle-of-attack and in approximating the $(V/H)K_\omega$ gain could result in a still simpler system. However, with all the simplifications considered, the system took the form shown in Figure 5-12. A comparison with the nominal load-relief controller as shown in Figure 5-10 quickly illustrates that the system can be greatly simplified. This information supports the ideas behind the synthesis technique which is the basis for this study. That is to say, that the technique first derives a "best" system (in terms of performance), and then, with the application of engineering approximations, a practical controller is derived from this best system. This approach to system design is much more appealing than the conventional trial and error design which is currently in practice.

Performance Evaluation of Simplified System

The simplified system performance was evaluated for the mean wind, random wind, and the NASA winds. Figures N-36 through N-38 illustrate the performance of this system for those wind inputs. The performance was compared to that of the nominal load-relief system in terms of the performance requirements. Table 5-4 tabulates the maximum bending moment and terminal drift error for both systems. These were the most significant responses. For the

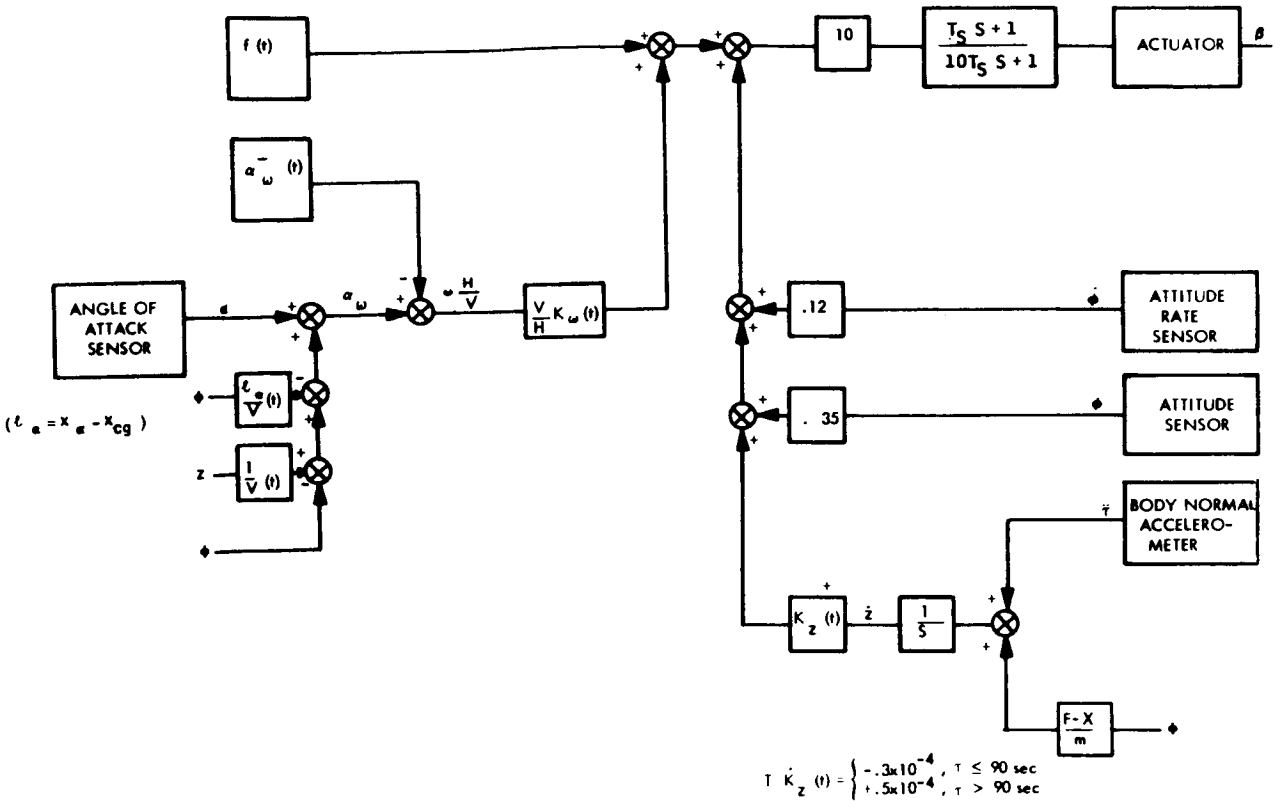

Figure 5-12. Simplified Load-Relief Controller with Realistic Sensing

mean-wind disturbance the bending moment is three to four times larger for the simplified system, and the terminal drift is 500 meters as opposed to no drift for the nominal system. However, the simplified system's performance was acceptable in terms of the performance requirements. For the NASA wind, the systems are quite comparable in terms of the bending moment, but the simplified system always had a larger terminal drift. These results indicate that the system can be greatly simplified without a serious degradation in performance.

Table 5-4. Performance Comparisons Between the Nominal Load-Relief System and the Simplified Load-Relief System

Controller	Maximum Bending Moment (kp-m)	Terminal Drift (m)
Performance Requirement	2.25×10^6	3000
Mean-Wind Disturbance		
Nominal Load Relief	0.15×10^6	0.0
Simplified Load Relief	0.80×10^6	500
48-Second NASA Wind Disturbance		
Nominal Load Relief	1.4×10^6	0
Simplified Load Relief	1.8×10^6	650
56-Second NASA Wind Disturbance		
Nominal Load Relief	1.8×10^6	0
Simplified Load Relief	2.3×10^6	250
64-Second NASA Wind Disturbance		
Nominal Load Relief	2.4×10^6	0
Simplified Load Relief	2.65×10^6	820
72-Second NASA Wind Disturbance		
Nominal Load Relief	2.6×10^6	0
Simplified Load Relief	2.4×10^6	600
80-Second NASA Wind Disturbance		
Nominal Load Relief	1.5×10^6	0
Simplified System	1.4×10^6	300

COMPARISON STUDIES

The load-relief control system was compared with two other control systems on the basis of performance and complexity. These two systems were the minimax controller and a conventional controller, both of which were defined under NASA contract NAS 8-11206 (see Ref. 12, 15). The reason for conducting this comparison study was to establish what improvement in performance could be obtained with the load-relief control technique relative to these other techniques. Further, it was the objective to determine the cost in terms of complexity that must be paid to achieve the improvement in performance. Before these systems can be compared, it is necessary to describe both the minimax and conventional controllers in terms of their respective block diagrams and the assumptions underlying their design. The performance of each of the systems is presented for various vehicle and controller parameter variations using the wind disturbances defined above.

Description of Minimax Controller

Figure 5-13 is a block diagram of the minimax control system. It consists of attitude, attitude-rate, and angle-of-attack feedbacks. The system configuration was derived from a drift-minimum controller configuration, and the primary objective of the design was to provide a load-relief capability. The gains for the controller were defined by applying optimal control theory to a piecewise constant approximation of the vehicle for only the first 84 seconds of flight. This period was divided into seven intervals with a different constant approximation of the vehicle in each interval. The disturbances used in the design were winds of bounded amplitude which cause the maximum of any of several cost items to occur in each flight interval, and each cost item is proportional to some physical quantity of interest. The cost of a given controller is the maximum of its several cost items. Optimal control theory provides a straightforward method of

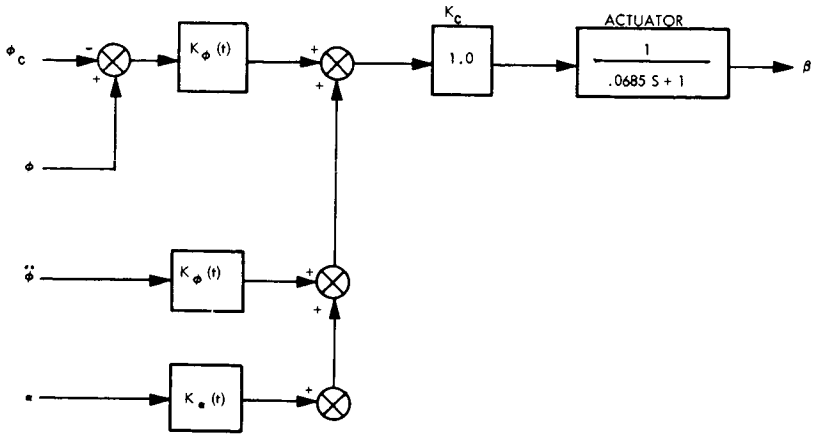

Figure 5-13. Minimax Controller

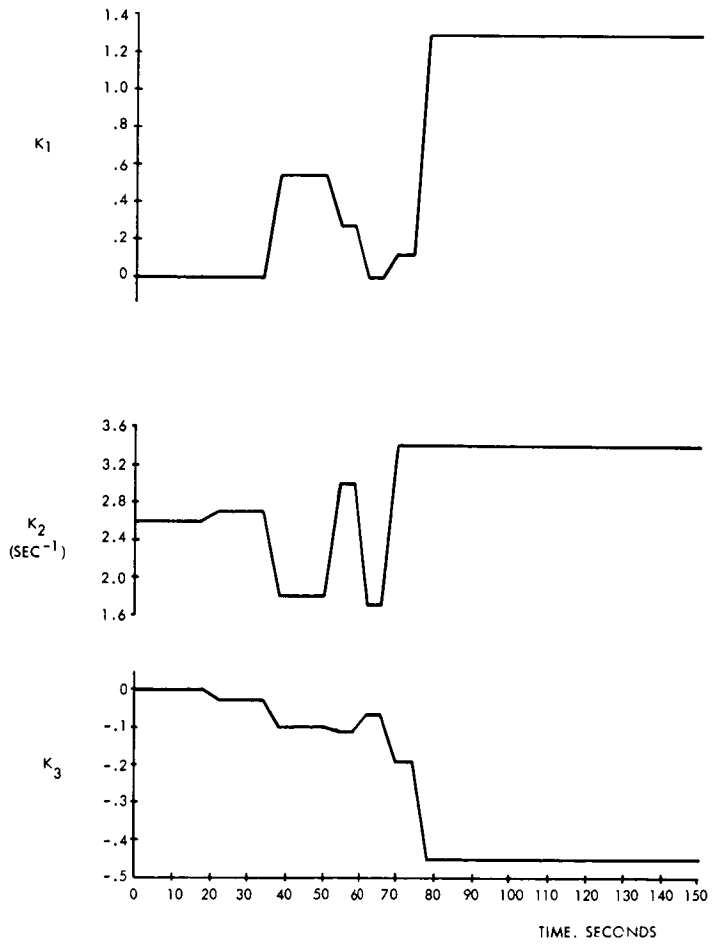

Figure 5-14
Minimax Control Gains

computing the cost of a finite set of controllers. The controller of the set with minimum cost is called the minimax controller of that set. Bending moment is weighed heavily in the cost items for the computations of the gains.

The gains which were computed for the controller are shown in Figure 5-14. For the simulation, the gains computed for interval seven were also used for the time from 84 seconds until the end of flight. In the design of the controller, gains were not computed for the last half of the flight. The system was designed for a rigid vehicle without consideration of actuator and sensor dynamics and the actual location of the angle-of-attack sensor.

Response of the nominal minimax controller to the mean wind, random, and the NASA winds are shown in Figures N-39 through N-41. These responses show satisfactory performance for the random-wind and mean-wind disturbances. However, the allowable bending moment is exceeded for all NASA wind cases with the exception of the 48-second wind. This system was designed to meet a maximum bending moment of 2.7×16^6 kp-m instead of 2.25×10^6 kp-m. A large switching transient occurs in the gimbal-angle response when the K_1 and K_3 gains are switched at 74 seconds into the flight. In practice, this transient could be minimized by an improved blending of the gains. The magnitudes of the significant parameters have been tabulated in Table 5-5. As can be seen from this table, the bending moment for the 72-second NASA wind is nearly double the maximum allowable value. Other performance parameters (e.g., $\dot{\phi} + 0.388\alpha$) were not tabulated as they were well within the allowed limits.

The controller and aerodynamic parameter variations evaluated with the minimax controller were as follows:

Table 5-5. Minimum Performance Results

Wind Disturbance	Maximum Bending Moment (kp-m)	Terminal Drift (m)	Terminal Drift Rate (m/sec)
Mean Wind	1.45×10^6	800	14.5
48 sec NASA	1.9×10^6	1800	30
56 sec NASA	2.5×10^6	1600	27
64 sec NASA	3.1×10^6	550	11
72 sec NASA	3.9×10^6	0	3
80 sec NASA	2.9×10^6	200	2
Performance Requirement	2.25×10^6	3000	40

<u>Controller</u>

$\pm$ 20% K_1

$\pm$ 20% K_2

$\pm$ 20% K_3

<u>Vehicle</u>

$\pm$ 20% c_1

$\pm$ 20% c_2

$\pm$ 20% $\frac{F-X}{m}$

$\pm$ 20% V

$\pm$ 20% N'/m

$\pm$ 20% R'/m

Responses of the system for these variations are shown in Figures N-42 through N-48. The data from these responses show the system to be somewhat sensitive to the K_3 gain and the longitudinal acceleration $\frac{F-X}{m}$ in terms of the drift error at burnout. However, this is to be expected. It is the ratio of the angle-of-attack feedback gain to attitude gain which determines the drift error. Further, the desired ratio of these gains depends heavily on the time history of the longitudinal acceleration $\frac{F-X}{m}$.

Description of Conventional Controller

Figure 5-15 is a block diagram of the conventional control system. It is basically an attitude control system with added acceleration feedback to provide the minimum required load-relief capability. All gains were constant with the exception of the forward-loop gain K_c. This gain took on two discrete values over the flight.

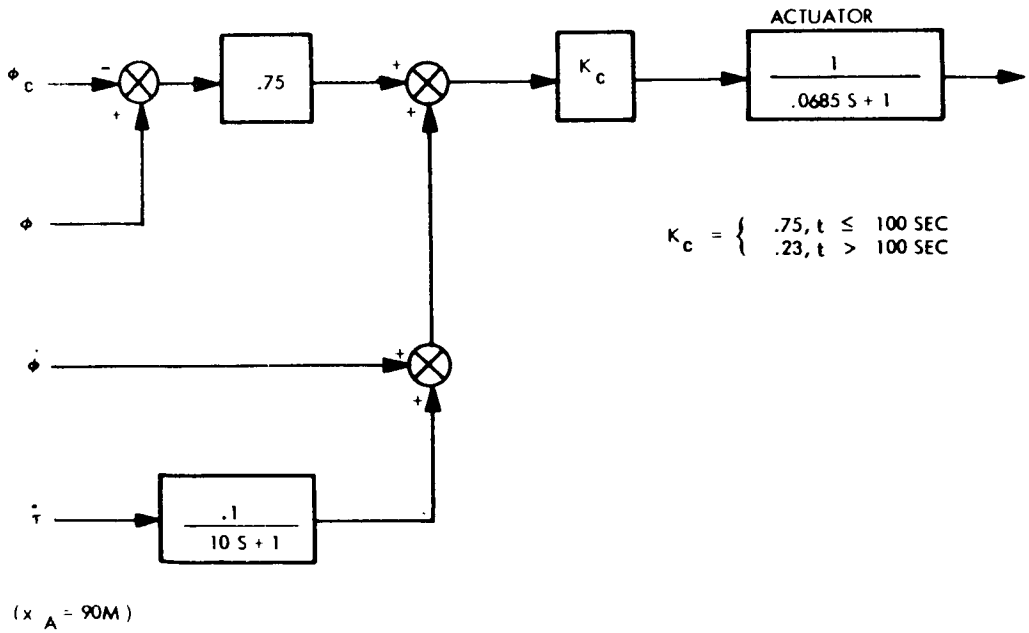

Figure 5-15. Conventional Controller

The conventional controller was not designed to provide primarily load relief; rather the emphasis was placed on designing a system to provide positive control of the first two structural bending modes. If a rigid-body vehicle had been assumed, there would have been no need to schedule the forward-loop gain K_c; i.e., all controller gains would be constant over the entire flight. The load-relief capability built into the system was based on meeting a bending-moment constraint of 2.7×10^6 kp-m instead of the 2.25×10^6 kp-m required of the load-relief controller. However, the system load-relief capability was designed using a flexible vehicle and assuming that the 64-second NASA wind was the worst wind. The system was designed assuming third-order actuator dynamics but no sensor dynamics. Further, the system was constrained to have a minimum response frequency of 0.5 rad/sec in response to attitude commands. This constraint was not imposed on either the minimax system or the load-relief system. This constraint severely restricts the load-relief capability of the system. Since the conventional controller was designed for a flexible vehicle, the system contained additional filtering for bending-mode compensation. This filtering was not necessary for a rigid-body study, and thus was not used.

Responses of the conventional controller to the mean wind, random wind, and the NASA winds are shown in Figures N-49 through N-55. Significant parameters for each of these responses are tabulated in Table 5-6. In addition to the nominal conventional controller, responses to the NASA winds were obtained for a drift-minimum controller and pure-attitude controller. These systems were derived from the conventional controller by simply setting the acceleration feedback gain to that required for drift-minimum operation (i.e., $K_A \cong 0.07$) or to zero for pure attitude control. Table 5-6 and the responses show that the conventional controller is nearly identical in load-relief capability to the minimax controller. For all winds considered, the maximum bending moment is nearly the same. However, for the 48-second, 56-second, and 64-second winds, the conventional controller has a smaller drift error at burnout. The minimax controller, on the other hand, has smaller drift errors for the 72-second and 80-second

Table 5-6. Conventional Controller Performance Summary

Wind Disturbance	Maximum Bending Moment (Kp-m)	Terminal Drift (m)	Terminal Drift Rate (m/sec)
Performance Requirement	2.25×10^6	3000	40
Nominal Conventional Controller			
Mean Wind	1.65×10^6	550	12
48-sec NASA	2.0×10^6	700	12.5
56-sec NASA	2.7×10^6	850	15
64-sec NASA	3.3×10^6	900	17.5
72-sec NASA	4.1×10^6	750	17
80-sec NASA	2.8×10^6	400	12
Conventional Controller - Drift Minimum Gains			
Mean Wind			
48-sec NASA	2.1×10^6	100	5
56-sec NASA	2.8×10^6	150	5
64-sec NASA	3.6×10^6	100	5
72-sec NASA	4.2×10^6	100	4
80-sec NASA	3.0×10^6	200	0
Conventional Controller - No Acceleration Feedback			
Mean Wind			
48-sec NASA	2.2×10^6	1050	9
56-sec NASA	3.2×10^6	1350	10
64-sec NASA	4.3×10^6	1800	20
72-sec NASA	4.8×10^6	2350	30
80-sec NASA	3.4×10^6	2000	27

winds. It is of interest to note that there is almost no significant reduction in bending moment when going from the drift-minimum acceleration feedback gain to the conventional controller acceleration feedback gain. This is not the case, however, between a pure-attitude controller and the drift-minimum controller.

Thus, one might argue that the drift-minimum gain would be more desirable when comparing the change in bending moments and the corresponding change in drift error at burnout. It was noted in the design of the conventional controller that the bending moment was significantly reduced when the first structural bending mode was included in the analysis. In fact, the analysis showed that an acceleration feedback gain of 0.4 rad/m/sec^2 was required to meet the bending moment constraint for the rigid-body model. However, with the addition of the first structural mode, an acceleration feedback gain of only 0.1 rad/m/sec was required to meet the bending -moment constraint.

The following parameter variations were analyzed for the conventional controller:

Control	Vehicle
$\pm$ 20% K_c	$\pm$ 20% c_1
$\pm$ 20% K_A	$\pm$ 20% c_2
$\pm$ 20% K_c	$\pm$ 20% N'/m
$\pm$ 20% T_A	$\pm$ 20% R'/m
$\pm$ 20% ℓ_A	$\pm$ 20% $\frac{F-X}{m}$
	$\pm$ 20% V

Responses with conventional controller to the mean wind for these parameter variations are shown in Figures N-56 through N-63.

Analogous to the minimax controller, only variations in the accelerometer feedback gain K_A and the longitudinal acceleration term $\frac{F-X}{m}$ had any significant effect on performance. The principal effect was in the drift at burnout.

Performance Comparison With Load-Relief Controller

Table 5-7 lists the significant performance parameters for the nominal load-relief controller, the simplified load-relief controller, the minimax controller, and the conventional controller. All systems easily meet the terminal condition constraints and the maximum allowable gimbal-angle constraint. Further, all systems meet the bending-moment constraint for the mean winds, but all systems fail to meet the bending moment constraint for two or more of the NASA winds. However, it should be noted that the load-relief controller produces a maximum bending moment for the mean-wind disturbance which is a factor of 10 better than either the conventional controller or the minimax controller. The reason for this significant reduction in the bending moment can be attributed to the deterministic input in the load-relief controller. This suggests that if wind biasing (i.e., deterministic input) were to be added to the other controllers then perhaps they also could achieve a significant reduction in the bending moment. In fact, this has already been demonstrated to some degree on the present Saturn C-1 vehicle. In response to the NASA winds, the load-relief controller again demonstrates a significant reduction in the bending moment over that obtained from the minimax and conventional controllers. However, the improvement is not as marked as in the case of the mean wind.

For the random wind it is difficult to determine which system has the superior performance; to do so would require making several runs with each configuration and then averaging the maximum bending moments to establish a trend.

Table 5-7. Performance Comparisons - Sissenwine Winds

Controller	$I_b \times 10^{-6}$ (kp-m)	z (m)	$\dot{z}$ (m/sec)	$\dot{\phi} + 0.388\alpha$ (rad/sec)	β (deg)
Performance Requirement	2.25	3000	40	0.0453	5
Mean-Wind Disturbance					
Nominal Load Relief	0.15	0	0	0.005	0.10
Simplified Load Relief	0.80	500	2.5	0	0.60
Minimax	1.45	800	14.5	0.0025	0.75
Conventional	1.65	550	12	0.002	0.65
48-Second NASA Wind Disturbance					
Nominal Load Relief	1.4	0	0	0.005	0.58
Simplified Load Relief	1.8	650	2.5	0	0.60
Minimax	1.9	1800	30	0.0025	1.7
Conventional	2.0	700	12.5	0	0.55
56-Second NASA Wind Disturbance					
Nominal Load Relief	1.8	0	0	0.005	0.65
Simplified Load Relief	2.3	250	2.5	0	1.3
Minimax	2.5	1600	27	0.0025	1.2
Conventional	2.7	850	15	0	0.50

Table 5-7. Performance Comparisons - Sissenwine Winds (continued)

Controller	$I_b \times 10^{-6}$ (kp-m)	z (m)	$\dot{z}$ (m/sec)	$\dot{\phi} + 0.388\alpha$ (rad/sec)	β (deg)
Performance Requirement	2.25	3000	40	0.0453	5
64-Second NASA Wind Disturbance					
Nominal Load Relief	2.4	0	0	0.0075	0.82
Simplified Load Relief	2.65	820	2.0	0	2.0
Minimax	3.1	550	11	0	0.90
Conventional	3.3	900	17.5	0	1.2
72-Second NASA Wind Disturbance					
Nominal Load Relief	2.6	0	0	0.005	0.55
Simplified Load Relief	2.4	600	2.5	0	1.6
Minimax	3.9	0	3	0	1.3
Conventional	4.1	750	17	0.0025	1.8
80-Second NASA Wind Disturbance					
Nominal Load Relief	1.5	0	0	0.005	0.72
Simplified Load Relief	1.4	300	2	0	0.90
Minimax	2.9	200	2	0	1.5
Conventional	2.8	400	12	0	1.6

Another significant difference between the load-relief controller and the other controllers is the errors produced at burnout. Again the load-relief controller is superior to the others since it brings all terminal errors to nearly zero. With a simplified system, small terminal drift errors resulted. However, these drift errors were well within the allowable limits.

Comparing the controllers on the basis of complexity, it is evident the conventional controller is by far the simplest system, and the load-relief controller is the most complex. Even the simplified version of the load-relief controller is more complex than the conventional controller. Thus, it is seen that the improvement in performance has been obtained at the expense of a significant increase in complexity. It is anticipated, however, that further refinement of the load-relief controller could result in a more competitive system in terms of complexity.

Stability

Another area of comparison among the controllers is with regard to stability. Both the load-relief controller, and the minimax controllers do not provide a stable vehicle system configuration at all flight conditions, as shown in the root locus diagrams of Appendix O. The conventional controller, however, was designed to provide a stable system with specified gain and phase margins at any given fixed flight condition (see Ref. 16). The root locus of the load-relief controller was computed both with and without the drift-rate term. This term affects the stability of the flight-path root. The drift term was not included in the analysis since this feedback was insignificant for point stability. Since all controllers satisfactorily controlled the vehicle over the trajectory in the presence of wind disturbances, the question must be asked; "Is stability at any one given flight condition necessary?" Without going into an exhaustive analysis, it seems a reasonable conclusion can be made. Since the flight is of bounded time (i.e., 150 seconds) any instability of a low-frequency nature such as an unstable flight-path root should not seriously degrade the system

performance (so long as the terminal drift constraint is met). However, higher-frequency instabilities such as the short-period mode or one of the bending modes would most likely result in unsatisfactory performance.

It is interesting to note that the frequency of the short-period mode for the load-relief controller and the minimax controller was around 0.1 rad/sec which is rather low. The conventional controller was constrained to have a short-period-mode minimum-allowable-frequency of 0.5 rad/sec to assure proper following of the attitude pitch command program. This frequency constraint was not imposed on either of the other controllers. Since the other controllers exhibited a very-low-frequency short-period mode, it is anticipated they would have difficulty following a pitch program with any degree of accuracy. It is conceivable the pitch program (and, hence, the trajectory) could be modified to accommodate this low-frequency controller characteristic. Whether or not this is a practical solution was not determined. It is rather clear that the minimax controller would have considerable difficulty following any pitch program since its attitude gain is zero for the first 20 seconds of flight. However, it is expected this gain could be set at a finite value for this interval without seriously degrading the system's load-relief capability.

CONCLUSIONS

To summarize, it has been shown that the load-relief controller has demonstrated superior performance over the other systems but at the expense of a significant increase in system complexity. The system achieved a superior load-relief capability primarily through the use of wind biasing and feedforward signals based on an assumed knowledge of the vehicle parameters and wind models. The system minimized the terminal-condition errors by computing the drift and drift-rate buildup and integrating them to zero during the last portion of flight. It was demonstrated that the system could be greatly simplified. This fact verifies the philosophy behind the synthesis technique developed in the study. This philosophy was to first design, using an analytical

synthesis technique, a control system which would provide the "best" performance. This step would then indicate how well one could expect to do in terms of performance. Then by simplifying this "best" system one could readily define a practical controller in terms of system complexity. This approach differs from the more conventional technique of trial and error wherein the analyst tries to find any system which will meet the requirements and does this by relying entirely on past experience and engineering intuition. Although the simplified load-relief controller was still more complex than the conventional controller, it is anticipated that further refinements in the synthesis technique will produce a more competitive control system.

It was pointed out that factors such as imposing stability constraints and a requirement for following a pitch program were not considered in the design of either the load-relief controller or the minimax controller. Yet, all systems successfully controlled the vehicle. This suggests that the performance requirements be carefully reviewed in order to define a common set of criteria for future studies.

It is recommended that possibly some flexible modes be included in further development of the synthesis technique in order to make the vehicle model more representative. It is also recommended that a complete time-varying simulation be made which would include the steady-state terms in the equations so that any techniques used for following a pitch program could be amply demonstrated for a multitude of wind disturbances. By so doing, the total gimbal deflection and, hence, total bending moment could also be computed.

SECTION VI
CONCLUSIONS AND RECOMMENDATIONS

The "Design of a Load-Relief Control System" study is examined in retrospect in this section. Significant results, recommendations for future studies, doubtful areas, open questions, etc., are discussed.

RESULTS

The goal of the study was to develop a load-relief controller design technique. The goal was met. The design technique developed consists of casting the load-relief problem as a linear, stochastic minimization problem, solving that problem, and simplifying the resulting optimum controller. It was demonstrated that the stochastic optimum controller is a good controller and that it can be successfully simplified.

Significant Results

The following aspects of the design technique are considered significant:

(1) The stochastic formulation of the load-relief problem is meaningful and tractable. It incorporates into the design the stochastic nature of the incident winds, the time-varying booster dynamics, and the finite-time nature of the control problem. It treats the terminal rotation and translation constraints together, it handles high-order system descriptions, and it handles arbitrary sensor arrangements and sensor noise levels. The formulation defines an optimum controller and it provides a criterion for measuring the quality of any linear controller. Its basis, minimizing an upper bound on the likelihood that one or more booster responses will fall outside preselected limits, is a meaningful and appealing design motivation.

(2) Through quadratic equivalence, the technique takes full advantage of the wealth of quadratic theory results. These results define the form and mathematical properties of the optimum controller, and they provide an easy means for calculating its parameters.

(3) The technique makes the physical nature of the control problem evident. The coefficients of the first variation of the upper-bound functional show what is easy to control, what is hard to control, and where the control emphasis should be placed. The characteristics of the optimum controller show how the difficult-to-control responses should be handled. This insight is perhaps the most useful result of applying the technique.

Less Significant Results

Quadratic equivalence implies two additional results:

(4) It provides a means of choosing quadratic coefficients in quadratic theory applications. The inability to choose these coefficients has been the major stumbling block preventing wide application of quadratic theories.

(5) It establishes an equivalence between linear control problems. This is a somewhat philosophical result; it permits determining whether two cost functionals are equivalent in that their minimizations produce identical controllers.

Good Luck Results

Two results of the study must be considered fortuitous:

(6) The optimum load-relief controller was shown to be parameter insensitive. Reasonable variations in the booster and controller parameters did not seriously degrade over-all system performance.

(7) The optimum controller was successfully simplified to an essentially constant-gain form without severely degrading over-all system performance.

These latter results may be general properties of quadratic controllers or they may be particular properties of the "Model Vehicle No. 2" and the nature of the load-relief problem. No mathematical analysis of why these properties were obtained was made, and it was not known beforehand whether the optimum controller would possess them. The insensitivity and simplification results must therefore be regarded as good luck.

Very Minor Results

Among the minor results were the following:

(8) The derivation of the expected number of occasions that a non-stationary, non-zero mean, Gaussian random process exceeds a preselected limit in a given time interval is novel. But the derivation is really nothing more than carrying through the algebra of Middleton's formulation (Ref. 16).

(9) Showing that J^*-functional is an upper bound to the likelihood of mission failure is also novel. But the proof is very easy.

Physical Insight

The third result above claims that the stochastic design technique provides insight into the load-relief problem. Regarding the "Model Vehicle No. 2" examples run in the study, it showed that:

(10) Meeting the terminal-response constraints is easy.

(11) Meeting the gimbal-actuator constraints is easy.

(12) The load-relief problem reduces to controlling the bending covariances in the high-dynamic-pressure (max-q) region of the flight.

(13) The feedback part of the optimum controller should be a low-frequency, angle-of-attack controller because large gimbal motions would cause more bending than angle-of-attack variations.

(14) The feedforward deterministic input and the wind-estimator inputs significantly improve the load-relief controller's performance. They do this by bucking the wind-induced angle of attack.

RECOMMENDATIONS FOR FUTURE WORK

A lack of time prevented investigating many interesting issues that came up in the course of the study.

Mathematical Recommendations

(1) The separation theorem should be proved for continuous time systems. This theorem is the key to incomplete state measurement problems; it permits dividing those problems into known control and estimation problems.

(2) The existence and uniqueness of extremal solutions to the J^*-minimization should be established for reasons of rigor.

(3) The conditions under which quadratic equivalence can be guaranteed should be derived. Quadratic equivalence is a powerful tool, and it deserves better verification than it got in this study.

Convergence

(4) We erred in not spending more effort on getting a better match of the quadratic coefficients and the coefficients of the first variation of the J^*-functional. As a result we do not know how much smaller J^* and the peak bending covariances can be made.

(5) The "direct iteration" technique employed was simple and fairly efficient. It could undoubtedly be made much more efficient with a little tuning. With quadratic equivalence, it is an easier way to find optimum control gains than direct minimization of the J^* functional would be.

Doubts

(6) The J^*-functional is extremely sensitive to small variations in peak covariances. The sensitivity is due to the Gaussianess assumption; the Gaussian exponential $e^{-1/2 \frac{\gamma}{\sigma}^2}$ is a very sharp function of the standard deviation σ for $\sigma << \gamma$. This sensitivity is undesirable in that it makes controller performance too sensitive to small vehicle parameter variations. No way out of this dilemma is presently seen.

(7) The J^*-functional appears to be sensitive to bending moment rates. The rate expression employed in the study was conjured for convenience. Whether or not booster performance is sensitive to force rates and high-frequency winds should be established.

Physical Problems

The booster model employed in the study was quite simple; the design technique can easily handle more complex physical problems. The following are of interest and can be treated:

(8) Inclusion of realistic sensors, sensor noises, and sensor drifts.

(9) Inclusion of the pitch attitude program in the formulation.

(10) Inclusion of bending modes, fuel slosh, and engine inertia effects.

(11) Inclusion of second-axis control.

FINAL COMMENTS

A fairly powerful design technique was developed in the study. The technique employs statistics, optimization theory, and a significant amount of digital computation. The optimum controller it produces is a very good controller, but it is time-varying and complex, and it must eventually be simplified.

We feel that a bright engineer could design almost as good a controller without all of the sophisticated theories the design technique requires. He could, that is, if he had a great deal of insight into the physical nature of the control problem.

The value of the design technique is not in its mathematics. It is that it provides that physical insight. The insight makes it easier to design a workable controller by simplifying an optimal controller than by conventional cut-and-try methods.

REFERENCES

1. "Model Vehicle No. 2 for Advanced Control Studies". A data package supplied by personnel at Marshall Space Flight Center.

2. Bendat, J. S., Principles and Applications of Random Noise Theory. Wiley, 1958. Chapter 10.

3. Kalman, R. E., and Bucy, R. S., "New Results in Linear Filtering and Prediction Theory". ASME Trans. (J. of Basic Eng.), Vol. 83D, March, 1961, pp. 95-108. Many of the results presented in this paper appear also in:
Kalman, R. E., "A New Approach to Linear Filtering and Prediction Problems". ASME Trans. (J. of Basic Eng.), Vol. 83D, March, 1960, pp. 35-45.

4. Kalman, R. E., "New Methods and Results in Linear Prediction and Estimation Theory". Tech. Rept. 61-1, Research Inst. for Advanced Studies, Baltimore, Md. 1961.

5. Bryson, A. E.; Johansen, D. E., "Linear Filtering for Time-Varying Systems Using Measurements Containing Colored Noise". IEEE Trans. on Automatic Control, Vol. AC-10, No. 1, January, 1965.

6. Kalman, R. E., "Contributions to the Theory of Optimal Control". Bol. Soc. Mat. Mex., 1961.

7. Tou, J. S., Optimum Design of Digital Control Systems. Academic Press, N.Y., 1963.

8. Vaughan, W. W., "Interlevel and Intralevel Correlations of Wind Components for Six Geographic Locations". NASA TN D-561, December, 1960.

9. Lenhard, R. W., Court, A. and Samela, H. A., "Variability Shown by Hourly Wind Soundings". J. of App. Meteorology, Vol. 2, 1963, pp. 99-104.

10. Davenport, W. B. and Root, W. L., Random Signals and Noise. McGraw Hill, N. Y., 1958, Chapter 8.

11. Bliss, G. A., Lectures on the Calculus of Variations. Univ. of Chicago Press, Chicago, Ill., 1946, Part II.

12. Graham, K. D., Final Technical Report Number 1, "Minimax Control of Large Launch Boosters", Honeywell Report 12003-FTR 1, NASA Contract NAS8-11206, Sept., 1965.

13. Gilmore, Arthur, et al., "Investigation of Dynamical Stability Derivatives of Vehicles Flying at Hypersonic Velocity". Air Force Flight Dynamics Laboratory Report ASD-TDR-62-460, September, 1963.

14. Ashley, H.; Zartarian, G., "Piston Theory - A New Aerodynamic Tool for the Aeroelastician", Journal of the Aeronautical Sciences, December, 1956, pp. 1109-1118.

15. Edinger, L. D.; White, G. D., Final Technical Report Number 2, Vol. I, "Data Requirements for In-flight Synthesis and Multiple Blender Studies", Honeywell Report 12003-FTR 2, NASA contract NAS8-11206, December, 1965.

16. Middleton, D., An Introduction to Statistical Communication Theory. McGraw Hill, N. Y., 1960, Section 9.4.

17. Tricomi, F. G., Integral Equations, Interscience Publishers, N. Y., 1957.

APPENDIX A
COEFFICIENTS

The coefficients of the "Model Vehicle No. 2" booster differential equations are presented in this appendix as Figures A-1 through A-28.

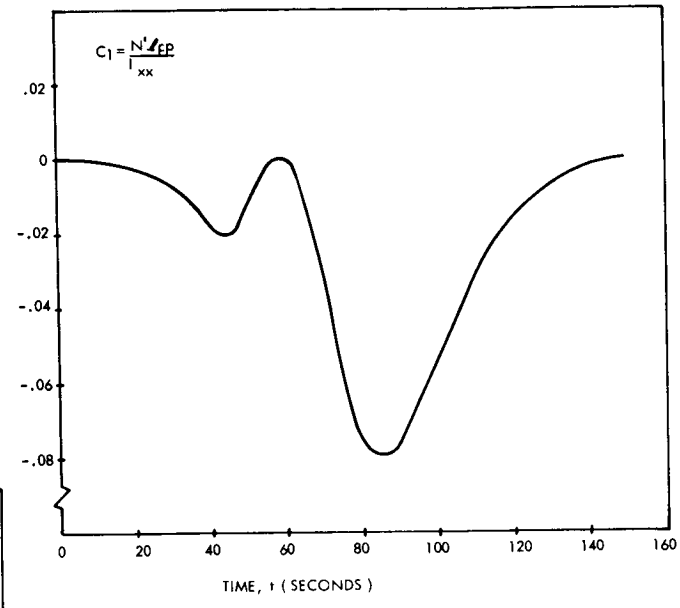

Figure A-1

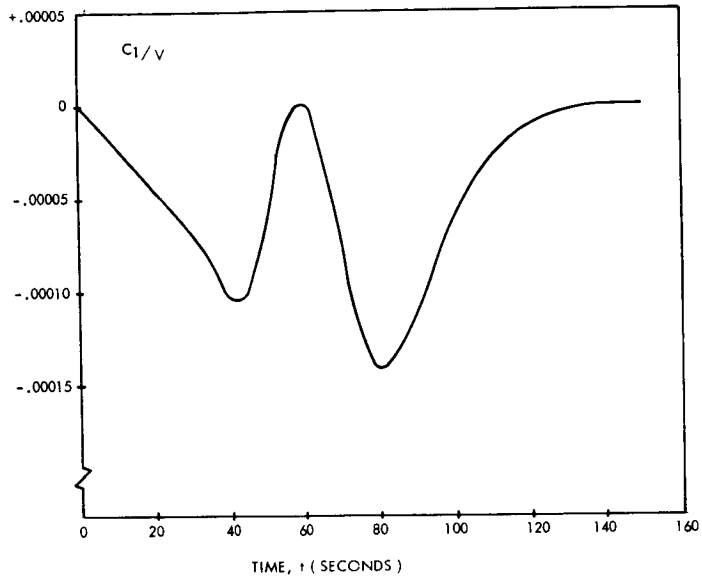

Figure A-2

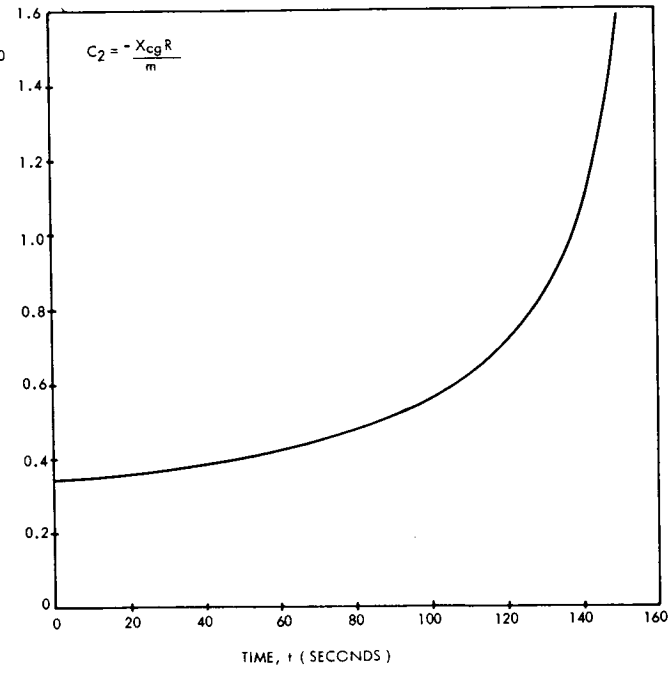

Figure A-3

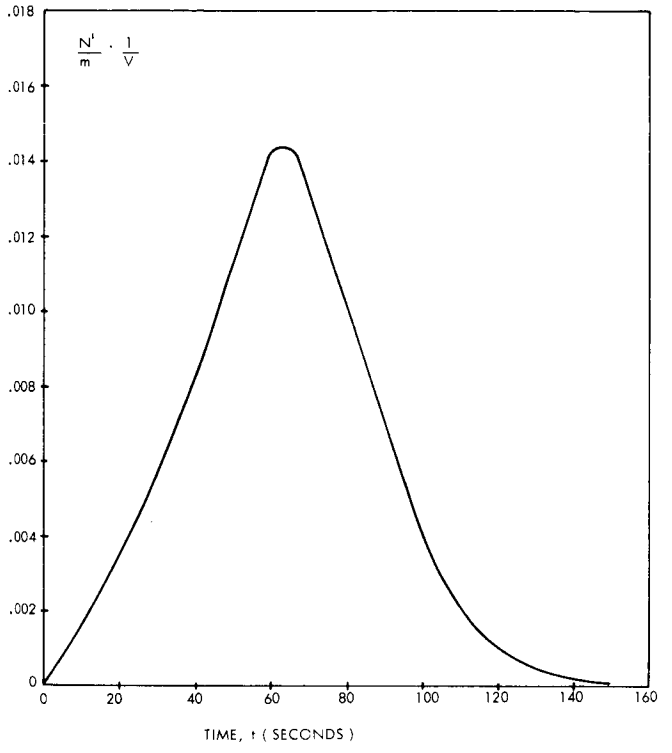

Figure A-4

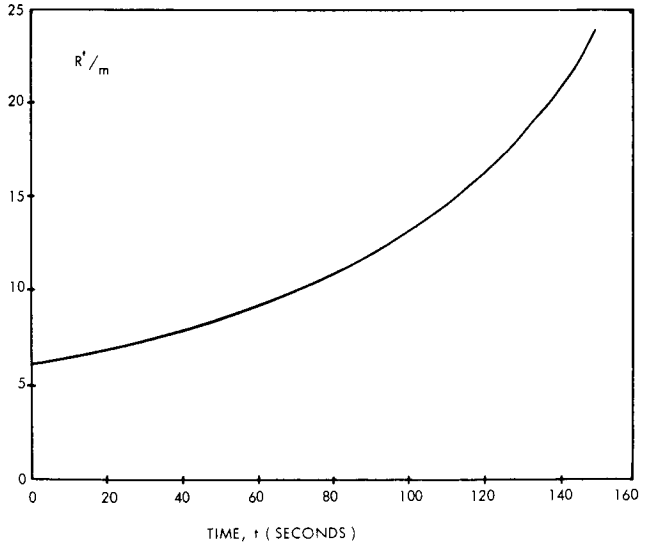

Figure A-5

Figure A-6

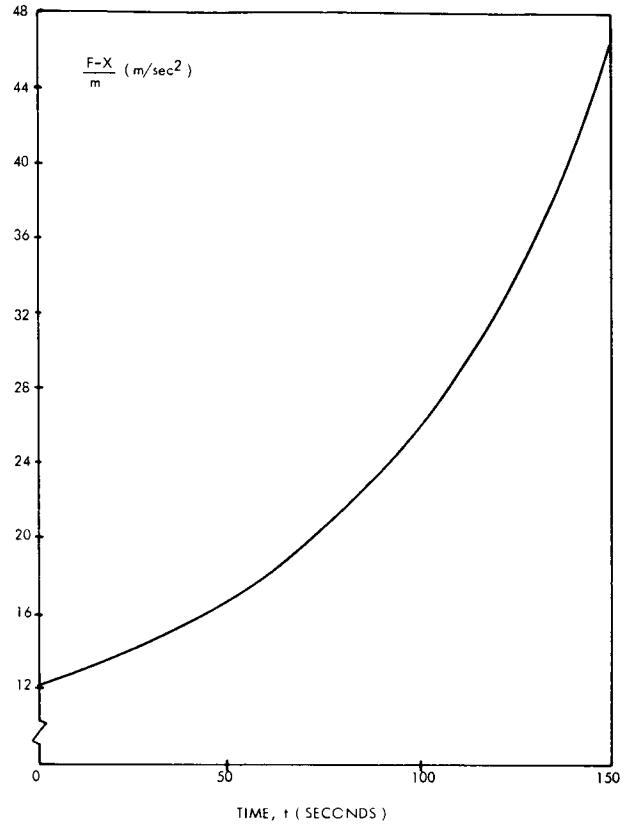

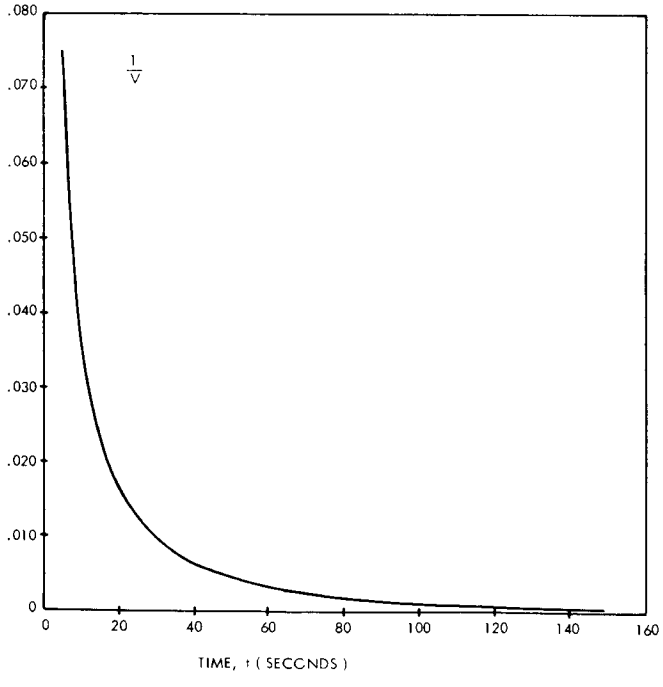

Figure A-7

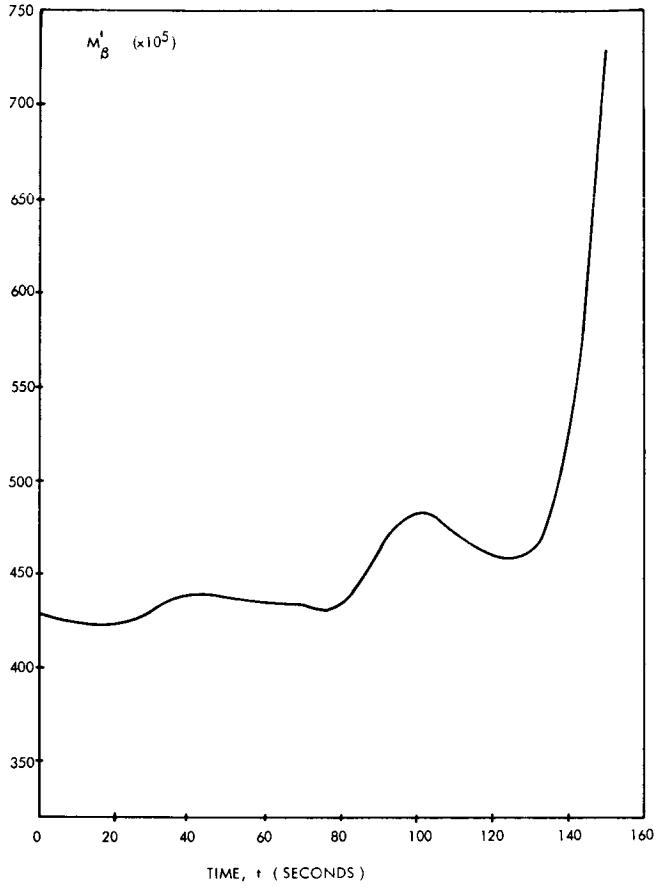

Figure A-8

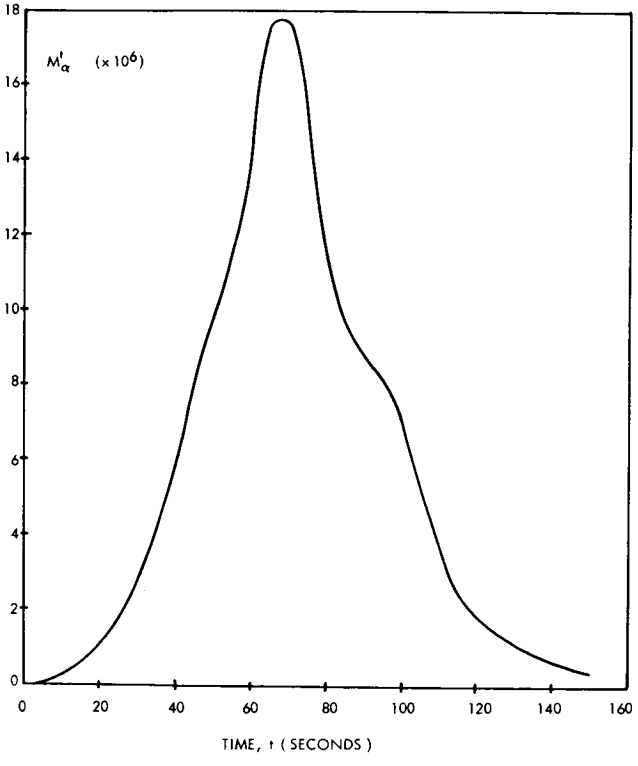

Figure A-9

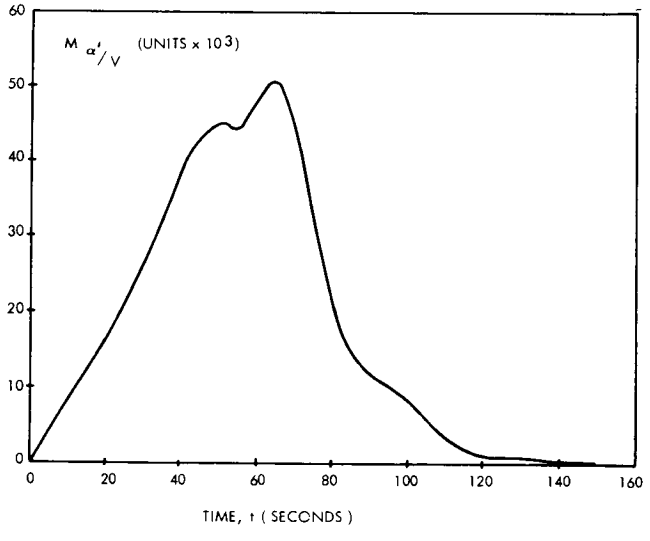

Figure A-10

Figure A-11

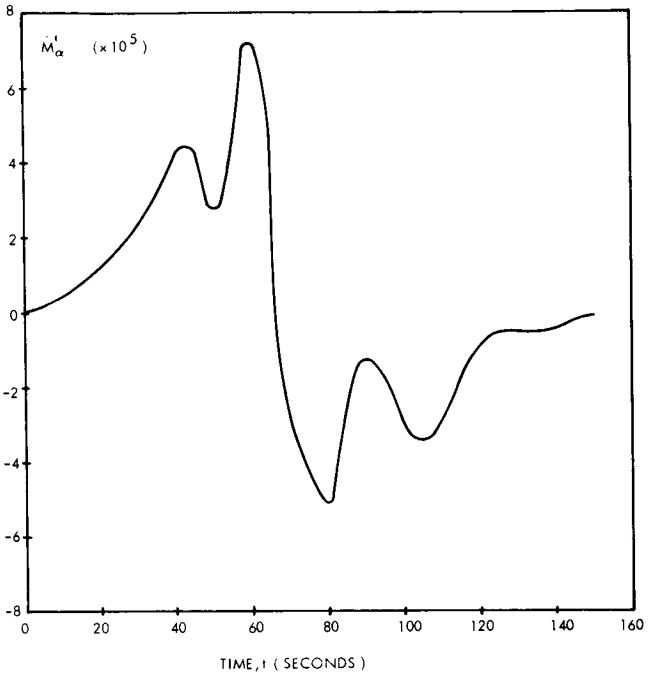

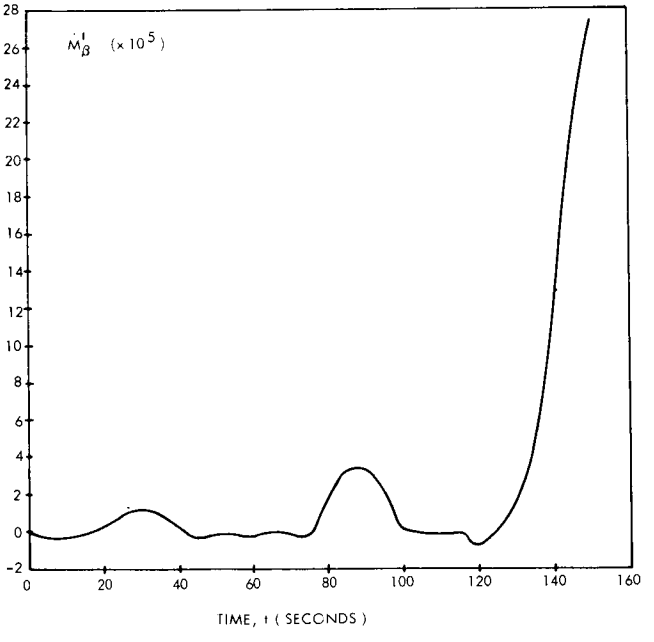

Figure A-12

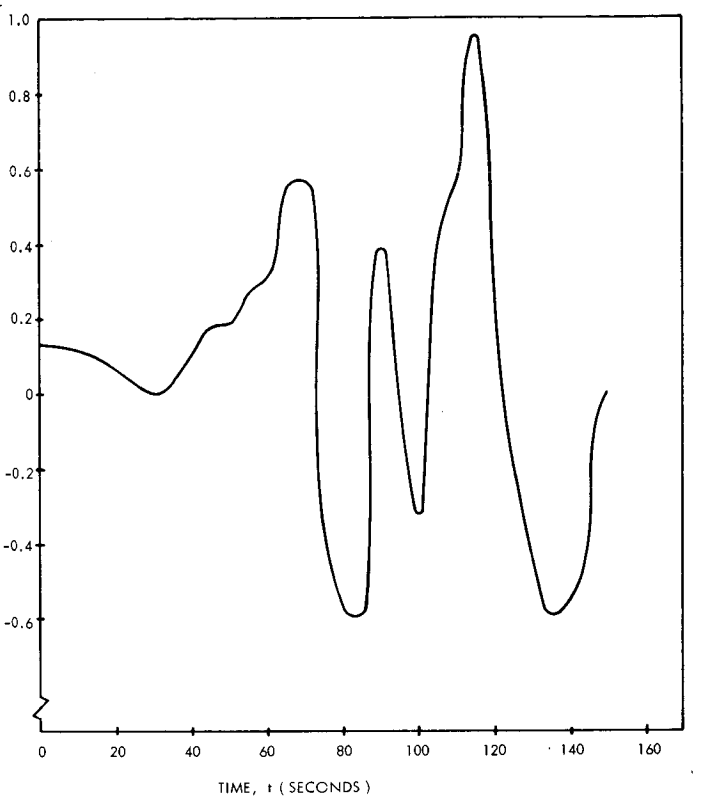

Figure A-13

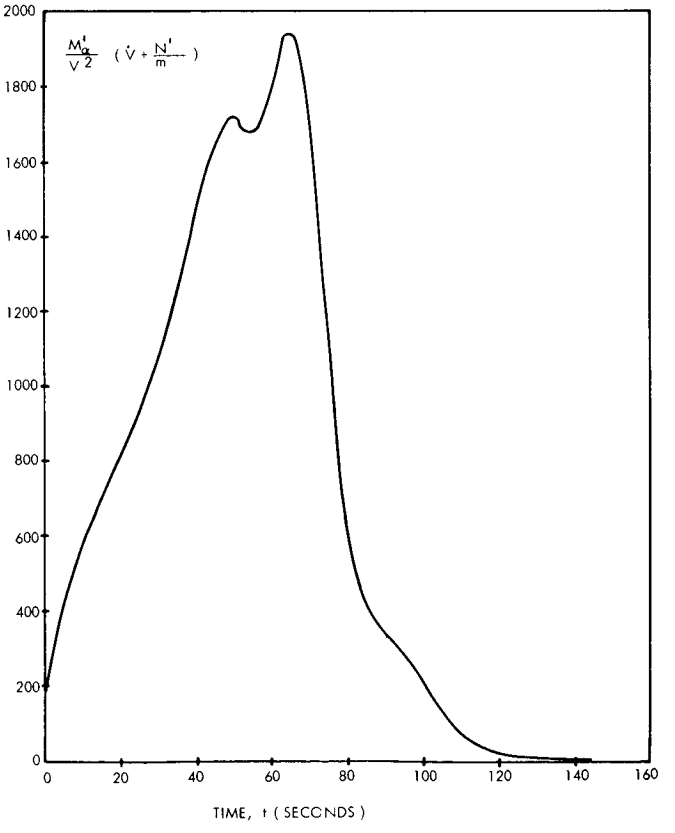

Figure A-14

Figure A-15

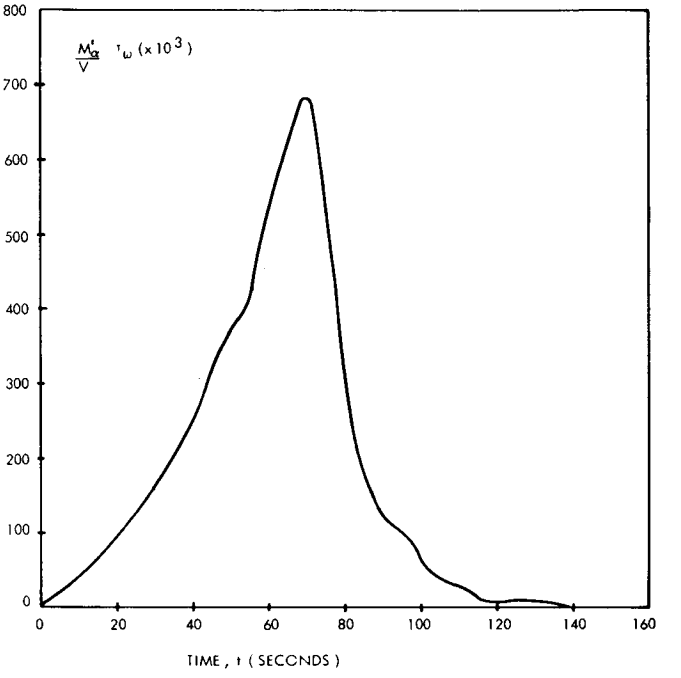

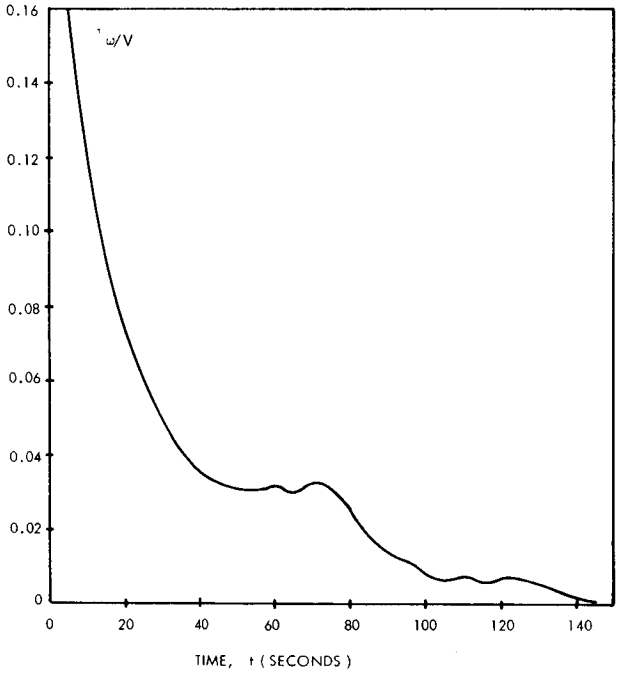

Figure A-16

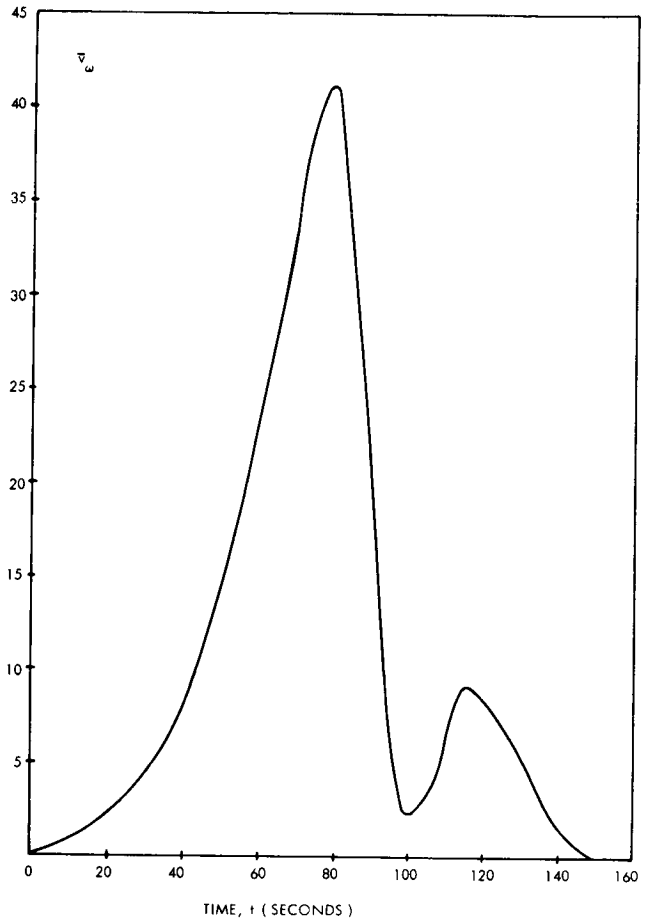

Figure A-17

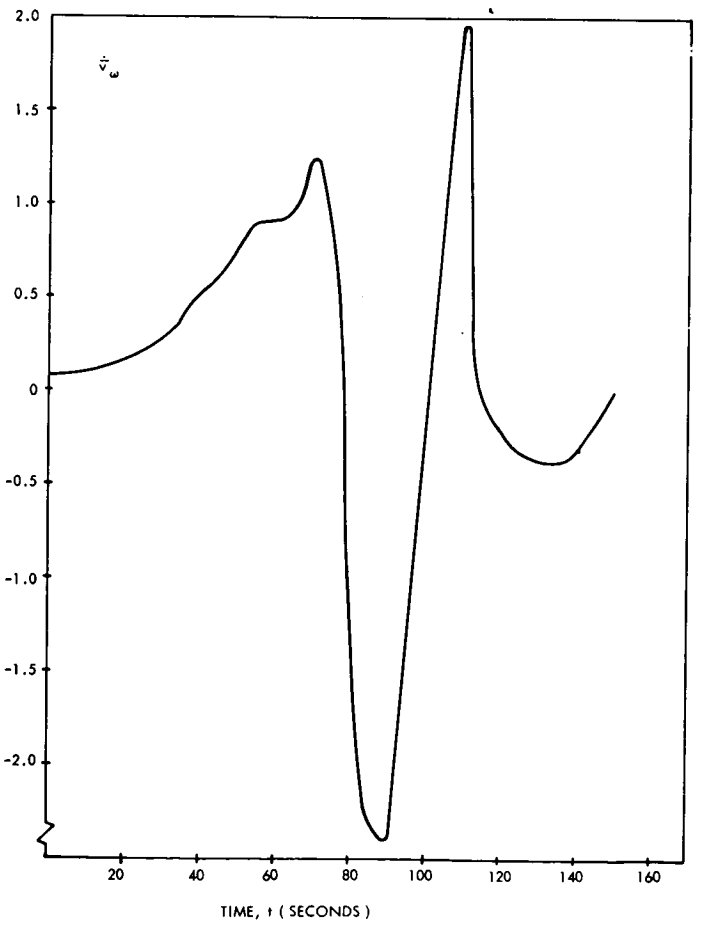

Figure A-18

Figure A-19

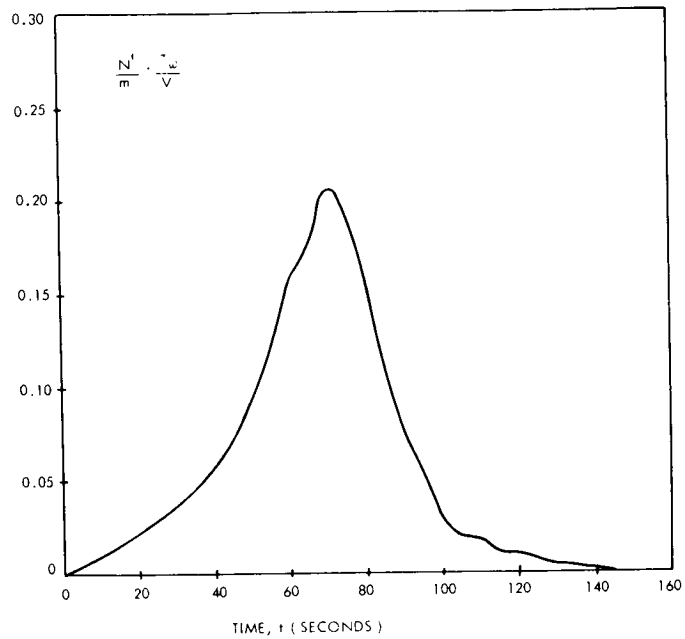

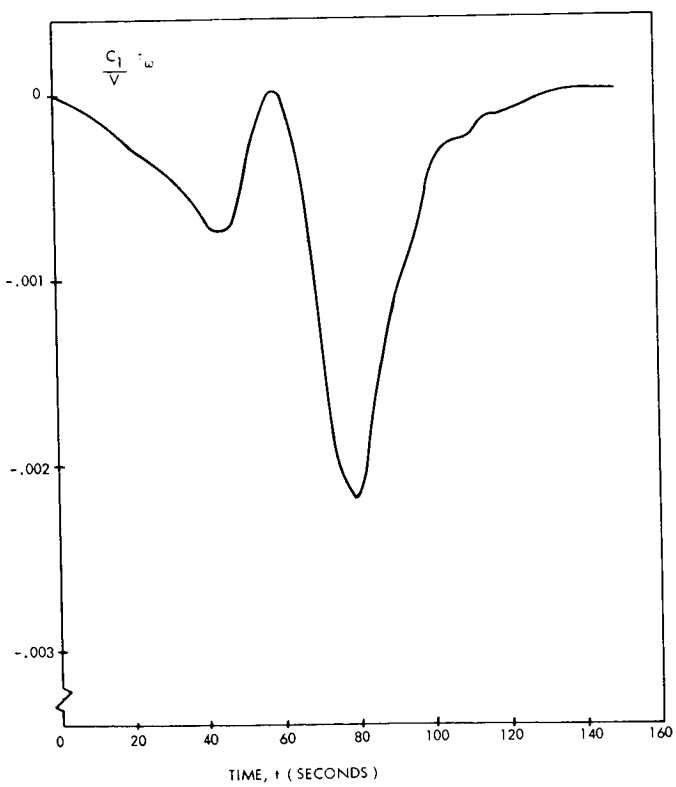

Figure A-20

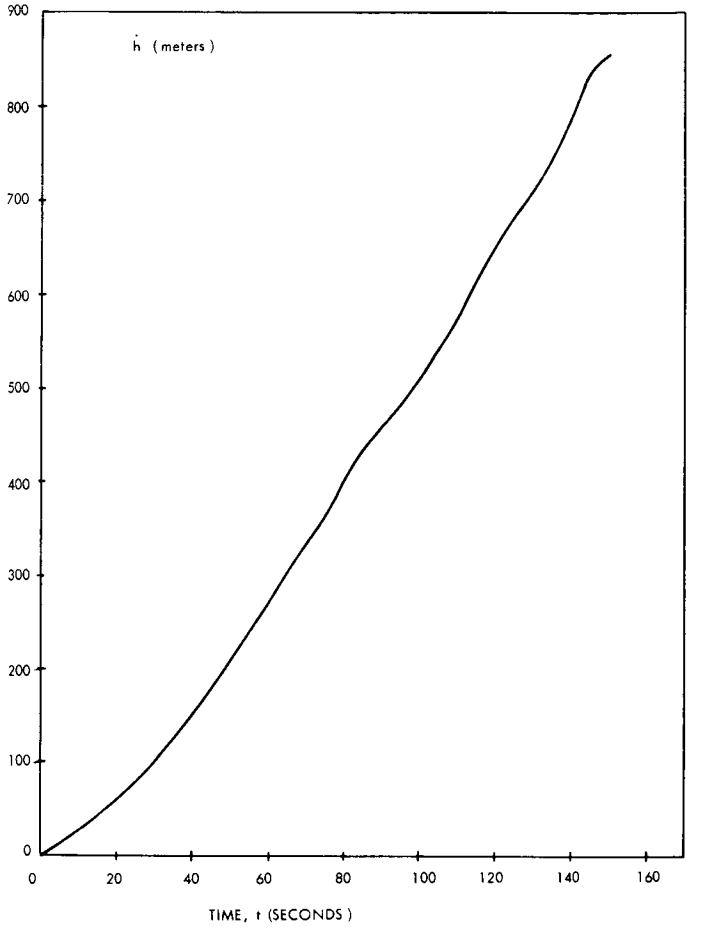

Figure A-21

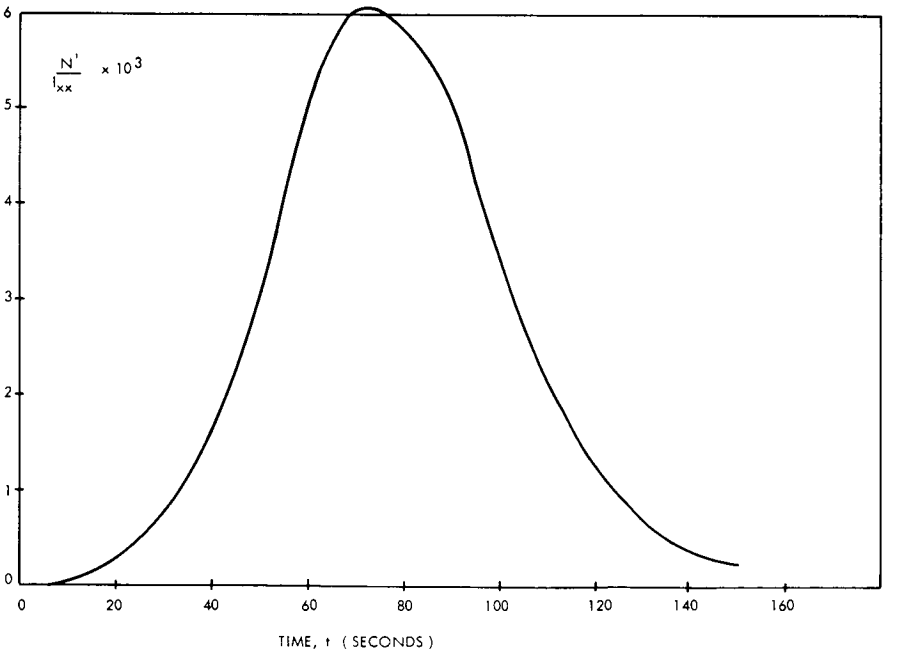

Figure A-22

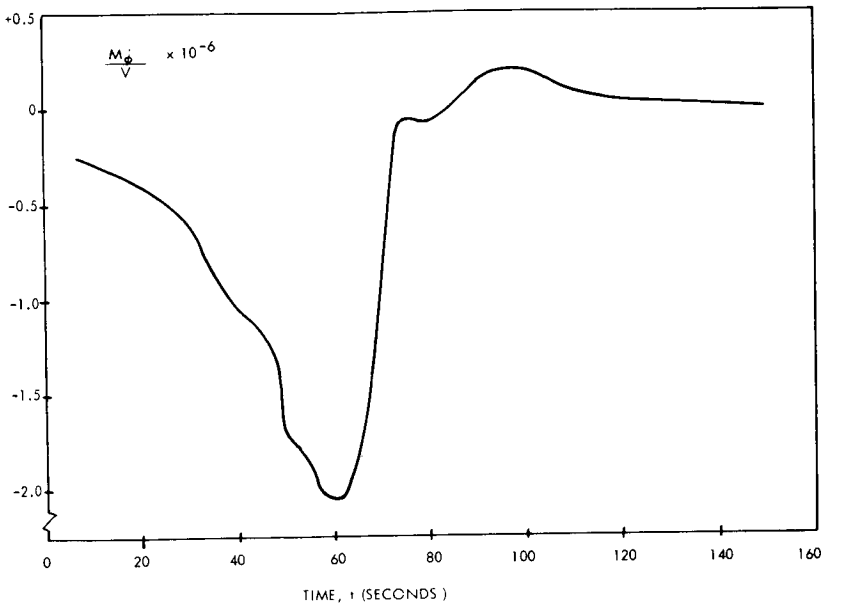

Figure A-23

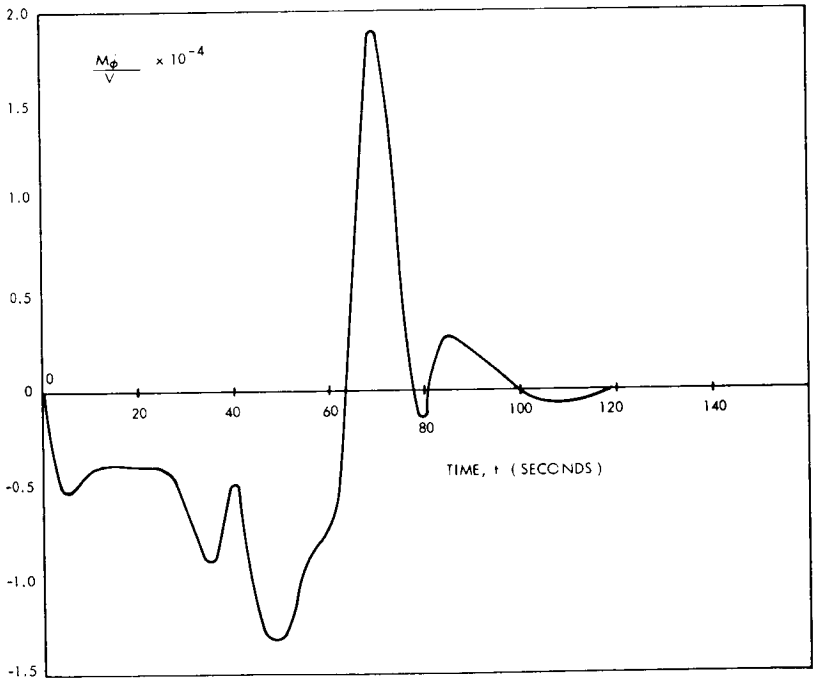

Figure A-24

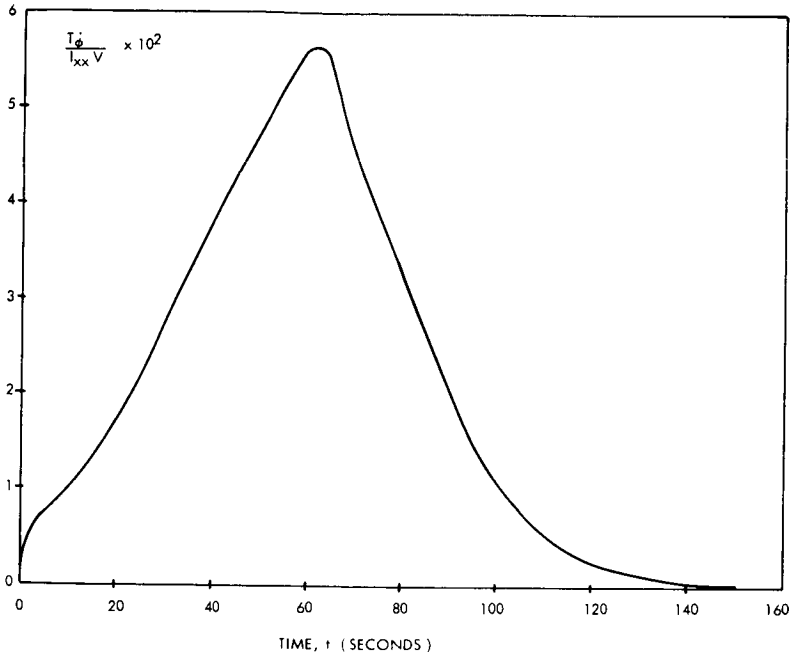

Figure A-25

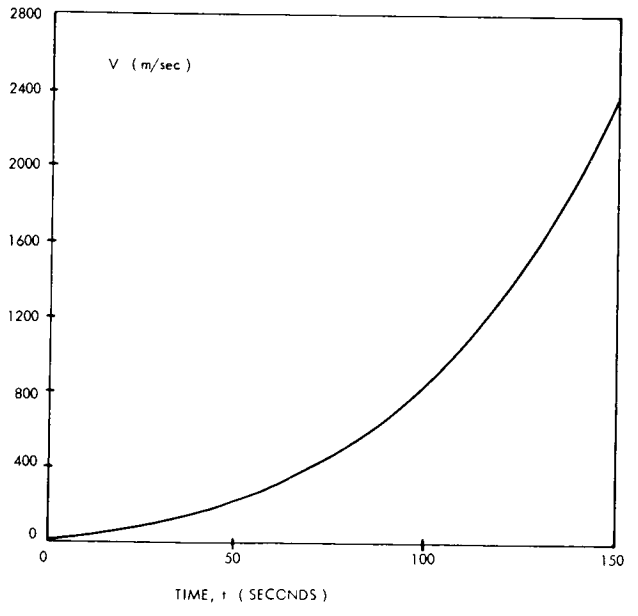

Figure A-26

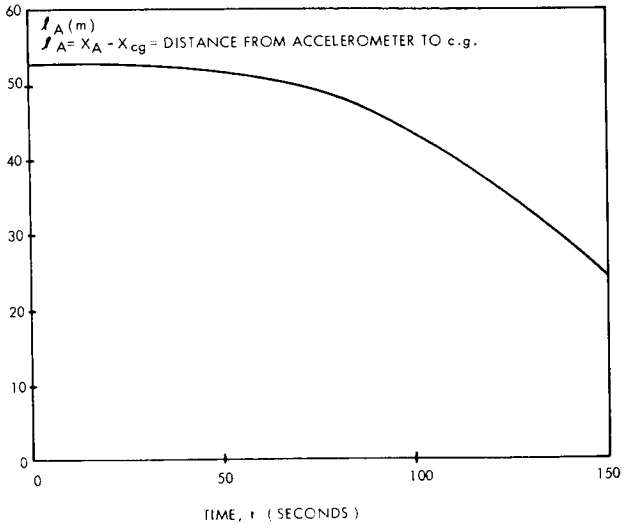

Figure A-27

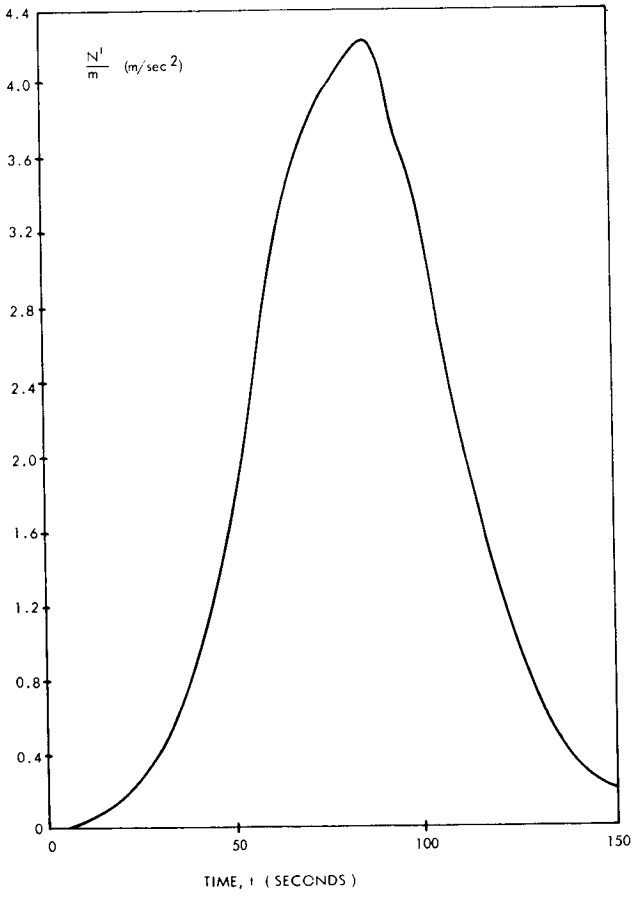

Figure A-28

APPENDIX B
WIND FILTER DETERMINATION

Three topics are discussed in this appendix, the selection of autocorrelation parameters to best fit given wind covariances by a gradient method, the derivation of the impulse response of the linear filter, white noise driven, whose output autocorrelation is the exponential cosine

$$E\left\{\omega(h_1)\,\omega(h_1+h)\right\} = (\cos a_2|h| + a_3 \sin a_2|h|)\exp(a_1|h|)$$

and the conversion of that filter from an altitude scale to a time scale.

GRADIENT METHOD

Given an autocorrelation that is a function of unchosen parameters a_1, a_2, a_3

$$E\left\{\omega(h_1)\,\omega(h_1+h)\right\} = f(a_1, a_2, a_3, h),$$

the quality-of-fit measure of Section II can be written in the form

$$J = g(a_1, a_2, a_3)$$

Letting

$$a_i = \alpha_i + \epsilon\,\beta_i$$

and expanding J in ϵ produces

$$J = g(\alpha_1, \alpha_2, \alpha_3) + \epsilon \sum_{i=1}^{3} \left(\frac{\partial g}{\partial a_i}\Big|_{\alpha_i}\right)\beta_i + \epsilon^2 \sum_{i=1}^{3}\sum_{j=1}^{3} \left(\frac{\partial^2 g}{\partial a_i \partial a_j}\Big|_{\alpha_i}\right)\beta_i\beta_j$$

$$+ \text{ higher order terms in } \epsilon$$

If the values $a_i = \alpha_i$ minimize J, then

$$\left.\frac{\partial g}{\partial a_i}\right|_{\alpha_i} = 0 \text{ for } i = 1, \ldots 3$$

for if this were not true one could always find ϵ and β_i such that the left side of the above equation would be less than the minimized J.

The gradient iteration seeks stationary values of g $\left(\text{values where } \frac{\partial g}{\partial a_i} = 0\right)$ by the following procedure. Let α_i^k be the kth guess at the minimizing a_i, and let the $k + 1^{th}$ guess be

$$\alpha_i^{k+1} = \alpha_i^k - \left(\rho \left.\frac{\partial g}{\partial a_i}\right|_{\alpha_i^k}\right)$$

where ρ is a small positive constant. It is clear that if the kth guess α_i^k is correct, then the corrections

$$-\rho\left(\left.\frac{\partial g}{\partial a_i}\right|_{a_i^k}\right)$$

applied to subsequent iterations will be zero, and the iterative process will have converged. If the kth guess is not the minimizing a_i, then the correction

$$-\rho\left(\left.\frac{\partial g}{\partial a_i}\right|_{\alpha_i^k}\right)$$

will produce a $k+1^{th}$ guess in the direction of minimizing J (i.e., if $\frac{\partial g}{\partial a_i} > 0$, decreasing α should decrease J, etc.).

The gradient procedure does not always converge, and often, when it does, a great many iterations are required. Fortunately, it converged for the exponential-cosine autocorrelation function to within two significant digits in 500 iterations.

IMPULSE RESPONSE

The impulse response of the linear filter, white noise driven, whose output has the above exponential-cosine autocorrelation can be obtained by computing the output power spectrum.

The power spectrum of the output of above exponential cosine filter is

$$\phi_{\omega\omega}(s) = \int_{-\infty}^{\infty} e^{-sh} \, e^{-a_1 |h|} (\cos a_2 |h| + a_3 \sin a_2 |h|) \, dh$$

$$= \int_{0}^{\infty} e^{-sh} \, e^{-a_1 h} (\cos a_2 h + a_3 \sin a_2 h) \, dh$$

$$+ \int_{0}^{\infty} e^{sh} \, e^{-a_1 h} (\cos a_2 h + a_3 \sin a_2 h) \, dh$$

Performing the integrations,

$$\phi_{\omega\omega}(s) = \frac{s+a_1+a_2a_3}{(s+a_1)^2 + a_2^2} + \frac{-s+a_1+a_2a_3}{(-s+a_1)^2 + a_2^2} = F(s)\,F(-s)$$

where

$$F(s) = \sqrt{2(a_1 - a_2a_3)} \left(\frac{s+a_0}{(s+a_1)^2 + a_2^2} \right),$$

and

$$a_0 = \frac{\sqrt{(a_1+a_2a_3)\,(a_1^2 + a_2^2)}}{a_1 - a_2a_3} .$$

the output of a linear filter with an impulse response f(h), driven by unity white noise $\eta(h)$

$$E\left\{\eta(h_1)\ \eta(h_1+h)\right\} = \delta(h)\ ,$$

where $\delta(h)$ is the Dirac delta function is the convolution

$$\omega(h_1) = \int_{-\infty}^{\infty} f(h_2)\ \eta(h_1-h_2)\ dh_2$$

The output autocorrelation is

$$E\left\{\omega(h_1)\omega(h_1+h)\right\} = E\left\{\left[\int_{-\infty}^{\infty} f(h_2)\eta(h_1-h_2)dh_2\right]\left[\int_{-\infty}^{\infty} f(h_3)\eta(h_1+h-h_3)dh_3\right]\right.$$

$$= E\left\{\int_{-\infty}^{\infty}\int_{-\infty}^{\infty} f(h_2)f(h_3)\eta(h_1-h_2)\eta(h_1+h-h_3)dh_2dh_3\right.$$

$$= \int_{-\infty}^{\infty}\int_{-\infty}^{\infty} f(h_2)f(h_3)E\left\{\eta(h_1-h_2)\eta(h_1+h-h_3)\right\} dh_2\ dh_3$$

$$= \int_{-\infty}^{\infty}\int_{-\infty}^{\infty} f(h_2)f(h_3)\ \delta(h-h_3+h_2)\ dh_2\ dh_3$$

$$= \int_{-\infty}^{\infty} f(h_3-h)\ f(h_3)\ dh_3\ .$$

The output power spectrum is

$$\phi_{\omega\omega}(s) = \int_{-\infty}^{\infty} e^{-sh} \int_{-\infty}^{\infty} f(h_3-h)\, f(h_3)\, dh_3 dh$$

$$= \int_{-\infty}^{\infty} e^{-sh_3} f(h_3) \left[\int_{-\infty}^{\infty} e^{s(h_3-h)} f(h_3-h)\, dh \right] dh_3$$

$$= \int_{-\infty}^{\infty} e^{-sh_3} f(h_3)\, F(-s)\, dh_3$$

$$= F(s)\, F(-s)$$

Hence, to achieve the desired exponential-cosine autocorrelation function, a filter with a transfer function

$$F(s) = \sqrt{2(a_1 - a_2 a_3)} \quad \frac{s+a_0}{(s+a_1)^2 + a_2^2}$$

is required. The impulse response f(h) is then

$$f(h) = \frac{1}{2\pi j} \int_{-j\infty}^{+j\infty} e^{sh} F(s)$$

$$= \frac{\sqrt{2(a_1 - a_2 a_3)}}{a_2} \left[(a_0 - a_1)^2 + a_2^2 \right]^{1/2} e^{-a_1 h} \sin(a_2 h + \Psi)\, u_{-1}(h)$$

where $u_{-1}(h)$ is the unit step

$$u_{-1}(h) = \begin{cases} 1 \text{ for } h > 0 \\ 0 \text{ for } h \leq 0, \end{cases}$$

and

$$\Psi = \tan^{-1}\left(\frac{a_2}{a_0 - a_1}\right) .$$

CONVERSION TO TIME SCALE

The above wind-filter impulse-response is expressed in terms of altitude h. The booster control problem is expressed in terms of time t, and it is necessary to change the filter scale to time via the relation

$$h(t) = \int_0^t \dot{h}(t)\, dt$$

where $\dot{h}(t)$ is the vertical component of booster velocity.

The simplest way to do this is to convert the wind filter to state vector form. The transfer function F(s) above can be synthesized on an analog computer with the simulation:

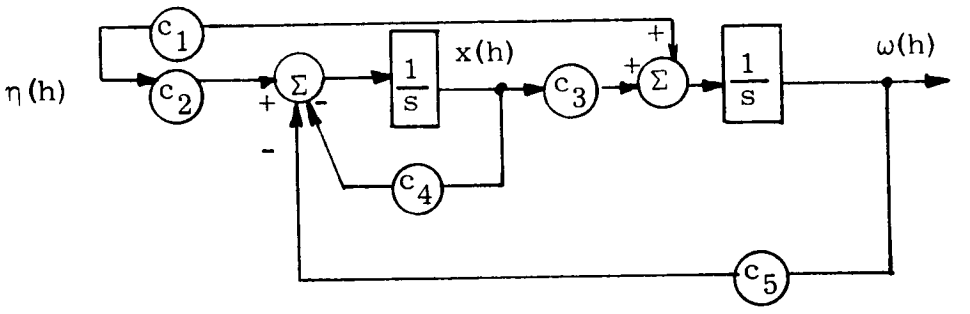

where

$$c_1 = \sqrt{2(a_1 - a_2 a_3}$$

$$c_2 = \sqrt{2(a_1 + a_2 a_3)\,(a_1^2 + a_2^2) - 2a_1 c_1}$$

$$c_3 = 1$$

$$c_4 = 2a_1$$

$$c_5 = \left(a_1^{\,2} + a_2^{\,2}\right)$$

This simulation can be described by the vector differential equation

$$\frac{d}{dh}\begin{bmatrix}\omega(h)\\ x(h)\end{bmatrix} = \begin{bmatrix}0 & c_3\\ -c_5 & -c_4\end{bmatrix}\begin{bmatrix}\omega(h)\\ x(h)\end{bmatrix} + \begin{bmatrix}c_1\\ c_2\end{bmatrix}\eta(h)$$

This, in turn, can be rewritten in the matrix notation

$$\frac{d}{dh}\,[\,z(h)\,] = A[\,z(h)] + B\,\eta(h)$$

The goal of the scale conversion is to find a similar time-scale form

$$\frac{d}{dt}\,[\,z(t)] = F(t)\,z(t) + G(t)\,\eta(t)$$

where $\eta(t)$ is white noise

$$E\left\{\eta(t_1)\;\eta(t_1+t)\right\} = R(t_1)\,\delta(t)\;.$$

Values for F(t), G(t) and R(t) can be found by examining the coefficients of the response-covariance differential equations. Let $\phi(t_1, t_2)$ be the fundamental matrix

$$\frac{d}{dt}\,\phi(t_1, t_2) = F(t_1)\,\phi(t_1, t_2)$$

$$\phi(t_1, t_1) = I.$$

The solution of the time-scale differential equation is

$$z(t) = \phi(t, t_o)\, z(t_o) + \int_o^t \phi(t, \tau)\, G(\tau)\, \eta(\tau)\, d\tau$$

The response covariance matrix is the matrix $E\left\{z(t)\, z(t)'\right\}$, the prime (′) superscript indicating a transpose. That is, the ij^{th} component of this matrix is the expected value of the ith component of the vector $z(t)$ times the jth component of that vector. The response covariance matrix is then

$$E\left\{z(t)z(t)'\right\} = E\left\{\left[\phi(t, t_o)\, z(t_o) + \int_o^t \phi(t, \tau)\, G(\tau)\, \eta(\tau)\, d\tau\right] \bullet \right.$$

$$\left. \bullet \left[z(t_o)'\, \phi(t, t_o)' + \int_o^t \eta(\tau)'\, G(\tau)'\, \phi(t, \tau)'\, d\tau\right]\right\}$$

$$= \phi(t, t_o)\, E\left\{z(t_o)\, z(t_o)'\right\} \phi(t, t_o)'$$

$$+ \int_o^t \int_o^t \phi(t, \tau)\, G(\tau)\, E\left\{\eta(\tau)\, \eta(\rho)'\right\} G(\rho)'\, \phi(t, \rho)'\, d\tau d\rho$$

$$+ \int_o^t \phi(t, t_o)\, E\left\{z(t_o)\, \eta(\tau)'\right\} G(\tau)'\, \phi(t, \tau)'\, d\tau$$

$$+ \int_o^t \phi(t, \tau)\, G(\tau)\, E\left\{\eta(\tau)\, z(t_o)'\right\} \phi(t, t_o)'\, d\tau$$

The last two terms are identically zero because, with a white noise input, present states $[z(t_o)]$ are statistically independent of present and future inputs $[\eta(\tau)]$. Substituting the noise covariance $R(\tau)\, \delta(\rho - \tau)$ into the above produces:

$$E\left\{z(t)\ z(t)'\right\} = \phi(t, t_o)\ E\left\{z(t_o)\, z(t_o)\right\} \phi(t, t_o)'$$
$$+ \int_o^t \phi(t, \tau)\ G(\tau)\ R(\tau)\ G(\tau)'\ \phi(t, \tau)'\ d\tau$$

Differentiating with respect to time produces the covariance differential equation

$$\frac{d}{dt} E\left\{z(t)\ z(t)'\right\} = F(t)\ E\left\{z(t)\ z(t)'\right\} + E\left\{z(t)\, z(t)'\right\} F(t)' + G(t)\, R(t)\, G(t)'$$

A similar derivation with the altitude-scale differential equation produces

$$\frac{d}{dh} E\left\{z(h)\ z(h)'\right\} = AE\left\{z(h)\, z(h)'\right\} + E\left\{z(h)\ z(h)'\right\} A'$$

By application of the chain rule

$$\frac{d}{dt} E\left\{z(t)\ z(t)'\right\} = \left(\frac{d}{dh} E\left\{z(h)\ z(h)'\right\}\right) \frac{dh}{dt}$$

there results

$$F(t) = \dot{h}(t)\ A$$

$$G(t)\ R(t)\ G(t)' = \dot{h}(t)\ BB'.$$

By choosing

$$R(t) = 1$$

then

$$G(t) = \sqrt{\dot{h}(t)}\ B.$$

The wind filter is then

$$\frac{d}{dt}\begin{bmatrix}\omega(t)\\ (t)\end{bmatrix} = \begin{bmatrix}0 & c_3\dot{h}\\ -c_5\dot{h} & -c_4\dot{h}\end{bmatrix}\begin{bmatrix}\omega(t)\\ x(t)\end{bmatrix} + \begin{bmatrix}c_1\varepsilon\sqrt{\dot{h}}\\ c_2\varepsilon\sqrt{\dot{h}}\end{bmatrix}\eta(t)$$

where

$$E\left\{\eta(t_1)\ \eta(t_2)'\right\} = \delta(t_1-t_2)\ .$$

APPENDIX C

DISTRIBUTED AERODYNAMIC (TRANSVERSE) STRIP FORCES FOR A LAUNCH VEHICLE

In this appendix, data for the "Model Vehicle No. 2" are modified to exhibit aerodynamic forces distributed along the length of the vehicle. This modification eliminates unrealistic impulses in bending-moment-rate due to step winds. The distributed loads can be approximated by adding more dynamics to the plant representation.

The data package for "Model Vehicle No. 2" uses a lumped model approximation of the distributed aerodynamic forces. The lumped model seriously neglects gust penetration dynamics. In particular, it estimates infinite bending-moment-rates due to step winds. To eliminate this anomaly, an integration that was performed in developing the lumped model is left undone. Some "finagle" factors are introduced to permit using inconsistent aerodynamic data. Unsteady aerodynamic loads are estimated by the use of simple theories and consistency with static loads is enforced by use of the finagle factors.

The objective for the model developed here is a model that will yield qualitatively correct trends for the load alleviation study. The model is the simplest that can be conceived. Results obtained from synthesizing load alleviation controls for this model should be interpreted with caution and should be used to determine the next iteration on the model.

The equations are derived on the assumption that, at a given flight condition (dynamic pressure and Mach number), the aerodynamic load at a point on the vehicle is due solely to the motion of that point. Integrating these loads across the vehicle yields the force on a transverse strip. Herein, the unsteady aerodynamic forces are computed from Newtonian Impact Theory (Ref. 13) and Piston Theory (Ref. 14) in a manner that is consistent with the lumped parameter data for Model Vehicle No. 2 supplied by NASA (Ref. 1).

Impact Theory is used to estimate the unsteady aerodynamic loads over the portion of the vehicle where there is axial symmetry. Modified first-order piston theory is used to estimate the unsteady aerodynamic loads over the finned portion of the vehicle. Modifications consist of replacing the Mach number effect of Piston Theory with the Prandtl-Ackert and Prandtl-Glauert correction factors for supersonic and subsonic speeds. Transonically the factors are limited to 2. Fin-trip leakage at supersonic speeds is estimated by using a linear variation between the tip and the Mach cone.

Consistency between Model Vehicle No. 2 data and the unsteady aerodynamic loads estimated by the above procedure is developed by enforcing agreement between the old and revised models for constant wind gusts.

The unsteady loads are summarized next. The finagle factors are then presented. Following the presentation of the finagle factors there is a discussion lumping the distributed loads. The air loads are then derived.

AIR LOADS

The normal air load on a transverse strip at station x is called $\tilde{t}_o$; it is the integral of the pressure across the vehicle at station x. The integral of $\tilde{t}$ from tail to nose would yield the total normal force. Estimated $\frac{1}{q}\frac{dt_o}{d\alpha}$ (called $\frac{1}{q}\frac{d\tilde{t}_o}{d\alpha}$) is tabulated below; q is dynamic pressure in kg/m^2, α is the angle of attack in radians, M_A is Mach number, and $\tilde{t}_o$ is the estimated transverse force in kg/m.

$$\frac{1}{q}\frac{d\tilde{t}_o}{d\alpha} = 21.223 - 2.45x \qquad \text{for } 0.63 \leq x \leq 1.63$$

$$= \frac{4}{\sqrt{1-M_A^2}}\left\{9.17\right\} \qquad \text{for } M_A < \frac{\sqrt{3}}{2} \text{ and for } 1.63 < x \leq 2.54$$

$$= 8 \quad 9.17 - \frac{(2M_A - \sqrt{3})}{(\sqrt{5} - \sqrt{3})} \frac{3.14 - x}{\sqrt{\frac{5}{4} - 1}} \Bigg\} \quad \text{for } \sqrt{\frac{3}{2}} \leq M_A \leq \sqrt{\frac{5}{2}} \text{ and for } 1.63 < x \leq 2.54$$

$$= \frac{4}{\sqrt{M_A^2 - 1}} \left\{ 9.17 - \frac{3.14 - x}{\sqrt{M_A^2 - 1}} \right\} \quad \text{for } \sqrt{\frac{5}{2}} < M_A \quad \text{and for } 1.63 < x \leq 2.54$$

$$\frac{1}{q} \frac{d\tilde{t}_o}{d\alpha} = \frac{4}{\sqrt{1 - M_A^2}} \left\{ 19.22 \right\} \quad \text{for } M_A < \sqrt{\frac{3}{2}} \quad \text{and for } 2.54 < x \leq 3.14$$

$$= 8 \left\{ 19.22 - \frac{(2M_A - \sqrt{3})}{(\sqrt{5} - \sqrt{3})} \frac{3.14 - x}{\sqrt{\frac{5}{4} - 1}} \right\} \quad \text{for } \sqrt{\frac{3}{2}} \leq M_A \leq \sqrt{\frac{5}{2}} < M \text{ and for } 2.54 \leq x \leq 3.14$$

$$= \frac{4}{\sqrt{M_A^2 - 1}} \left\{ 19.22 - \frac{3.14 - x}{\sqrt{M_A^2 - 1}} \right\} \quad \text{for } \sqrt{\frac{5}{2}} < M_A \quad \text{and for } 2.54 \leq x \leq 3.14$$

$$\frac{1}{q} \frac{d\tilde{t}_o}{d\alpha} = \frac{4}{\sqrt{1 - M_A^2}} \left\{ 31.26 - 3.805x \right\} \quad \text{for } M_A < \sqrt{\frac{3}{2}} \quad \text{and for } 3.14 < x \leq 5.05$$

$$= 8 \left\{ 31.26 - 3.805x \right\} \quad \text{for } \sqrt{\frac{3}{2}} \leq M_A \leq \sqrt{\frac{5}{2}} \text{ and for } 3.14 < x \leq 5.05$$

$$= \frac{4}{\sqrt{M_A^2 - 1}} \left\{ 31.26 - 3.805x \right\} \quad \text{for } \sqrt{\frac{5}{2}} < M_A \quad \text{and for } 3.14 < x \leq 5.05$$

$$= 21.6056 - 2.455x \quad \text{for } 5.05 < x \leq 8.32$$

$$= 1.1850 \quad \text{for } 8.32 < x \leq 84.08$$

$$= 7.28 - 0.1830 \left\{ x - 84.08 \right\} \quad \text{for } 84.08 < x \leq 90.31$$

$$= 0.9875 \quad \text{for } 90.31 < x \leq 122.09$$

$$= 15.82 - 0.448\{x-122.09\} - 0.092\{x-122.09\}^2 \qquad \text{for } 122.09 < x \leq 126.51$$

$$= 0.6583 \qquad \text{for } 126.51 < x \leq 142.30$$

$$= 3.91\{144.86 - x\} \qquad \text{for } 142.30 < x \leq 144.86$$

FINAGLE FACTORS

If there were no other aerodynamic data for Model Vehicle No. 2 than the estimates just presented, they would be used without modification. The data packages do present the side-force derivative, center of pressure, and bending moments at some flight conditions. The transverse-strip estimates and the gross data are reconciled by introducing three finagle factors. These finagle factors are functions of Mach number and dynamic pressure (flight condition). They enforce agreement for steady-state conditions. Once the factors are known, the strip estimates for use in the heave, pitch, and moment equations become

$$\frac{d\tilde{t}_1}{d\alpha} = (ff)_1 \frac{d\tilde{t}_o}{d\alpha}$$

$$\frac{d\tilde{t}_2}{d\alpha} = (ff)_2 \frac{d\tilde{t}_o}{d\alpha}$$

$$\frac{d\tilde{t}_3}{d\alpha} = (ff)_3 \frac{d\tilde{t}_o}{d\alpha}$$

where

$$(ff)_1 = \frac{\left|\frac{N}{M}\right|^1_m}{\int_{x_T}^{x_N} \frac{d\tilde{t}_o}{d\alpha}\, dx}$$

$$(ff)_2 = \frac{-c_1 I_{xx}}{\int_{x_T}^{x_N} \frac{d\tilde{t}}{d\alpha}(x - x_{cg})\, dx}$$

$$(ff)_3 = \frac{M'_\alpha}{V} \div \left\{ \int_{x_T}^{x} \left[- \frac{d\tilde{t}_o}{d\alpha} \frac{(x - x')}{V} \right] \right\} dx' + \int_{x_T}^{x} M'(x - x') \int_{x_T}^{x_N} \frac{d\tilde{t}_o}{d\alpha} \frac{1}{V} \cdot$$

$$\cdot \left[\frac{(ff)_2}{m} (x'' - x_{cg})(x' - x_{cg}) + \frac{(ff)_1}{m} \right] dx'' \Bigg\} dx'$$

The first two factors are presented in Figures C-1 and C-2. These figures indicate the distributed estimates are reasonably accurate for slow motions.

LUMPING THE LOADS

The equations previously presented may be revised to replace the distributed air loads with equivalent lumped-parameter dynamic load build-up functions. This would permit replacing the lumped-parameter representation that has been used with one of higher order that correctly represents the distributed air load. The revised equations would not display impulses in bending-moment rate due to step winds.

The estimation of the lumped-parameter model for the side force will be used to illustrate the procedure.

Figure C-3 presents the unsteady air load at the high-dynamic-pressure flight condition. Integrating this and normalizing yields the normalized step response for side force as presented in Figure C-4. The rapid changes in load are due to the nose cone, first and second cone frustrum transition sections, and the fins.

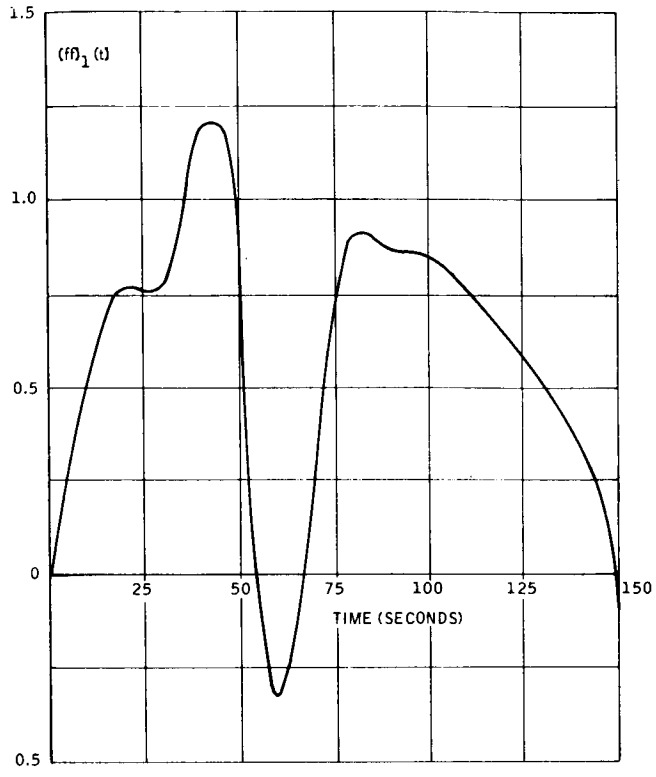

Figure C-1
$(ff)_1(t)$ versus Time

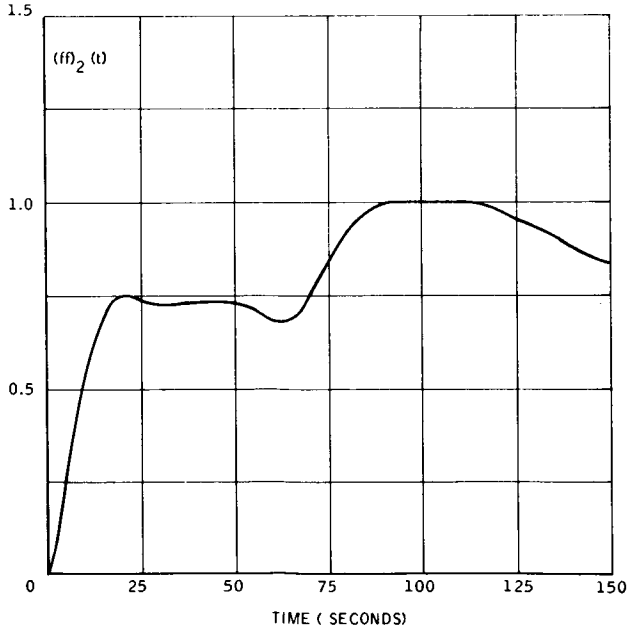

Figure C-2
$(ff)_2(t)$ versus Time

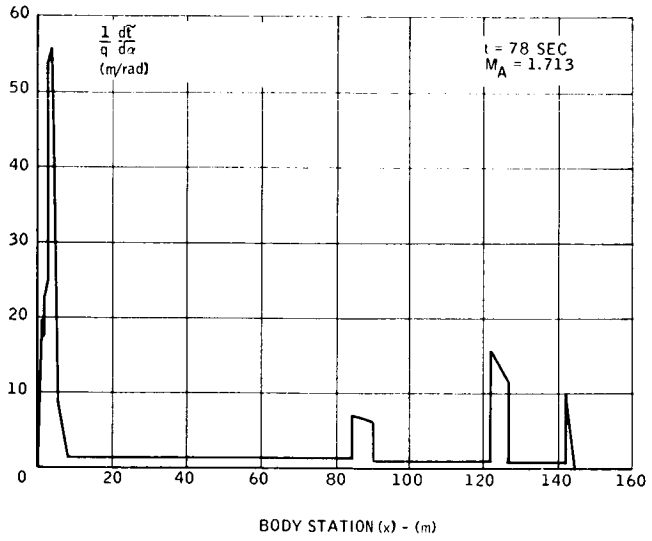

Figure C-3. Unsteady Air Loads

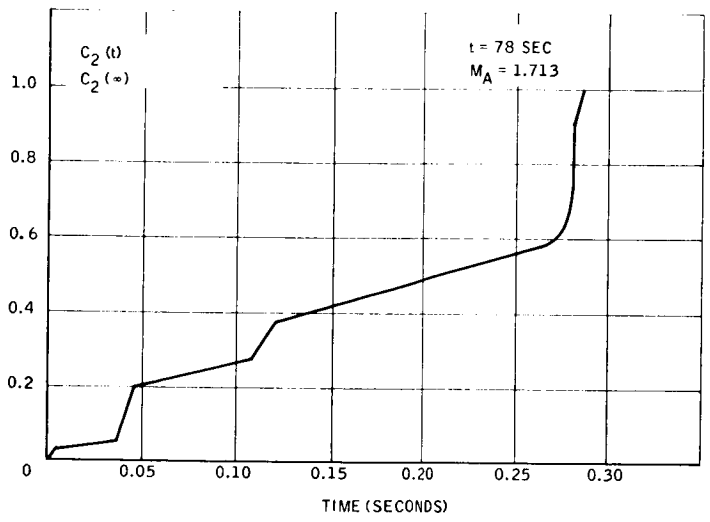

Figure C-4. Normalized Side-Force Step Response

The lumping problem is thus the approximation of the step response of Figure C-4 with dynamics that have a similar step response. Once the form of the approximating dynamics have been determined, optimization of the parameters can be accomplished in a straightforward manner.

ESTIMATION OF UNSTEADY AIR LOADS

The sources of and approximations to the aerodynamic theories are discussed first. These results are then used to estimate the loads on the two and three dimensional parts of the vehicle.

Aerodynamic Theories

Piston theory is the basis for estimating the loads over the two-dimensional (finned) regions and impact theory is used for the three-dimensional axially symmetric regions.

Two-Dimensional -- First-order piston theory (Ref. 15) states that the unsteady pressure difference Δp across a two-dimensional surface at high Mach number is given by

$$\Delta p = \frac{4}{M_A} q\alpha \tag{C. 1}$$

The average steady-state Δp for thin airfoils at supersonic speeds is given by the Prandtl-Ackert expression

$$\Delta p = \frac{4}{\sqrt{M_A^2 - 1}} q\alpha \tag{C. 2}$$

and for subsonic speeds by the Prandtl-Glauert

$$\Delta p = \frac{C_{L_{\alpha_o}}}{\sqrt{1 - M_A^2}} 2q\alpha \qquad \text{(C-3)}$$

Considering the fin aspect ratio and present intentions it seems reasonable to take $C_{L_{\alpha_o}} = 4$.

Equations (C. 2) and (C. 3) agree at Mach 1. Equations (C. 1) and (C. 2) are about equal at high Mach numbers. It thus appears reasonable to replace M_A in Equation (C. 1) by $\sqrt{\left| M_A^2 - 1 \right|}$.

At unity Mach number $\sqrt[2]{\left| M_A^2 - 1 \right|}$ goes to infinity, and it is larger at all transonic speeds than experiments show. The Prandtl correction factors will be arbitrarily truncated at 2. Hence, the final two-dimensional piston theory pressure difference will be taken as

$$\Delta p = \begin{cases} \dfrac{4}{\sqrt{\left| M_A^2 - 1 \right|}} q\alpha & \text{if } \dfrac{1}{\sqrt{\left| M_A^2 - 1 \right|}} < 2 \\ 8\, q\alpha & \text{if } \dfrac{1}{\sqrt{\left| M_A^2 - 1 \right|}} \geq 2 \end{cases} \qquad \text{(C. 4)}$$

Tip leakage is assumed to be lumped in $C_{L_\alpha} = 4$ for $M_A < \frac{\sqrt{3}}{2}$. For $M_A > \frac{.5}{2}$ tip leakage is accounted for by linearly reducing the Δp calculated by Equation (C. 4) by the inboard Mach line and the fin tip, i.e.,

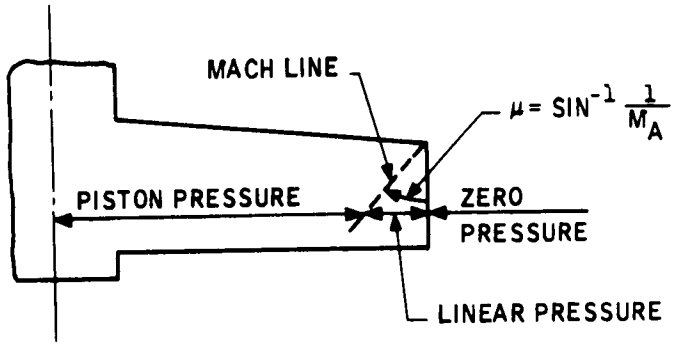

For $\sqrt{3}/2 < M_A < \sqrt{5}/2$ tip leakage is assumed to vary linearly.

Three-Dimensional -- The air loads on the axially symmetric and engine shroud parts of the body are calculated from impact theory (Ref. 14) which estimates the pressure on unshielded portions (unobstructed line of sight to the relative wind) as

$$p = \rho V_N^2 \tag{C. 5}$$

where

ρ is the air density

V_N is air velocity normal to the surface

the pressure on shielded portions is taken as zero

Vehicle Dimensions

The vehicle dimensions are assumed to be those presented in Figure C-5; this comes from page 53 of Reference 13.

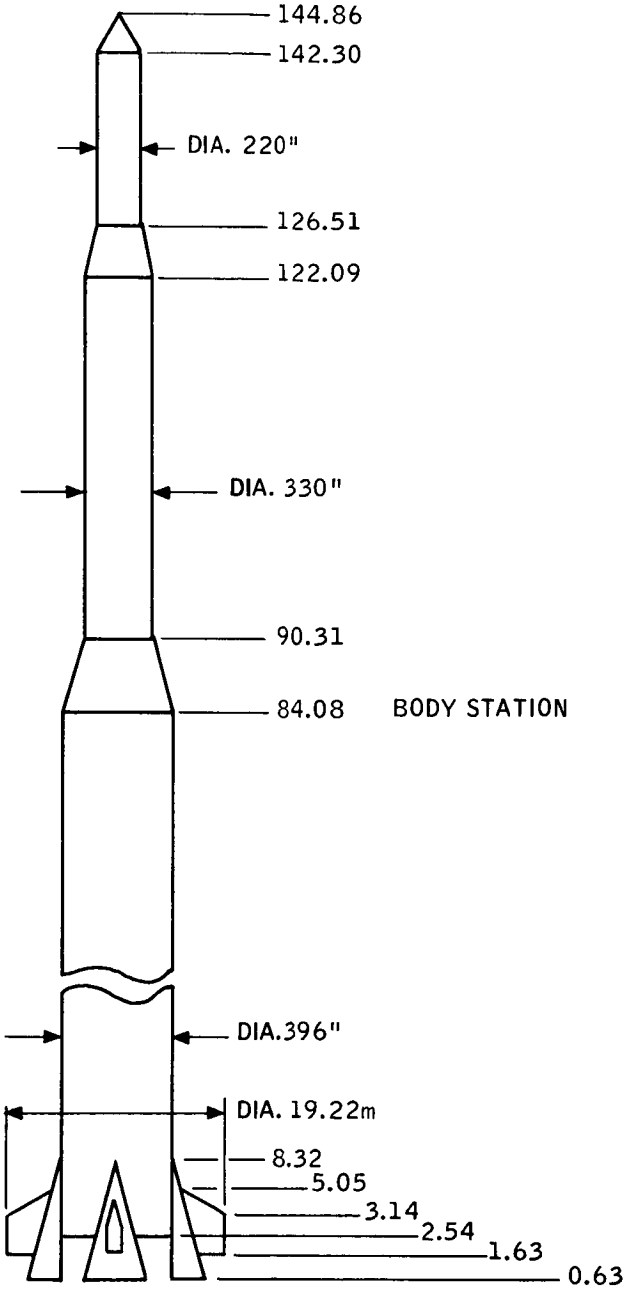

Figure C-5. Model Vehicle No. 2

Impact theory is used to estimate air loads on the parts of the vehicle except for those between 1.63 and 5.05. Two two-dimensional area excludes the 396-inch strip between body stations 1.63 and 2.54.

Two-Dimensional

Application of the piston theory results presented in Equation (C.4) to the geometry just defined is immediate. The results are presented in the equations for body stations 1.63 to 5.05 under "Air Loads".

Three-Dimensional

The application of impact theory to unsteady air loads estimation is presented in detail in order to display some assumptions made. The order of presentation is nose cone, cylindrical sections, transition sections, and shrouds and aft body.

None Cone -- The surface of the cone in rectangular coordinate is:

$$f(\zeta, \eta, \zeta) = \zeta^2 + \eta^2 - \zeta^2 \tan^2 \theta = 0 \qquad \text{(C. 6)}$$

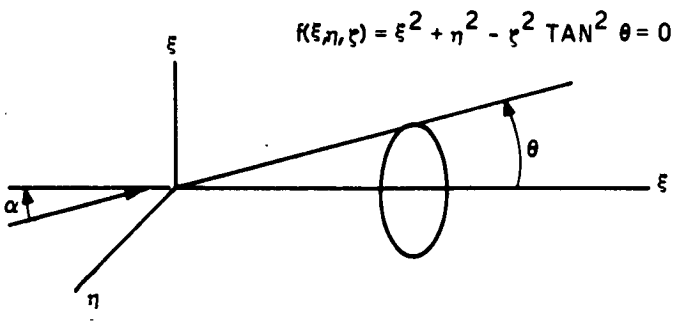

To integrate pressures around the cone, it is desirable to use polar coordinates

$$\xi = \zeta \sin\omega \tan\theta$$

$$\eta = \zeta \cos\omega \tan\theta. \qquad \text{(C. 7)}$$

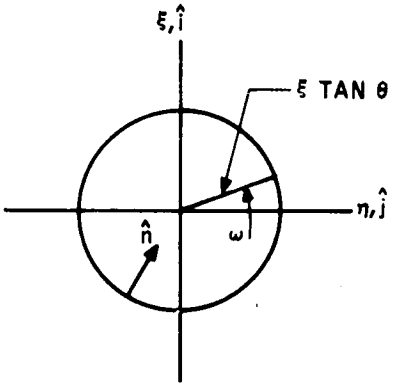

The unit inward normal to the cone is

$$\hat{n} = \frac{\nabla f}{|\nabla f|} = \frac{-\xi\hat{i} - \eta\hat{j} + \zeta\tan^2\theta\hat{k}}{\sqrt{\xi^2 + \eta^2 + \zeta^2 \tan^4\theta}}$$

$$= -\cos\theta \sin\omega\hat{i} - \cos\theta \cos\omega\hat{j} + \sin\theta\hat{k} \qquad \text{(C. 8)}$$

The wind vector is taken in the $\xi - \zeta$ plane so

$$\bar{V} = V \sin\alpha\hat{i} + V \cos\alpha\hat{k} \qquad \text{(C. 9)}$$

The velocity and pressure normal to the cone are

$$\bar{V}_n = (\bar{V}\cdot\hat{n})\hat{n} = V_n\hat{n} = V(-\sin\alpha \cos\theta \sin\omega + \cos\alpha \sin\theta)\hat{n} \qquad \text{(C. 10)}$$

$$(\bar{V}\cdot\hat{n})^2 = \frac{V^2(\sin^2\omega \sin^2\alpha - 2\sin\omega \sin\alpha \cos\alpha \tan\theta + \cos^2\alpha \tan^2\theta)}{\sec^2\theta} \qquad \text{(C. 11)}$$

$$\bar{p} = \rho V_n^2 \hat{n} \qquad \text{(C. 12)}$$

For $\bar{p}$ it was assumed that $|\alpha| \leq |\theta|$ so the formula is valid around the entire cone; no part of the surface lies in the shadow.

The ζ running load $(\tilde{t})$ in the ξ direction is the integral of the component of pressure in the ξ direction

$$\tilde{t} = -\int_{\zeta\tan\theta}^{-\zeta\tan\theta} \bar{p}\cdot\tilde{i}\, d\eta + \int_{-\zeta\tan\theta}^{\zeta\tan\theta} \bar{p}\cdot\hat{i}\, d\eta$$

$$= +2\ q \frac{\sin\theta}{\sec^2\theta}\ \zeta \left\{ \int_0^{\pi} f(\alpha, \theta, \omega)\, d\omega - \int_{\pi}^{2\pi} f(\alpha, \theta, \omega)\, d\omega \right\} \tag{C. 13}$$

where

$$f(\alpha, \theta. \omega) = -\sin^2\alpha \sin^4\omega + 2 \sin\alpha \cos\alpha \tan\theta \sin^3\omega - \cos^2\alpha \tan^2\theta \sin^2\omega$$

The integral

$$\int_{\omega_L}^{\omega_u} f(\alpha, \theta, \omega)\, d\omega = -\sin^2\alpha \left\{ -\frac{\sin^3\omega \cos\omega}{4} - \frac{3}{8} \cos\omega \sin\omega + \frac{3}{8}\omega \right\}_{\omega_L}^{\omega_u}$$

$$+ 2 \sin\alpha \cos\alpha \tan\theta \left\{ -\frac{1}{3} \cos\omega(\sin^2\omega + 2) \right\}_{\omega_L}^{\omega_u}$$

$$- \cos^2\alpha \tan^2\theta \left\{ -\frac{1}{2} \cos\omega \sin\omega + \frac{\omega}{2} \right\}_{\omega_L}^{\omega_u} \tag{C. 14}$$

Hence, for the nose cone

$$\tilde{t} = q\zeta\ \frac{16}{3}\ \frac{\sin^2\theta}{\sec\theta}\ \sin 2\alpha \tag{C. 15}$$

$$\frac{d\tilde{t}}{d\alpha} = q\zeta\ \frac{32}{3}\ \frac{\sin^2\theta}{\sec\theta}\ \cos 2\alpha \tag{C. 16}$$

Figure C-5 indicates the nose cone is between $142.30 < x \leq 144.86$

The cone semi-angle θ is

$$\theta - \tan^{-1} \frac{\frac{110}{39.37}}{2.56} \cong 47.6°$$

so for small α

$$\frac{1}{\bar{q}} \frac{d\tilde{t}}{d\alpha} = (3.91)(144.86 - x) = 566.4026 - 3.91x \tag{C.17}$$

for

$$142.30 < x \leq 144.86$$

Cylindrical Sections

The surfaces of the cylinders in rectangular coordinates are taken as

$$f(\xi, \eta, \zeta) = 0 = \xi^2 + \eta^2 - R^2 \tag{C.18}$$

The surfaces in polar coordinates are

$$\begin{aligned} \xi &= R \sin \omega \\ \eta &= R \cos \omega \end{aligned} \tag{C.19}$$

The unit inward normal to a cylinder is

$$\hat{n} = \frac{\nabla f}{|\nabla f|} = \frac{-\xi \hat{i} - \eta \hat{j}}{\sqrt{\xi^2 + \eta^2}}$$

$$= - \sin \omega \hat{i} - \cos \omega \hat{j} \tag{C.20}$$

The wind vector is taken in the $\xi - \zeta$ plane so $\bar{V} = V \sin \alpha \hat{i} + V \cos \alpha \hat{k}$
The velocity and pressure normal to a cylinder

$$\bar{V}_n = (-\bar{V} \cdot \hat{n}) \hat{n} = V_n \hat{n} = (-V \sin \alpha \sin \omega) \hat{n} \tag{C.21}$$

$$(\bar{V} \cdot \hat{n})^2 = V^2 \sin^2 \alpha \sin^2 \omega \tag{C.22}$$

$$\bar{p} = \begin{cases} 0 & \text{if } \sin\alpha \sin\omega \geq 0 \\ \rho V_n^2 \hat{n} = \rho V^2 \sin^2\alpha \sin^2\omega \hat{n} & \text{if } \sin\alpha \sin\omega \leq 0 \end{cases} \tag{C.23}$$

The pressure formula indicates that pressures on the backside is taken as zero.

The ζ running load in the ξ direction is the integral of the component of pressure in the ξ direction

$$\tilde{t} = -\int_{R}^{-R} \bar{p} \cdot \hat{i}\, d\eta + \int_{-R}^{R} \bar{p} \cdot \hat{i}\, d\eta$$

$$= +R\int_{0}^{\pi} \bar{p} \cdot \hat{i} \sin\omega\, d\omega - R\int_{\pi}^{2\pi} \bar{p} \cdot \hat{i} \sin\omega\, d\omega \tag{C.24}$$

If $\alpha > 0$, the first integral on the right is zero; if $\alpha < 0$, the second integral on the right is zero.

So for $\alpha > 0$

$$\tilde{t} = q\, D \sin^2\alpha \int_{\pi}^{2\pi} \sin^4\omega\, d\omega$$

$$= q\, D \sin^2\alpha \left\{ -\frac{\sin^3\omega \cos\omega}{4} - \frac{3}{8}\cos\omega + \frac{3}{8}\omega \right\}_{\pi}^{2\pi}$$

$$= q\, D \frac{3\pi}{8} \sin^2\alpha \tag{C.25}$$

for $\alpha \geq 0$

For any α

$$\tilde{t} = q D \frac{3\pi}{8} \sin^2 \alpha \text{ sign } \alpha \tag{C.26}$$

This infamous result will be linearized and agreement will be enforced at 0.1 radian so

$$\frac{1}{q} \frac{d\tilde{t}}{d\alpha} \cong D \frac{0.3\pi}{8} \tag{C.27}$$

From this and Figure C-3

$$\frac{1}{q} \frac{d\tilde{t}}{d\alpha} = 0.6583 \text{ for } 126.51 < x \leq 142.20 \tag{C.28}$$

$$\frac{1}{q} \frac{d\tilde{t}}{d\alpha} = 0.9875 \text{ for } 90.31 < x \leq 122.09 \tag{C.29}$$

$$\frac{1}{q} \frac{d\tilde{t}}{d\alpha} = 1.1850 \text{ for } 8.32 < x \leq 84.08 \tag{C.30}$$

Transition Sections -- The difference in the impact pressure formulae between the cone frustrum transition sections and the nose cone is in the shielding on the former:

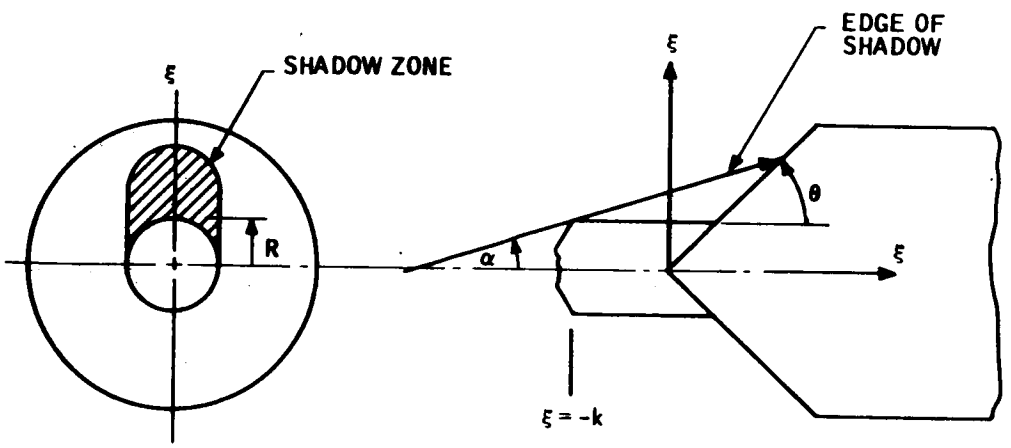

Again assuming the cone angle is greater than the angle of attack ($\theta > \alpha$), it is seen that the nose cone formula, (C-13), previously developed can be used except the area of integration should not include the shadow zone of the sketch.

The edge of the shadow is

$$\pi^2 + (\xi - [k + \zeta] \tan \alpha)^2 - R^2 = 0 \tag{C. 31}$$

The polar coordinates of the surface of the cone are

$$\xi = \zeta \sin \omega \tan \theta \tag{C. 32}$$

$$\eta = \zeta \cos \omega \tan \theta$$

Thus, the intersection of the edge of the shadow and the cone frustrum is given by

$$\omega_s = \sin^{-1} \frac{\zeta^2 \tan^2 \theta + [k + \zeta]^2 \tan^2 \alpha - R^2}{2\zeta [k + \zeta] \tan \alpha \tan \theta} \tag{C. 33}$$

where

$$0 \leq \omega_s \leq \pi/2.$$

This and Equation (C. 13) yield

$$\tilde{t} = 2q \frac{\sin \theta}{\sec^2 \theta} \zeta \left\{ \int_0^{\pi} f(\alpha, \theta, \omega)\, d\omega - \int_{\pi}^{2\pi} f(\alpha, \theta, \omega)\, d\omega - \int_{\omega_s}^{\pi - \omega_s} f(\alpha, \theta, \omega)\, d\omega \right\} \tag{C. 34}$$

This could be differentiated with respect to α, but it is sufficient for present purposes to develop numerical results. As for the cylinder, it will be assumed adequate to linearize and to take the derivative such that $\tilde{t}$ is correct at an angle of attack of 0. 1 radian.

$$\tilde{t} = q\zeta \left\{ \frac{16}{3} \frac{\sin^2\theta}{\sec\theta} \sin 2\alpha \left[1 - \frac{1}{4} \cos \omega_s (\sin^2\omega_s + 2) \right] \right.$$

$$+ 2 \frac{\sin\theta}{\sec^2\theta} \sin^2\alpha \left[\sin 2\omega_s \left(\frac{1}{4} \sin^2 \omega_s + \frac{3}{8}\right) + \frac{3}{8} (\pi - 2\omega_s) \right]$$

$$\left. + \sin^3\theta \cos^2\alpha \left[\sin 2\omega_s + \pi - 2\omega_s \right] \right\} \qquad \text{(C. 35)}$$

There are two cone frustrums to which the above formulae [Equations (C. 33) and (C. 35)] are to be applied. Figure C-5 puts the front one between 122. 09 and 125. 51 and the aft one between 84. 08 and 90. 31. The sketch below (taken from Figure C-5) shows that the aft cone frustrum is affected only by the cylindrical section between stations 90. 31 and 122. 09; the cylinder between 126. 51 and 142. 30 meters does not shadow the aft cone frustrum.

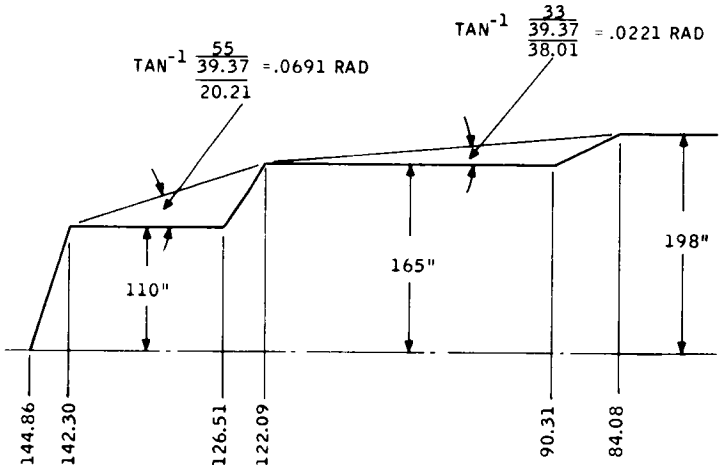

The sketch and Equations (C. 33) and (C. 35) yield:

x (m)	ζ (m)	ω_s (deg)	$\frac{1}{q}\frac{d\tilde{t}}{d\alpha}$
126. 51	8. 84	16. 45	12. 04
125. 04	10. 31	30. 90	13. 65
123. 56	11. 79	43. 20	15. 02
122. 09	13. 26	54. 40	15. 82
90. 31	31. 15	22. 40	6. 14
88. 23	33. 23	27. 40	6. 52
86. 16	35. 30	31. 70	6. 90
84. 09	37. 38	34. 70	7. 28

These data can be approximated by

$$\frac{1}{q}\frac{d\tilde{t}}{d\alpha} = 15.82 - 0.448\left\{x - 122.09\right\} - 0.092\left\{x - 122.09\right\}^2 \qquad \text{(C. 36)}$$

for $122.09 < x \leq 126.51$ and

$$\frac{1}{q}\frac{d\tilde{t}}{d\alpha} = 7.28 - 0.1830\left\{x - 84.08\right\} \qquad \text{(C. 37)}$$

for $84.08 < x \leq 90.31$

Engine Shrouds and Aft Body -- The shrouds are assumed to be cones centered about the control engines. This permits estimating the loads (less the fin loads) by use of the cone and cylinder formulae if the angles ω_o, ω_1, ω_2, ω_3, and ω_4 are known.

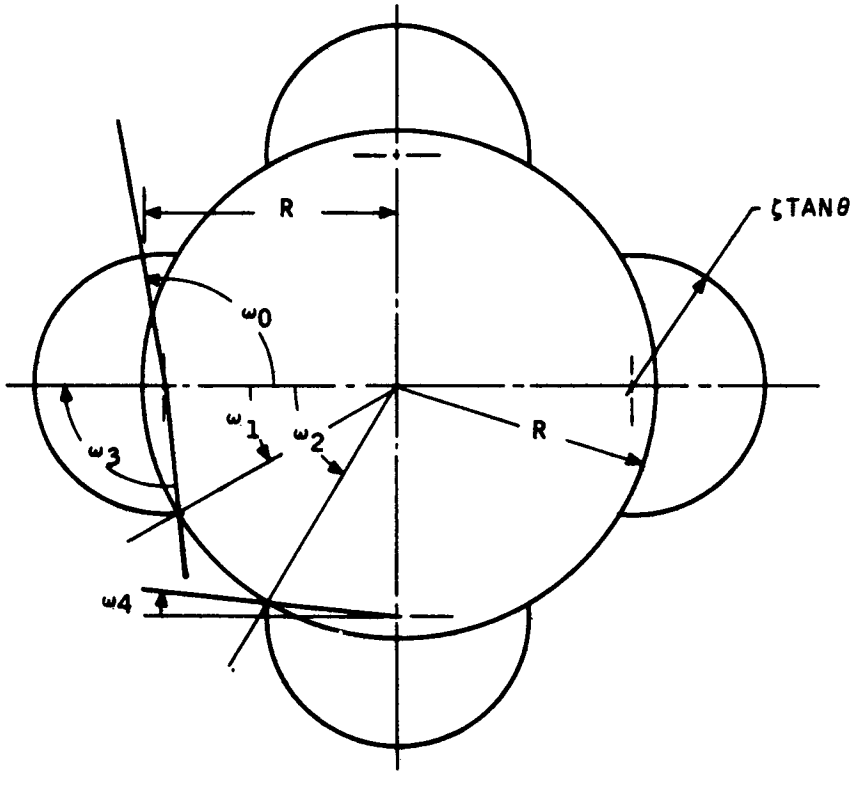

It is assumed the crosswise component of the wind is coming from below. The upward pressures on the cones and the cylinder are given by

$$\tilde{t} = 2q \frac{\sin\theta}{\sec^2\theta} \zeta \left\{ +\int_{\omega_o}^{\pi} 2 - \int_{\pi}^{\pi+\omega_3} 2 + (\text{sign}\,\omega_4)\int_0^{\omega_4} 2 - \int_{\pi}^{2\pi} +1 \right\} f(\alpha, \theta, \omega)\,d\omega \quad \text{(C. 38)}$$

$$\tilde{t} = q\,2R\,\sin^2\alpha \int_{\pi+\omega_1}^{\pi+\omega_2} \sin^4\omega\,d\omega$$

$$= q\,4R\,\sin^2\alpha \left\{ -\frac{1}{16}\sin 4\omega_1 + \frac{3\pi}{16} - \frac{3\omega_1}{4} \right\} \quad \text{(C. 39)}$$

The above will be evaluated at an angle of attack of 0. 1 radian and the assumption will be made again that the derivatives are linear and agree at 0. 1 radian. At 0. 1 radian the top of the side cones between the body and the horizontal tangent is shielded by the side of 396-inch section. The top of the cylinder and the entire top engine shroud are shielded from the air blast.

Impact pressures will be determined at four equidistant points along the cone shrouds and aft cylindrical section:

x (m)	ζ (m)	$\frac{1}{q}\frac{d\tilde{t}}{d\alpha}$	ω_o (deg)	ω_1 (deg)	ω_2 (deg)	ω_3 (deg)	ω_4 (deg)
8. 320	1. 352	0. 0	180. 00			0. 0	-90. 00
5. 757	3. 915	6. 91	110. 25			76. 5	-13. 5
3. 193	6. 479	13. 38	102. 08			89. 35	- 0. 65
0. 630	9. 042	19. 68	98. 62			97. 65	+ 7. 65
8. 320	1. 352	1. 180		00. 00	90. 00		
6. 390	3. 279	0. 8160		10. 50	79. 50		
4. 470	5. 205	0. 5930		17. 60	72. 40		
2. 540	7. 132	0. 3545		26. 60	63. 40		

The top data are for the engine shrouds and the lower are for the cylinder. These loads were combined to develop the load equations for $0.63 < x < 1.63$ and for $5.05 < x < 8.32$. The equations are presented in the "Air Loads" subsection.

CONCLUSIONS

Simple air loads estimates have been made. They should prove satisfactory for developing qualitative conclusions on the effects of gust penetration in load relief control.

APPENDIX D
VECTOR DIFFERENTIAL EQUATIONS

In this appendix, the vehicle and wind filter equations described in Section II are written in the first-order vector equation form

$$\dot{x} = F(t)\,x(t) + G_1(t)\,u(t) + G_2(t)\,\eta(t) + G_3(t)\,\bar{v}_\omega(t)$$

$$r(t) = H_1(t)\,x(t) + D_1(t)\,u(t) + D_2(t)\,\bar{v}_\omega(t)$$

CONSTANT-ANGLE-OF-ATTACK CASE

The case where the angle of attack is assumed constant over vehicle length reduces to a seventh-order system. The above equations are

$$\begin{bmatrix} \ddot{\phi} \\ \dot{x} \\ \ddot{z} \\ \dot{\theta} \\ \dot{\phi} \\ \dot{\omega} \\ \dot{z} \end{bmatrix} = \begin{bmatrix} 0 & 0 & \frac{-N\ell cp}{I_{xx}V} & \frac{-x_{cg}R}{I_{xx}} & \frac{-N\ell cp}{I_{xx}} & \frac{N\ell cp}{I_{xx}V}H & 0 \\ 0 & -\dot{h}c_4 & 0 & 0 & 0 & -\dot{h}c_5 & 0 \\ 0 & 0 & \frac{-N}{mV} & \frac{R}{m} & \frac{F-X}{m} + \frac{N}{m} & \frac{N}{mV}H & 0 \\ 0 & 0 & 0 & -14.6 & 0 & 0 & 0 \\ 1 & 0 & 0 & 0 & 0 & 0 & 0 \\ 0 & \dot{h} & 0 & 0 & 0 & 0 & 0 \\ 0 & 0 & 1 & 0 & 0 & 0 & 0 \end{bmatrix} \begin{bmatrix} \dot{\phi} \\ x \\ \dot{z} \\ \theta \\ \phi \\ \omega \\ z \end{bmatrix} + \begin{bmatrix} 0 \\ 0 \\ 0 \\ 14.6 \\ 0 \\ 0 \\ 0 \end{bmatrix} u + \begin{bmatrix} \frac{N\ell cp}{I_{xx}V} \\ 0 \\ \frac{N}{mV} \\ 0 \\ 0 \\ 0 \\ 0 \end{bmatrix} \bar{v}_\omega + \begin{bmatrix} 0 \\ c_2\sqrt{\dot{h}} \\ 0 \\ 0 \\ 0 \\ c_1\sqrt{\dot{h}} \\ 0 \end{bmatrix} \eta$$

$$
\begin{bmatrix} \beta \\ \dot{\beta} \\ I_b \\ \dot{I}_b \\ \dot{\phi}+0.388\alpha \\ z \\ \dot{z} \end{bmatrix}
=
\begin{bmatrix}
0 & 0 & 0 & 1 & 0 & 0 & 0 \\
0 & 0 & 0 & -14.6 & 0 & 0 & 0 \\
0 & R_x & \frac{-M_\alpha'}{V} & M_\beta' & M_\alpha' & \frac{M_\alpha' H}{V} & 0 \\
R_{\dot{\phi}} & 0 & R_{\dot{z}} & R_\beta & R_\phi & R_\omega & 0 \\
1 & 0 & \frac{-0.388}{V} & 0 & 0.388 & \frac{0.388H}{V} & 0 \\
0 & 0 & 0 & 0 & 0 & 0 & 1 \\
0 & 0 & 1 & 0 & 0 & 0 & 0
\end{bmatrix}
\begin{bmatrix} \phi \\ x \\ \dot{z} \\ \beta \\ \phi \\ \omega \\ z \end{bmatrix}
+
\begin{bmatrix} 0 \\ 14.6 \\ 0 \\ 14.6M_\beta \\ 0 \\ 0 \\ 0 \end{bmatrix} u +
\begin{bmatrix}
0 & 0 \\
0 & 0 \\
\frac{M_\alpha'}{V} & 0 \\
R_V & \frac{M_\alpha'}{V} \\
\frac{0.388}{V} & 0 \\
0 & 0 \\
0 & 0
\end{bmatrix}
\begin{bmatrix} \bar{v}_\omega \\ \dot{\bar{v}}_\omega \end{bmatrix}
$$

where

$$R_{\dot{\phi}} = \frac{-M_\alpha'}{V}$$

$$R_x = \frac{M_\alpha' H}{V} \dot{h}$$

$$R_{\dot{z}} = -(\dot{M}_\alpha' - M_\alpha' \frac{N}{mV}) \frac{1}{V}$$

$$R_\beta = \dot{M}_\beta' - 14.6 M_\beta' - \frac{M_\alpha'}{V} \frac{R}{m}$$

$$R_\phi = - V R_{\dot{z}}$$

$$R_\omega = R_\phi \frac{H}{V} + \frac{M_\alpha'}{V} \dot{H}$$

$$R_V = -R_{\dot{z}}$$

$$H = \sigma_{V_\omega}$$

WIND LOAD APPROXIMATION

The case where the distribution of loads over the vehicle length is approximated by a third-order filter reduces to a tenth-order system. The above equations become those shown on the next two pages.

$$
\begin{bmatrix} \ddot{\phi} \\ \ddot{z} \\ \dot{x}_2 \\ \dot{x}_3 \\ \dot{\omega} \\ \dot{x} \\ \dot{x}_1 \\ \dot{\theta} \\ \dot{\phi} \\ \dot{z} \end{bmatrix}
=
\begin{bmatrix}
\frac{-T_\phi}{I_{xx}V} & \frac{-N\ell cp}{I_{xx}V} & \frac{-Na_4}{I_{xx}} & 0 & 0 & 0 & \frac{Na_3}{I_{xx}} & \frac{-x_{cg}R}{I_{xx}} & \frac{N\ell cp}{I_{xx}} & 0 \\
\frac{-N\ell cp}{mV} & \frac{-N}{mV} & \frac{N a_2}{m} & 0 & 0 & 0 & \frac{N a_1}{m} & \frac{R}{m} & \frac{F-X}{m} + \frac{N}{m} & 0 \\
0 & 0 & \frac{-4V}{X_2} & \frac{-6V}{X_2} & \frac{-5H}{X_2} & 0 & 0 & 0 & 0 & 0 \\
0 & 0 & \frac{V}{X_2} & 0 & \frac{-H}{X_2} & 0 & 0 & 0 & 0 & 0 \\
0 & 0 & 0 & 0 & 0 & \dot{h} & 0 & 0 & 0 & 0 \\
0 & 0 & 0 & 0 & -c_5\dot{h} & -\dot{h}c_4 & 0 & 0 & 0 & 0 \\
0 & 0 & 0 & 0 & \frac{H}{X_1} & 0 & \frac{-V}{X_1} & 0 & 0 & 0 \\
0 & 0 & 0 & 0 & 0 & 0 & 0 & -14.6 & 0 & 0 \\
1 & 0 & 0 & 0 & 0 & 0 & 0 & 0 & 0 & 0 \\
0 & 1 & 0 & 0 & 0 & 0 & 0 & 0 & 0 & 0
\end{bmatrix}
\begin{bmatrix} \dot{\phi} \\ \dot{z} \\ x_2 \\ x_3 \\ \omega \\ x \\ x_1 \\ \theta \\ \phi \\ z \end{bmatrix}
+
\begin{bmatrix} 0 \\ 0 \\ 0 \\ 0 \\ 0 \\ 0 \\ 0 \\ 14.6 \\ 0 \\ 0 \end{bmatrix}
u +
\begin{bmatrix} 0 \\ 0 \\ \frac{-5}{X_2} \\ \frac{-1}{X_2} \\ 0 \\ 0 \\ \frac{1}{X_1} \\ 0 \\ 0 \\ 0 \end{bmatrix}
\bar{v}_\omega +
\begin{bmatrix} 0 \\ 0 \\ 0 \\ 0 \\ c_1\sqrt{\dot{h}} \\ c_2\sqrt{\dot{h}} \\ 0 \\ 0 \\ 0 \\ 0 \end{bmatrix}
$$

$$
\begin{bmatrix} \theta \\ \dot{\theta} \\ I_b \\ \dot{I}_b \\ \dot{\phi}+0.388\alpha \\ \alpha \\ \dot{\phi} \\ \dot{z} \\ \phi \\ z \end{bmatrix}
=
\begin{bmatrix}
0 & 0 & 0 & 0 & 0 & 0 & 0 & 1 & 0 & 0 \\
0 & 0 & 0 & 0 & 0 & 0 & 0 & -14.6 & 0 & 0 \\
\frac{-M_{\dot{\phi}}}{V} & \frac{-M_{\alpha}'}{V} & M_{\alpha}'a_6 & 0 & 0 & 0 & M_{\alpha}'a_5 & M_{\theta}' & M_{\alpha}' & 0 \\
R_{\dot{\phi}} & \frac{-R_{\phi}}{V} & R_{x_2} & -R_{x_3} & HR_V & 0 & R_{x_1} & R_{\theta}' & R_{\phi} & 0 \\
1 & \frac{-0.388}{V} & 0 & 0 & \frac{0.388H}{V} & 0 & 0 & 0 & 0.388 & 0 \\
0 & \frac{-1}{V} & 0 & 0 & \frac{H}{V} & 0 & 0 & 0 & 1 & 0 \\
1 & 0 & 0 & 0 & 0 & 0 & 0 & 0 & 0 & 0 \\
0 & 1 & 0 & 0 & 0 & 0 & 0 & 0 & 0 & 0 \\
0 & 0 & 0 & 0 & 0 & 0 & 0 & 0 & 1 & 0 \\
0 & 0 & 0 & 0 & 0 & 0 & 0 & 0 & 0 & 1
\end{bmatrix}
\begin{bmatrix} \phi \\ \dot{z} \\ x_2 \\ x_3 \\ w \\ x \\ x_1 \\ \theta \\ \phi \\ z \end{bmatrix}
+
\begin{bmatrix} 0 \\ 14.6 \\ 0 \\ 14.6M_{\theta}' \\ 0 \\ 0 \\ 0 \\ 0 \\ 0 \\ 0 \end{bmatrix}
u+
\begin{bmatrix} 0 \\ 0 \\ 0 \\ R_V \\ \frac{0.388}{V} \\ \frac{1}{V} \\ 0 \\ 0 \\ 0 \\ 0 \end{bmatrix}
\bar{v}_w
$$

where

$$R_{\dot{\phi}} = M_\alpha{}' \left(1 + \frac{N\ell cp}{mV^2}\right) + \frac{M_{\dot{\phi}} T_{\dot{\phi}}}{I_{xx} V^2} - \frac{\dot{M}_\phi}{V}$$

$$R_{x_2} = \left(\dot{M}_\alpha{}' - \frac{4V}{X_2} M_\alpha{}'\right) a_6 - \frac{M_\alpha{}' N}{mV} a_2 + \frac{M_{\dot{\phi}} N}{I_{xx} V} a_4$$

$$R_{x_3} = M_\alpha{}' \frac{6V}{X_2} a_6$$

$$R_v = M_\alpha{}' \left(\frac{a_5}{X_1} - \frac{a_6}{X_2}\right)$$

$$R_{x_1} = \left(\dot{M}_\alpha{}' - \frac{V}{X_1} M_\alpha{}'\right) a_5 - \frac{M_\alpha{}' N}{mV} a_1 - \frac{M_{\dot{\phi}} N}{I_{xx} V} a_3$$

$$R_\beta = \dot{M}_\beta{}' - 14.6\, M_\beta{}' - \frac{M_\alpha{}'}{V} \frac{R}{m} + \frac{M_{\dot{\phi}}}{V} \frac{Rx_{cg}}{I_{xx}}$$

$$R_\phi = \dot{M}_\alpha{}' - M_\alpha{}' \frac{N}{mV} - \frac{M_\phi}{V} \frac{N\ell cp}{I_{xx}}$$

$$H = \sigma_{v_\omega}$$

APPENDIX E
THE UPPER-BOUND J*

In this appendix, it is shown that the functional J* defined by Equation (3.8) is an upper bound for the likelihood of failure J defined by Equation (3.6).

Derivations of the terminal likelihoods $P(\bar{a}_i)$ and the in-flight expectations $E\left\{N_i\right\}$ making up J* are also presented.

NOTATION

The notation is that employed in Section III. Given n response perturbations $r_i(t)$ and n finite, positive constants γ_o, define a_i to be the event

$$\left| r_i(T) \right| < \gamma_i,$$

and $\bar{a}_i$ to be the event

$$\left| r_i(T) \right| \geq \gamma_i.$$

Let $b_i(j)$ be the event that the two conditions

$$\left| r_i(t) \right| = \gamma_i$$

$$\frac{d}{dt} \left| r_i(t) \right| > 0$$

are met simultaneously exactly j times in the interval [0, T]. Let $\bar{b}_i(0)$ be the event that one of the events $b_i(j)$, $j > 0$, occurs. Let $P(\bar{a}_i)$ be the probability of the event $\bar{a}_i$, and $P(b_i(j))$ be the probability of the event $b_i(j)$.

The failure likelihood J is the likelihood that not all of the events $a_1, \ldots a_m$, $b_{m+1}(0), \ldots b_n(0)$ occur. This is by definition the joint likelihood J,

$$J = 1 - P[a_1, \ldots b_n(0)]$$

The functional J* was defined by

$$J^* = \sum_{i=0}^{m} P(\bar{a}_i) + \sum_{i=m+1}^{n} E(N_i)$$

where $E(N_i)$ was the expected number of occasions that $|r_i(t)|$ exceeded γ_i in (0, T).

$$E\{N_i\} = \sum_{j=0}^{\infty} j\, P(b_i(j)).$$

PROOF OF THE UPPER-BOUND PROPERTY

The upper-bound property is that

$$J^* \geq J$$

This inequality can be proved by considering the ways the mission can fail.

The ways the mission can fail are if the event

$\bar{a}_1$	occurs, or the events
$a_1, \bar{a}_2$	occur, or the events

$a_1, a_2, \bar{a}_3$ occur, or the events

$\vdots$

$a_1, \ldots a_m, \bar{b}_{m+1}(0)$ occur, or the events

$\vdots$

$a_1, \ldots a_m, b_{m+1}(0), \ldots b_{n-1}(0), \bar{b}_n(0)$ occur

These are mutually exclusive events, so that

$$J = 1 - P[a_1, a_2, \ldots a_m, b_{m+1}(0), \ldots b_n(0)] = P(\bar{a}_1) + P(a_1, \bar{a}_2) +$$

$$P(a_1, a_2, \bar{a}_3) + \ldots P[a_1, \ldots a_m, b_{m+1}(0), \ldots b_{n-1}(0), \bar{b}_n(0)]$$

Now

$$P(a_1, \ldots a_j, \bar{a}_{j+1}) = P(a_1, \ldots a_j | \bar{a}_{j+1}) \; P(\bar{a}_{j+1})$$

where $P(a_1, \ldots a_j | \bar{a}_{j+1})$ is the conditional probability that events $a_1, \ldots a_j$ occur given that event $\bar{a}_{j+1}$ occurs. Since these conditional probabilities lie in the range

$$0 \leq P(a_1, \ldots a_j | \bar{a}_{j+1}) \leq 1$$

then

$$P(a_1, \ldots a_j, \bar{a}_{j+1}) \leq P(\bar{a}_{j+1})$$

and therefore

$$J \leq \sum_{i=1}^{m} P(\bar{a}_i) + \sum_{i=m+1}^{n} P(\bar{b}_i(0))$$

Since $\bar{b}_i(0)$ is the event that one of the events $b_i(j)$, $j \geq 1$ occurs, and since these are mutually exclusive events, then

$$P[\bar{b}_i(0)] = \sum_{j=1}^{\infty} P[b_i(j)]$$

Since

$$P[b_i(j)] \leq j\, P[b_i(j)] \quad \text{for } j \geq 1$$

and

$$0 = j\, P[b_i(j)] \quad \text{for } j = 0$$

then

$$P\left[\bar{b}_i(0)\right] \leq \sum_{j=0}^{\infty} j\, P[b_i(j)]$$

or

$$P[\bar{b}_i(0)] \leq E(N_i)$$

which, coupled with the above inequality for J, leads to

$$J \leq \sum_{i=1}^{m} P(\bar{a}_i) + \sum_{i=m+1}^{n} E(N_i).$$

Q.E.D.

DERIVATION OF THE TERMINAL LIKELIHOODS $P(\bar{a}_i)$

It is assumed that the terminal response $r_i(T)$ is a Gaussian random variable with a mean

$$E[r_i(T)] = \bar{r}_i(T)$$

and a variance

$$E[(r_i(T) - \bar{r}_i(T))^2] = \sigma_{r_i}(T)^2$$

The probability $P(\bar{a}_i)$ that $|r_i(T)| > \gamma_i$ is

$$\text{Prob}\,(|r_i(T)| > \gamma_i) = 1 - \text{Prob}\,(|r_i(T)| \leq \gamma_i)$$

where

$$\text{Prob}\,(|r_i(T)| \leq \gamma_i) = \int_{-\gamma_i}^{\gamma_i} P_{r_i(T)}(x)\,dx$$

where $P_{r_i(T)}(x)$ is the Gaussian density

$$P_{r_i(T)}(x) = \frac{1}{\sqrt{2\pi\,\sigma_{r_i}(T)}} \exp\left(\frac{-(x-\bar{r}_i(T))^2}{2\,\sigma_{r_i}(T)^2}\right)$$

Letting

$$y = \frac{x-\bar{r}_i(T)}{\sigma_{r_i}(T)}$$

the terminal likelihood $P(\bar{a}_i)$ may be rewritten

$$P(\bar{a}_i) = 1 - \int_{\frac{-\gamma_i-\bar{r}_i(T)}{\sigma_{r_i}(T)}}^{\frac{\gamma_i-\bar{r}_i(T)}{\sigma_{r_i}(T)}} \frac{1}{\sqrt{2\pi}} \exp\left(\frac{-y^2}{2}\right) dy$$

DERIVATION OF THE EXPECTATIONS $E(N_i)$

$E(N_i)$ is the expected number of occasions that the two conditions

$$\left| r_i(t) \right| = \gamma_i$$

$$\frac{d}{dt} \left| r_i(t) \right| > 0$$

are met in the interval $[0, T]$. That is, it is the expected number of occasions that $\left| r_i(t) \right|$ exceeds the limit γ_i.

To derive an expression for $E(N_i)$, let $x(t)$ and $y(t)$ be the random processes

$$x(t) = r_i(t) - \gamma_i$$

$$y(t) = - r_i(t) - \gamma_i,$$

and let A_x and A_y be the events

$$A_x : [x(t) = 0 \text{ with } \dot{x}(t) > 0]$$

$$A_y : [y(t) = 0 \text{ with } \dot{y}(t) > 0]$$

Then the expected number of occasions that $\left| r_i(t) \right|$ exceeds γ_i in $(0, T)$ is the sum of the expected number of occasions that the events A_x and A_y occur.

$$E(N_i) = E[N(A_x)] + E[N(A_y)].$$

Consider the function $x(t)$. Assuming $r_i(t)$ is Gaussian, $x(t)$ is Gaussian, and $x(t)$ and its time derivative $\dot{x}(t)$ have the joint Gaussian density

$$P_{x\dot{x}}(\alpha, \beta) = \frac{1}{2\pi\sqrt{\mathrm{Det}\ M}} \exp\left(- \frac{\begin{bmatrix} \alpha - \bar{x} \\ \beta - \bar{\dot{x}} \end{bmatrix}' M^{-1} \begin{bmatrix} \alpha - \bar{x} \\ \beta - \bar{\dot{x}} \end{bmatrix}}{2} \right)$$

where

$$\bar{x} = E[r_i(t)] - \gamma_i = \bar{r}_i(t) - \gamma_i$$

$$\bar{\dot{x}} = E[\dot{r}_i(t)] = \frac{d}{dt}(\bar{r}_i(t))$$

and

$$M = \begin{bmatrix} E\left\{(r_i(t) - \bar{r}_i(t))^2\right\} & E\left\{(r_i(t) - \bar{r}_i(t))\ (\dot{r}_i(t) - \bar{\dot{r}}_i(t))\right\} \\ E\left\{(r_i(t) - \bar{r}_i(t))\ (\dot{r}_i(t) - \bar{\dot{r}}(t))\right\} & E\left\{(\dot{r}_i(t) - \bar{\dot{r}}_i(t))^2\right\} \end{bmatrix}$$

$$= \begin{bmatrix} M_{11} & M_{12} \\ M_{12} & M_{22} \end{bmatrix}$$

In a time interval $\tau \leq t < \tau + d\tau$, the fraction of time that $x(t)$ and $\dot{x}(t)$ lie in the ranges

$$\alpha \leq x(t) < \alpha + d\alpha$$

$$\beta \leq \dot{x}(t) < \beta + d\beta$$

is the product

$$P_{x\dot{x}}(\alpha, \beta)\ d\alpha\ d\beta$$

The expected time spent in this "rectangle" is then

$$P_{x\dot{x}}(\alpha, \beta)\, d\alpha\, d\beta\, d\tau$$

The time x(t) spends crossing from α to $\alpha + d\alpha$ (or vice versa) is the distance $d\alpha$ divided by the velocity $|\dot{x}| = \beta$, or

$$dt = \frac{dx}{|\dot{x}|} = \frac{d\alpha}{\beta}$$

This is the time spent in the above rectangle on each occasion of crossing it. The expected number of occasions that x(t) and $\dot{x}(t)$ lie in this rectangle is then the expected time spent in the rectangle divided by the time spent in the rectangle on each occasion of crossing it, or

$$\frac{P_{x\dot{x}}(\alpha, \beta)\, d\alpha\, d\beta\, d\tau}{dt} = |\beta|\, P_{x\dot{x}}(\alpha, \beta)\, d\beta\, d\tau$$

The expected number of instances in the interval $\tau \leq t < \tau + d\tau$ that the event A_x occurs is then the sum, over all the rectangles for which $\alpha = 0$ and $\beta > 0$, of the expected number of instances per rectangle,

$$\int_0^\infty |\beta|\, P_{x\dot{x}}(0, \beta)\, d\beta\, d\tau$$

Finally, the expected number of instances that A_x occurs in $[0, T]$ is the sum over all $d\tau$ intervals of the expected number of instances per interval

$$E\{N(A_x)\} = \int_0^T \left[\int_0^\infty |\beta|\, P_{x\dot{x}}(0, \beta)\, d\beta \right] d\tau$$

Computing the inner integral

$$|\beta|\ P_{x\dot{x}}(0,\beta) = \frac{|\beta|}{2\pi\sqrt{M_{11}M_{22}-M_{12}^{2}}}\ e^{-1/2\ \frac{\begin{bmatrix}-\bar{x}\\ \beta-\bar{\dot{x}}\end{bmatrix}'\begin{bmatrix}M_{22} & -M_{12}\\ -M_{12} & M_{11}\end{bmatrix}\begin{bmatrix}-\bar{x}\\ \beta-\bar{\dot{x}}\end{bmatrix}}{M_{11}\ M_{22}-M_{12}^{2}}}$$

$$= \frac{|\beta|}{2\pi\sqrt{M_{11}M_{22}-M_{12}^{2}}}\ e^{-1/2\ \frac{(\bar{x})^{2}M_{22}+(\beta-\bar{\dot{x}})^{2}M_{11}+2M_{12}(\beta-\bar{\dot{x}})\bar{x})}{M_{11}M_{22}-M_{12}^{2}}}$$

$$= \frac{1}{\sqrt{2\pi M_{11}}}\ e^{-\frac{\bar{x}^{2}}{2M_{11}}}\ \frac{|\beta|}{\sqrt{2\pi\left(M_{22}-\frac{M_{12}^{2}}{M_{11}}\right)}}\ e^{-\frac{\left(\beta-\bar{\dot{x}}+\bar{x}\frac{M_{12}}{M_{11}}\right)^{2}}{2\left(M_{22}-\frac{M_{12}^{2}}{M_{11}}\right)}}$$

Defining

$$r_x = -\bar{\dot{x}} + \bar{x}\frac{M_{12}}{M_{11}}$$

$$\sigma_x = \sqrt{M_{22}-\frac{M_{12}^{2}}{M_{11}}}$$

then

$$\int_0^\infty |\beta| P_{x\dot{x}}(0,\beta)d\beta = \frac{1}{\sqrt{2\pi M_{11}}} e^{-\frac{\bar{x}^2}{2M_{11}}} \int_0^\infty \frac{\beta}{\sqrt{2\pi}\sigma_x} e^{-\frac{(\beta + r_x)^2}{2\sigma_x^2}}$$

Letting

$$z = \frac{\beta + r_x}{\sigma_x}$$

This becomes

$$\frac{1}{\sqrt{2\pi M_{11}}} e^{-\frac{\bar{x}^2}{2M_{11}}} \int_{\frac{r_x}{\sigma_x}}^\infty \frac{\sigma_x z - r_x}{2\pi} e^{-1/2z^2} dz$$

Defining

$$\Phi(V) = \int_{-\infty}^{V} \frac{1}{\sqrt{2\pi}} e^{-1/2z^2} dz$$

and noting that

$$\frac{d}{dz} e^{-1/2z^2} = -ze^{-1/2z^2}$$

then

$$\int_0^\infty |\beta| \, P_{x\dot{x}}(0,\beta)d\beta = \frac{1}{\sqrt{2\pi M_{11}}} \, e^{-\frac{\bar{x}^2}{2M_{11}}} \left[\frac{\sigma_x}{\sqrt{2\pi}} \, e^{-\frac{(r_x)^2}{2\sigma_x^2}} + r_x \left(\Phi\left(\frac{r_x}{\sigma_x}\right) - 1 \right) \right]$$

The derivation of E $N(A_y)$ is similar, differing only in a few sign changes. Combining all of these results,

$$E\left\{N_i\right\} = \int_0^T \left[P_x(t) + P_y(t)\right] dt$$

where

$$P_x(t) = \frac{1}{\sqrt{2\pi M_{11}}} \, e^{-\frac{\bar{x}^2}{2M_{11}}} \left[\frac{\sigma_x}{\sqrt{2\pi}} \, e^{-\frac{(r_x)^2}{2\sigma_x^2}} + r_x \left(\Phi\left(\frac{r_x}{\sigma_x}\right) - 1 \right) \right]$$

$$P_y(t) = \frac{1}{\sqrt{2\pi M_{11}}} \, e^{-\frac{\bar{y}^2}{2M_{11}}} \left[\frac{\sigma_x}{\sqrt{2\pi}} \, e^{-\frac{(r_y)^2}{2\sigma_x^2}} = r_y \left(\Phi\left(\frac{r_y}{\sigma_x}\right) - 1 \right) \right]$$

where

$$\bar{x} = \bar{r}_i(t) - \gamma_i$$

$$\bar{y} = -\bar{r}_i(t) - \gamma_i$$

$$r_x = \bar{x} \, \frac{M_{12}}{M_{11}} - \dot{\bar{r}}(t)$$

$$r_y = \bar{y}\,\frac{M_{12}}{M_{11}} + \bar{r}(t)$$

$$\sigma_x = \sqrt{M_{22} - \frac{M_{12}^{\;2}}{M_{11}}}$$

$$M_{11} = E\left\{ (r_i(t) - \bar{r}_i(t))^2 \right\}$$

$$M_{22} = E\left\{ (\dot{r}_i(t) - \dot{\bar{r}}_i(t))^2 \right\}$$

$$M_{12} = E\left\{ (r_i(t) - \bar{r}_i(t))\,(\dot{r}_i(t) - \dot{\bar{r}}_i(t)) \right\}$$

This completes the derivation of the $E\{N_i\}$ expectations.

The above derivation follows the derivation of the Rice formula for stationary Gaussian processes presented by Bendat (Ref. 2). The extension of Bendat's derivation to non-stationary processes involved only including the general Gaussian density in the integral

$$\int_0^\infty |\beta|\, P_{x\dot{x}}(0, \beta)\, d\beta$$

A slightly different derivation, employing impulse functions, is given in Middleton (Ref. 16).

MOMENTS

It is to be noted that the expressions for both $P(\ddot{a}_i)$ and $E\{N_i\}$ are functions only of first and second response moments (means and covariances). This is, of course, due to the fact that Gaussian random processes are completely described by their first and second moments.

The upper-bound functional J* is thus a functional of first and second moments.

Define $\bar{r}(t)$

$$\bar{r}(t) = E\{r(t)\}$$

to be the vector of mean responses, R(t)

$$R(t) = \bar{r}(t)\,\bar{r}(t)'$$

to be the matrix of mean response products, and S(t)

$$S(t) = \mathrm{cov}\{r(t)\,r(t)'\}$$

to be the response covariance matrix. The ij^{th} component of R(t) is then

$$R_{ij}(t) = \bar{r}_i(t)\,\bar{r}_j(t)$$

and the ij^{th} component of S(t) is

$$S_{ij}(t) = E\{(r_i(t) - \bar{r}_i(t))\,(r_j(t) - \bar{r}_j(t))\}$$

In this notation the upper-bound J* may be written in the form

$$J^* - f_1(S(T),\ R(T)) + \int_0^T f_2(S(t),\ R(t))\,dt$$

where the functions f_1, f_2 are defined by the above equations.

The fact that J* can be written as a functional of first and second response moments is essential to the quadratic equivalence described in Section III.

APPENDIX F
TAYLOR'S SERIES MOMENT EXPANSION

Response covariance and mean-response-product matrices were defined in Section III. The quadratic equivalence assertion presented there was based on being able to expand these matrices in finite Taylor's series.

In this appendix it is shown first that these moment matrices exist (their coefficients are defined and are not infinite for $t \in [0, T]$). Their existence is then used to validate constructions of finite Taylor's series expansions.

FORMULATION

Given the linear system

$$\dot{x}(t) = F(t)\,x(t) + G_1(t)\,u(t) + G_2(t)\,\eta_1(t) + G_3(t)\,\bar{v}_\omega(t)$$

$$r(t) = H_1(t)\,x(t) + D_1(t)\,u(t) + D_2(t)\,\bar{v}_\omega(t)$$

$$m(t) = H_2(t)\,x(t) + \eta_2(t)$$

where

$x(t)$ = system state vector

$u(t)$ = control input vector

$r(t)$ = responses to be controlled

$m(t)$ = measured responses

$\bar{v}_\omega(t)$ = vector of deterministic inputs ($\bar{v}_\omega(t)$ known for all $t \geq 0$)

$\eta_1(t)$ = vector of white noise processes

$$E\left\{\eta_1(t)\,\eta_1(\tau)'\right\} = I\,\delta(t-\tau)$$

$\eta_2(t)$ = vector of white noise processes

$$E\left\{\eta_2(t)\,\eta_2(\tau)'\right\} = V(t)\,\delta(t-\tau)$$

$$E\left\{\eta_1(t)\,\eta_2(\tau)'\right\} = W(t)\,\delta(t-\tau)$$

Let F(t) be the mean response vector,

$$\bar{r}(t) = E\left\{r(t)\right\}$$

let R(t) be a matrix of mean response products

$$R(t) = \bar{r}(t)\,\bar{r}(t)'$$

and let S(t) be the response covariance matrix

$$S(t) = \text{cov}\,[r(t)\,r(t)'] = E\left\{[r(t) - \bar{r}(t)]\,[r(t) - \bar{r}(t)]'\right\}$$

EXISTENCE OF S(t), R(t)

Given a controller

$$u(t) = L(t, m[0, t]),$$

let y(i, j, t, τ) be the system impulse responses

$$y(1, j, t, \tau) = r(t) \text{ when} \qquad \begin{aligned} \eta_{1_j}(t) &= \delta(t-\tau) \\ \eta_{1_i}(t) &= 0 \qquad i \neq j \\ \eta_2(t) &= 0 \\ \bar{v}_\omega(t) &= 0, \end{aligned}$$

$y(2, j, t, \tau) = r(t)$ when

$$\eta_{2j}(t) = \delta(t-\tau)$$

$$\eta_{2i}(t) = 0 \qquad i \neq j$$

$$\eta_1(t) = 0$$

$$\bar{v}_\omega(t) = 0$$

and $y(3, j, t, \tau) = r(t) - D_3(t)\,\bar{v}_\omega(t)$ when

$$\bar{v}_{\omega_j}(t) = \delta(t-\tau)$$

$$\bar{v}_{\omega_i}(t) = 0, \; i \neq j$$

$$\eta_1(t) = 0$$

$$\eta_2(t) = 0$$

Let $\gamma(i, t, \tau)$ be the matrices

$$\gamma(i, t, \tau) = [y(i, 1, t, \tau)\; y(i, 2, t, \tau) \ldots y(i, m, t, \tau]$$

Assuming for the moment that the functions $y(i, j, t, \tau)$ exist, from linearity

$$\bar{r}(t) = D_3(t)\,\bar{v}_\omega(t) + \int_0^t \gamma(3, t, \tau)\,\bar{v}_\omega(\tau)\,d\tau$$

so that

$$R(t) = \int_0^t \int_0^t \gamma(3, t, \tau)\,\bar{v}_\omega(\tau)\,\bar{v}_\omega(z)'\,\gamma(3, t, z)'\,d\tau dz \; +$$

$$+\int_0^t [\gamma(3,\ t,\ \tau)\ \bar{v}_\omega(\tau)\ \bar{v}_\omega(t)'\ D_3(t)' + D_3(t)\ \bar{v}_\omega(t)\ \bar{v}_\omega(\tau)'\ \gamma(3,\ t,\ \tau)']\ d\tau$$

$$+\ D_3(t)\ \bar{v}_\omega(t)\ \bar{v}_\omega(t)'\ D_3(t)'.$$

Similarly

$$S(t) = \int_0^t [\gamma(1,\ t,\ \tau)\ \gamma(1,\ t,\ \tau)' + \gamma(1,\ t,\ \tau)\ V(\tau)\ \gamma(2,\ t,\ \tau)'$$

$$+\ \gamma(2,\ t,\ \tau)\ V(\tau)'\ \gamma(1,\ t,\ \tau)' + \gamma(2,\ t,\ \tau)\ W(\tau)\ \gamma(2,\ t,\ \tau)']d\tau$$

Both $S(t)$ and $R(t)$ will be continuous if it is specified that the coefficients of $\bar{v}_\omega(t)$, $D_3(t)$, $V(t)$ $W(t)$ are continuous, and it can be shown that the functions $y(i,\ j,\ t,\ \tau)$ are bounded.

Consider the Volterra integral equation of the second kind

$$\int_0^t K(t,\ \tau)\ x(\tau)\ d\tau - x(t) = \mu(t)$$

Given $K(t,\ \tau)$, $\mu(\tau)$, this equation has a solution for $x(t)$ ($x(t)$ exists) if $\mu(t)$ is piecewise continuous and the integral

$$\int_0^t K(t,\ \tau)\ d\tau$$

is piecewise continuous[1]. The solution is

$$x(t) = \mu(t) + \int_o^t \left(\sum_{i=o}^{\infty} K_{i+1}(t, \tau) \right) u(\tau)\, d\tau$$

where

$$K_1(t, \tau) = K(t, \tau)$$

$$K_{i+1}(t, \tau) = \int_o^t K(t, z)\, K_i(z, \tau)\, dz$$

The impulse response equations can be put into this form by appropriately limiting the class of admissible controllers L.

Limiting L to the form

$$u(t) = L(t, m[o, t])$$

$$= C(t)\, m(t) + \int_o^t A(t, \tau)\, m(\tau)\, d\tau$$

$$= C(t)\, H_2(t)\, x(t) + \int_o^t A(t, \tau)\, H_2(\tau)\, x(\tau)\, d\tau + C(t)\, \eta_2(t) + \int_o^t A(t, \tau)\, \eta_2(\tau) d\tau$$

---

[1] F. G. Tricomi, Integral Equations, Interscience Publishers, Inc., N.Y., 1957.

then

$$\dot{x}(t) = [F(t) + g_1(t)C(t)\,H_2(t)]x(t) + \int_0^t G_1(t)\,A(t,\ \tau)\,H_2(\tau)\,x(\tau)\,d\tau + G_2(t)\eta_1(t)$$

$$+G_3(t)\,\bar{v}_w(t) + G_1(t)C(t)\,\eta_2(t) + \int_0^t G_1(t)\,A(t,\ \tau)\,\eta_2(\tau)\,d\tau$$

Integrating both sides of this equation, by defining

$$\mu(t) = -x(0) - \int_0^t [G_2(\tau)\,\eta_1(\tau) + G_3(\tau)\,\bar{v}_w(\tau) + G_1(\tau)C(\tau)\,\eta_2(\tau)$$

$$+ \int_0^\tau G_1(\tau)\,A(\tau,\ t_1)\,\eta_2(t_1)\,dt_1]\,d\tau$$

and

$$K(t,\ \tau) = F(\tau) + G_1(\tau)\,c(\tau)\,H_2(\tau) + \int_\tau^t G_1(t_1)A(t_1,\ \tau)\,H_2(\tau)\,dt_1$$

the equation reduces to the above Volterra equation. Then x(t) exists if the coefficients of F(t), $G_1(t)$, C(t), $H_2(t)$ and the integral

$$\int_\tau^t G_1(t_1)\,A(t_1,\ \tau)\,dt_1$$

are all piecewise continuous. Adding that $H_1(t)$, $D_1(t)$, $D_2(t)$ are bounded, $r(t)$ then exists, and the impulse responses $y(i, j, t, \tau)$ therefore exist.

EXPANSION IN FINITE TAYLOR'S SERIES

Let

$$u(t) = L_o(t, m[o, t]) + \epsilon L_1(t, m[o, t])$$

where ϵ is in the range $-1 < \epsilon < +1$, and let

$$x(t) = x_o(t) + \epsilon x_1(t) + \epsilon^2 x_2(t) + \ldots + \epsilon^{n-1} x_{n-1}(t)$$

Substituting these expressions into the system equations and equating terms in ϵ, there results

$$\dot{x}_o(t) = F(t)\, x_o(t) + G_1(t)\, L_o(t, m_o[o, t]) + G_2(t)\, \eta_1(t) + G_3(t)\, \bar{v}_\omega(t)$$

$$m_o(t) = H_2(t)\, x_o(t) + \eta_2(t),$$

$$\vdots$$

$$\dot{x}_i(t) = F(t)\, x_i(t) + G_1(t)\, [L_o(t, m_i[o, t]) + L_1(t, m_{i-1}[o, t])]$$

$$m_i(t) = H_2(t)\, x_i(t)$$

$$\vdots$$

$$\dot{x}_{n-1}(t) = F(t)\, x_{n-1}(t) + G_1(t)\, [L_o(t, m_{n-1}[o, t]) + L_1(t_1 m_{n-2}[o, t])]$$

$$+ \epsilon G_1(t)\, L_1(t, m_{n-1}[o, t])$$

$$m_{n-1}(t) = H_2(t)\, x_{n-1}(t).$$

The first n-1 terms, $x_o(t), \ldots x_{n-2}(t)$, are independent of ϵ, and by virtue of the above existence result, all n-2 terms $x_i(t)$ are bounded for any ϵ in the range $-1 < \epsilon < +1$.

The corresponding responses r(t) are

$$r(t) = r_o(t) + \epsilon r_1(t) + \ldots + \epsilon^n r_n(t)$$

where

$$r_o(t) = H_1(t)\, x_o(t) + D_1(t)\, L_o(t, m_o[o, t]) + D_2(t)\, \bar{v}_\omega(t)$$

$$\vdots$$

$$r_i(t) = H_1(t)\, x_i(t) + D_1(t)\, [L_o(t, m_i[o, t]) + L_1(t, m_{i-1}[o, t])]$$

$$\vdots$$

$$r_n(t) = D_1(t)\, L_1(t, m_{n-1}[o, t]).$$

The first n-1 terms, $r_o(t), \ldots r_{n-2}(t)$, are independent of ϵ. The impulse responses $y(i, j, t, \tau)$ are therefore expandable in a finite Taylor's series

$$y(i, j, t, \tau) = \sum_{K=o}^{n} \epsilon^K y_K(i, j, t, \tau)$$

where the first n-2 terms of the expansion are independent of ϵ and all n+1 terms are bounded for ϵ in the range $-1 < \epsilon < +1$.

R(t) and S(t) are then expandable in ϵ

$$R(t) = R_o(t) + \epsilon R_1(t) + \ldots + \epsilon^{2n} R_{2n}(t)$$

$$S(t) = S_o(t) + \epsilon S_1(t) + \ldots + \epsilon^{2n} S_{2n}(t)$$

where

$$\gamma_K(i, t, \tau) = [y_K(i, 1, t, \tau)\ y_K(i, 2, t, \tau) \ldots y_K(i, m, t, \tau)],$$

$$R_o(t) = \int_o^t \int_o^t \gamma_o(3, t, \tau)\ \bar{v}_\omega(\tau)\ \bar{v}_\omega(z)'\ \gamma_o(3, t, z)'\ dz d\tau$$

$$+ \int_o^t \gamma_o(3, t, \tau)\ \bar{v}_\omega(\tau)\ \bar{v}_\omega(t)' D_3(t)' + D_3(t)\ \bar{v}_\omega(t)\ \bar{v}_\omega(\tau)\ \gamma_o(3, t, \tau)]\ d\tau$$

$$+ D_3(t)\ \bar{v}_\omega(t)\ \bar{v}_\omega(t)'\ D_3(t)'$$

$$S_o(t) = \int_o^t [\gamma_o(1, t, \tau)\ \gamma_o(1, t, \tau)' + \gamma_o(1, t, \tau)\ V(\tau)\ \gamma_o(2, t, \tau)'$$

$$+ \gamma_o(2, t, \tau)\ V(\tau)' \gamma_o(1, t, \tau) + \gamma_o(2, t, \tau)\ W(\tau)\ \gamma_o(2, t, \tau)] d\tau$$

and for $1 \leq i \leq n$

$$R_i(t) = \sum_{j=o}^{i} \int_o^t \int_o^t \gamma_j(e, t, \tau)\ \bar{v}_\omega(\tau)\ \bar{v}_\omega(z)'\ \gamma_{i-j}(3, t, \tau)'\ dz d\tau$$

$$+ \int_o^t [\gamma_i(3, t, \tau)\ \bar{v}_\omega(\tau)\ \bar{v}_\omega(t)'\ D_3(t)' + D_3(t)'\ \bar{v}_\omega(t) \bar{v}_\omega(\tau) \gamma_i(3, t, \tau)'] d\tau$$

$$S_i(t) = \sum_{j=o}^{i} \int_o^t [\gamma_j(1, t, \tau)\, \gamma_{i-j}(1, t, \tau)' + \gamma_j(1, t, \tau)\, V(\tau)\, \gamma_{i-j}(2, t, \tau)'$$

$$+ \gamma_j(2, t, \tau) V(\tau)' \gamma_{i-j}(1, t, \tau)' + \gamma_j(2, t, \tau)\, W(\tau) \gamma_{i-j}(2, t, \tau)']d\tau$$

and for $n < i \leq 2n$

$$R_i(t) = \sum_{j=i-n}^{n} \int_o^t \int_o^t \gamma_j(3, t, \tau)\, \bar{v}_\omega(\tau)\, \bar{v}_\omega(z)'\, \gamma_{i-j}(3, t, \tau)' d\tau\, dz$$

$$S_i(t) = \sum_{j=i-n}^{n} \int_o^t [\gamma_j(1, t, \tau)\, \gamma_{i-j}(1, t, \tau)' + \gamma_j(1, t, \tau)\, V(\tau)\, \gamma_{i-2}(2, t, \tau)'$$

$$+ \gamma_j(2, t, \tau)\, V(\tau)'\, \gamma_{i-j}(1, t, \tau)' + \gamma_j(2, t, \tau)\, W(\tau)\, \gamma_{i-j}(2, t, \tau)']d\tau$$

Again, the first $n-2$ terms in these expansions are independent of ϵ, and all $2n+1$ terms are bounded for any ϵ in the range $-1 < \epsilon < +1$.

Choosing $n \geq 2$ and defining

$$\epsilon^2 R_2^*(t) = \sum_{i=2}^{2n} \epsilon^i R_i(t)$$

$$\epsilon^2 S_2^*(t) = \sum_{i=2}^{2n} \epsilon^i S_i(t)$$

The above series become

$$R(t) = R_o(t) + \epsilon\, R_1(t) + \epsilon^2 R_2^*(t)$$

$$S(t) = S_o(t) + \epsilon\, S_1(t) + \epsilon^2 S_2^*(t)$$

where R_o, S_o, R_1, S_1 are independent of ϵ and the coefficients of R_2^*, S_2^* are bounded for ϵ in the range (-1, 1). This is the form of the expansion employed in Section III in the expansion of J* and J**.

APPENDIX G
DIFFERENCE EQUATIONS

The solution to the difference equation formulation of quadratic control problem described in Section III is presented in this Appendix.

STATEMENT OF THE PROBLEM

Given the linear system

$$\dot{x}(t) = F(t)\, x(t) + G_1(t)\, u(t) + G_2(t)\, \bar{v}_\omega(t) + G_3(t)\, \eta_1(t)$$

$$r(t) = H_1(t)\, x(t) + D_1(t)\, u(t) + D_2(t)\, \bar{v}_\omega(t)$$

$$m(t) = H_2(t)\, x(t) + \eta_2(t)$$

where $\bar{v}_\omega(t)$ is a deterministic (known) time function, the inputs $\eta_1(t)$ and $\eta_2(t)$ are independent white noise processes

$$E\left\{\eta_1(t)\, \eta_1(t_1)'\right\} = W_1(t)\, \delta(t-t_1)$$

$$E\left\{\eta_2(t)\, \eta_2(t_1)'\right\} = W_2(t)\, \delta(t-t_1)$$

$$E\left\{\eta_1(t)\, \eta_2(t_1)'\right\} = W_3(t)\, \delta(t-t_1)$$

and the initial state mean and covariance are known

$$E\left\{x(o)\right\} = \bar{x}(o)$$

$$E\left\{(x(o) - \bar{x}(o))\,(x(o) - \bar{x}(o))'\right\} = X(o)$$

find the linear control functional of past and present measured outputs m(t)

$$u(t) = L(t, m[o, t]),$$

that minimizes the quadratic J**

$$J^{**} = TR[Q(T)\, S(T) + V(T)\, R(T) + \int_{o}^{T} (Q(t)\, S(t) + V(t)\, R(t))\, dt],$$

where R(t) is the matrix of mean response products

$$R(t) = \bar{r}(t)\, \bar{r}(t)'$$

and S(t) is the response covariance matrix

$$S(t) = E\left\{ (r(t) - \bar{r}(t))\, (r(t) - \bar{r}(t))' \right\}$$

The matrices Q(t), V(t) are assumed to be symmetric and non-negative definite for all $t \in [O, T]$, the matrices $D_1(t)'\, Q(t)\, D_1(t)$ and $D_1(t)'\, V(t)\, D_1(t)$ are assumed positive definite for all $t \in [O, T]$, and it is assumed that

$$Q(T)\, D_1(T) = V(T)\, D_1(T) = 0.$$

DIFFERENCE EQUATIONS FORMULATION

Choose a large, finite integer N and let

$$\Delta t = \frac{T}{N}.$$

Define

$$A(n) = I + \Delta t\, F(n\Delta t) \qquad H_1(n) = H_1(n\Delta t) \qquad W_1(n) = W_1(n\Delta t)$$

$$B_1(n) = \Delta t\, G_1(n\Delta t) \qquad D_1(n) = D_1(n\Delta t) \qquad W_2(n) = W_2(n\Delta t)$$

$$B_2(n) = \Delta t\, G_2(n\Delta t) \qquad D_2(n) = D_2(n\Delta t) \qquad W_3(n) = W_3(n\Delta t)$$

$$B_3(n) = \Delta t\, G_3(n\Delta t) \qquad H_2(n) = H_2(n\Delta t) \qquad Q(n) = Q(n\Delta t)$$

$$\bar{v}_\omega(n) = \bar{v}_\omega(n\Delta t) \qquad V(n) = V(n\Delta t).$$

The above quadratic problem may then be restated:

Given the linear system

$$x(n+1) = A(n)\, x(n) + B_1(n)\, u(n) + B_2(n)\, \bar{v}_\omega(n) + B_3(n)\, \eta_1(n)$$

$$r(n) = H_1(n)\, x(n) + D_1(n)\, u(n) + D_2(n)\, \bar{v}_\omega(n)$$

$$m(n) = H_2(n)\, x(n) + \eta_2(n)$$

where

$$E\left\{\eta_1(n)\, \eta_1(n_1)'\right\} = \frac{W_1(n)}{\Delta t} \quad \text{if } n = n_1$$

$$= 0 \qquad \text{if } n \neq n_1$$

$$E\left\{\eta_2(n)\, \eta_2(n_1)'\right\} = \frac{W_2(n)}{\Delta t} \quad \text{if } n = n_1$$

$$= \qquad \text{if } n \neq n_1,$$

$$E\left\{\eta_1(n)\ \eta_2(n_1)'\right\} = \frac{W_3(n)}{\Delta t} \qquad \text{if } n = n_1$$

$$= 0 \qquad \text{if } n \neq n_1$$

$$E\left\{x(o)\right\} = \bar{x}(o)$$

$$E\left\{(x(o) - \bar{x}(o))\ (x(o) - \bar{x}(o))'\right\} = X(o)$$

find the linear functional

$$u(n) = \sum_{i=o}^{n} L(n, i)\ m(i)$$

that minimizes the quadratic J**

$$J^{**} = TR[(Q(N)\ S(N) + V(N)\ R(N) + \sum_{n=o}^{n-1} \Delta t(Q(n)\ S(n) + V(n)\ R(n))].$$

where

$$R(n) = \bar{r}(n)\ \bar{r}(n)'$$

$$S(n) = E\left\{(r(n) - \bar{r}(n))\ (r(n) - \bar{r}(n))'\right\}$$

It is assumed that Q(n) and V(n) are symmetric and non-negative definite for N=0, . . . N, and $D_1(n)'\ Q(n)\ D_1(n)$ and $D_1(n)'\ V(n)\ D_1(n)$ are positive definite for $n < N$, and

$$Q(N)\ D_1(N) = V(N)\ D_1(N) = 0$$

SOLUTION OF THE DIFFERENCE EQUATION FORMULATION

The solution to the above difference equation problem follows that presented in Section III for the differential equations problem. The optimum control is of the form

$$u(n) = K_Q(n)\,\hat{x}(n) + [K_V(n) - K_Q(n)]\,\bar{x}(n) + f_V(n)$$

where $\bar{x}(n)$ is the apriori mean state

$$\bar{x}(n) = E\left\{x(n)\right\}$$

and $\hat{x}(n)$ is the conditional estimate

$$\hat{x}(n) = E\left\{x(n) \,\middle|\, m(o), \ldots m(n),\ u(o), \ldots u(n-1),\ \bar{v}_\omega(o), \ldots \bar{v}_\omega(n-1)\right\}.$$

The gains $K_V(n)$ and input $f_V(n)$ are the solutions of the backwards difference equations

$$P_V(N) = H_1(N)'\ V(N)\ H_1(N)$$

$$g(N) = H_1(N)'\ V(N)$$

$$K_V(n) = -\,[B_1(n)'\ P_V(n+1)\ B_1(n) + \Delta t\ D_1(n)'\ V(n)\ D_1(n)]^{-1}\,.$$

$$.\ [B_1(n)'\ P_V(n+1)\ A(n) + \Delta t\ D_1(n)'\ V(n)\ H_1(n)]\,\cdot$$

$$f_V(n) = -\,[B_1(n)'\ P_V(n+1)\ B_1(n) + \Delta t\ D_1(n)'\ V(n)\ D_1(n)]^{-1}.$$

$$.\ [B_1(n)'\ (g(n+1) + P_V(n+1)\ B_2(n)\ \bar{v}_\omega(n)) + \Delta t\ D_1(n)'\ V(n)\ D_2(n)\ \bar{v}_\omega(n)]$$

$$P_V(n) = [A(n) + B_1(n)\ K_V(n)]'\ P_V(n+1)\ [A(n) + B_1(n)\ K_V(n)]\ +$$

$$+ \Delta t\ [H(n) + D_1(n)\ K_V(n)]'\ V(n)\ [H(n) + D_1(n)\ K_V(n)]$$

$$g(n) = [A(n) + B_1(n)\ K_V(n)]'\ [g(n+1)\ (B_1(n)\ f(n) + B_2(n)\ \bar{v}_\omega(n))]$$

$$+ \Delta t\ [H(n) + D_1(n)\ K_V(n)]'\ V(n)\ [D_2(n)\ \bar{v}_\omega(n) + D_1(n)\ f(n)]$$

The gain $K_Q(n)$ is the solution to the above when $V(n)$ is replaced by $Q(n)$.

The solution to the Kalman's state estimation problem is

$$\hat{x}(n) = x_1(n) + \bar{x}(n)$$

$$x_1(n+1) = (A(n) - L(n)\ H(n))\ x_1(n) + L(n)\ m\ (n)$$

where $L(n)$ is the solution of the forward Riccati equation

$$P_\eta(o) = X(o)$$

$$\Delta t\ L(n) = [A(n)\ P_\eta(n)\ H(n)' + B_3(n)\ \frac{W_3(n)}{\Delta t}]\ [H_2(n)\ P_\eta(n)\ H_2(n) + \frac{W_2(n)}{\Delta t}]^{-1}$$

$$P_\eta(n+1) = A(n)\ P_\eta(n)\ A(n)' + B_3(n)\ \frac{W_1(n)}{\Delta t}\ B_3(n)'$$

$$- \Delta t\ L(n)\ [H_2(n)\ P_\eta(n)\ H_2(n) + \frac{W_2(n)}{\Delta t}]\ L(n)'\ \Delta t.$$

The matrix $P_\eta(n)$ in these equations is the covariance matrix of the estimation error $x(n) - \hat{x}(n)$

$$\tilde{x}(n) = x(n) - \hat{x}(n)$$

$$P_\eta(n) = \mathrm{cov}\left\{ \tilde{x}(n)\ \tilde{x}(n)' \right\}$$

$$= E\left\{ \tilde{x}(n)\ \tilde{x}(n)' \right\}$$

The estimation error $\tilde{x}(n)$ has zero mean,

$$E\left\{\hat{x}(n)\right\} = 0$$

A state covariance transition matrix can be derived from this property.

With

$$x(n+1) = A(n)\, x(n) + B_1(n)\, K(n)\, \hat{x}(n) + B_2(n)\, \bar{v}_\omega(n) + B_3(n)\, \eta_1(n)$$

$$\bar{x}(n+1) = A(n)\, \bar{x}(n) + B_1(n)\, K(n)\, \bar{x}(n) + B_2(n)\, \bar{v}_\omega(n)$$

then

$$x(n+1) - \bar{x}(n+1) = A(n)\,(x(n) - \bar{x}(n)) + B_1(n)\, K(n)\,(\hat{x}(n) - \bar{x}(n)) + B_3(n)\, \eta_1(n)$$

$$= (A(n) + B_1(n)\, K(n))\,(\hat{x}(n) - \bar{x}(n)) + A(n)\, \tilde{x}(n) + B_3(n)\, \eta_1(n)$$

Then

$$\mathrm{cov}\left\{x(n+1)\, x(n+1)'\right\} = E\left\{(x(n+1) - \bar{x}(n+1))\,(x(n+1) - \bar{x}(n+1))'\right\}$$

$$= (A(n) + B_1(n)K(n))E\left\{(\hat{x}(n) - \bar{x}(n))\,(\hat{x}(n) - \bar{x}(n))'\right\}(A(n) + B_1(n)K(n))'$$

$$+ (A(n) + B_1(n)K(n))E\left\{(\hat{x}(n) - \bar{x}(n))\,\tilde{x}(n)'\right\} A(n)'$$

$$+ (A(n) + B_1(n)K(n))E\left\{(\hat{x}(n) - \bar{x}(n))\,\eta_1(n)'\right\} B_3(n)'$$

$$+ A(n)E\left\{\tilde{x}(n)\,(\hat{x}(n) - \bar{x}(n))'\right\}(A(n) + B_1(n)K(n))'$$

$$+ A(n)E\left\{\tilde{x}(n)\tilde{x}(n)'\right\} A(n)' \; +$$

$$+ A(n)E\{\tilde{x}(n)\ \eta_1(n)'\}\ B_3(n)'$$

$$+ B_3(n)E\{\eta_1(n)\ (\hat{x}(n) - \bar{x}(n))'\}\ (A(n) + B_1(n)K(n))'$$

$$+ B_3(n)E\{\eta_1(n)\tilde{x}(n)'\}\ A(n)'$$

$$+ B_3(n)E\{\eta_1(n)\ \eta_1(n)'\}\ B_3(n)'$$

Since $x(n)$, $\hat{x}(n)$, and hence $\tilde{x}(n)$, are functions of past inputs, they are independent of the current (white) input $\eta_1(n)$, and

$$E\{(\hat{x}(n) - \bar{x}(n))\ \eta_1(n)'\} = E\{\tilde{x}(n)\ \eta_1(n)'\} = 0$$

From above

$$E\{(\hat{x}(n) - \bar{x}(n))\ \tilde{x}(n)'\} = E\{\hat{x}(n)\ \tilde{x}(n)'\} - \bar{x}(n)\ E\{\tilde{x}(n)'\}$$

$$= 0 - 0 = 0$$

Hence

$$\mathrm{cov}\{x(n+1)\ x(n+1)\} = (A(n) + B_1(n)\ K(n))\ E\{(\hat{x}(n) - \bar{x}(n))\ (\hat{x}(n) - \bar{x}(n))'\}$$

$$(A(n) + B_1(n)\ K(n))' + A(n)\ E\{\tilde{x}(n)\ \tilde{x}(n)'\}\ A(n)' + B_3(n)\ E\{\eta_1(n)\ \eta_1(n)'\}\ B_3(n)'$$

With $\hat{x} - \bar{x} = x - \bar{x} - \tilde{x}$,

$$E\{(\hat{x}(n) - \bar{x}(n))\ (\hat{x}(n) - \bar{x}(n)\} = E\{(x(n) - \bar{x}(n))\ (x(n) - \bar{x}(n))'\}$$

$$- E\{(x(n) - \bar{x}(n))\ \tilde{x}(n)'\} - E\{\tilde{x}(n)\ (x(n) - \bar{x}(n))'\}$$

$$+ E\{\tilde{x}(n)\ \tilde{x}(n)'\}$$

$$= \mathrm{cov}\{x(n)\ x(n)'\} - 2E\{\tilde{x}(n)\ \tilde{x}(n)'\} + E\{\tilde{x}(n)\ \tilde{x}(n)\},$$

then

$$\mathrm{cov}\{x(n+1)\, x(n+1)'\} = [(A(n) + B_1(n)\, K(n))]\, [\mathrm{cov}\{x(n)\, x(n)'\} - P_\eta(n)]\, (A(n) + B_1(n) K(n))' + A(n)\, P_\eta(n)\, A(n)' + B_3(n) \frac{W_1(n)}{\Delta t}\, B_3(n)'.$$

APPENDIX H
PARTIAL DERIVATIVES OF J*

The minimization of the upper-bound J* by the iteration procedure described in Section III requires calculation of various partial derivatives of J*. The formulas for these derivatives are presented in this appendix.

The functional J* as defined in Appendix E is the form

$$J^* = f_1(S(T),\ R(T)) + \int_0^T f_2(S(t),\ R(t))\ dt$$

where the functional f_1 is the sum of the terminal likelihoods $P(\bar{a}_i)$, and the functional f_2 is the sum of in-flight expectations $E\left\{N_i\right\}$. Defining the vector r(t) to be

$$r(t) = \begin{bmatrix} \beta(t) \\ \dot{\beta}(t) \\ I_b(t) \\ \dot{I}_b(t) \\ \dot{\phi}(t) + 0.388\,\alpha(t) \\ z(t) \\ \dot{z}(t) \end{bmatrix}$$

the terminal partial derivatives are

$$\frac{\partial f_1}{\partial R_{ij}} = \frac{\partial f_1}{\partial S_{ij}} = 0 \quad \text{for } i \neq j$$

$$\frac{\partial f_1}{\partial R_{ii}} = \frac{\partial f_1}{\partial S_{ii}} = 0 \quad \text{for } i < 5$$

$$\frac{\partial f_1}{\partial R_{ii}} = \frac{e^{-\frac{\gamma_i^2 + \bar{r}_i^2}{2S_{ii}}}}{\sqrt{2\pi S_{ii}}} - \frac{\sinh\left(\frac{\gamma_i \bar{r}_i}{S_{ii}}\right)}{\bar{r}_i} \quad \text{for } i = 5,\ 6,\ 7$$

$$\frac{\partial f_1}{\partial S_{ii}} = \frac{e^{-\frac{\gamma_i^2 + \bar{r}_i^2}{2S_{ii}}}}{\sqrt{2\pi S_{ii}}} \cdot \left[\frac{\gamma_i}{\sqrt{S_{ii}}} \cosh\left(\frac{\gamma_i \bar{r}_i}{S_{ii}}\right) - \frac{\bar{r}_i}{\sqrt{S_{ii}}} \sinh\left(\frac{\gamma_i \bar{r}_i}{S_{ii}}\right)\right]$$

$$\text{for } i = 5,\ 6,\ 7$$

The partial derivatives of the in-flight term $f_2(S(t),\ R(t))$ are a little more complex. The derivatives

$$\frac{\partial f_2}{\partial R_{ij}} = \frac{\partial f_2}{\partial S_{ij}} = 0 \quad \text{for} \quad \begin{cases} \text{all } i > 4 \\ \text{all } j > 4 \\ \quad i = 1,\ 2,\ j = 1,\ 2 \\ \quad i = 3,\ 4,\ j = 1,\ 2 \end{cases}$$

The derivations for the $i = 1,\ 2,\ j = 1,\ 2$ and the $i = 3,\ 4,\ j = 3,\ 4$ terms are similar. For the $i = 1,\ 2,\ j = 1,\ 2$ terms

$$P_x(t) = \frac{1}{\sqrt{2\pi M_{11}}} e^{-\frac{\bar{x}^2}{2M_{11}}} \left[\frac{\sigma_x}{\sqrt{2\pi}} e^{-\frac{1}{2}\left(\frac{r_x}{\sigma_x}\right)^2} + r_x \left(\Phi\left(\frac{r_x}{\sigma_x}\right) - 1\right)\right]$$

$$P_y(t) = \frac{1}{\sqrt{2\pi M_{11}}} e^{-\frac{\bar{y}^2}{2M_{11}}} \left[\frac{\sigma_x}{\sqrt{2\pi}} e^{-\frac{1}{2}\left(\frac{r_y}{\sigma_x}\right)^2} + r_y \left(\Phi\left(\frac{r_y}{\sigma_x}\right) - 1\right)\right]$$

where

$$\bar{x} = \bar{r}(t) - \gamma \qquad \bar{r} = \bar{r}_1$$

$$\bar{y} = -\bar{r}(t) - \gamma \qquad \dot{\bar{r}} = \bar{r}_2$$

$$r_x = \bar{x}\,\frac{M_{12}}{M_{11}} - \dot{\bar{r}}(t) \qquad M_{11} = S_{11}$$

$$M_{12} = S_{12} = S_{21}$$

$$r_y = \bar{y}\,\frac{M_{12}}{M_{11}} + \dot{\bar{r}}(t) \qquad M_{22} = S_{22}$$

$$\sigma_x = \sqrt{M_{22} - \frac{M_{12}^{\,2}}{M_{11}}} \qquad \Phi(z) = \int_{-\infty}^{z} \frac{e^{-\frac{1}{2}x^2}}{\sqrt{2\pi}}\,dx$$

The partial derivatives with respect to any variable z are

$$\frac{\partial f_2}{\partial z} = P_x\left[\frac{\partial M_{11}}{\partial z}\left(\frac{\bar{x}^2 - M_{11}}{2M_{11}^{\,2}}\right) - \frac{\partial \bar{x}}{\partial z}\left(\frac{\bar{x}}{M_{11}}\right)\right]$$

$$+ P_y\left[\frac{\partial M_{11}}{\partial z}\left(\frac{\bar{y}^2 - M_{11}}{2M_{11}^{\,2}}\right) - \frac{\partial y}{\partial z}\left(\frac{\bar{y}}{M_{11}}\right)\right]$$

$$+ \frac{e^{-\frac{\bar{x}^2}{2M_{11}}}}{\sqrt{2\pi M_{11}}}\left[\frac{\partial \sigma_x}{\partial z}\,\frac{e^{-\frac{1}{2}\left(\frac{r_x}{\sigma_x}\right)^2}}{\sqrt{2\pi}} + \frac{\partial r_x}{\partial z}\left(\Phi\left(\frac{r_x}{\sigma_x}\right) - 1\right)\right]$$

$$+ \frac{e^{-\frac{\bar{y}^2}{2M_{11}}}}{\sqrt{2\pi M_{11}}}\left[\frac{\partial \sigma_x}{\partial z}\,\frac{e^{-\frac{1}{2}\left(\frac{r_y}{\sigma_x}\right)^2}}{\sqrt{2\pi}} + \frac{\partial r_x}{\partial z}\left(\Phi\left(\frac{r_y}{\sigma_x}\right) - 1\right)\right]$$

where

$$\frac{\partial \bar{x}}{\partial S_{ij}} = \frac{\partial \bar{y}}{\partial S_{ij}} = 0 \text{ for all i, j}$$

$$\frac{\partial M_{11}}{\partial S_{11}} = 1$$

$$\frac{\partial M_{11}}{\partial S_{ij}} = 0 \text{ for i, j, } \neq 1$$

$$\frac{\partial \sigma_x}{\partial R_{ij}} = 0 \text{ for i, j}$$

$$\frac{\partial \sigma_x}{\partial S_{11}} = \frac{-M_{12}^{\ 2}}{2M_{11}^{\ 2}\sigma_x}$$

$$\frac{\partial \sigma_x}{\partial S_{22}} = \frac{1}{2\sigma_x}$$

$$\frac{\partial \sigma_x}{\partial S_{12}} = \frac{\partial \sigma_x}{\partial S_{21}} = \frac{-M_{12}}{2M_{11}\sigma_x}$$

$$\frac{\partial \bar{x}}{\partial R_{11}} = \frac{-\partial \bar{y}}{\partial R_{11}} = \frac{1}{2\bar{r}}$$

$$\frac{\partial \bar{x}}{\partial R_{22}} = \frac{\partial \bar{y}}{\partial R_{22}} = 0$$

$$\frac{\partial \bar{x}}{\partial R_{12}} = \frac{\partial \bar{x}}{\partial R_{21}} = \frac{-\partial \bar{y}}{\partial R_{12}} = \frac{-\partial \bar{y}}{\partial R_{21}} = \frac{1}{2\bar{r}}$$

$$\frac{\partial r_x}{\partial S_{11}} = \frac{-\bar{x}M_{12}}{M_{11}^{\ 2}}$$

$$\frac{\partial r_y}{\partial S_{11}} = \frac{-\bar{y} M_{12}}{M_{11}^{\ 2}}$$

$$\frac{\partial r_x}{\partial S_{12}} = \frac{\partial r_x}{\partial S_{21}} = \frac{\bar{x}}{2 M_{11}}$$

$$\frac{\partial r_y}{\partial S_{12}} = \frac{\partial r_y}{\partial S_{21}} = \frac{\bar{y}}{2 M_{11}}$$

$$\frac{\partial r_x}{\partial S_{22}} = \frac{\partial r_y}{\partial S_{22}} = 0$$

$$\frac{\partial r_x}{\partial R_{11}} = \frac{\partial \bar{x}}{\partial R_{11}} \left(\frac{M_{12}}{M_{11}} \right)$$

$$\frac{\partial r_y}{\partial R_{11}} = \frac{\partial \bar{y}}{\partial R_{11}} \left(\frac{M_{12}}{M_{11}} \right)$$

$$\frac{\partial r_x}{\partial R_{22}} = \frac{-\partial r_y}{\partial R_{22}} = \frac{-1}{2\bar{r}}$$

$$\frac{\partial r_x}{\partial R_{12}} = \frac{\partial r_x}{\partial R_{21}} = \frac{\partial \bar{x}}{\partial R_{12}} \left(\frac{M_{12}}{M_{11}} \right) + \frac{1}{2\bar{r}}$$

$$\frac{\partial r_y}{\partial R_{12}} = \frac{\partial r_y}{\partial R_{21}} = \frac{\partial \bar{y}}{\partial r_{12}} \left(\frac{M_{12}}{M_{11}} \right) + \frac{1}{2\bar{r}}$$

The partial derivatives of f_2 with respect to i = 3, 4, j = 3, 4 terms are the above with 1 replaced by 3 and 2 replaced by 4.

APPENDIX J
CONTROL GAINS AND RESPONSE MOMENTS

Control gains and response moments for the simplest case controller are presented in this appendix as Figures J-1 through J-22.

Figure J-1
K_ϕ versus Time

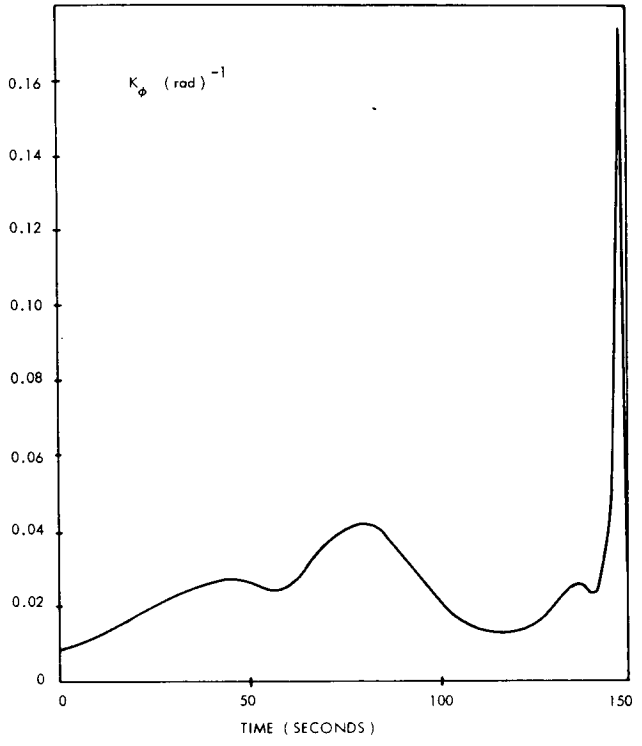

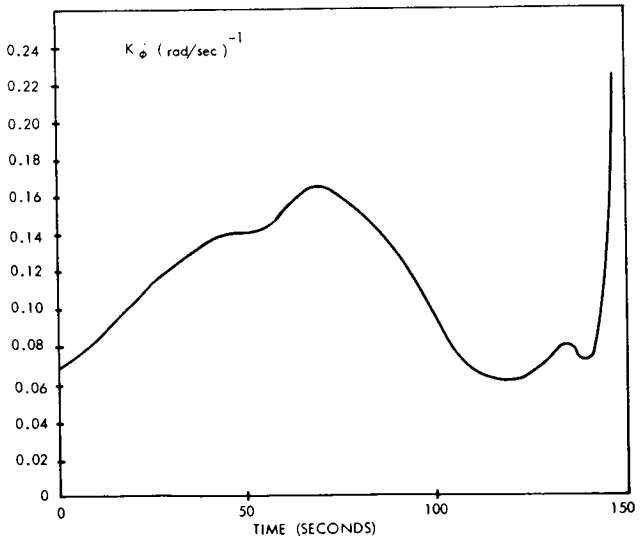

Figure J-2
$K_{\dot\phi}$ versus Time

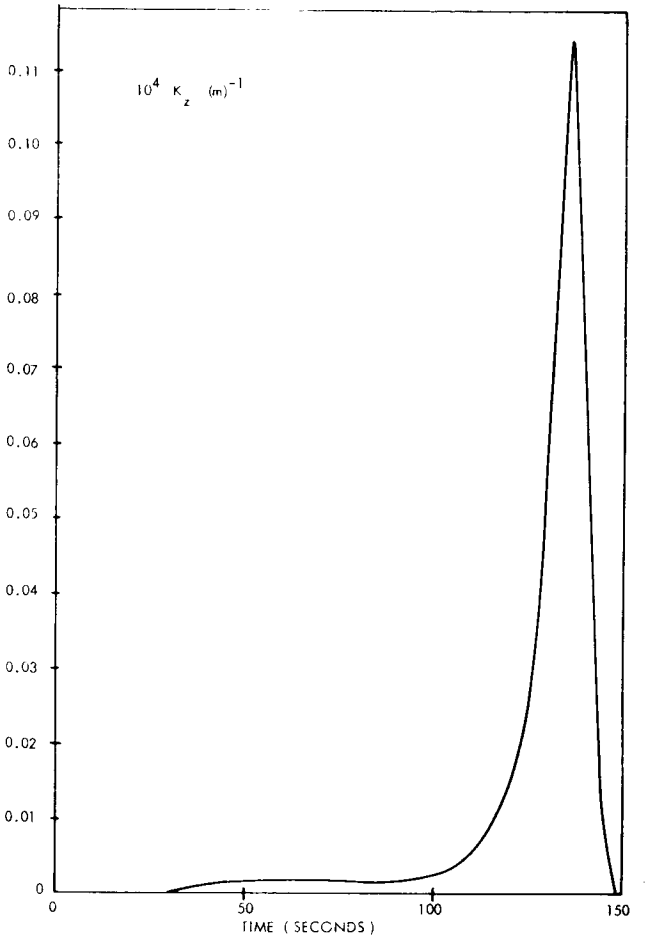

Figure J-3
K_z versus Time

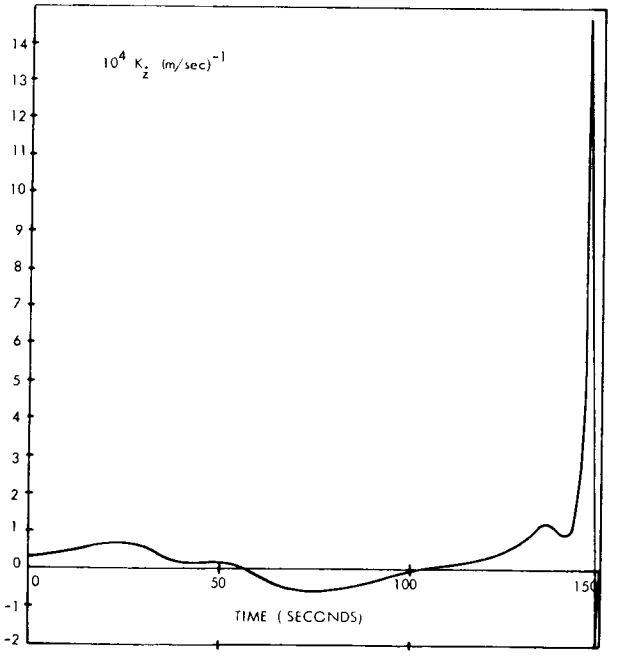

Figure J-4
K_z versus Time

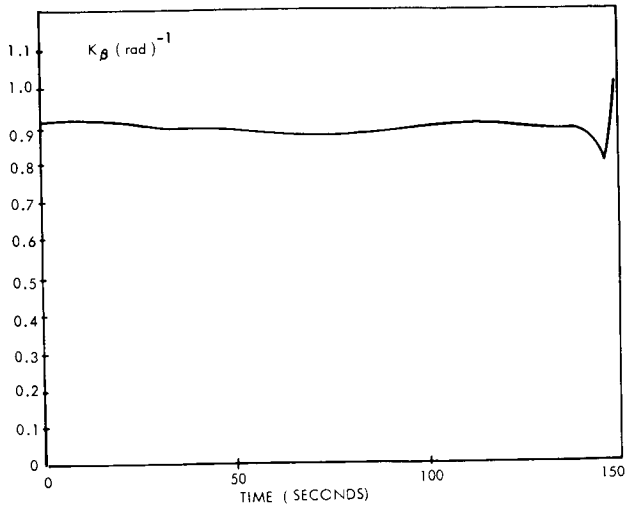

Figure J-5
K_β versus Time

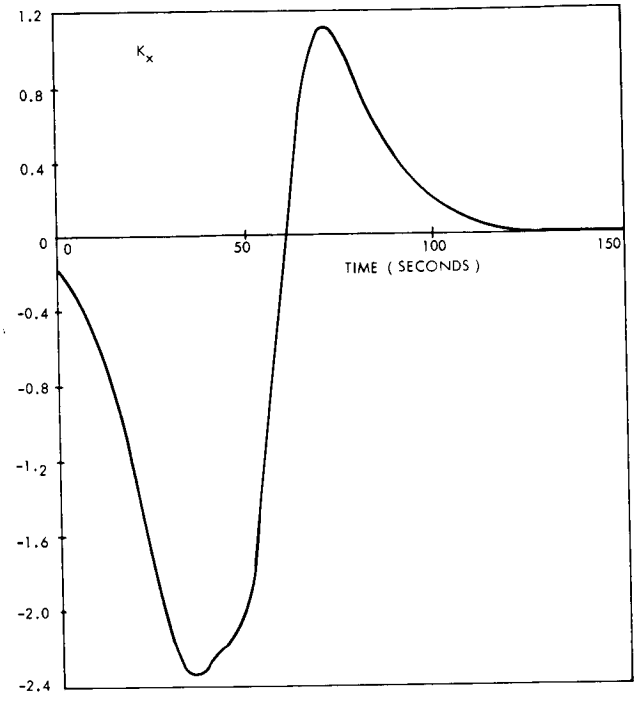

Figure J-6
K_x versus Time

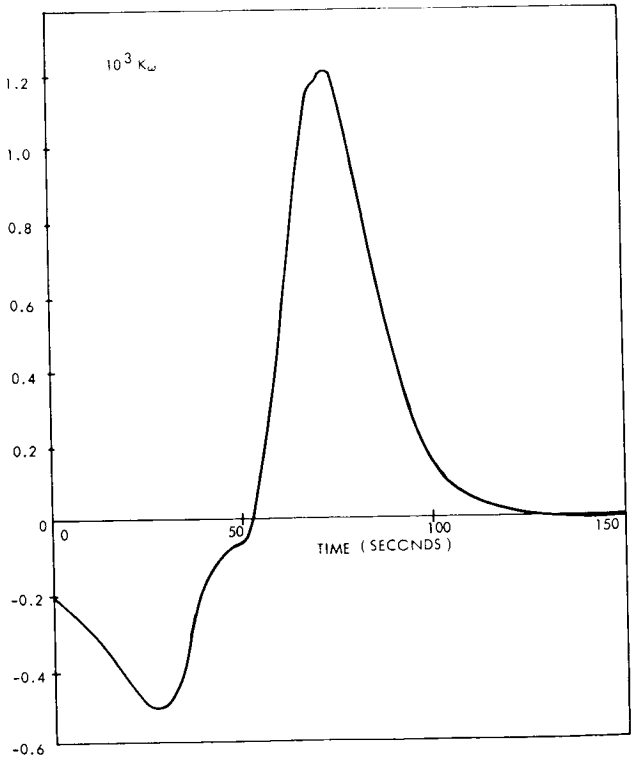

Figure J-7
f(t) versus Time

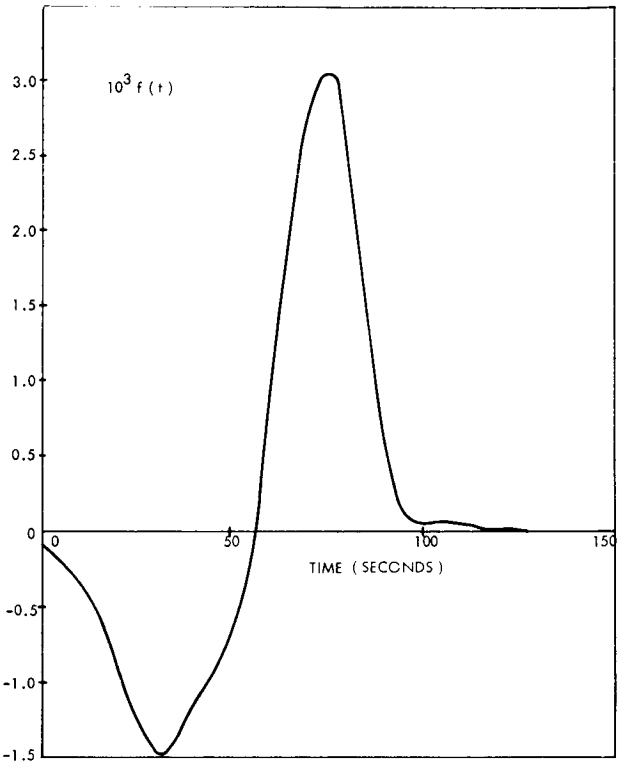

Figure J-8
f(t) versus Time

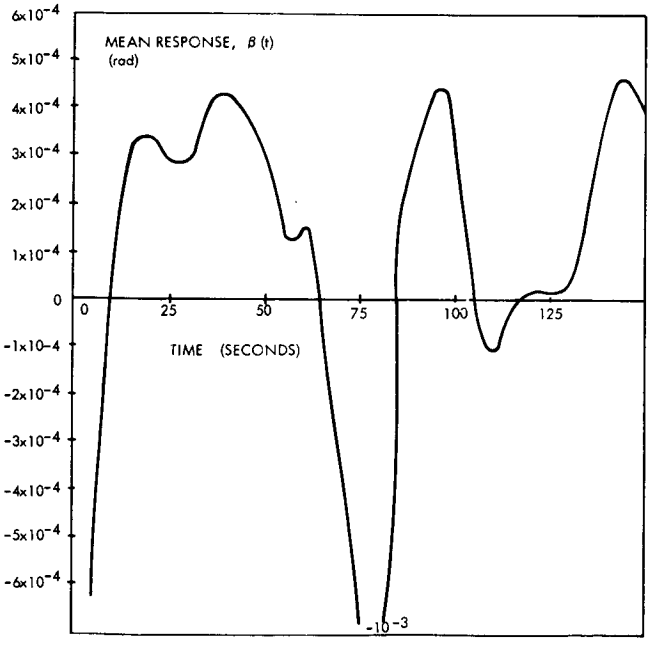

Figure J-9
Mean Response of Gimbal Angle for the Simplest Controller

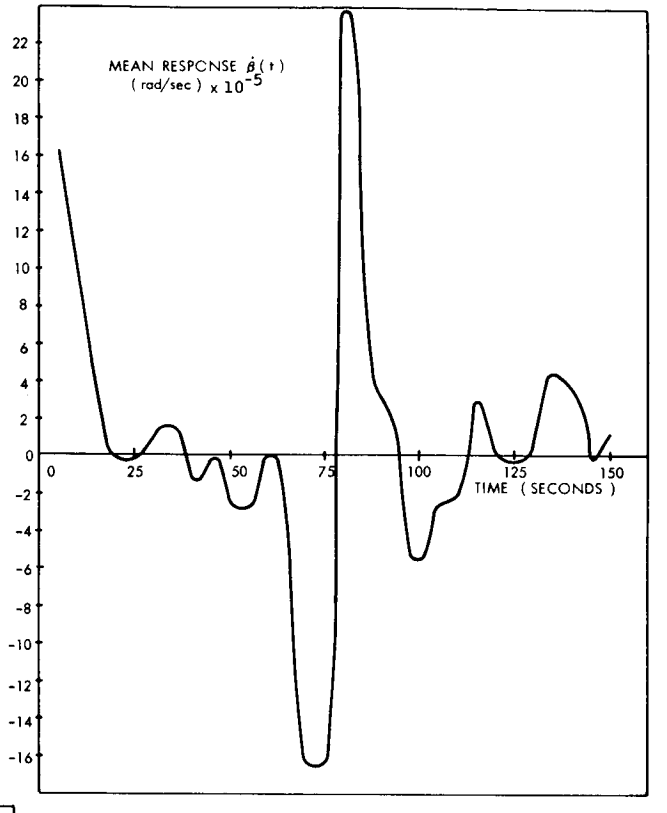

Figure J-10

Mean Response of Gimbal-Angle Rate for the Simplest Controller

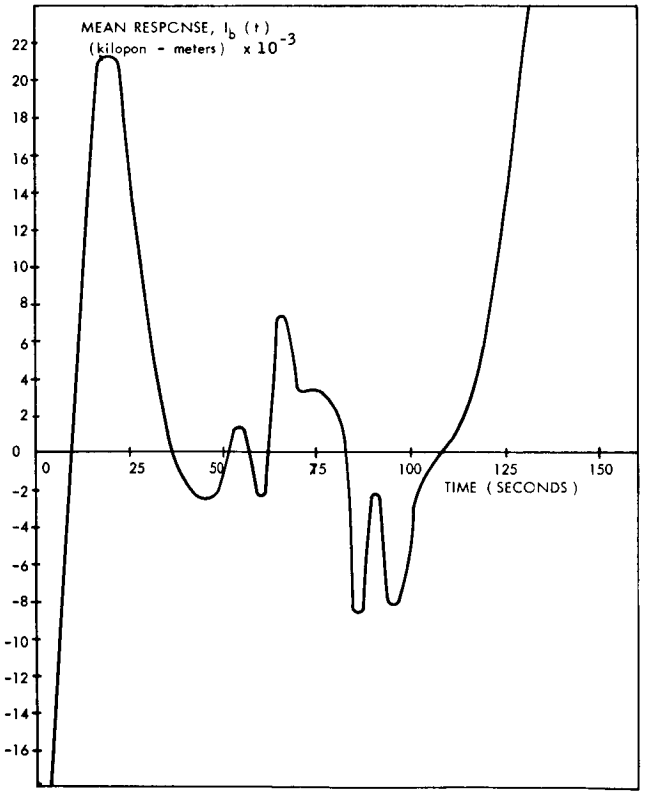

Figure J-11

Mean Response of Bending Moment for the Simplest Controller

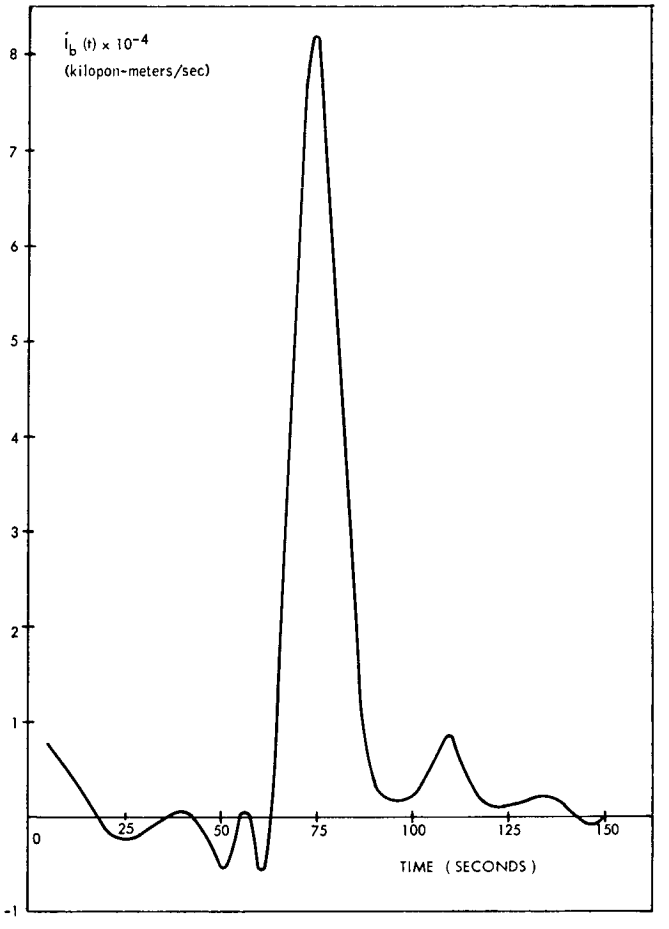

Figure J-12

Mean Response of Bending-Moment Rate for the Simplest Controller

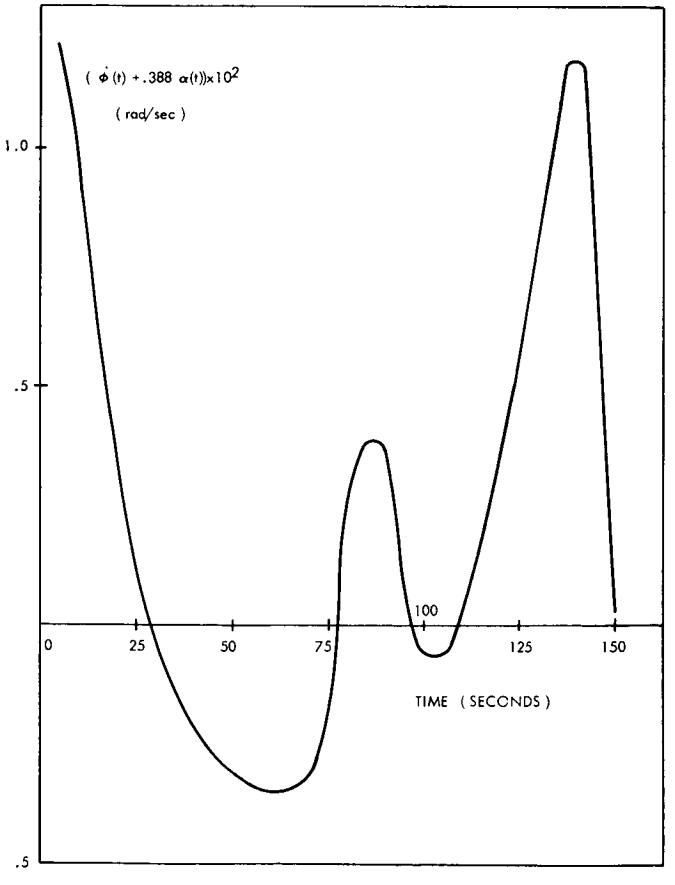

Figure J-13

Mean Response of ($\dot{\phi}$ + 0. 388 α) for the Simplest Controller

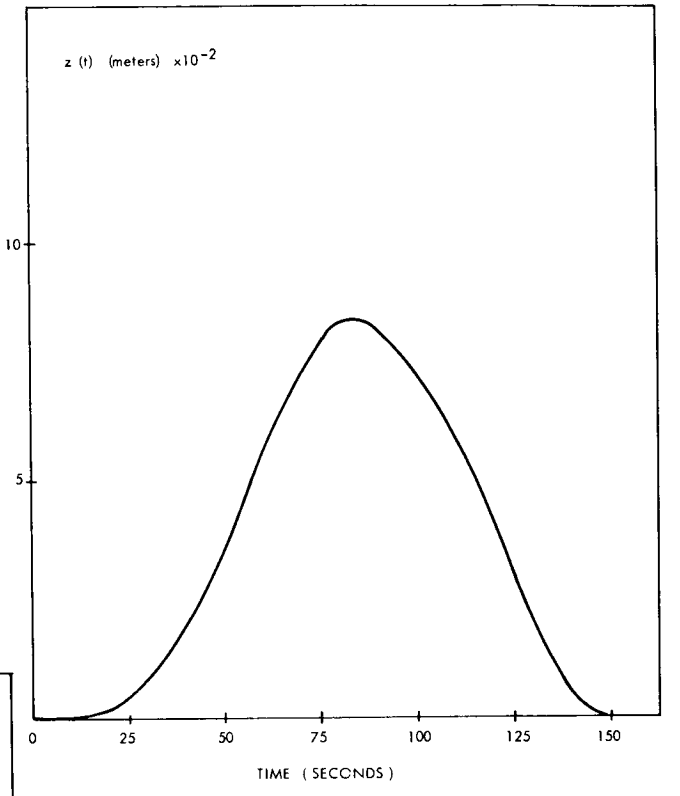

Figure J-14

Mean Response of the Drift for the Simplest Controller

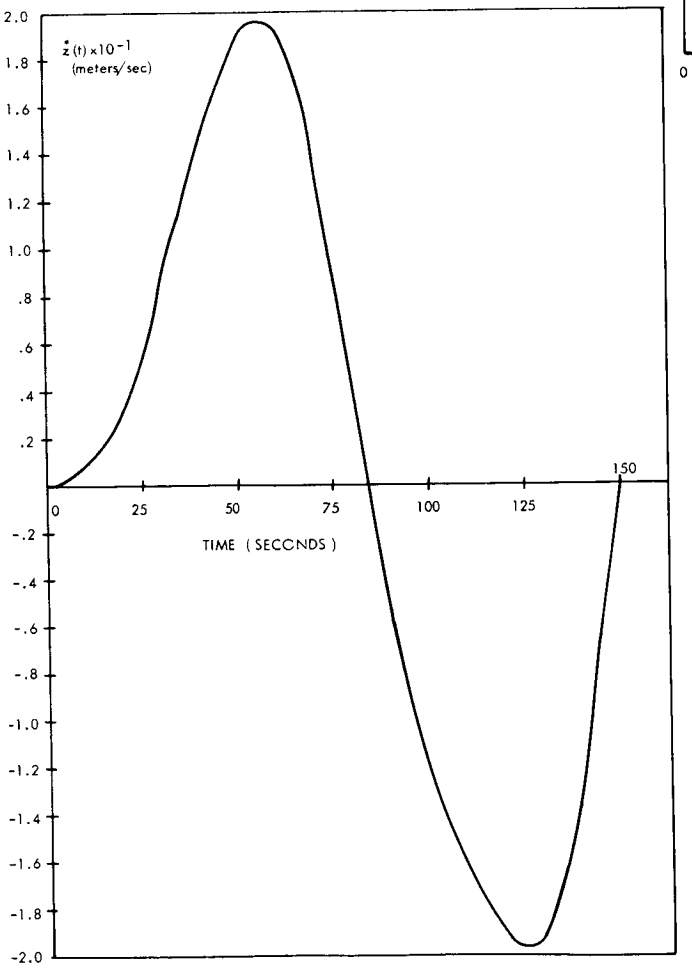

Figure J-15

Mean Response of the Drift Rate for the Simplest Controller

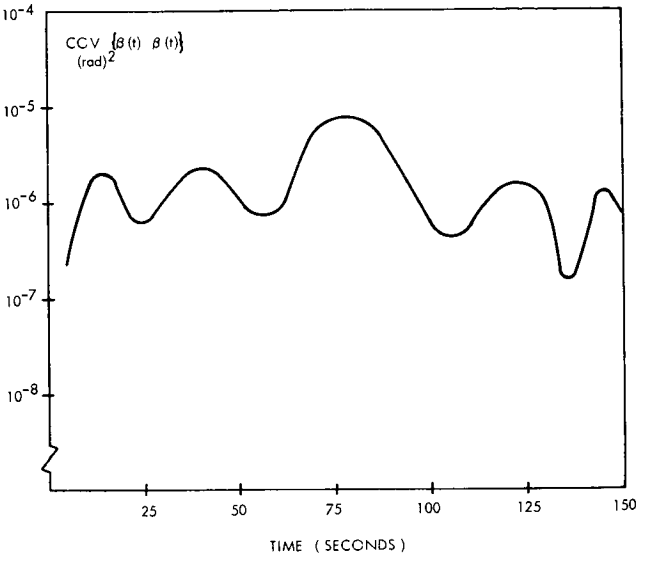

Figure J-16

Gimbal Covariance for the Simplest Controller

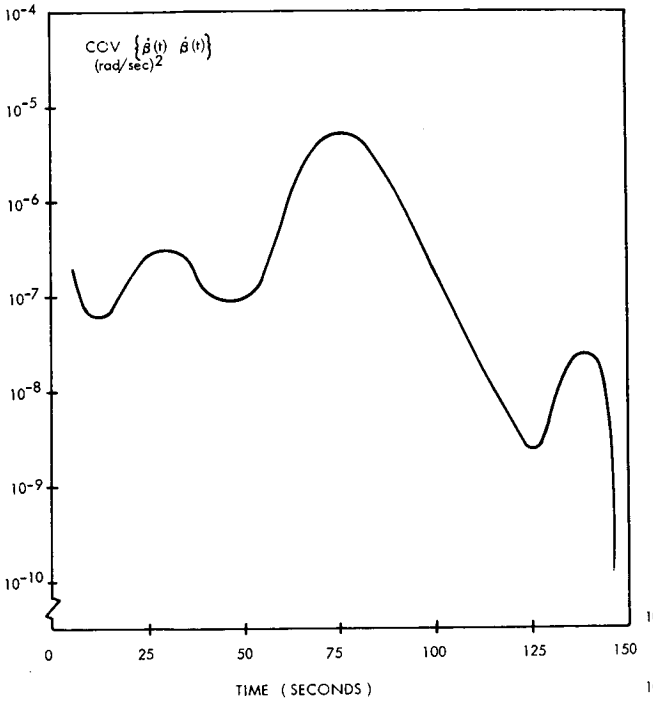

Figure J-17

Gimbal-Rate Covariance for the Simplest Controller

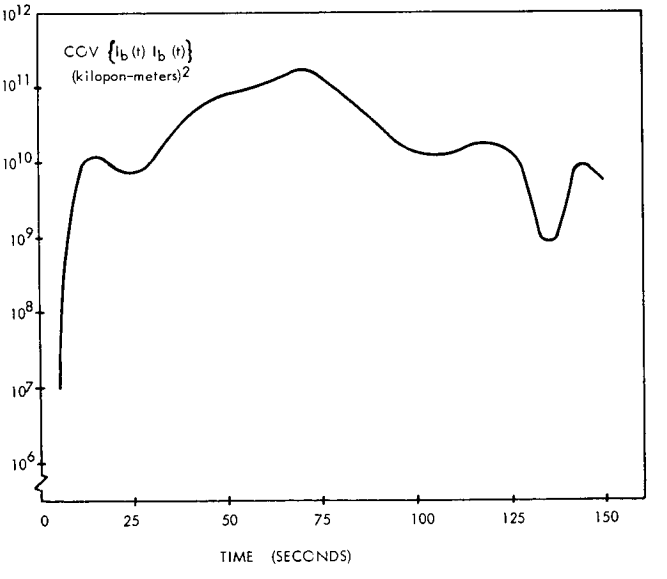

Figure J-18

Bending-Moment Covariance for the Simplest Controller

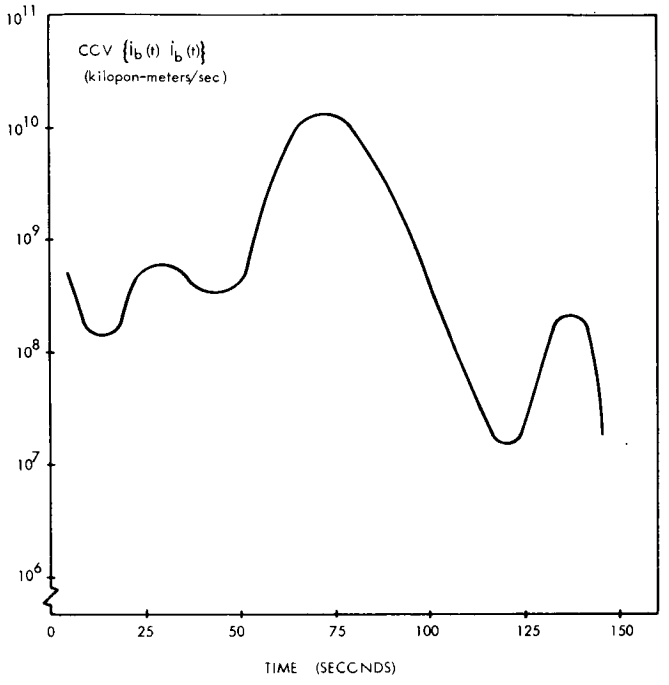

Figure J-19

Bending-Moment-Rate Covariance for the Simplest Controller

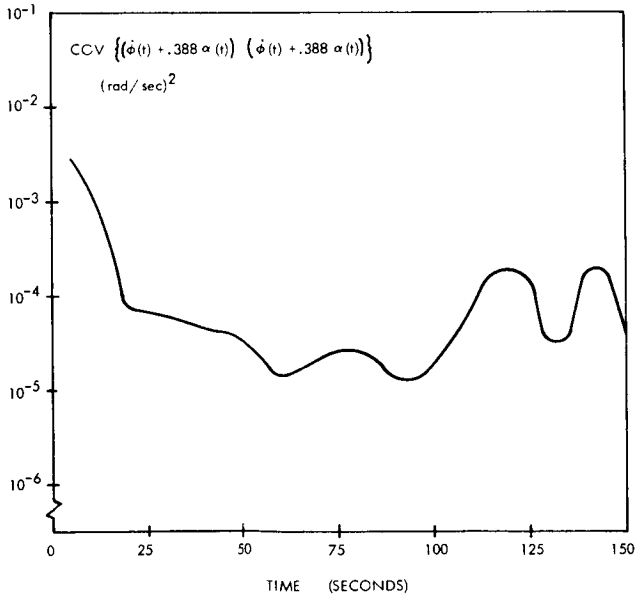

Figure J-20

($\dot{\phi}$ + 0. 388 α) Covariance for the Simplest Controller

Figure J-21

Drift Covariance for the Simplest Controller

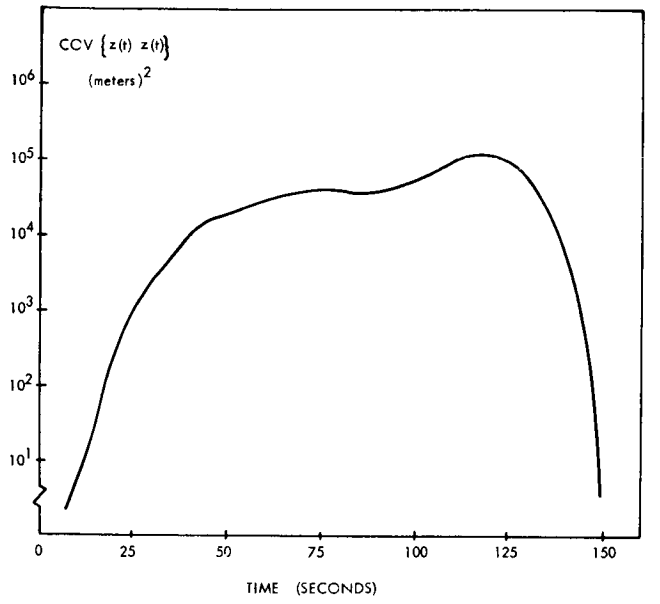

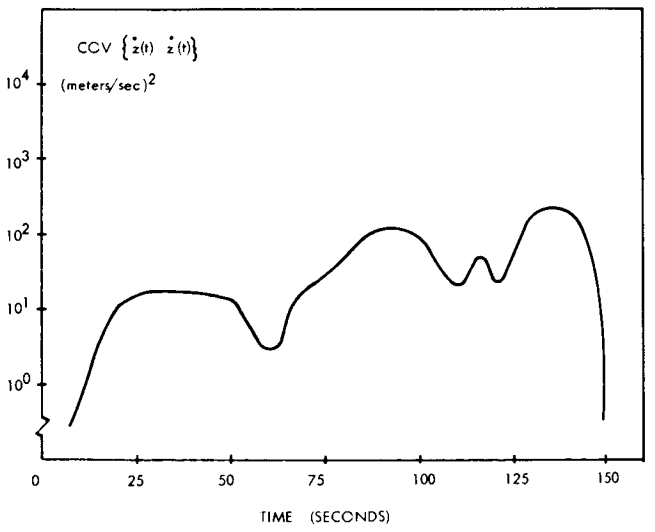

Figure J-22

Drift-Rate Covariance for the Simplest Controller

APPENDIX K
GAINS AND ESTIMATOR ERRORS

Gains and estimator errors for the Case I, Case II, and Case III Kalman estimators are presented in this appendix as Figures K-1 through K-6.

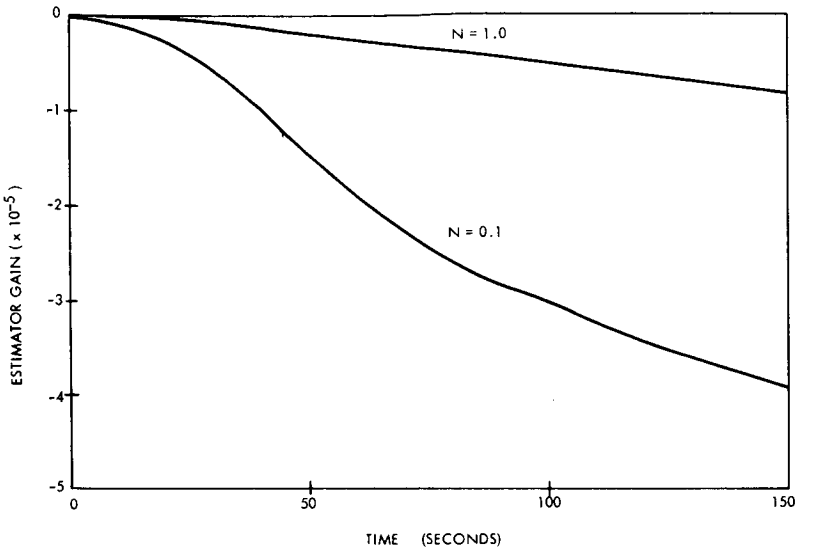

Figure K-1. Estimator Gains - Case I Estimator

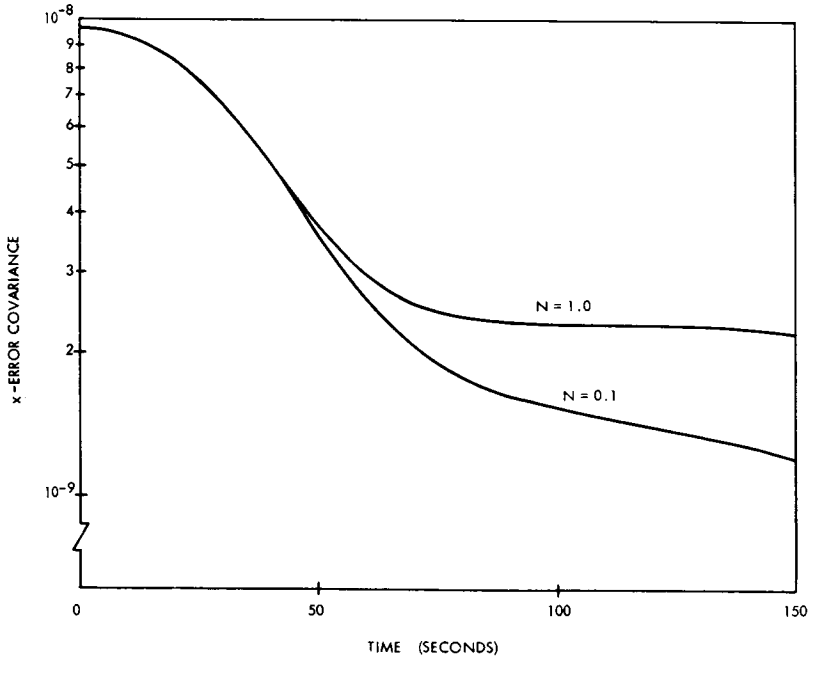

Figure K-2. x-Error Covariance - Case I Estimator

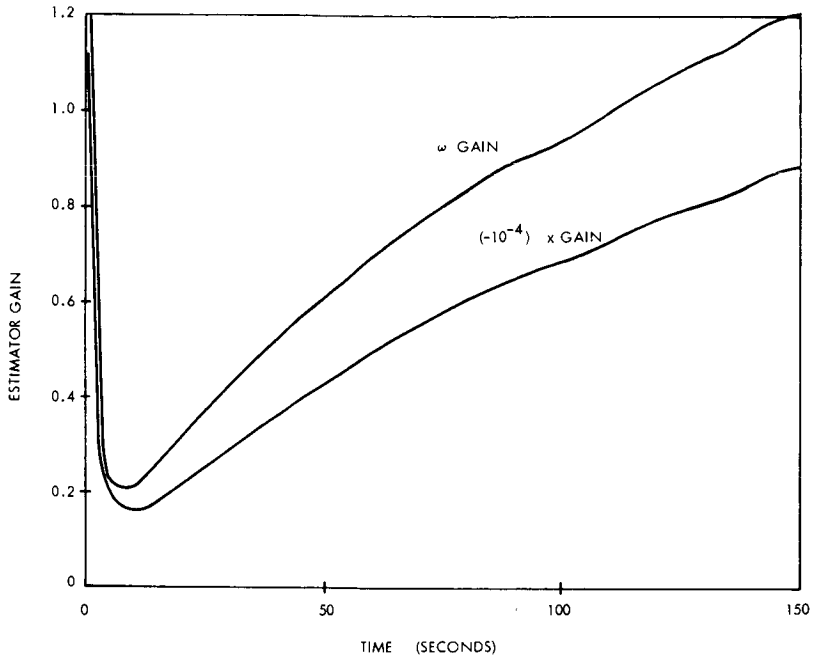

Figure K-3. Estimator Gains - Case II Estimator

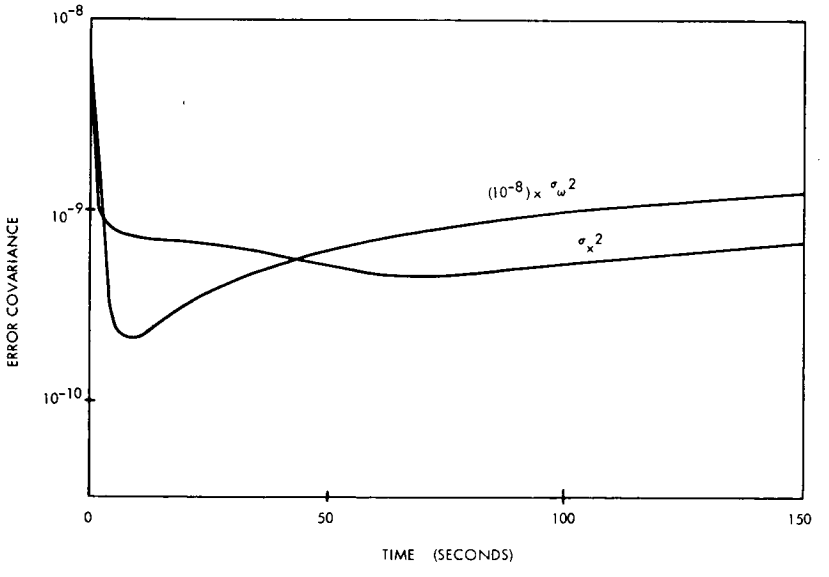

Figure K-4. Error Covariances - Case II Estimator

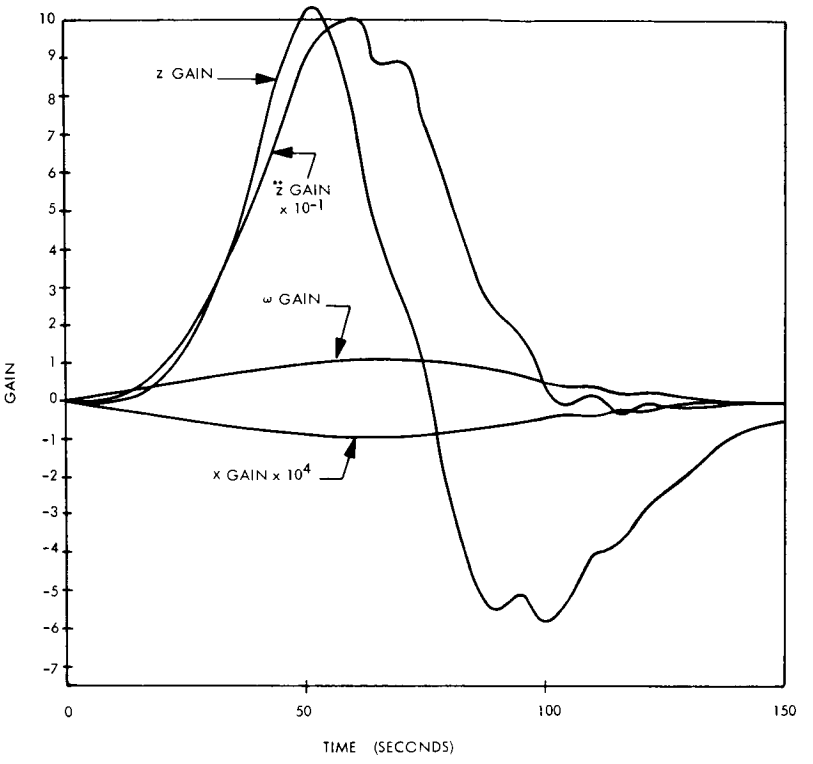

Figure K-5. Estimator Gains - Case III Estimator

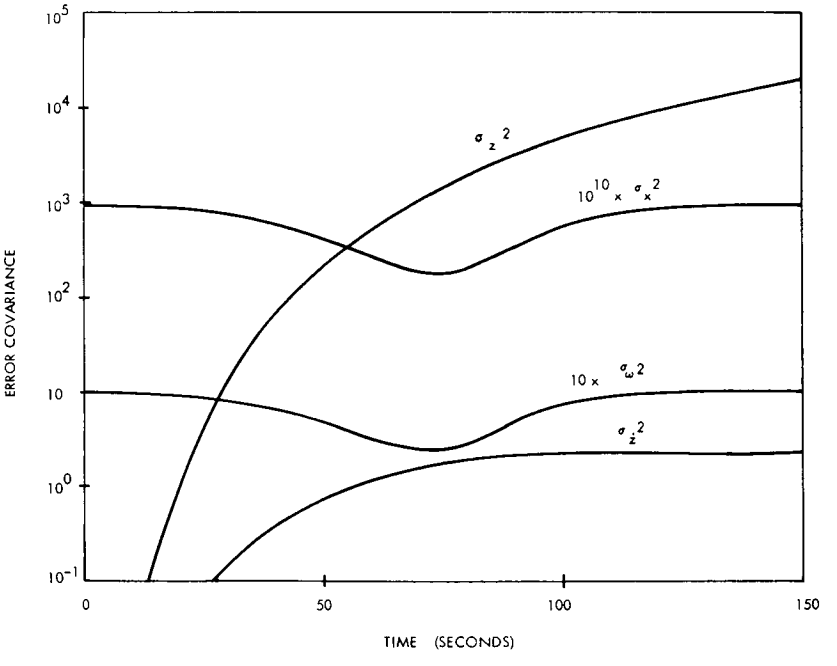

Figure K-6. Error Covariances - Case III Estimator

APPENDIX L
RESPONSE COVARIANCES

Response covariance comparisons for various controllers are presented in this appendix as Figures L-1 through L-20.

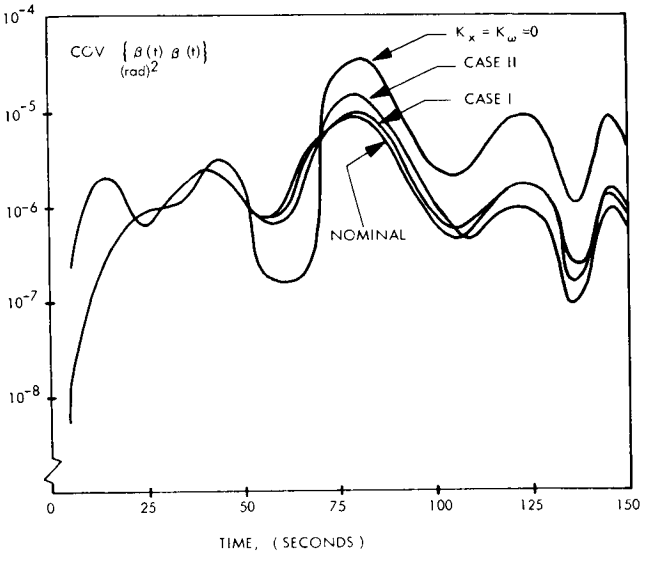

Figure L-1

Gimbal Covariances for Various Controllers

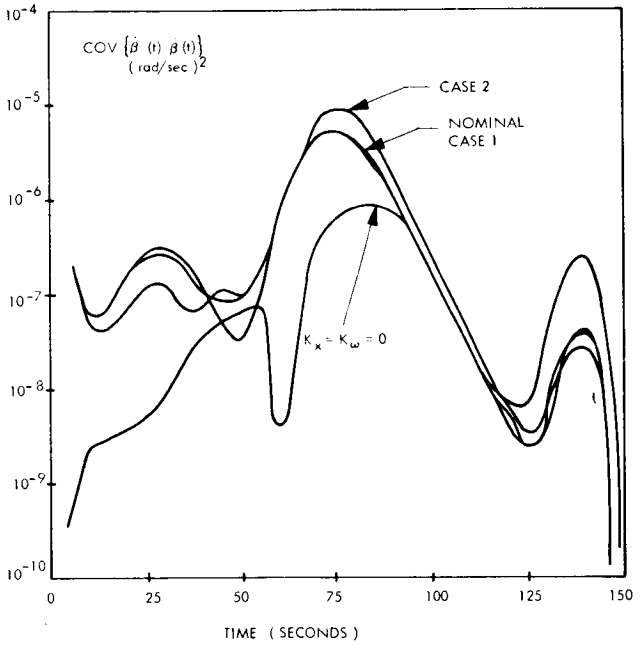

Figure L-2

Gimbal-Rate Covariances for Various Controllers

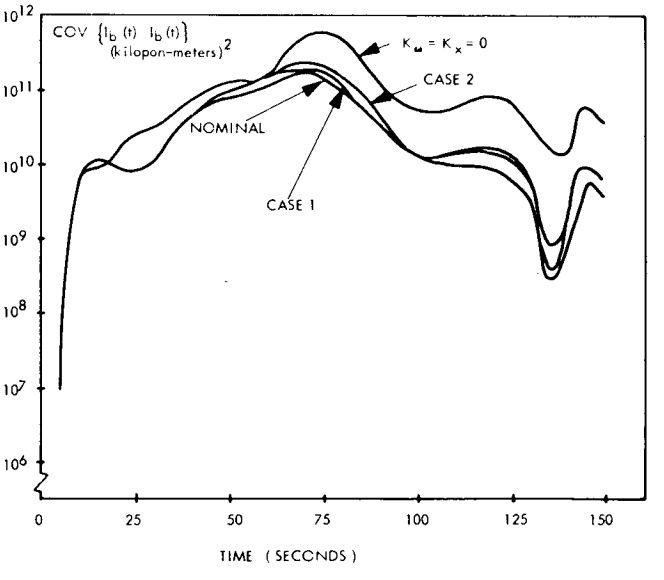

Figure L-3

Bending-Moment Covariances for Various Controllers

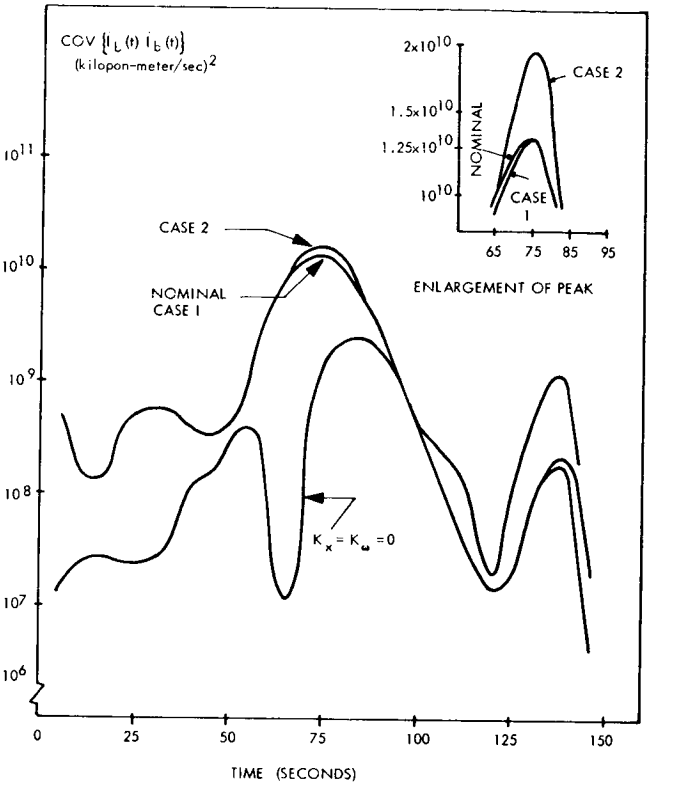

Figure L-4

Body-Bending Rate Covariances for Various Controllers

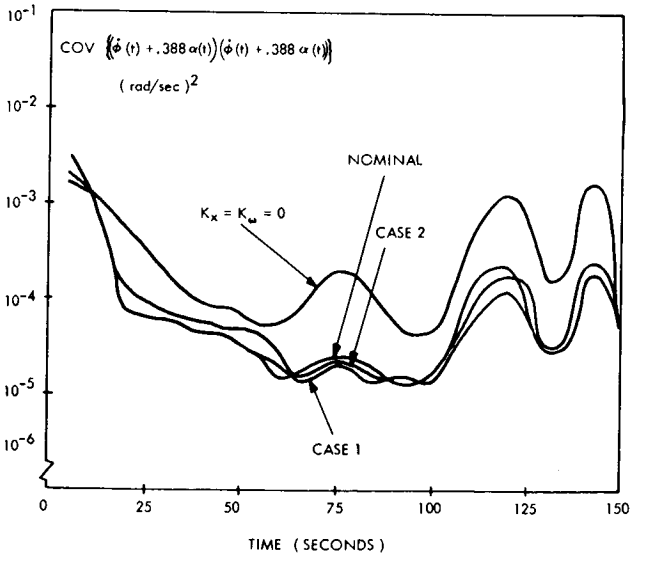

Figure L-5

(ϕ + 0. 388 α) Covariances for Various Controllers

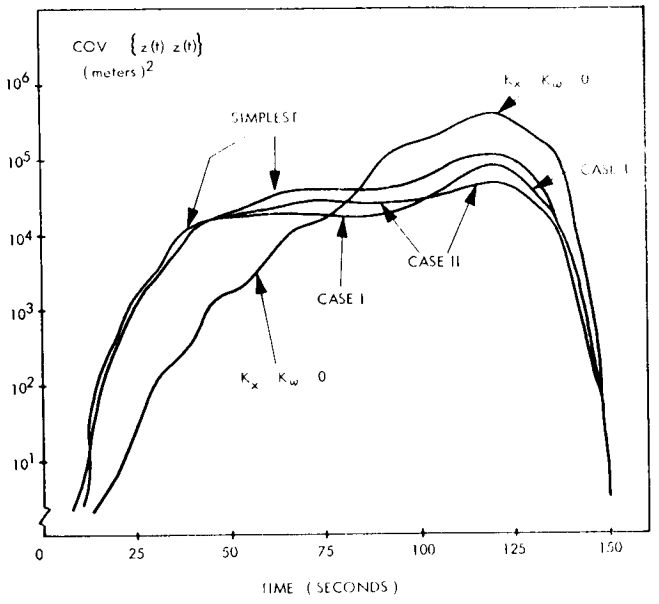

Figure L-6

Drift Covariances for Various Controllers

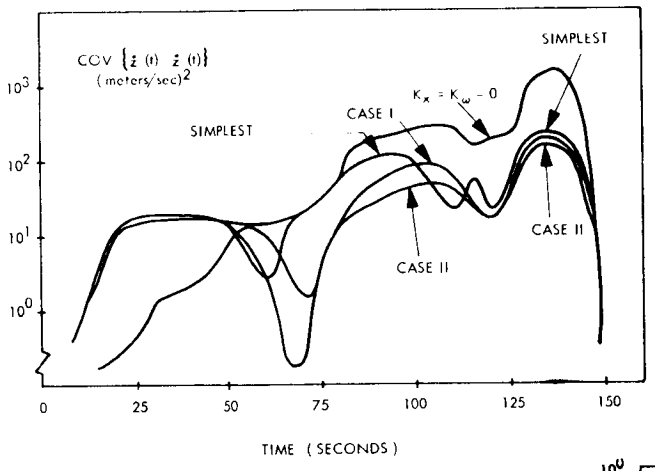

Figure L-7

Drift-Rate Covariances for Various Controllers

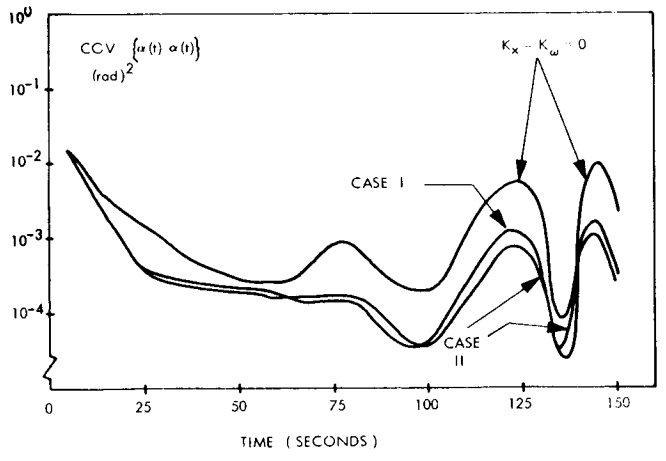

Figure L-8

Angle-of-Attack Covariances for Various Controllers

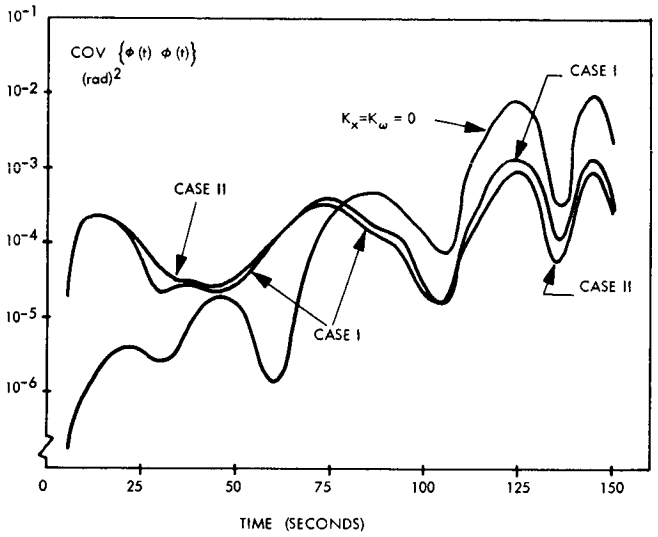

Figure L-9

Attitude Covariances for Various Controllers

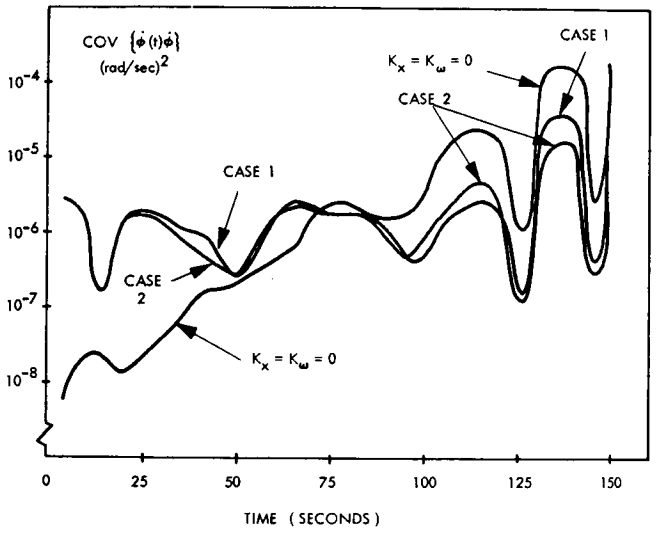

Figure L-10

Attitude-Rate Covariances for Various Controllers

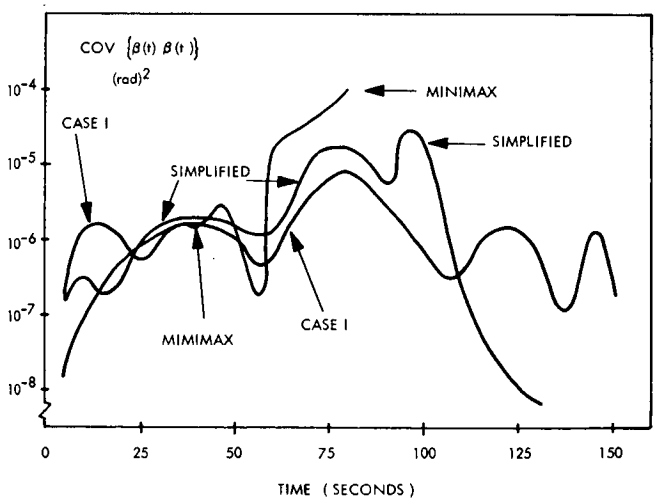

Figure L-11

Gimbal Covariances for Various Controllers

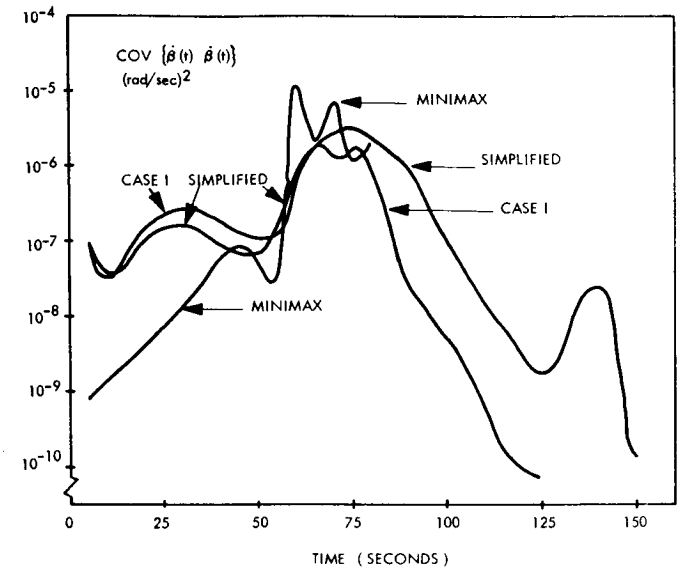

Figure L-12

Gimbal-Rate Covariances for Various Controllers

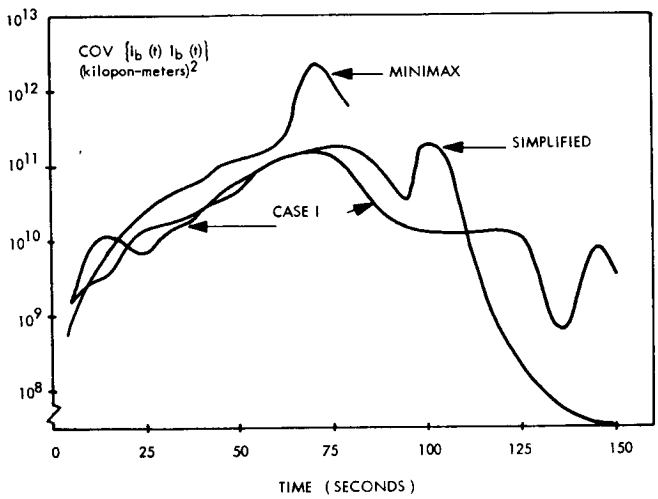

Figure L-13

Bending-Moment Covariances for Various Controllers

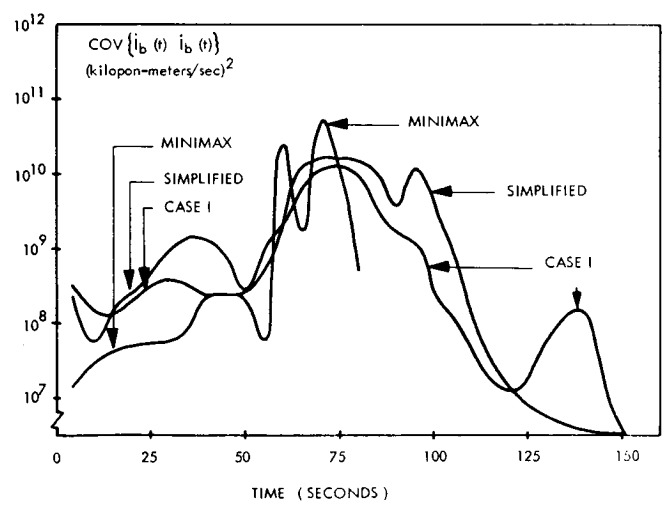

Figure L-14

Bending-Moment-Rate Covariances for Various Controllers

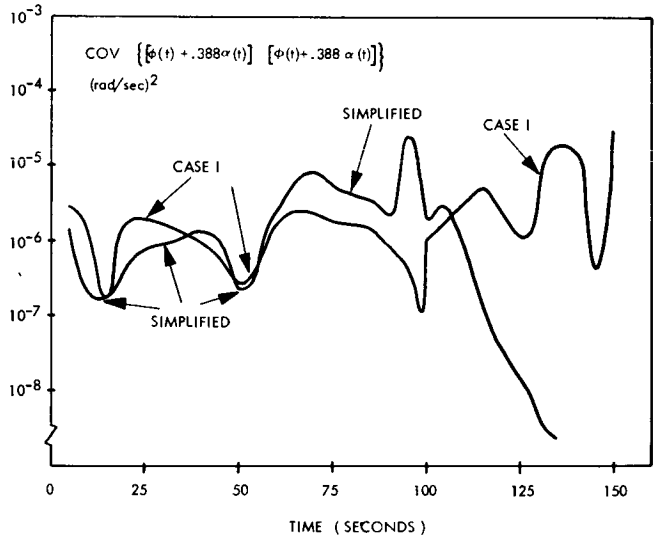

Figure L-15

(ϕ + 0. 388 α) Covariances for Various Controllers

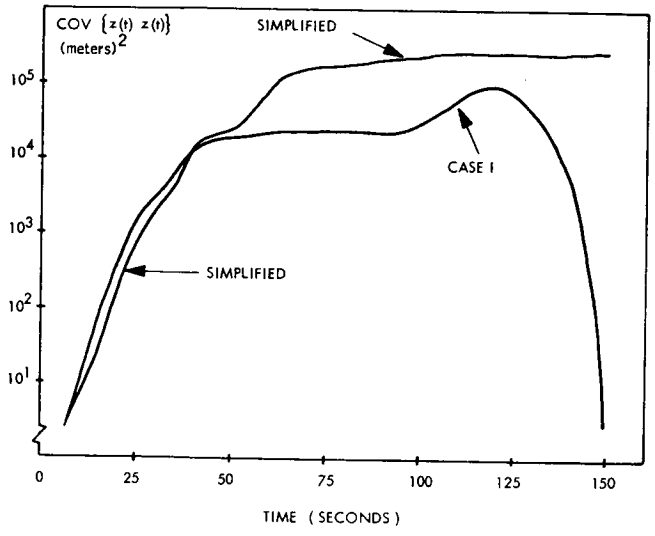

Figure L-16

Drift Covariances for Various Controllers

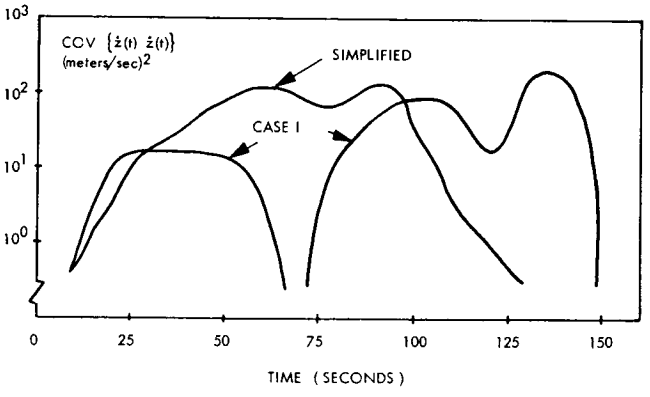

Figure L-17

Drift-Rate Covariances for Various Controllers

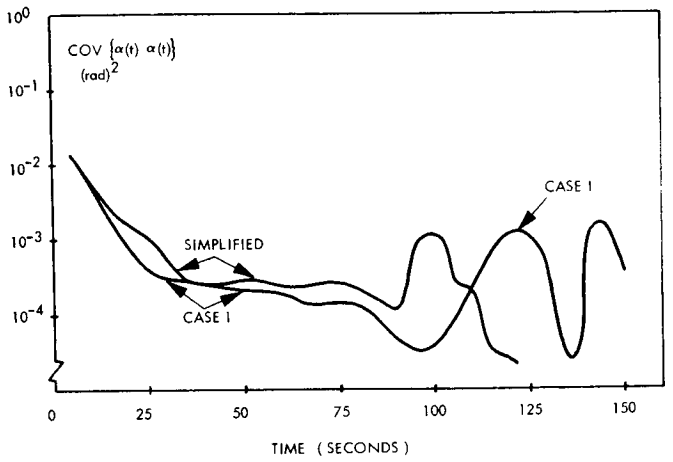

Figure L-18

Angle-of-Attack Covariances for Various Controllers

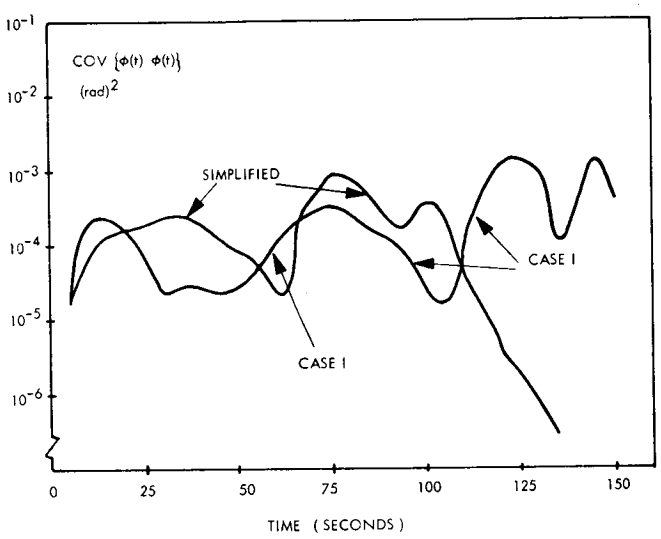

Figure L-19

Attitude Covariances for Various Controllers

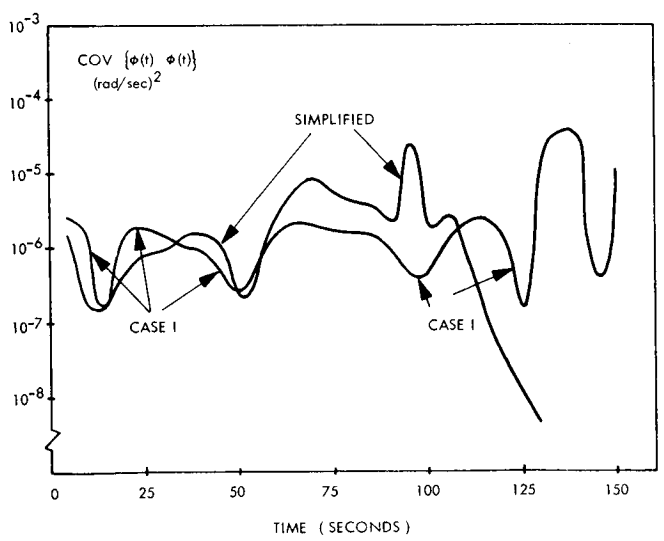

Figure L-20

Attitude-Rate Covariances for Various Controllers

APPENDIX M
ANALOG SIMULATION

This appendix contains a description of the time-varying flight simulation mechanized on a hybrid digital-analog computer. The simulator was used primarily to evaluate the load-relief controller using various wind disturbances. A conventional control system and minimax control system were also evaluated on the simulator for the purpose of comparison with the load relief control system.

The following vehicle equations of motion, wind generator, and conventional control system were simulated on the analog computer portion of the simulator:

- <u>Vehicle Equations</u>

$$\ddot{\phi} = c_1\alpha - c_2\beta$$

$$\ddot{z} = \frac{F-X}{m}\phi + \frac{N'}{m}\alpha + \frac{R'}{m}\beta$$

$$\ddot{\tau} = \ell_A\ddot{\phi} + \frac{N'}{m}\alpha + \frac{R}{m}\beta$$

$$= \ddot{z} - \ell_A\ddot{\phi} - \frac{F-X}{m}\phi$$

$$\alpha = \phi + \frac{v_w - z}{V}$$

$$I_b = M_\alpha{}'\alpha + M_\beta{}'\beta$$

- Actuator Dynamics

$$\dot{\beta} = -14.6\beta + 14.6u$$

- Conventional Control System

$$u = K_c \left[0.75\phi + \dot{\phi} + \frac{0.1}{10S+1} \ddot{\tau} \right]$$

$$x_A = 90 \text{ m}$$

$$K_c = \begin{cases} 0.75, & \tau \leq 100 \text{ sec} \\ 0.23, & \tau > 100 \text{ sec} \end{cases}$$

- Stochastic Wind Generator - The stochastic wind generator is shown in Figure M-1, where

$$d_1 = -0.97 \times 10^{-6} \text{ m}^{-3/2} \qquad \alpha_1 = 0.95 \times 10^{-4} \text{ m}^{-1}$$

$$d_2 = 1.38 \times 10^{-2} \text{ m}^{-1/2} \qquad \alpha_2 = 0.735 \times 10^{-4} \text{ m}^{-1}$$

and K is a scale factor adjusted to make $\omega(t)$ equal to unity.

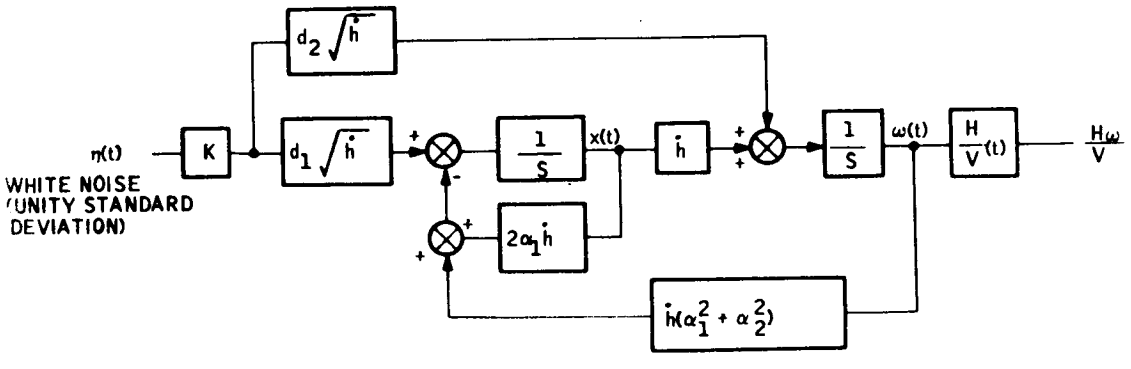

Figure M-1. Stochastic Wind Generator

The following load-relief control system and minimax control system were each simulated on the digital computer:

- Load Relief Controller

$$u = f(t) + K_{\phi}(t) + K_{\dot{\phi}}(t)\,\dot{\phi} + K_{\beta}(t)\,\beta + K_{\dot{z}}(t)\,\dot{z}$$

$$+ K_{z}(t)\,z + K_{\omega}(t)\,\omega + K_{x}(t)x$$

- Minimax Control System

$$u = K_1(t)\,\phi + K_2(t)\,\dot{\phi} + K_3(t)\,\alpha$$

In addition the Case I and Case II estimators were also simulated on the digital computer. Their block diagrams are as shown in Figures M-2 and M-3.

All the data used in the simulation is as plotted or tabulated in the text of the report and, hence, is not duplicated in this appendix.

The simulation employs the following equipment:

(1) Pace 231-R Analog Computer (100 amplifier) - This is the primary analog computer. The linear vehicle equations and linear portions of the wind generator and state estimators are simulated on it.

(2) Digital -Analog Hybrid Computer, consisting of:

(a) Scientific Data Systems 9300 Digital Computer. The digital computer is used to simulate the control law.

(b) Pace 231-R Analog Computer (20 amplifier)
This computer is used mainly as a link between the digital computer and the primary analog computer.

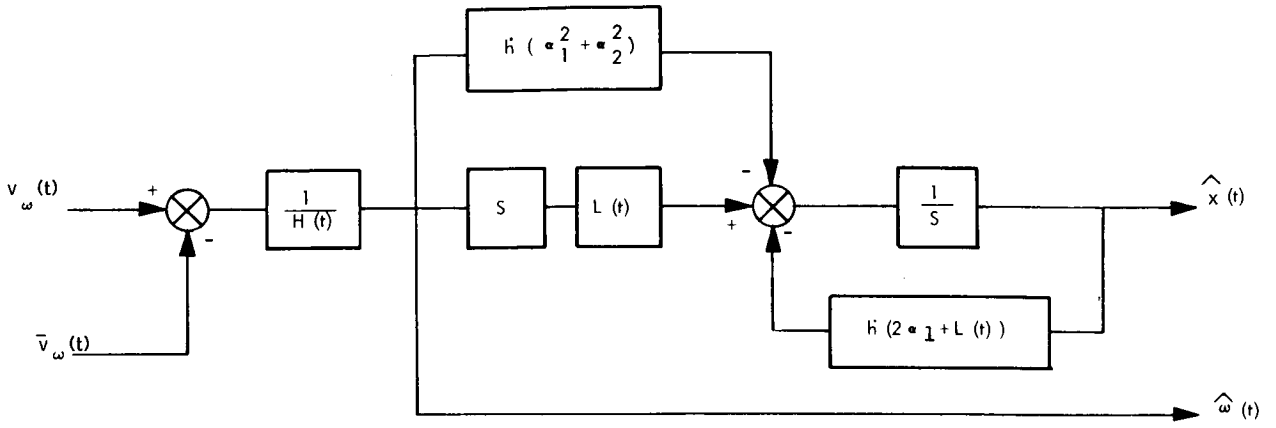

$$\hat{\omega}(t) = \frac{1}{H(t)} \left[\omega(t) - \bar{v}_\omega(t) \right]$$

$$\dot{\hat{x}}(t) = -\dot{h}(2\alpha_1 + L(t))\, x(t) + L(t)\,\dot{\hat{\omega}}(t) - h(\alpha_1^2 + \alpha_2^2)\,\hat{\omega}(t)$$

Figure M-2. Case I Kalman Estimator

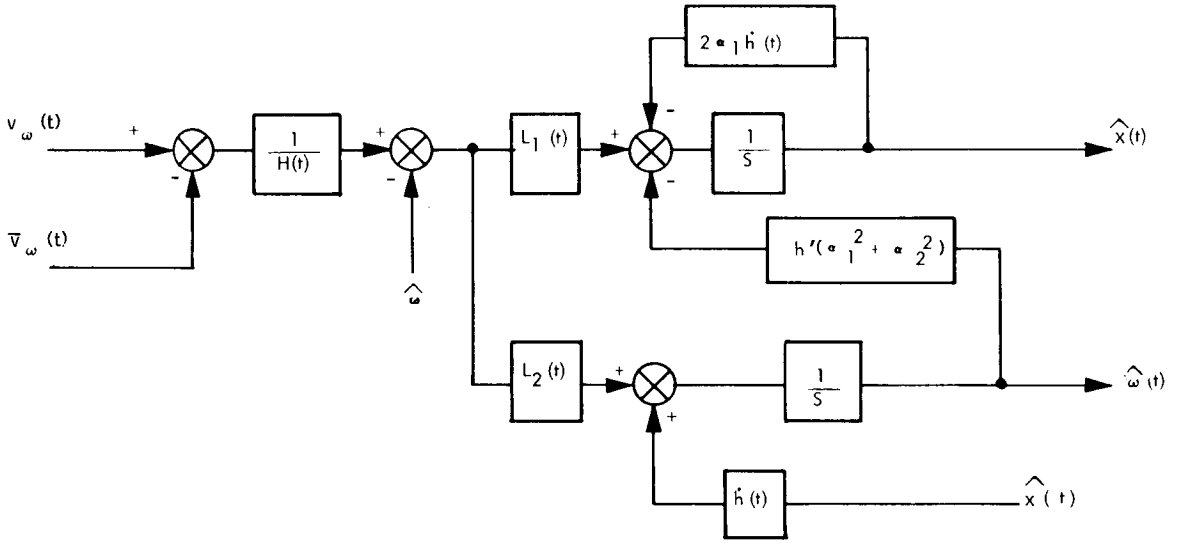

$$\dot{\hat{\omega}} = \dot{h}\hat{x} + L_2 \left(\frac{v_\omega - \bar{v}_\omega}{H(t)} - \hat{\omega} \right)$$

$$\dot{\hat{x}} = -2\alpha_1 \dot{h}\hat{x} - \dot{h}(\alpha_1^2 + \alpha_2^2)\,\hat{\omega} + L_1 \left(\frac{v_\omega - \bar{v}_\omega}{H(t)} - \hat{\omega} \right)$$

Figure M-3. Case II Kalman Estimator

(3) Nonlinear Equipment -

(a) Comcor - This is a nonlinear electronic device that generates four output variables as a function of a single input variable. For purposes of this simulation, time is used as the input variable.

(b) Pace Diode Function Generator (DFG) - The diode function generators are used to generate some of the time varying vehicle parameters (c_1, $\frac{N'}{m}$ M'_α etc.).

(c) Pace Servo Multipliers with Padded Potentiometers - This particular application of a servo multiplier is used to generate a time function and simultaneously multiply it with a second time function.

(d) Pace Electronic Multipliers - The electronic multipliers are used to obtain the product of two time-varying functions.

Analog diagram symbols are defined in Figure M-4, and a block diagram of the simulation is presented in Figure M-5. Analog computer patching diagrams are presented in Figures M-6 through M-10. Pot settings are tabulated in Table M-1. The digital computer program is not presented since the computer link language is not a standard language. Thus, the information would not be of much value to someone not familiar with the Addage 770 link.

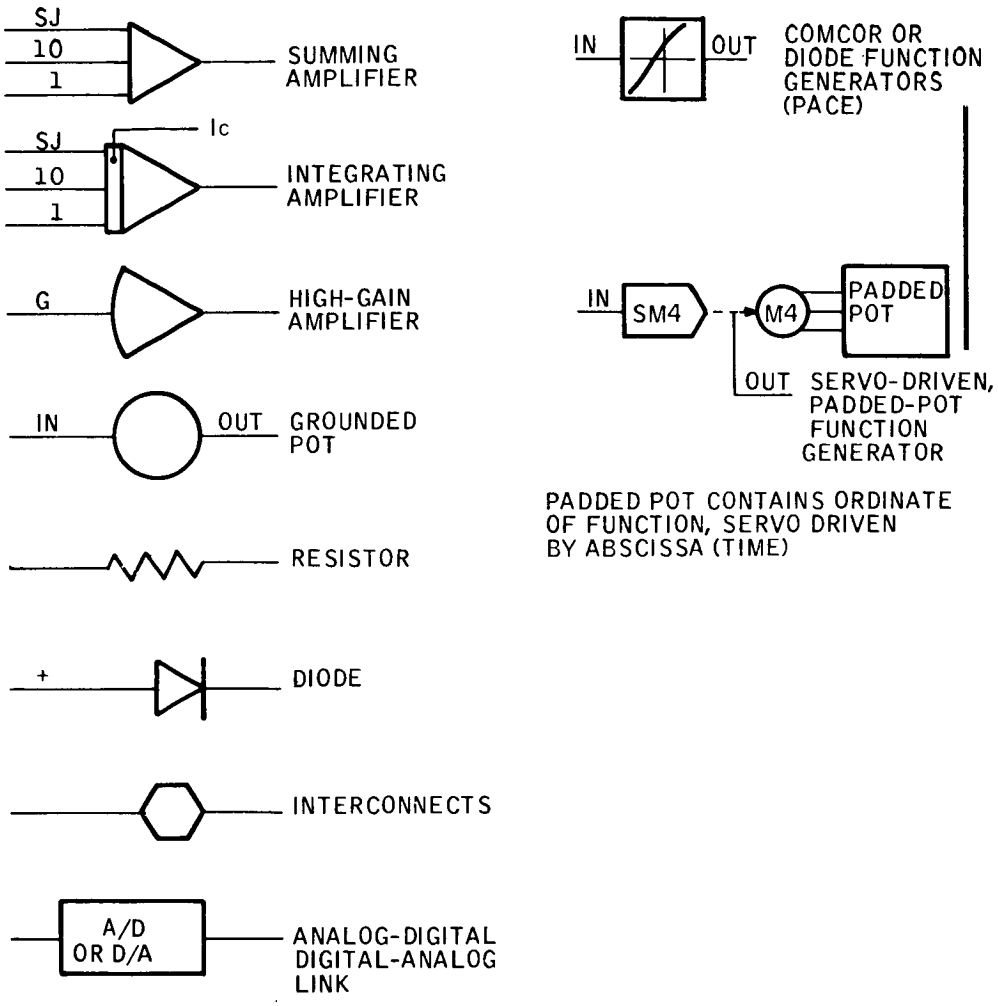

NOTE: PACE ELECTRONIC MULTIPLIERS ARE DRAWN WITH PATCHBOARD CONNECTIONS SHOWN

Figure M-4. Analog Diagram Symbols

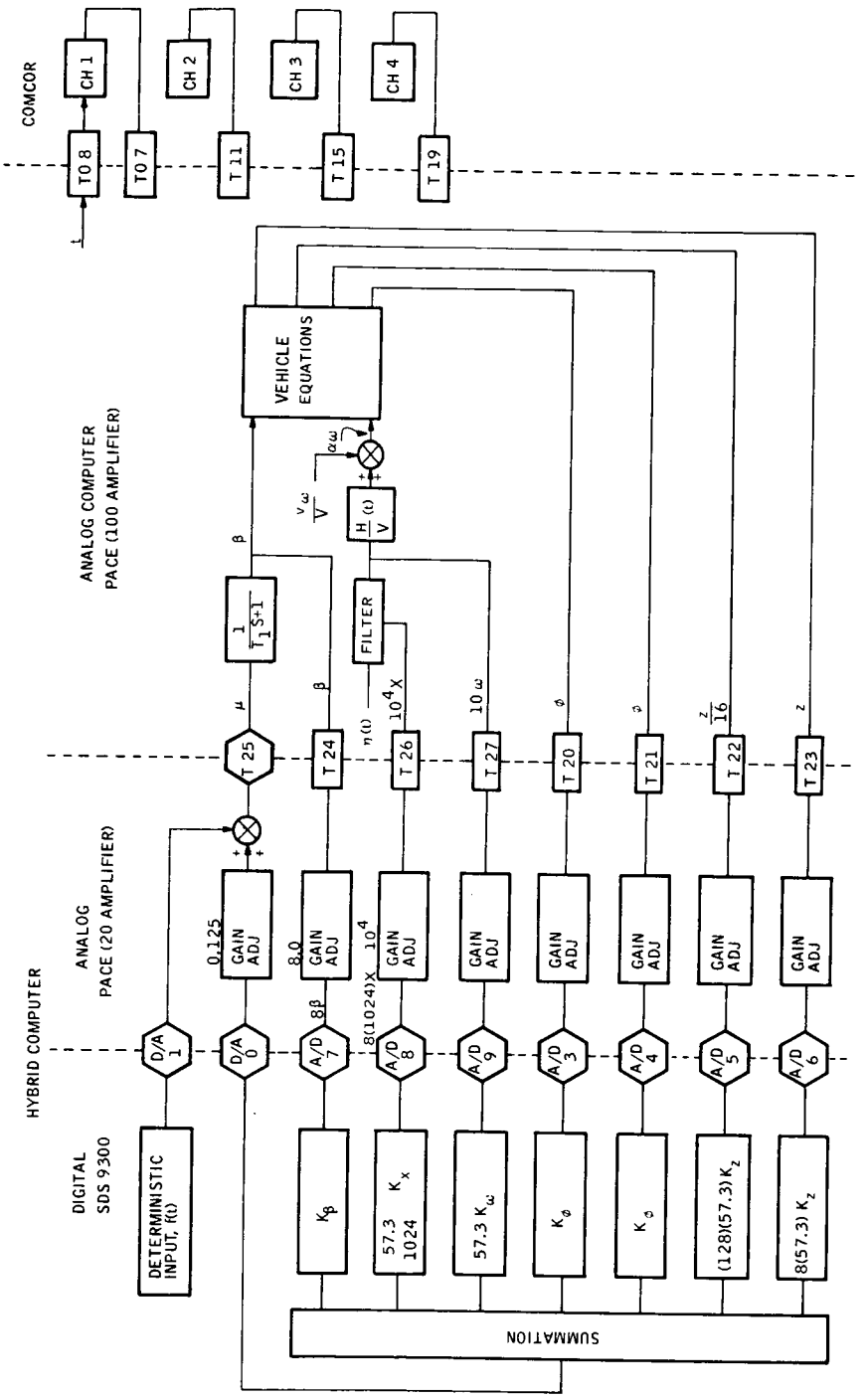

Figure M-5. Block Diagram of Simulation for Load Relief Study

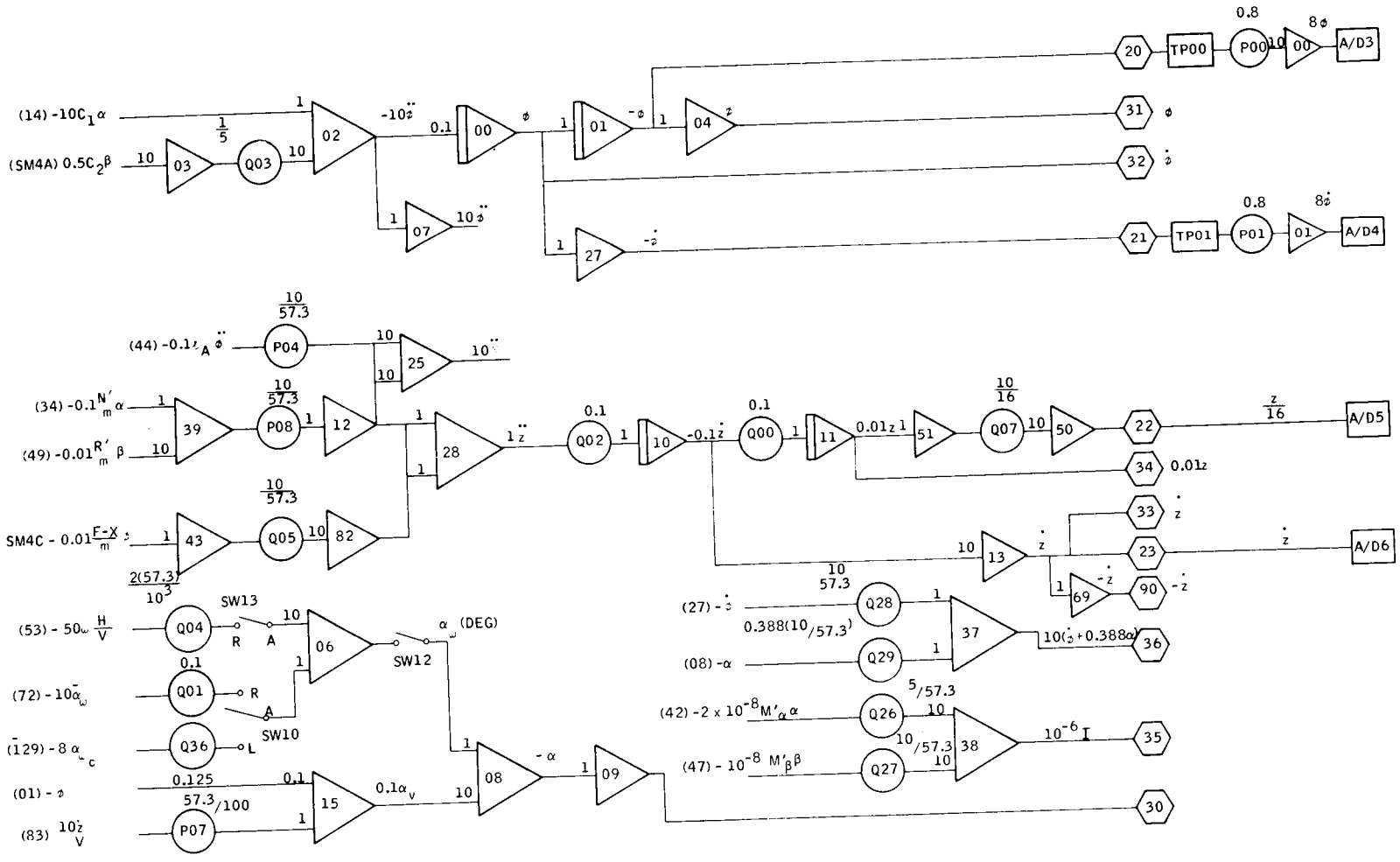

Figure M-6. Analog Simulation of Vehicle Equations of Motion

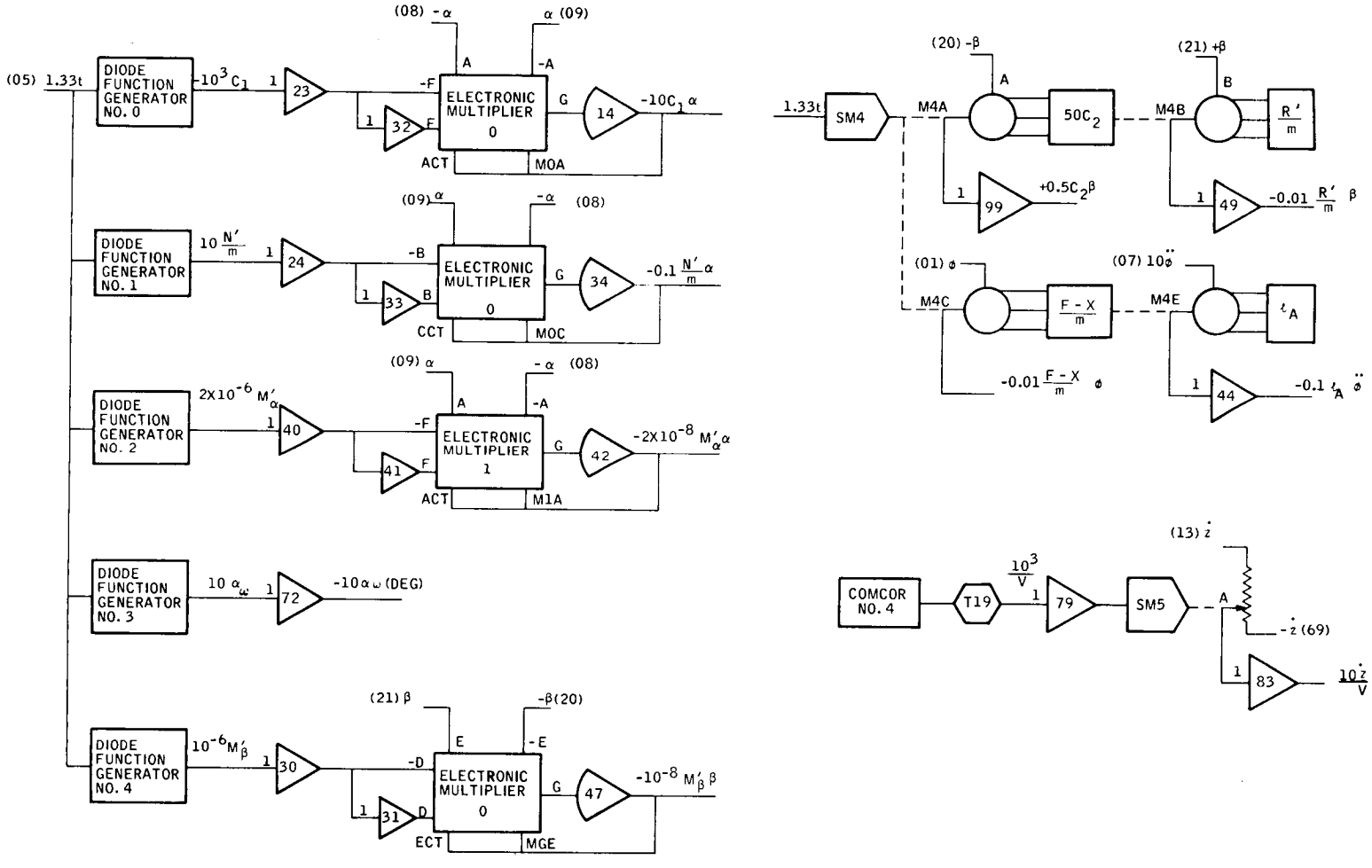

Figure M-7. Analog Derivation of Nonlinear Functions and Products

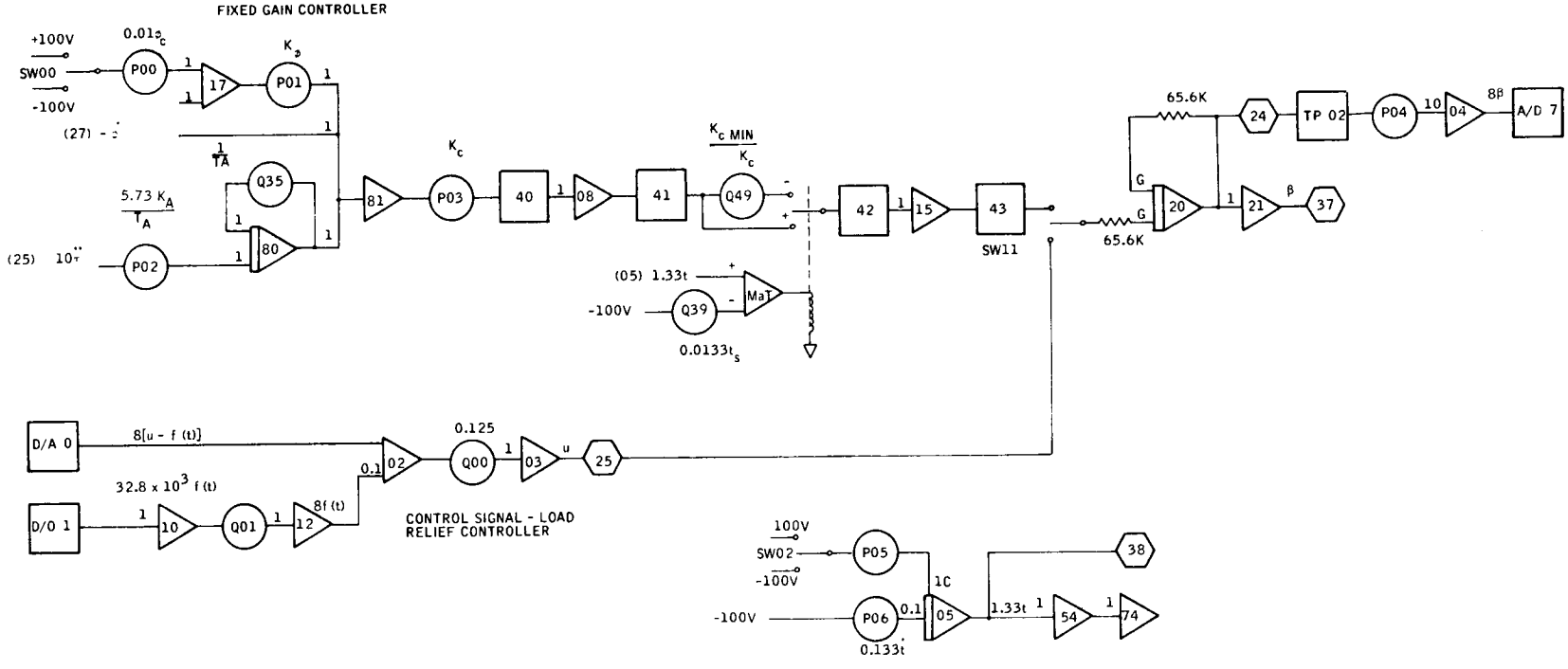

Figure M-8. Control System Configuration

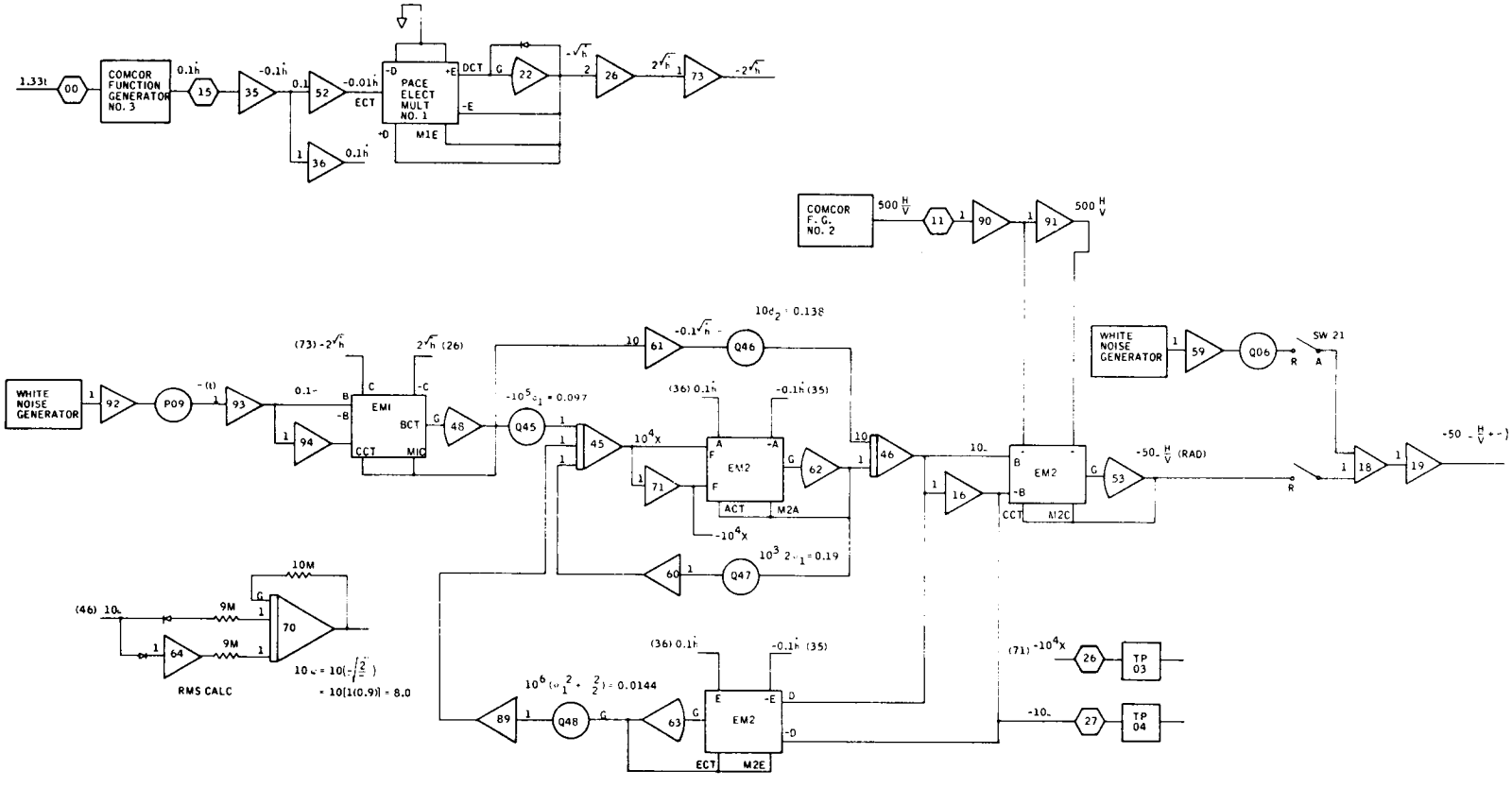

Figure M-9. Analog Simulation of Stochastic Wind Generator

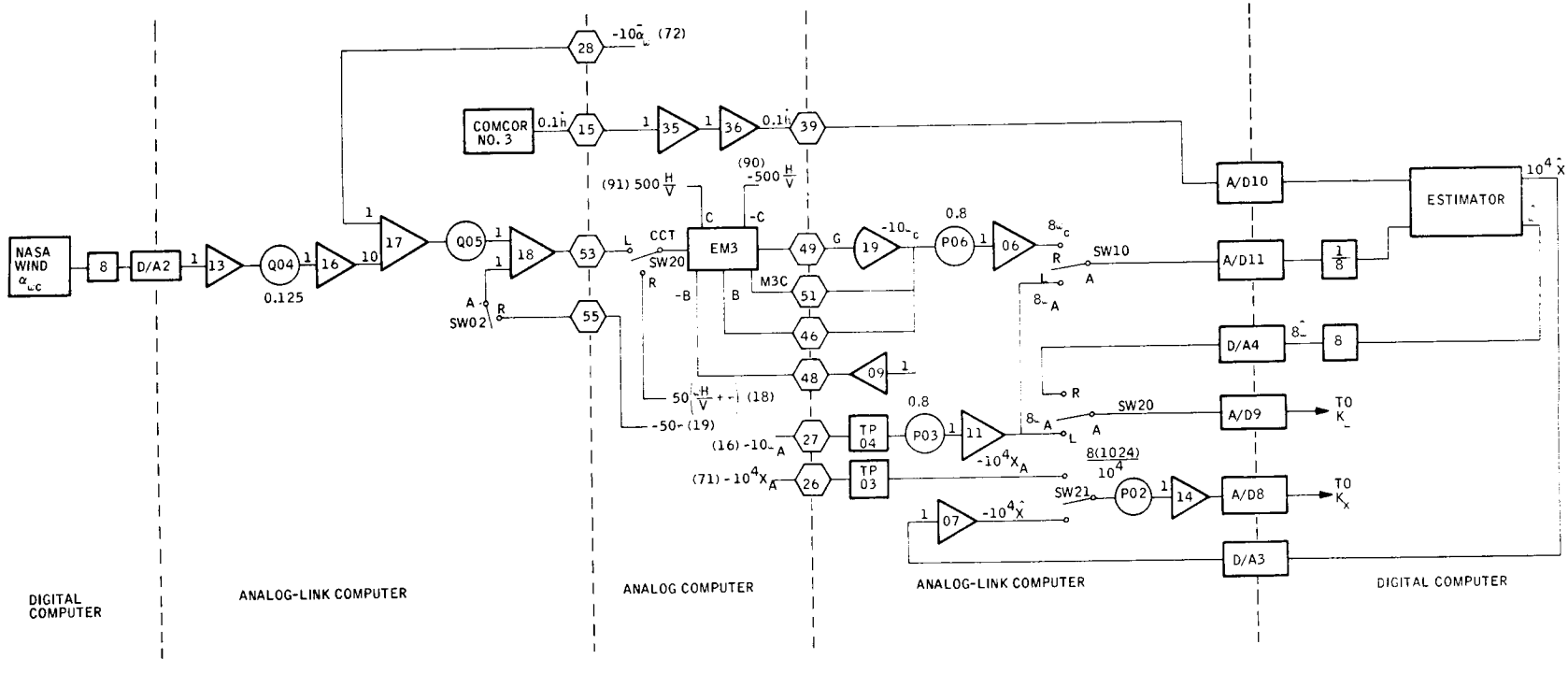

Figure M-10. Estimator Feedforward Simulation

Table M-1

Analog Simulation Potentiometer Settings

ANALOG

Parameter		
Pot	Description	Value
P00	$\phi_c/100$	Var
01	K_ϕ	0.7500
02	$(5.73\ K_A)/T_A$	0.5730
03	K_c	0.750
04	10/57.3	0.1750
05	Time Function	1.0000
06	Time Function	0.133
07	$57.3/10^2$	0.5730
08	10/57.3	0.1750
09	RMS Wind Adjust	Calib.
Q00		0.100
01	Scale Factor	0.01
02	Scale Factor	0.1000
03	Scale Factor	0.2000
04	$2(57.3)/10^3$	0.1145
05	10/57.3	0.1750
06	Scale Factor	
07	Scale Factor 1/16	0.625
08	α_g	Var
09		

HYBRID ANALOG

Parameter		
Pot	Description	Value
P00	Scale Factor	0.8000
01	Scale Factor	0.8000
02	$8(1024)/10^4$	0.8190
03	Scale Factor	0.8000
04	Scale Factor	0.8000
Q00	Scale Factor	0.1250
01	Scale Factor	0.139
04	α_{ω_c} Input	0.125
05	$0.1\ (\frac{50}{37.3})$	0.0873

Table M-1
Analog Simulation Potentiometer Settings (Cont.)

ANALOG

Parameter		
Pot	Description	Value
26	5/57.3	0.0872
27	10/57.3	0.1750
28	10/57.3	0.1750
29	0.388 (10/57.3)	0.0679
35	I/T_A	0.10
36	Scale Factor	0.125
39	Relay Switch	0.4600
45	$10^5 d_1$	0.097
46	10d	0.1379
47	$10^3 (2\alpha_1)$	0.1900
48	$10^6 (\alpha_1^2+\alpha_2^2)$	0.0144
49	$K_c \vert_t > 100$ sec	0.3070

APPENDIX N
ANALOG RESPONSE TRACINGS

The analog response tracings obtained in the analog-simulation tests discussed in Section V are presented in this appendix as Figures N-1 through N-63.

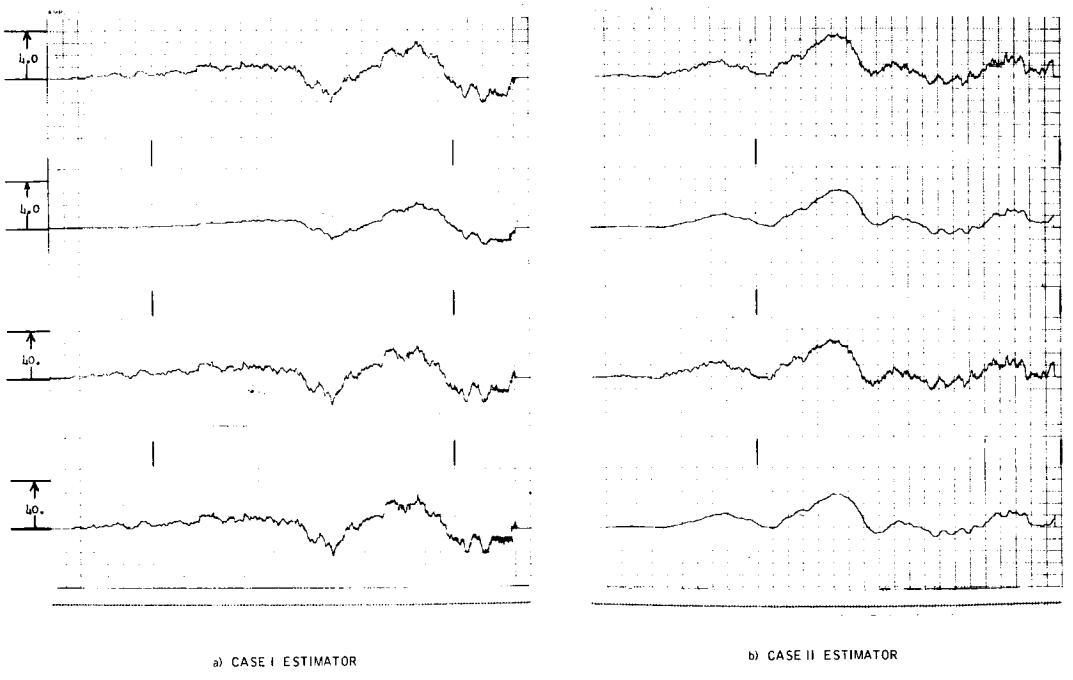

Figure N-1. Comparison of Actual x_A and ω_A Signals from Stochastic Wind Generator with Estimated $\hat{x}$ and $\hat{\omega}$ from Estimators

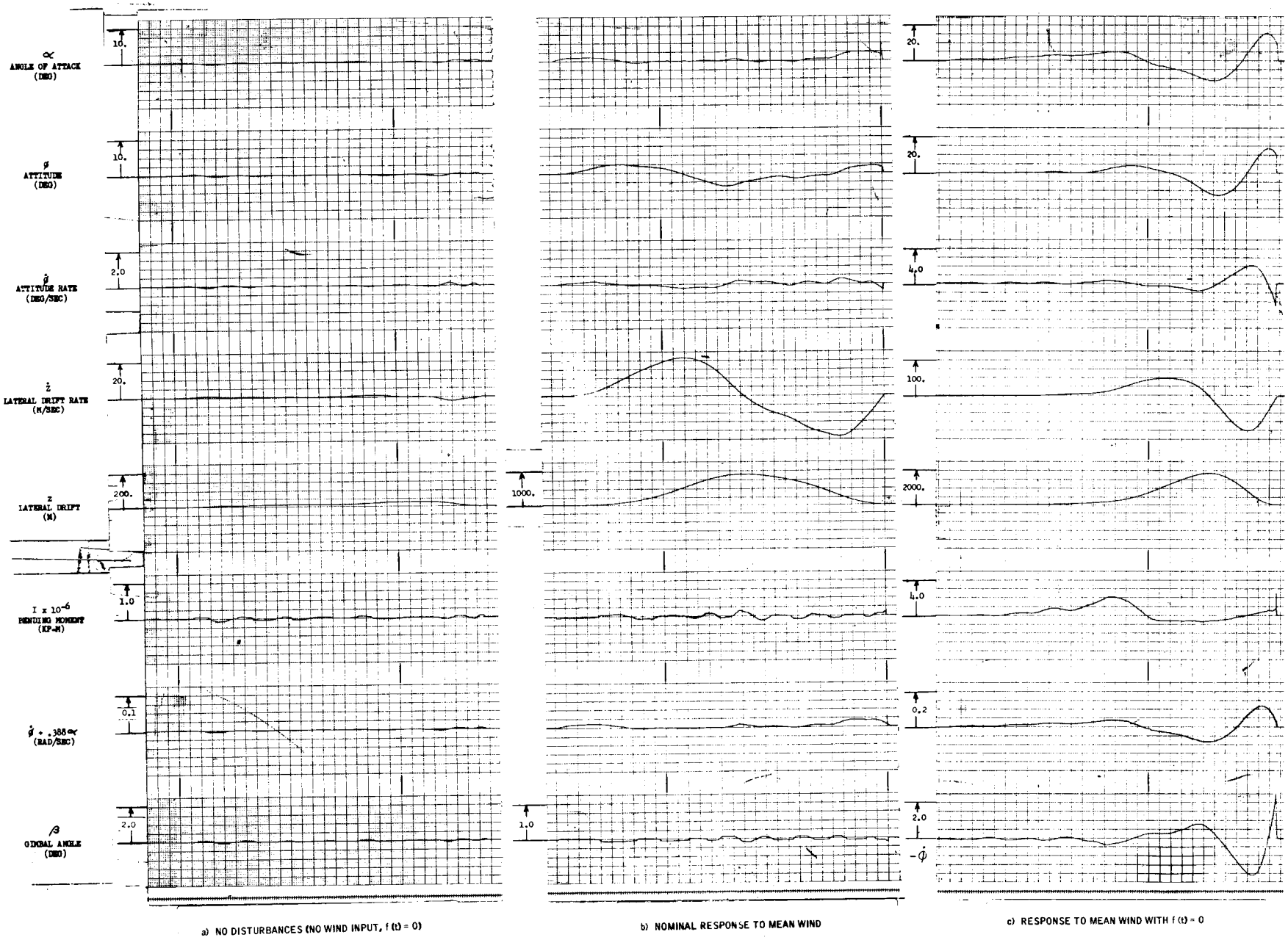

Figure N-2. Load-Relief Controller - Nominal Responses

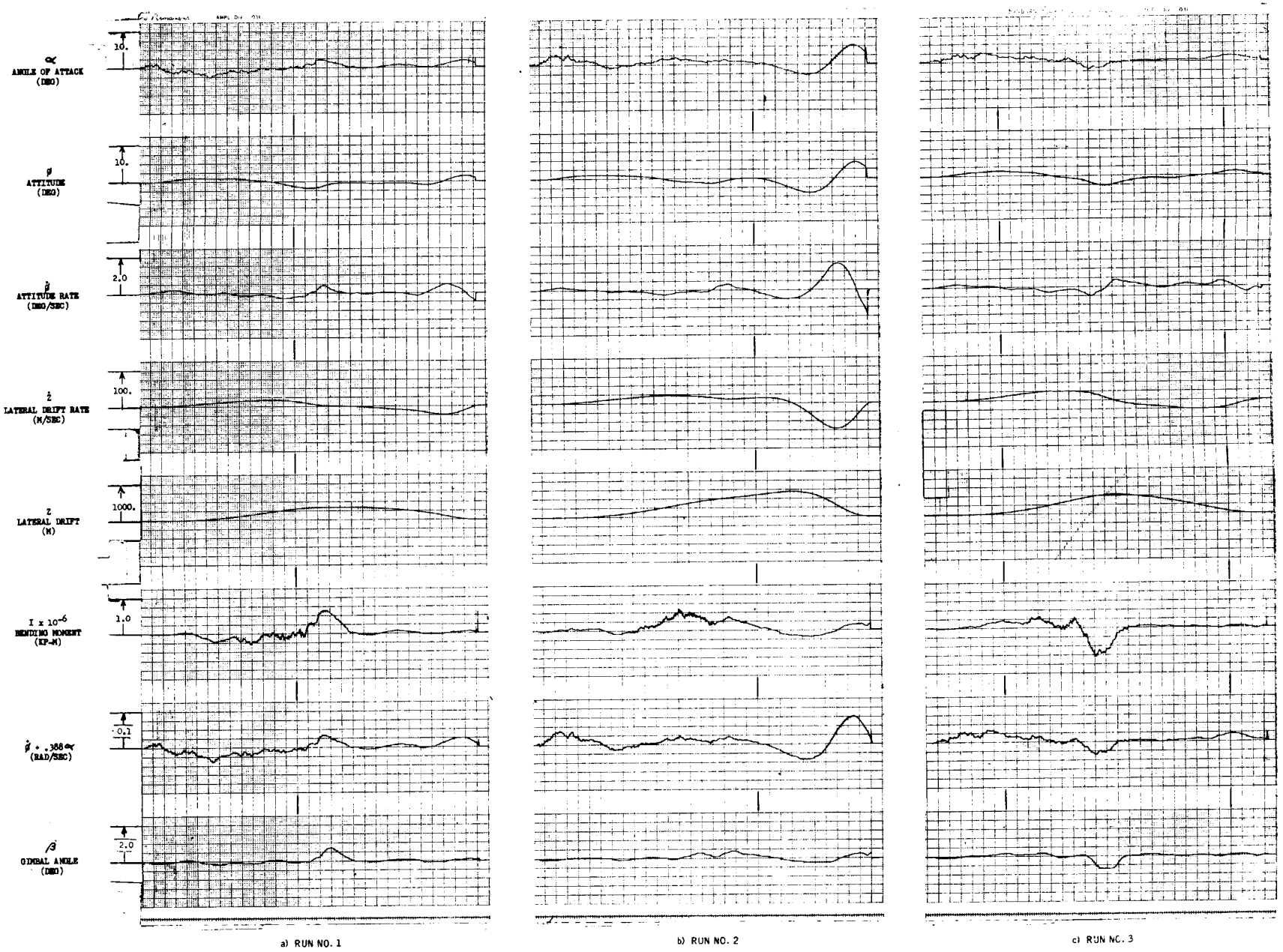

Figure N-3. Load-Relief Controller, No Estimator ($K_x = K_\omega = 0$) - Response to Random Wind

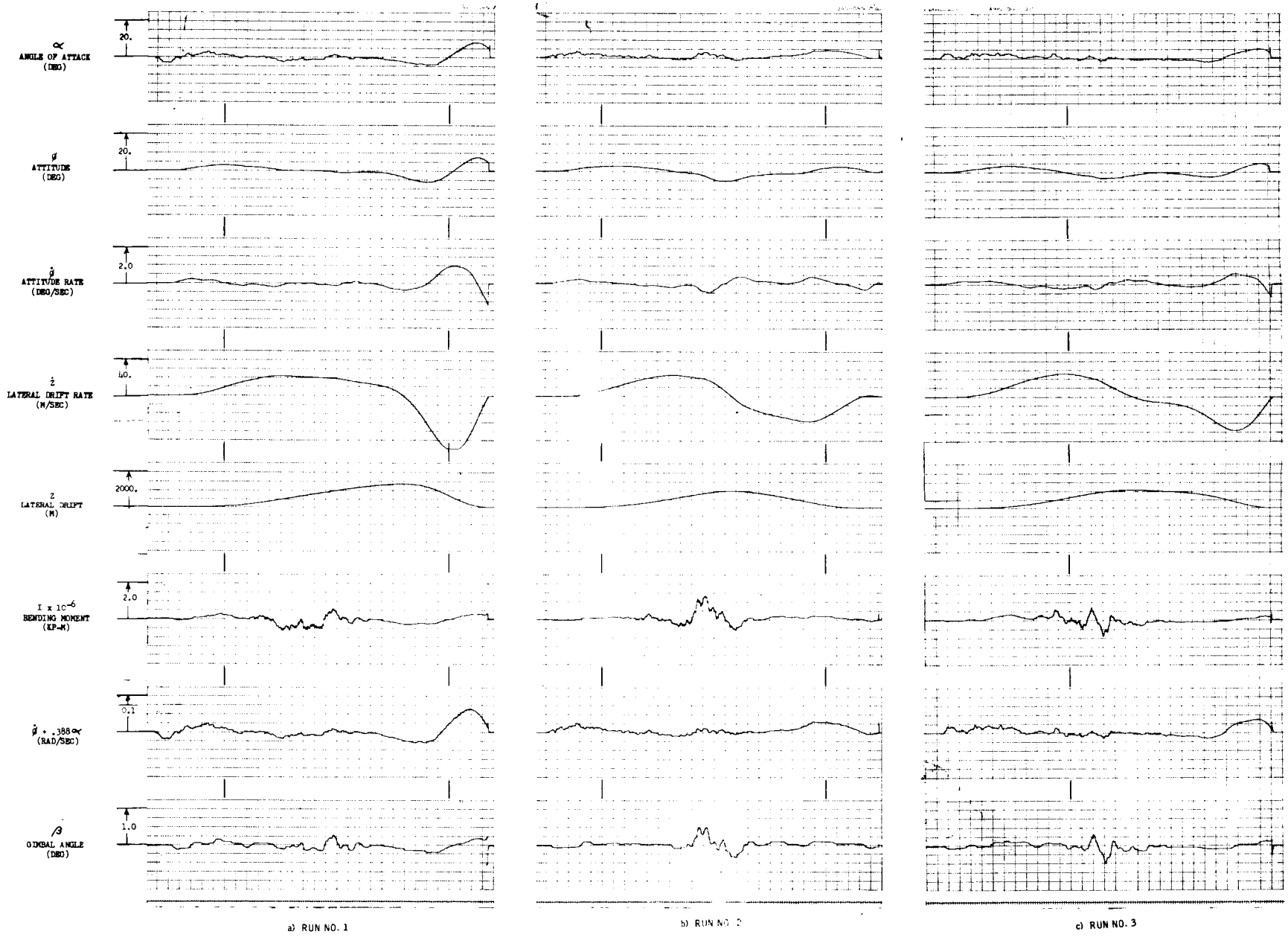

Figure N-4. Load-Relief Controller, Case I Estimator - Response to Random Wind

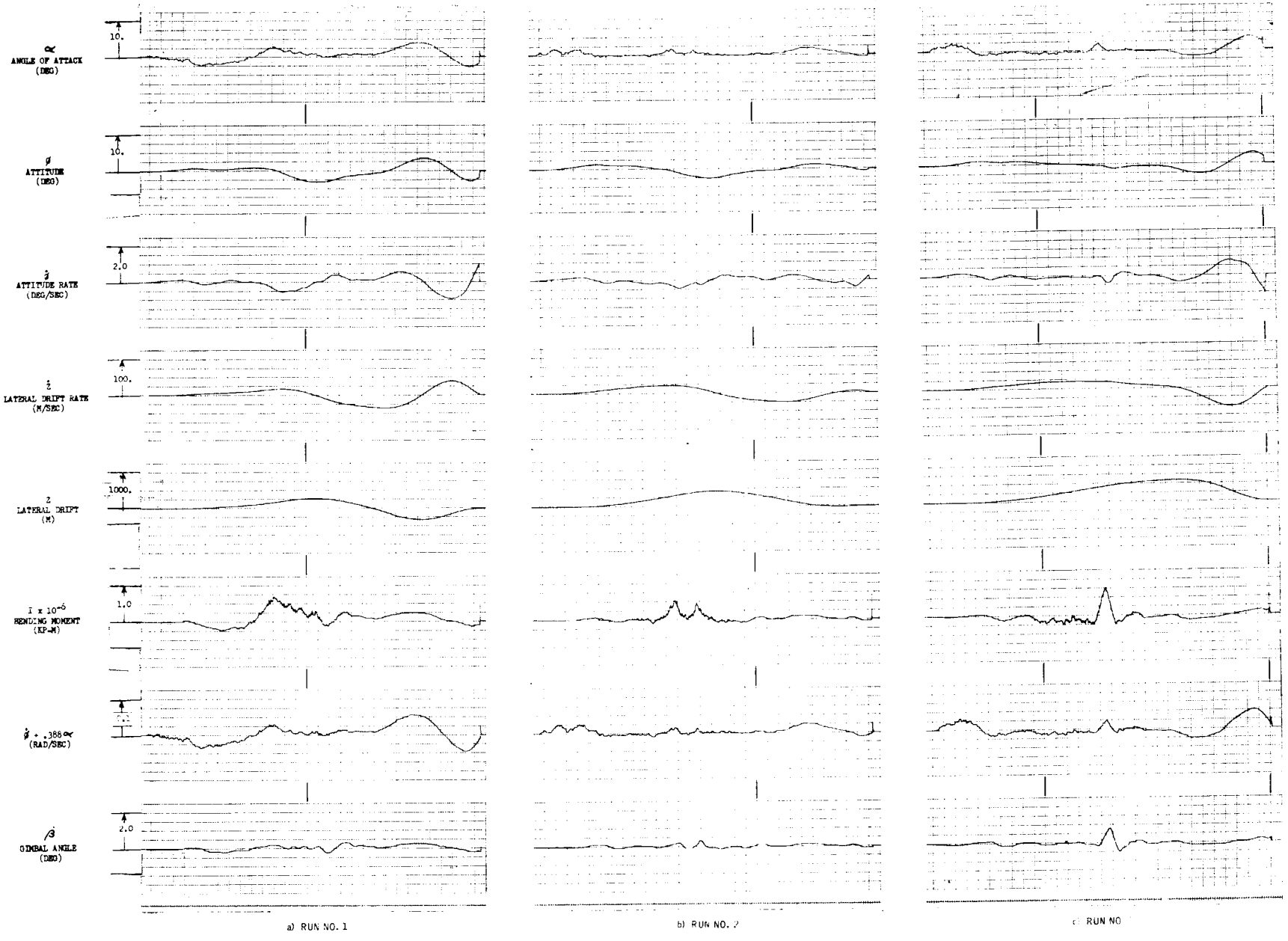

Figure N-5. Load-Relief Controller, Case II Estimator - Response to Random Wind

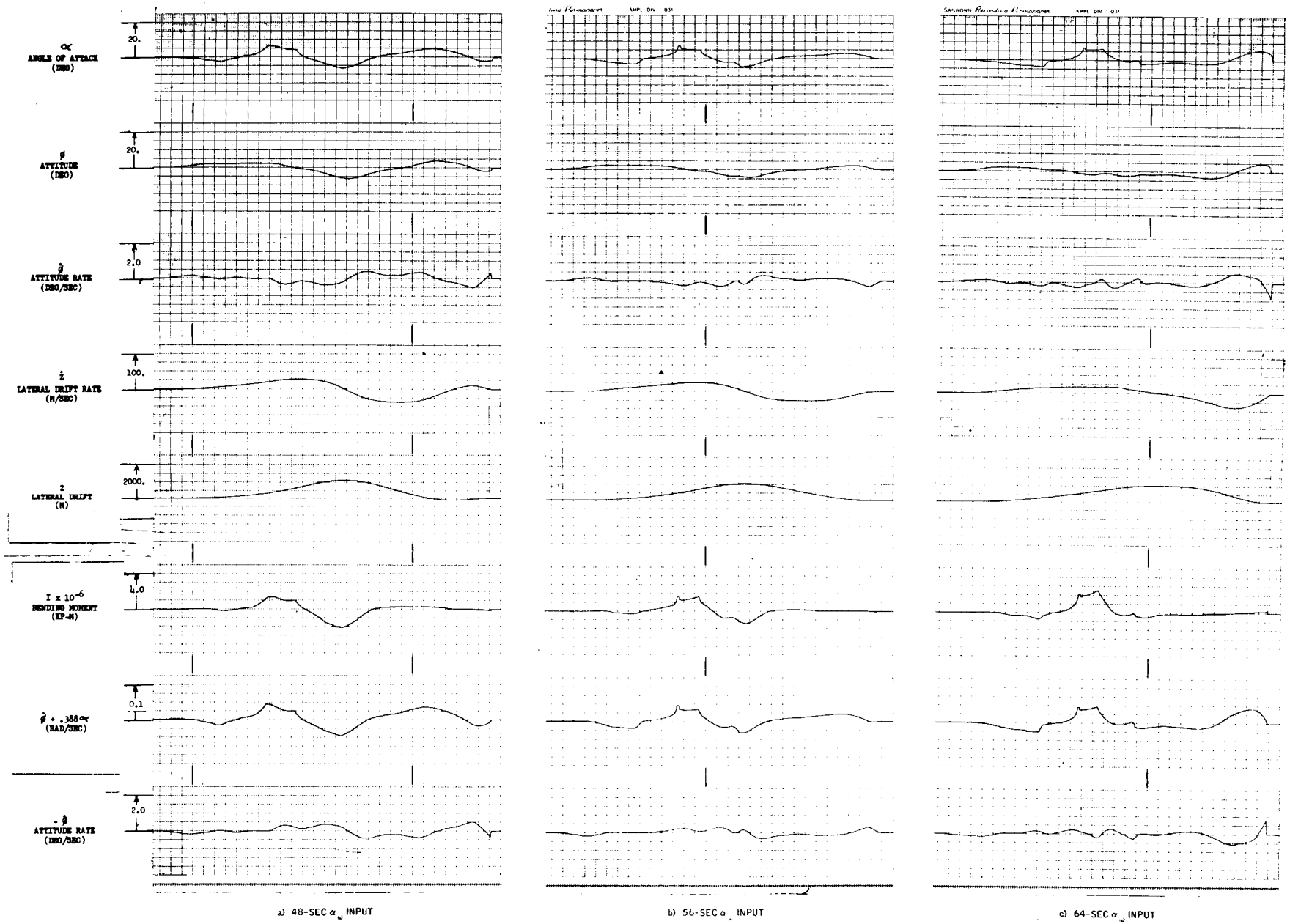

Figure N-6. Load-Relief Controller, No Estimator ($K_x = K_\omega = 0$) - NASA Wind Response (48-, 56-, and 64- second α_ω inputs)

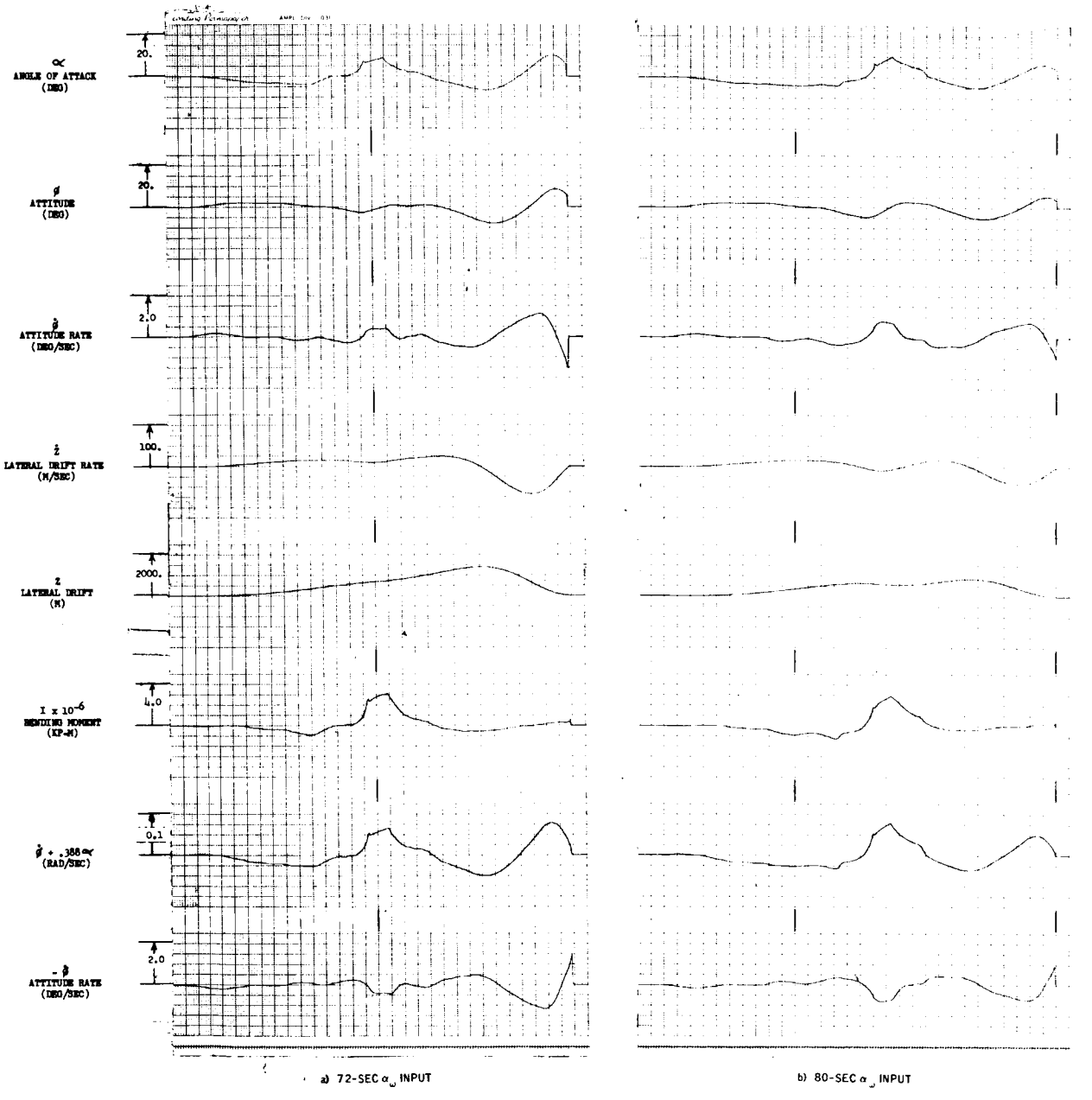

Figure N-7. Load-Relief Controller, No Estimator ($K_x = K_\omega = 0$) - NASA Wind Response (72- and 80-second α_ω inputs)

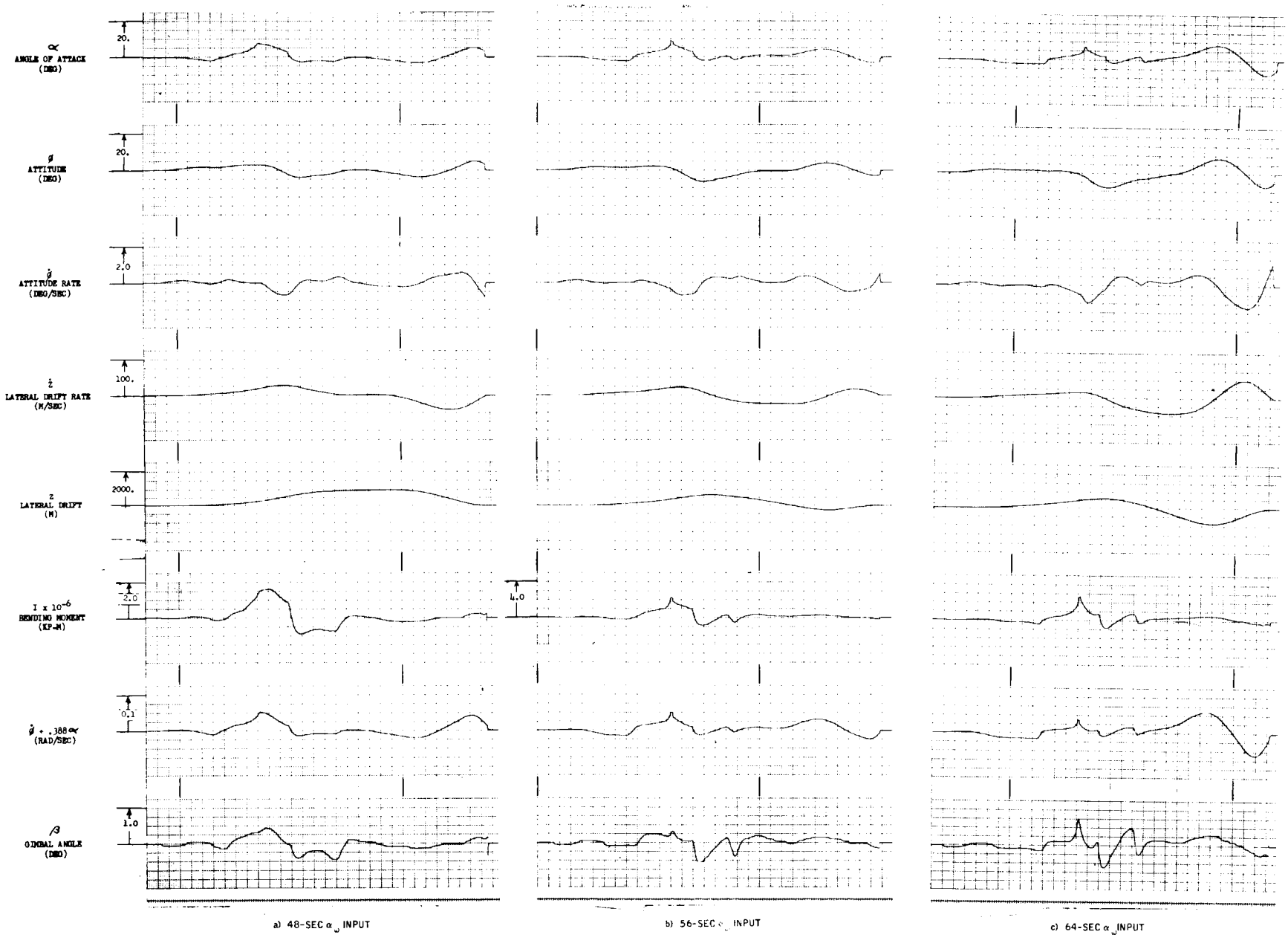

Figure N-8. Load-Relief Controller, Case I Estimator - NASA Wind Response (48-, 56-, and 64-second α_ω inputs)

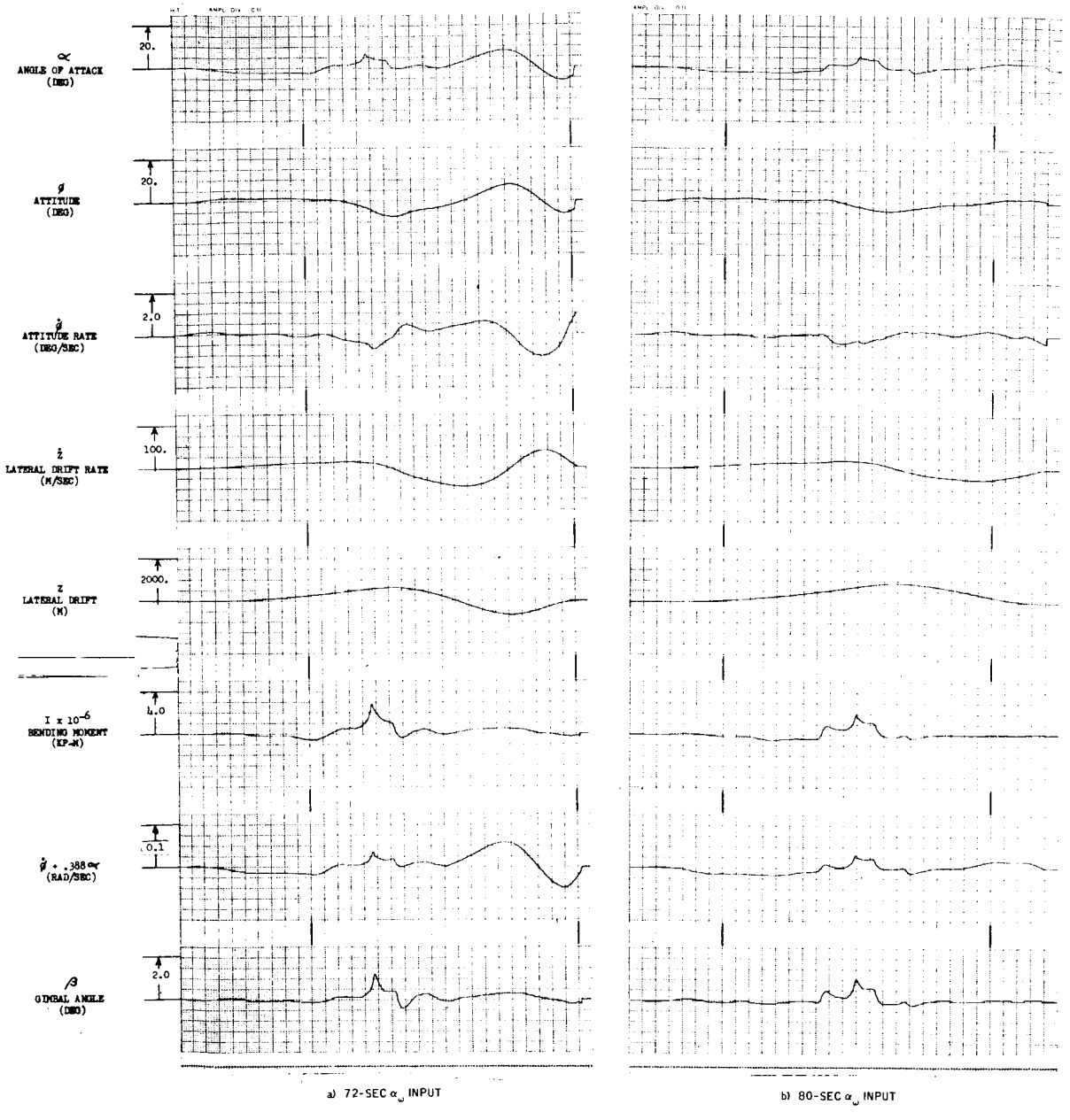

Figure N-9. Load-Relief Controller, Case I Estimator - NASA Wind Response (72- and 80-second α_ω inputs)

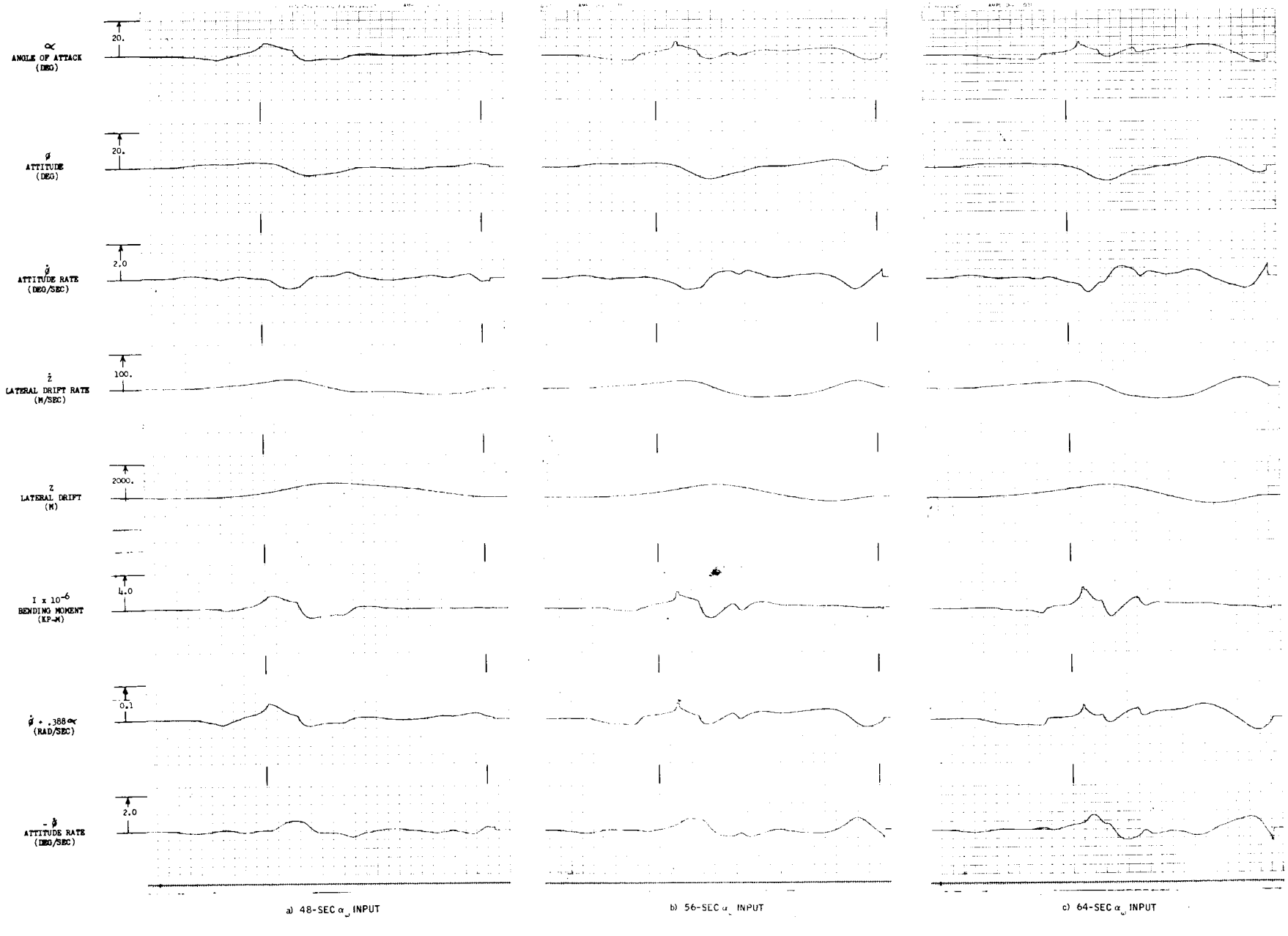

Figure N-10. Load-Relief Controller, Case II Estimator - NASA Wind Response (48-, 56-, and 64-second α_ω inputs)

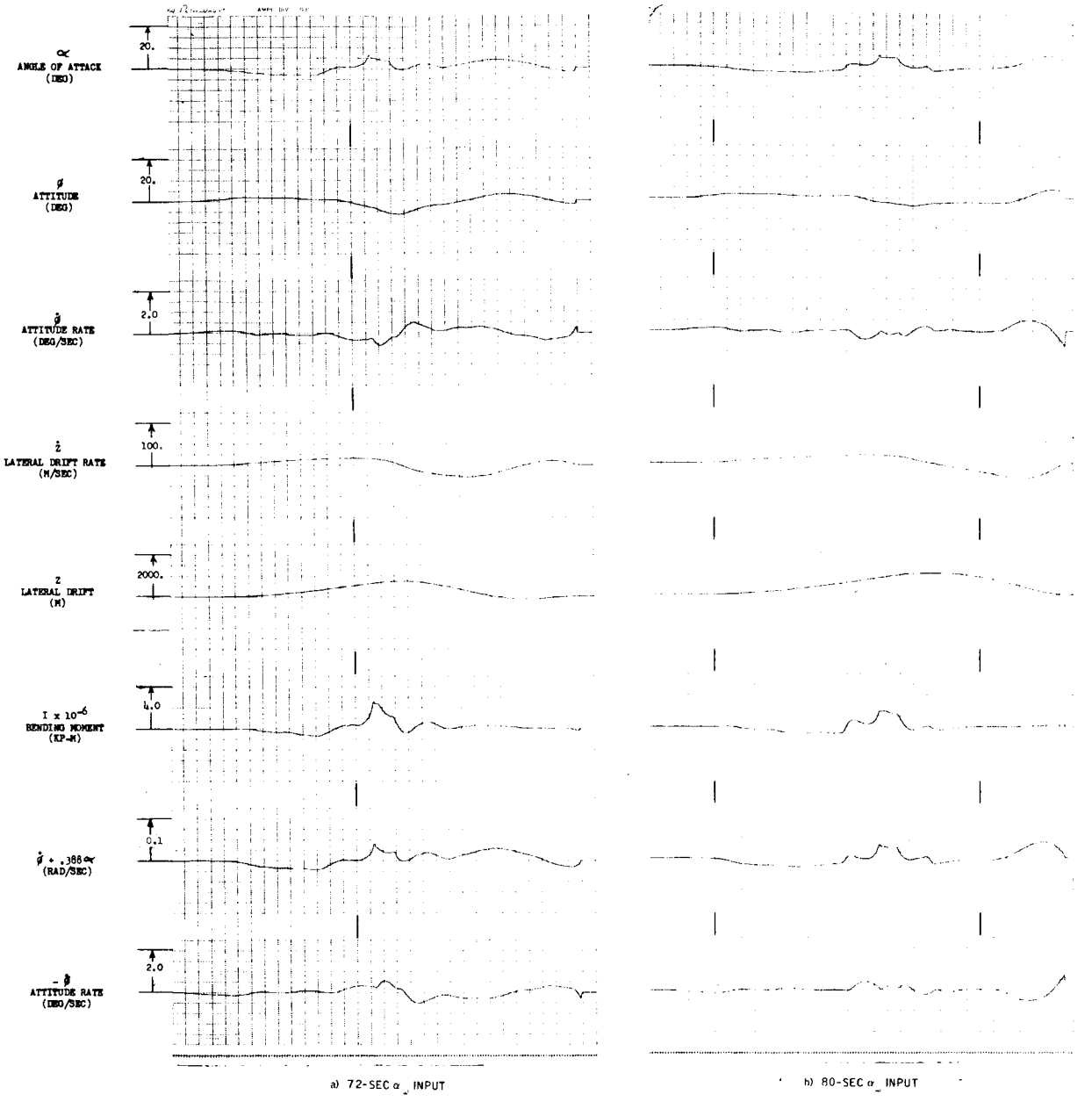

Figure N-11. Load-Relief Controller, Case II Estimator - NASA Wind Response (72- and 80-second α_ω inputs)

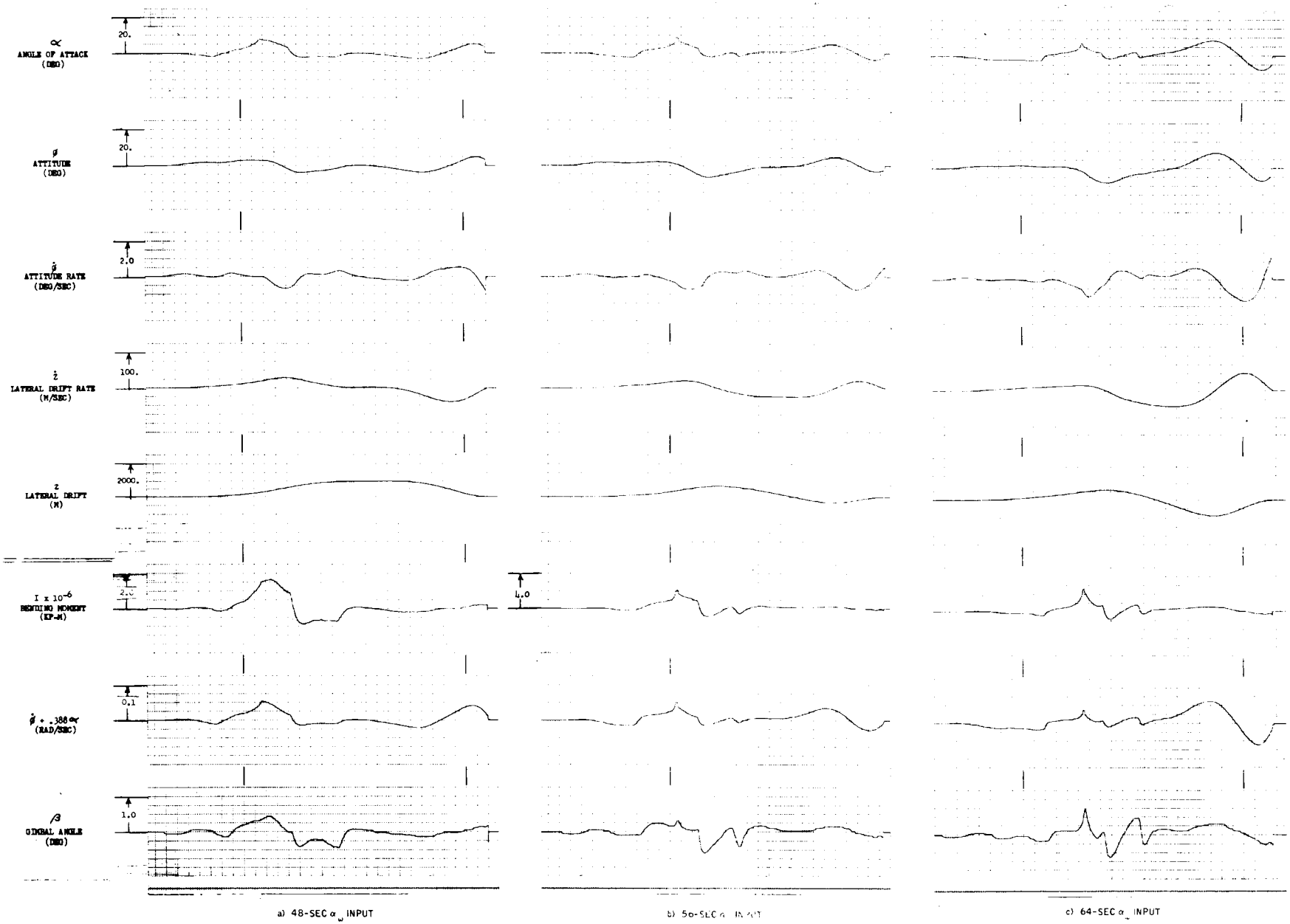

gure N-12. Load-Relief Controller, [illegible] I Estimator with 0.5-degree Sensor Noise - NASA Wind Response (48-, 56-, and 64-second α_ω inputs)

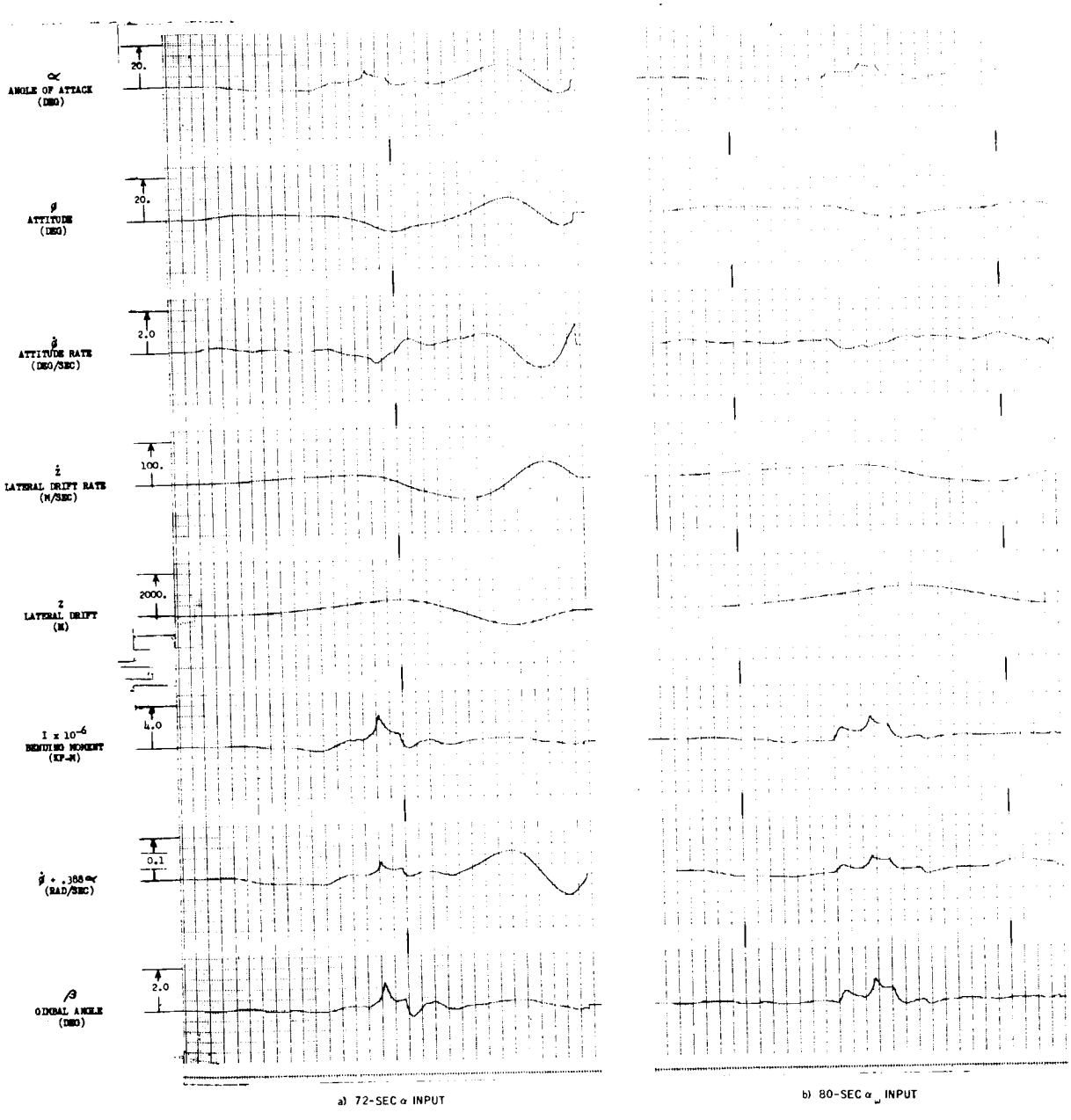

Figure N-13. Load-Relief Controller, Case I Estimator with 0.5-degree Sensor Noise - NASA Wind Response (72- and 80-second $\alpha_{(\omega)}$ inputs)

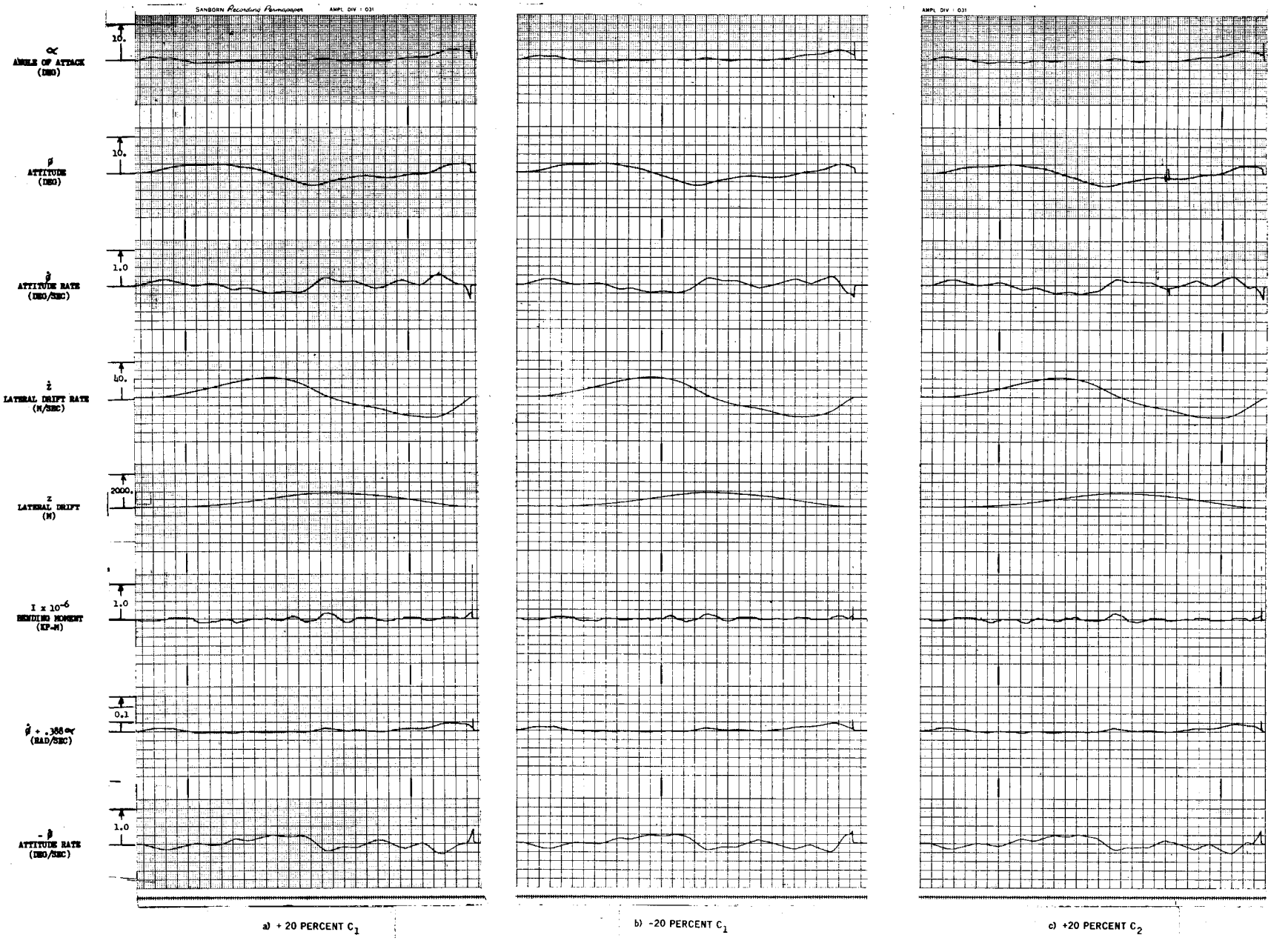

Figure N-14. Load-Relief Controller, Vehicle Parameter Variations - Response to Mean Wind [(a) +20% c_1, (b) -20% c_1, (c) +20% c_2]

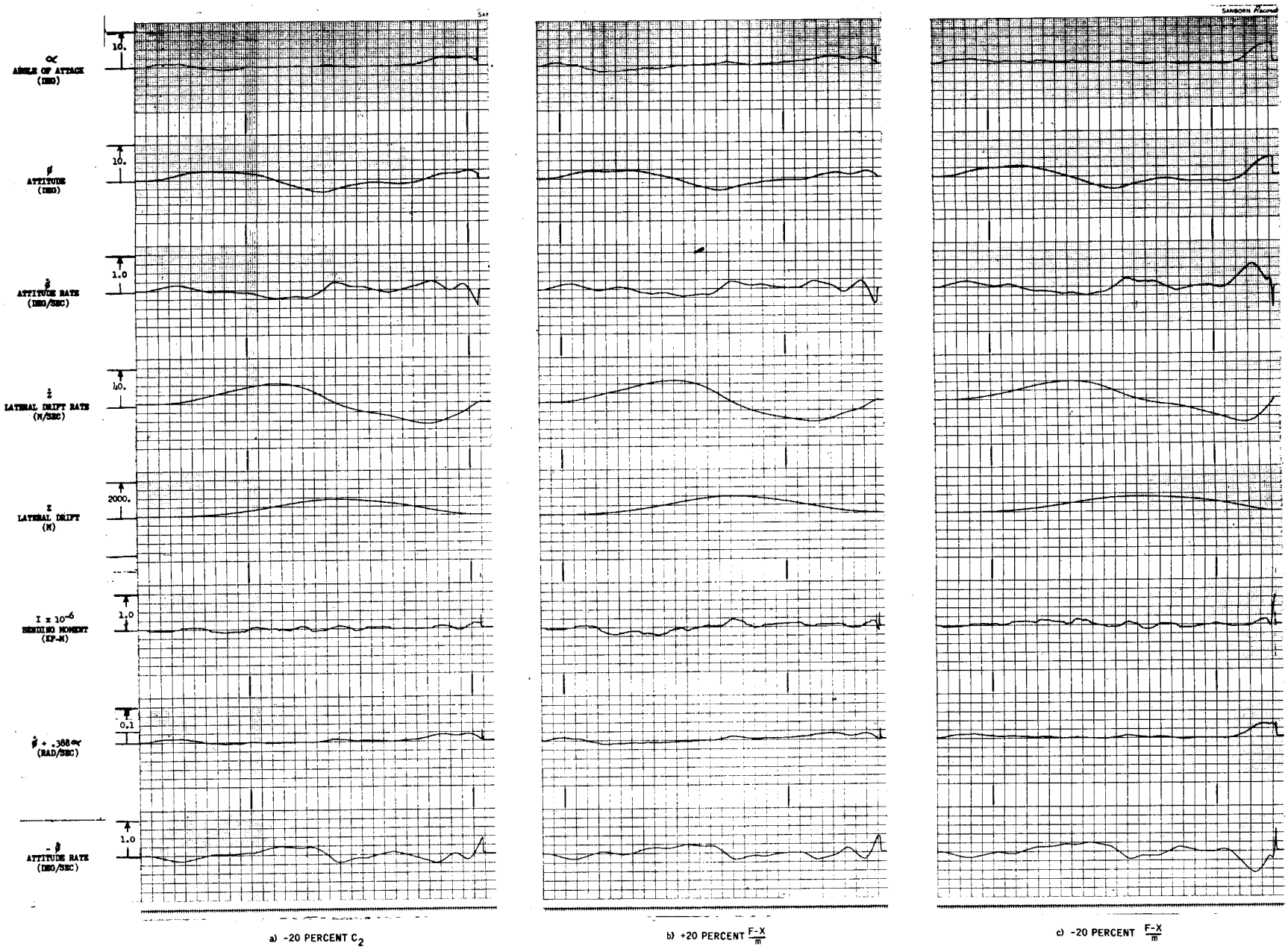

Figure N-15. Load-Relief Controller, Vehicle Parameter Variations - Response to Mean Wind [(a) -20% c_2, (b) +20% $\left(\frac{F-X}{m}\right)$, (c) -20% $\left(\frac{F-X}{m}\right)$]

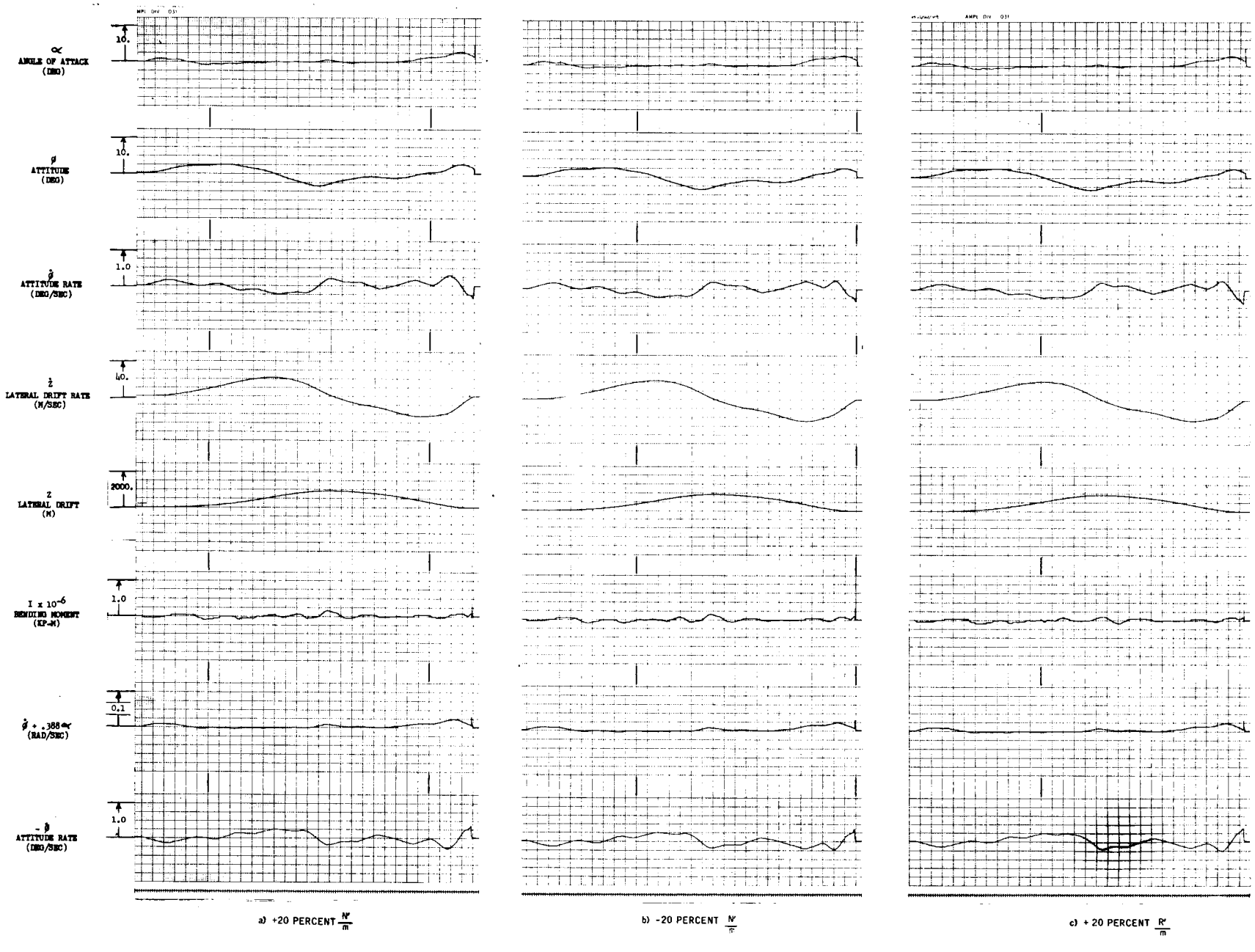

Figure N-16. Load-Relief Controller, Vehicle Parameter Variations - Response to Mean Wind [(a) -20% $\frac{N'}{m}$, (b) -20% $\frac{N'}{m}$, (c) +20% $\frac{R'}{m}$]

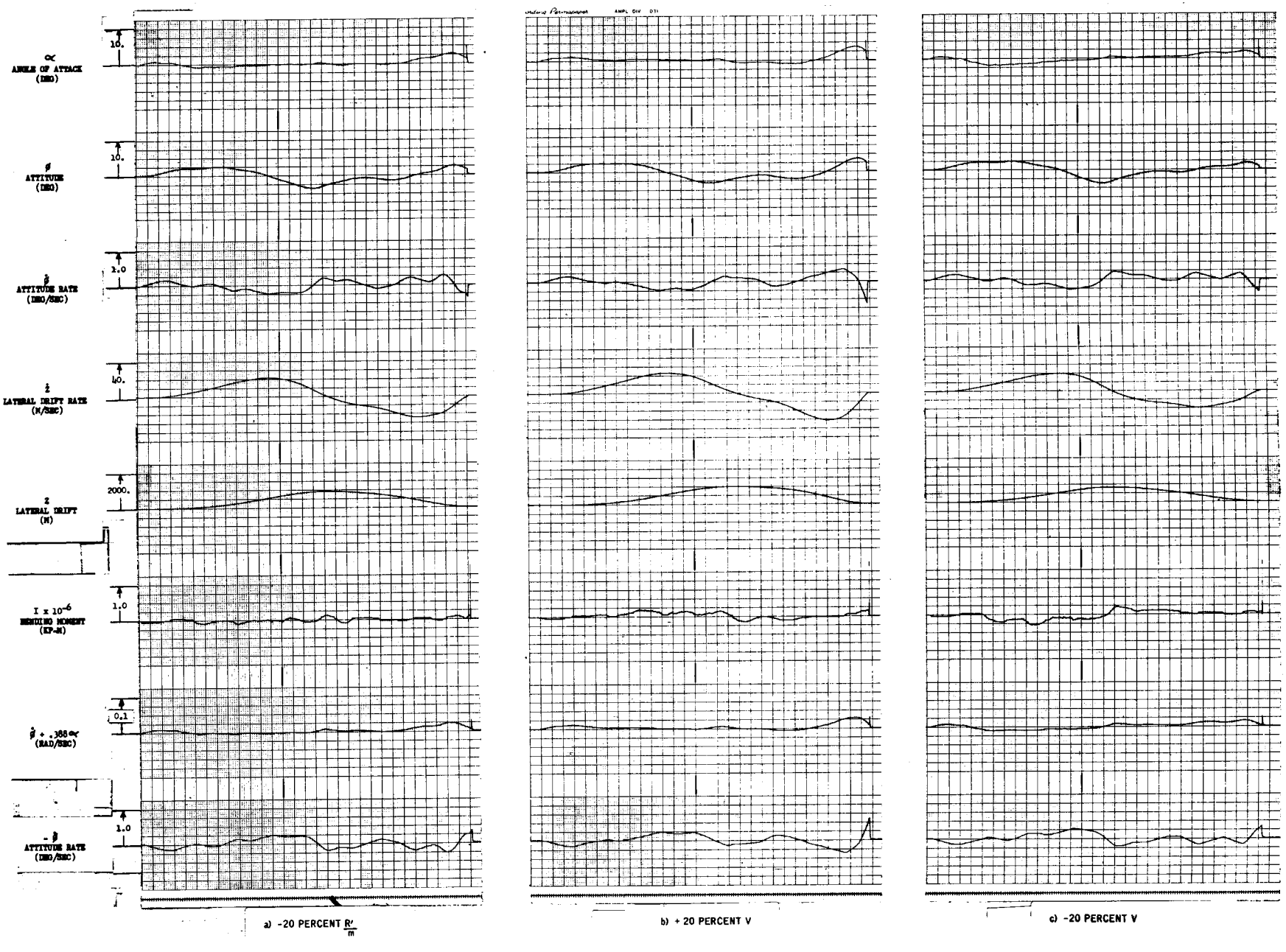

Figure N-17. Load-Relief Controller, Vehicle Parameter Variations - Response to Mean Wind [(a) -20% $\frac{R'}{m}$, (b) +20% v, (c) -20% v]

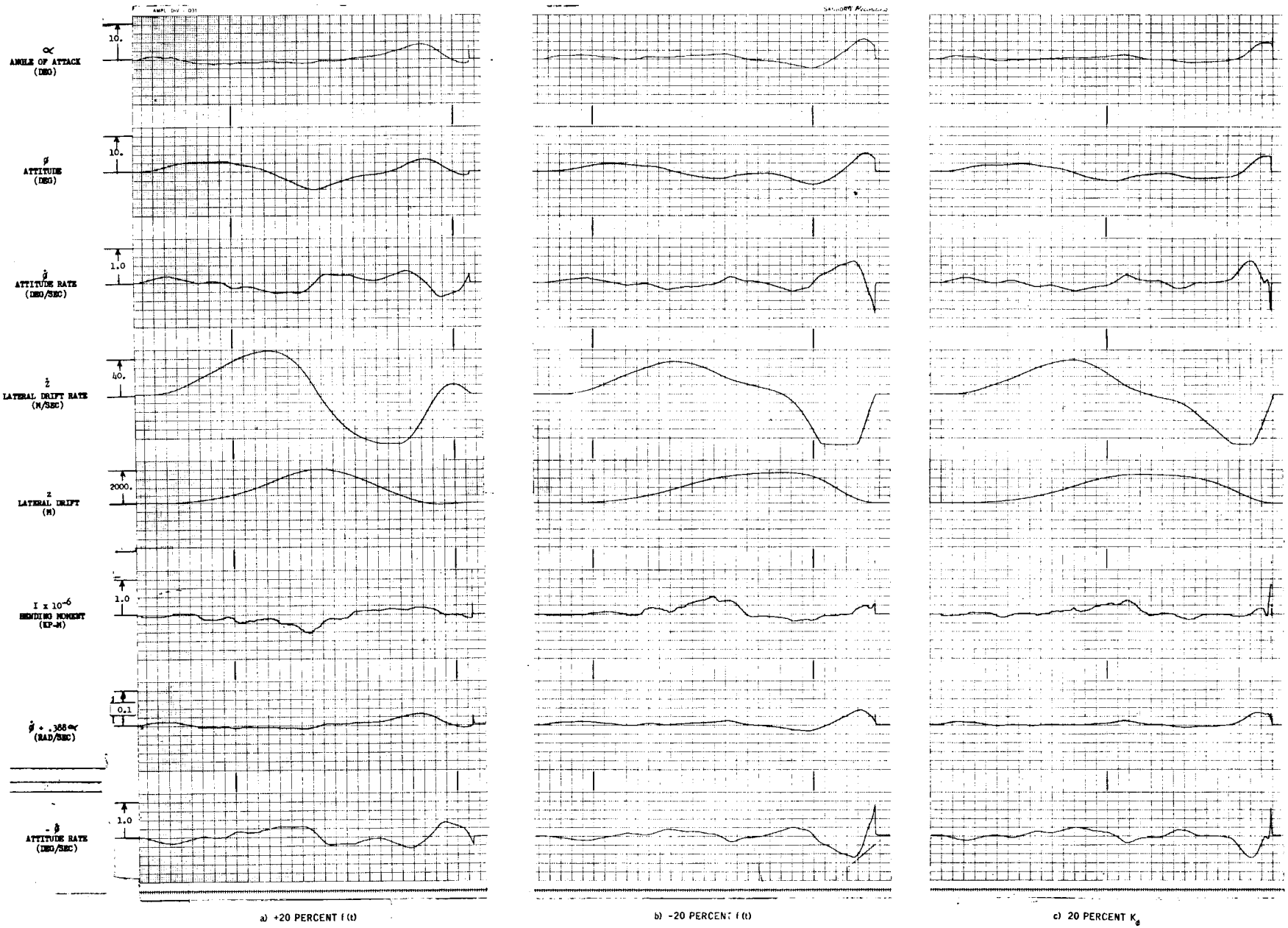

Figure N-18. Load-Relief Controller, Controller Parameter Variations - Response to Mean Wind [(a) +20% f(t), (b) -20% f (t), (c) +20% K_ϕ]

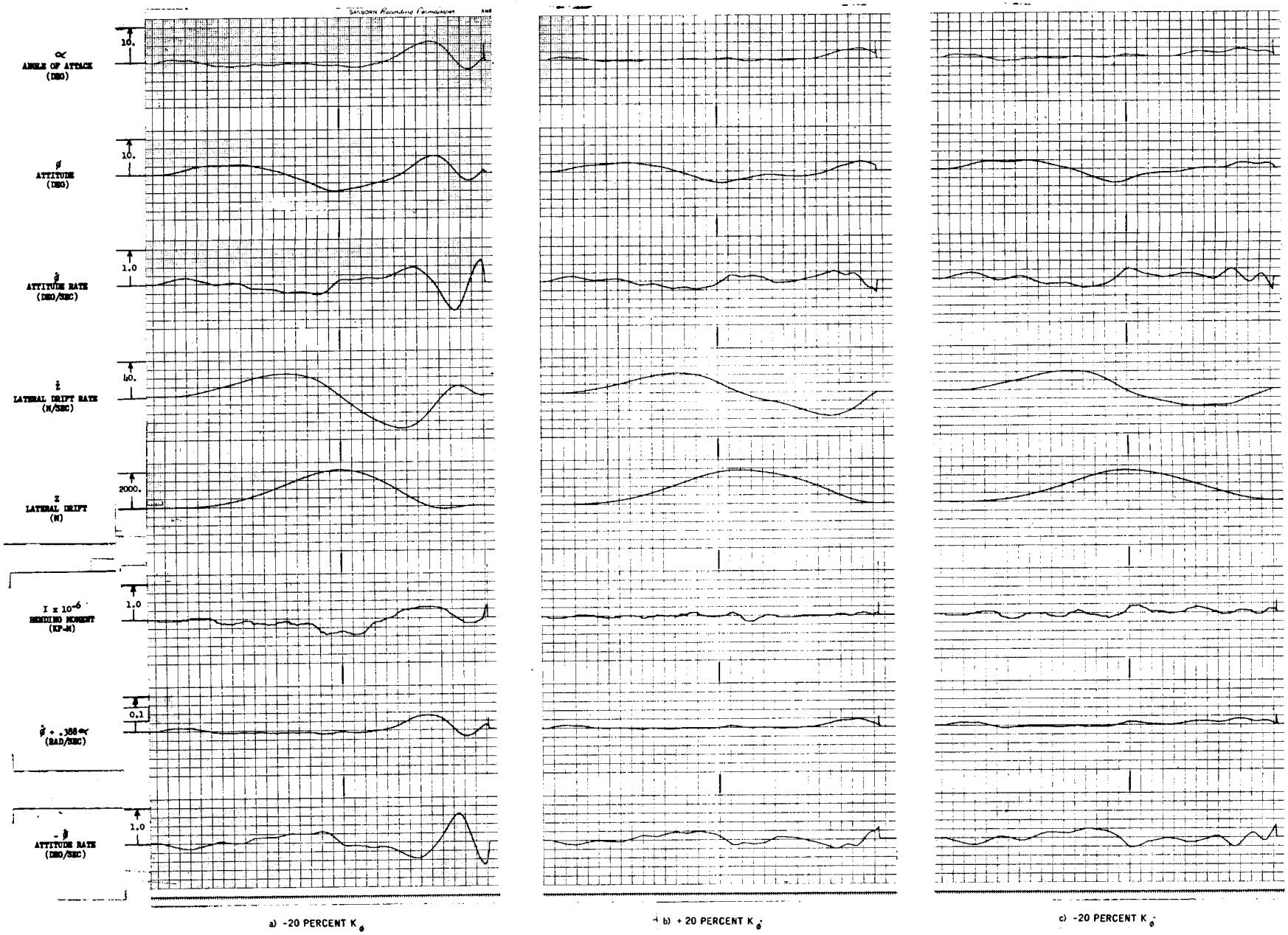

Figure N-19. Load-Relief Controller, Controller Parameter Variations - Response to Mean Wind [(a)+20% $K_{\dot{\phi}}$ (b)+20% $K_{\dot{\phi}}$, (c) -20% $K_{\dot{\phi}}$]

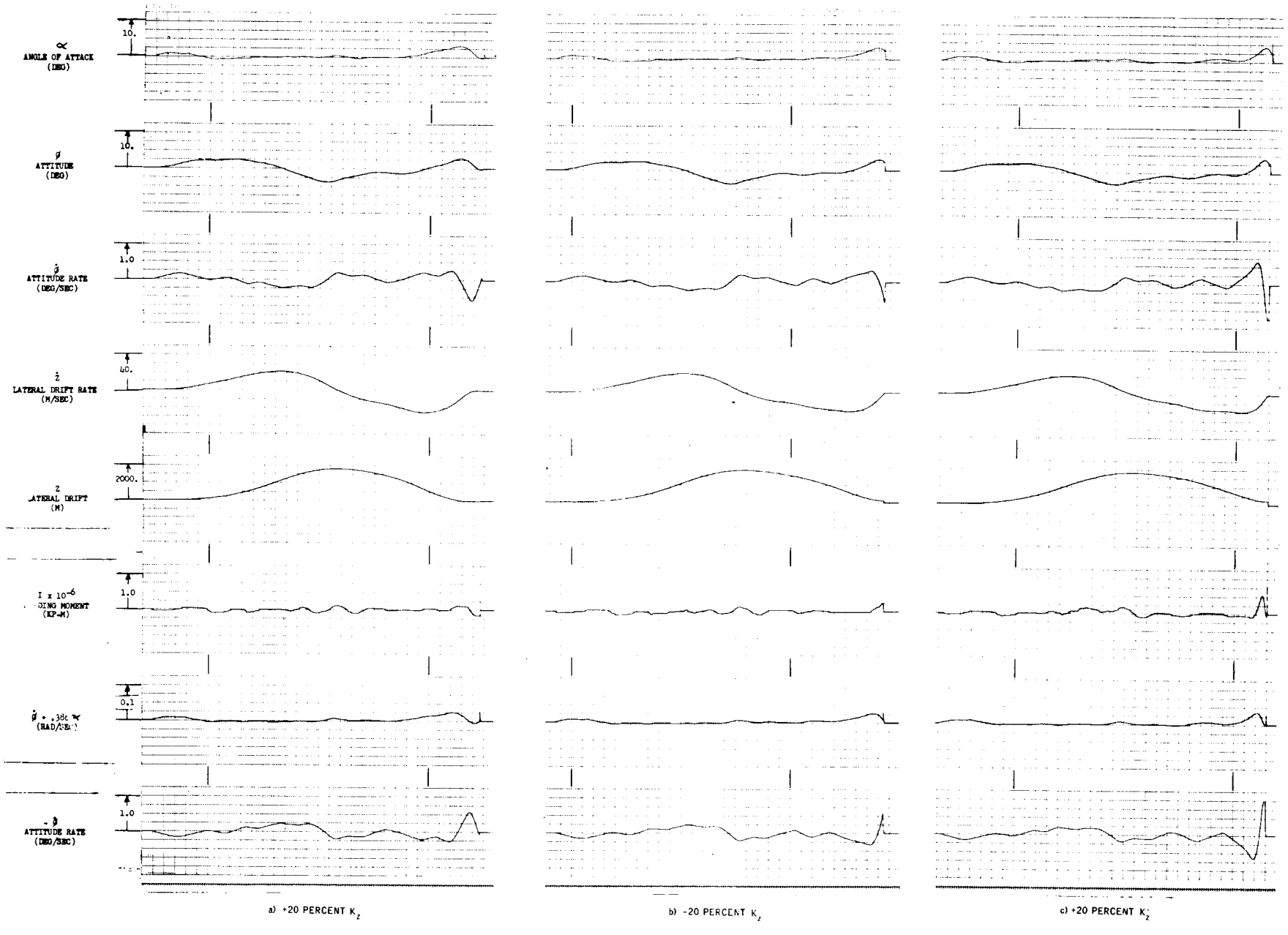

Figure N-20. Load-Relief Controller, Controller Parameter Variations - Response to Mean Wind [(a) +20% K_z, (b) -20% K_z, (c) +20% K_z]

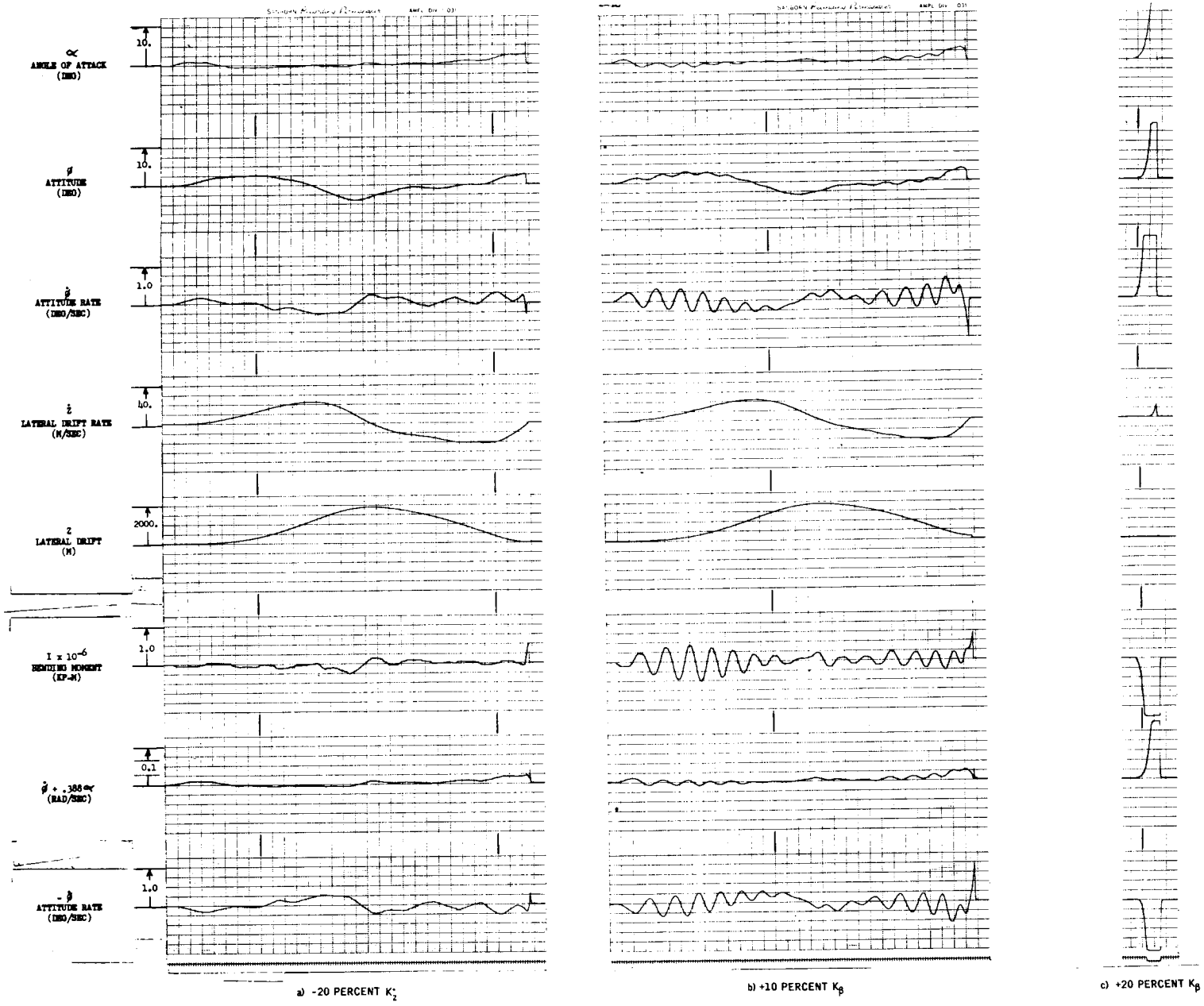

Figure N-21. Load-Relief Controller, Controller Parameter Variations - Response to Mean Wind [(a) +20% K_z, (b) +10% K_β, (c) +20% K_β]

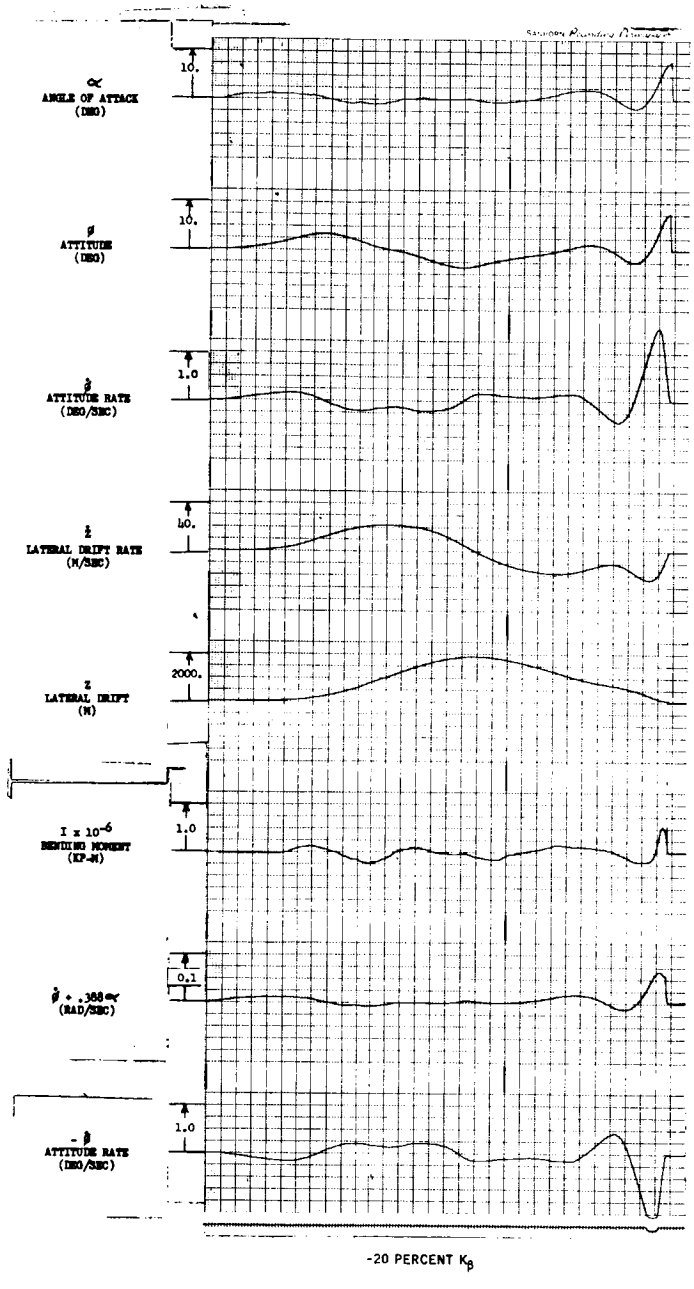

Figure N-22. Load-Relief Controller, Controller Parameter Variations - Response to Mean Wind (-20% K_β)

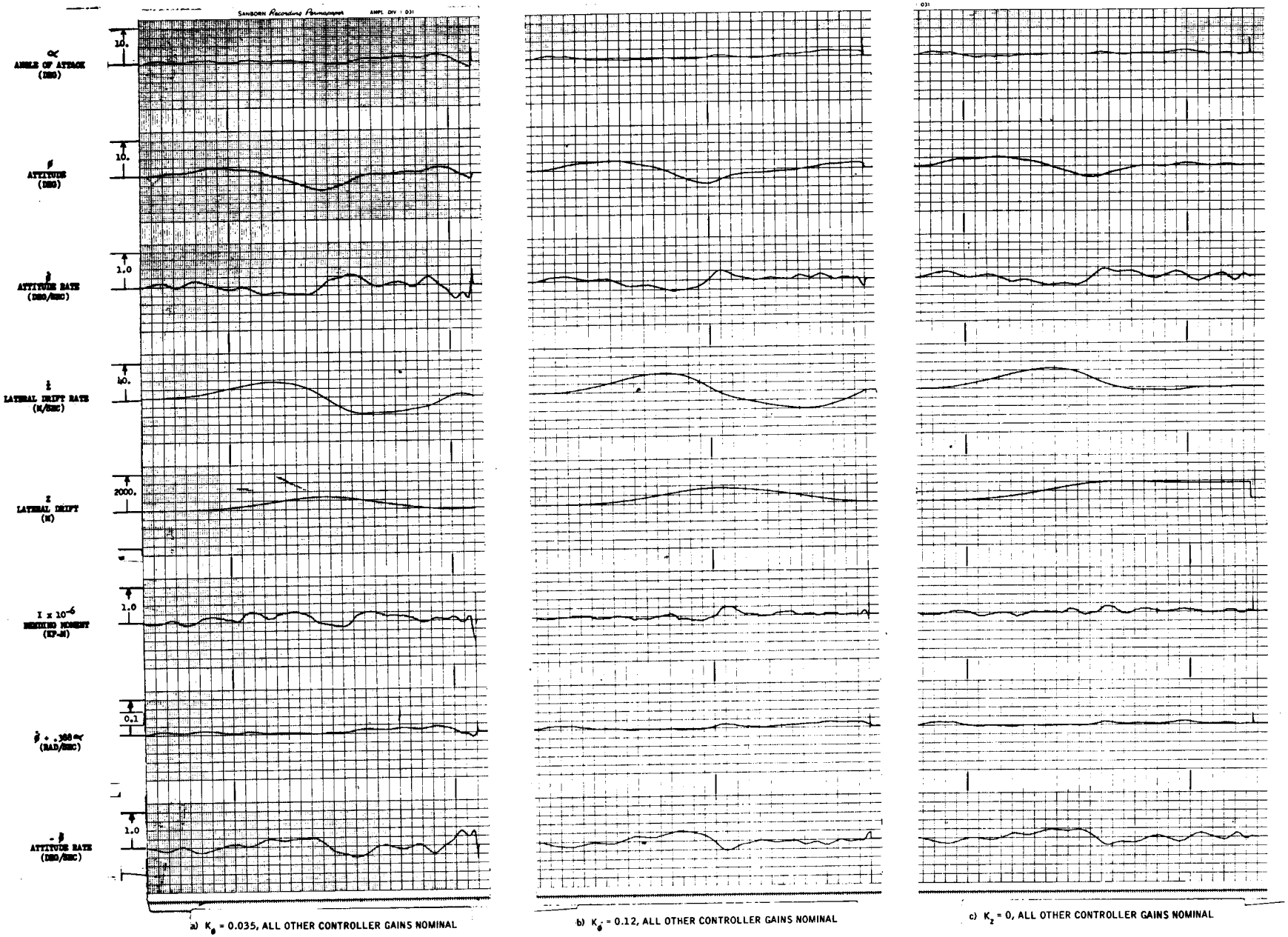

Figure N-23. Simplification Investigation of Load-Relief Controller - Response to Mean Wind [(a) $K_\phi = 0.035$, (b) $K_\phi = 0.12$, (c) $K_z = 0$]

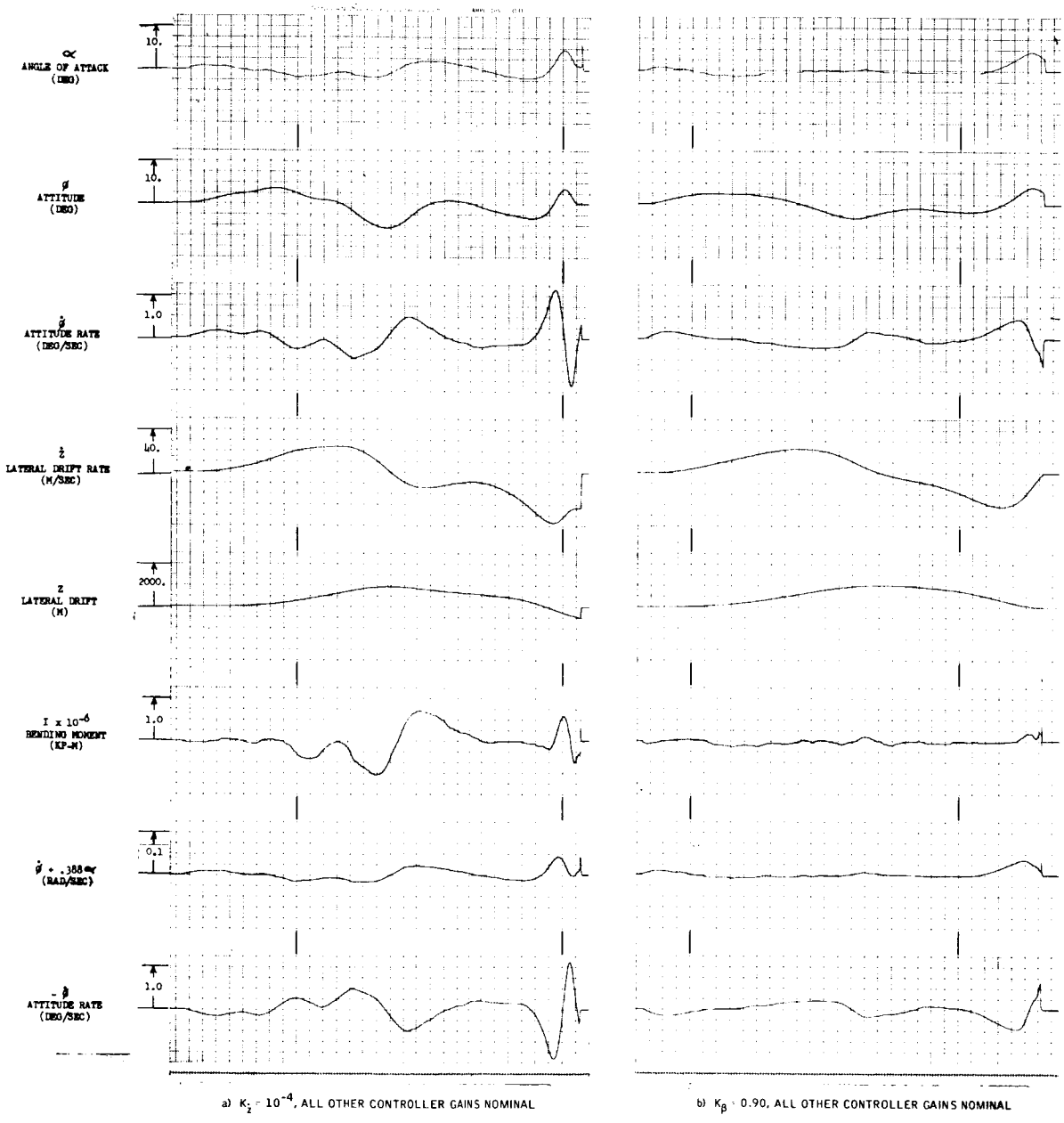

Figure N-24. Simplification Investigation of Load-Relief Controller - Response to Mean Wind [(a) $K_z = 10^{-4}$, (b) $K_\beta = 0.9$]

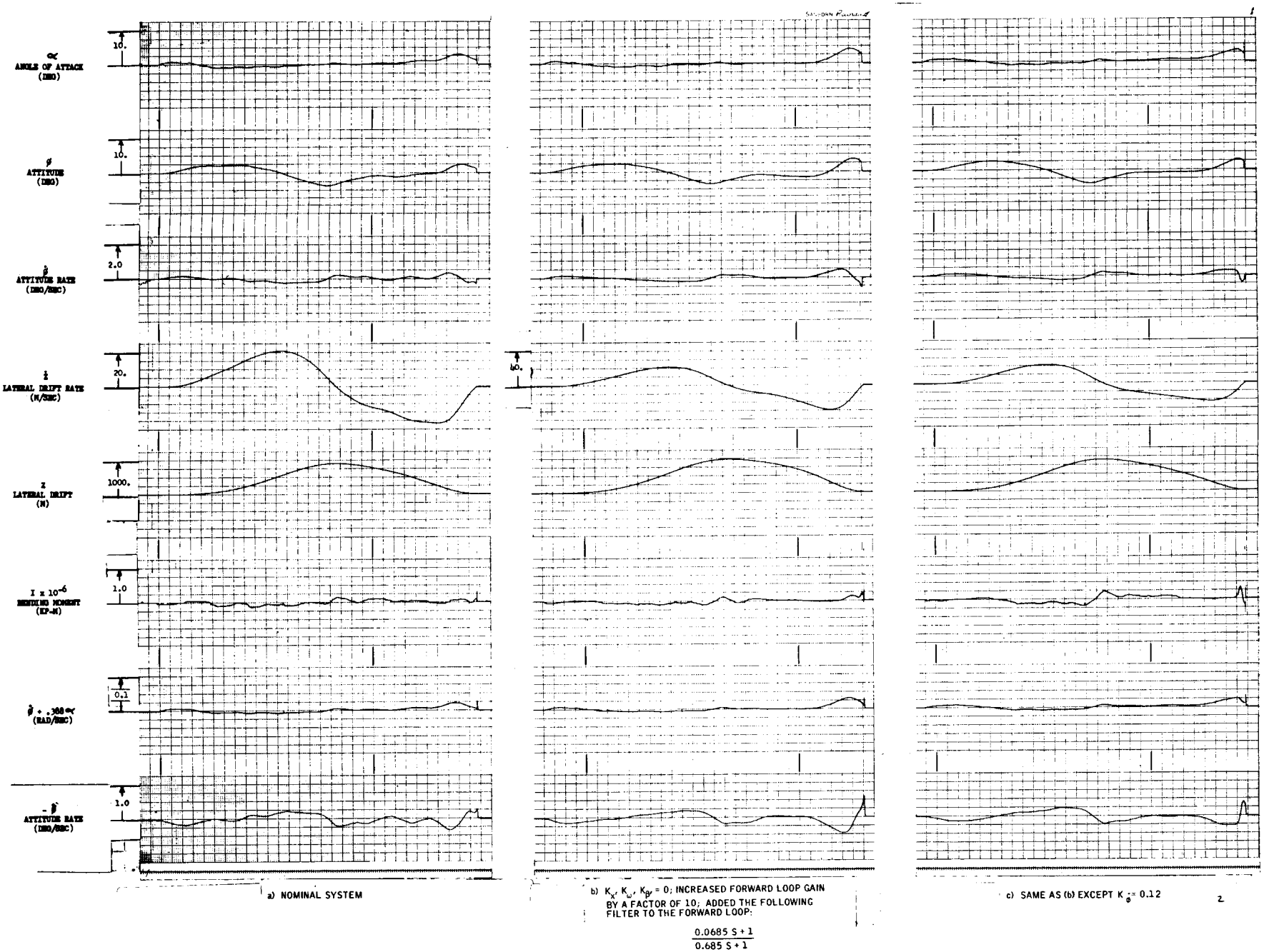

Figure N-25. Load-Relief System, System Simplifications - Mean-Wind Response

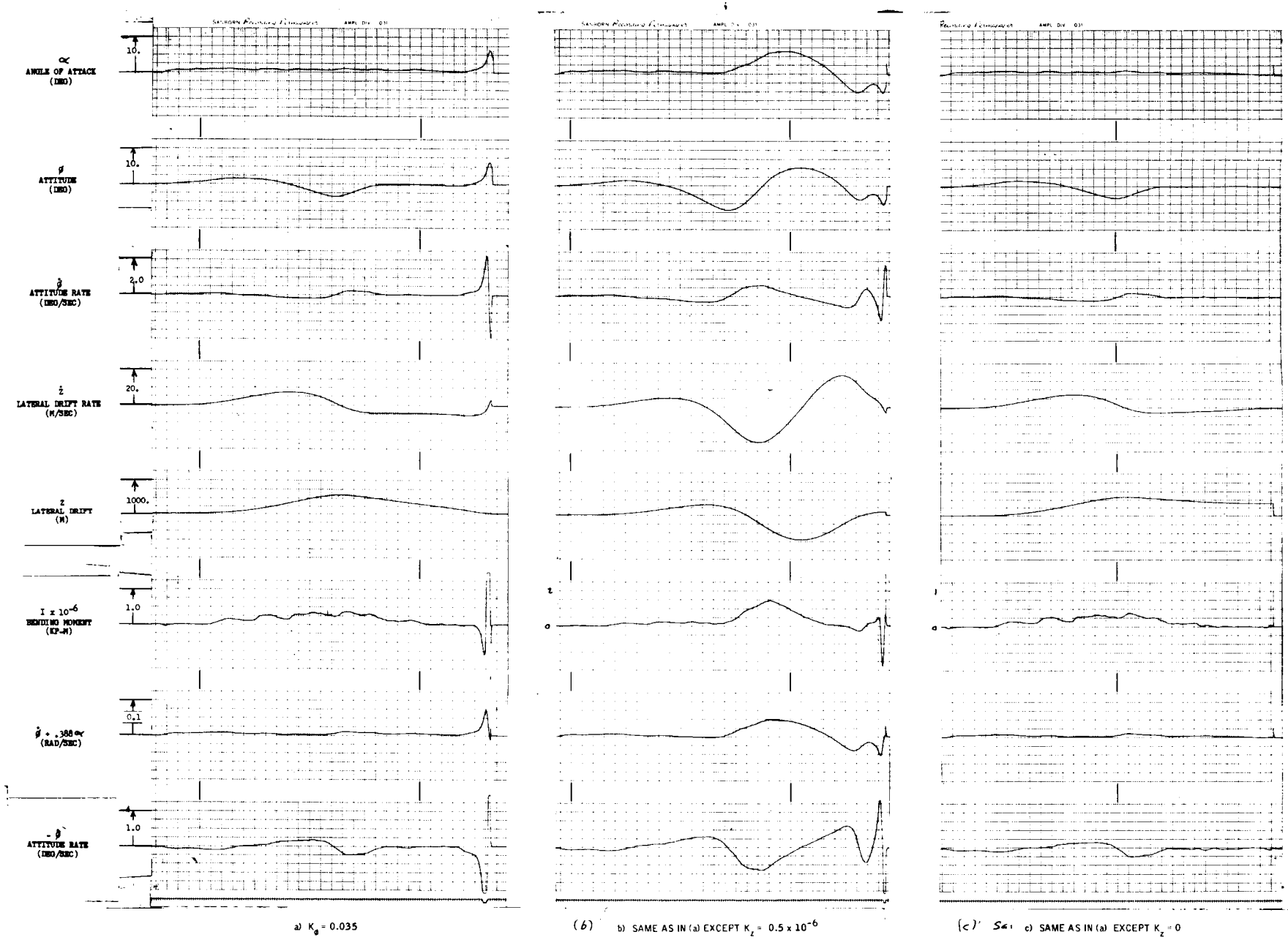

a) $K_\phi = 0.035$ (b) b) SAME AS IN (a) EXCEPT $K_z = 0.5 \times 10^{-6}$ (c) c) SAME AS IN (a) EXCEPT $K_z = 0$

Figure N-26. Load-Relief System, System Simplifications - Mean-Wind Response

$$U = 10\left[\frac{0.0685\,S+1}{0.685\,S+1}\right]\left[f(t) + K_\phi\phi + 0.12\dot{\phi} + K_{\dot{z}}\dot{z} + K_z z\right]$$

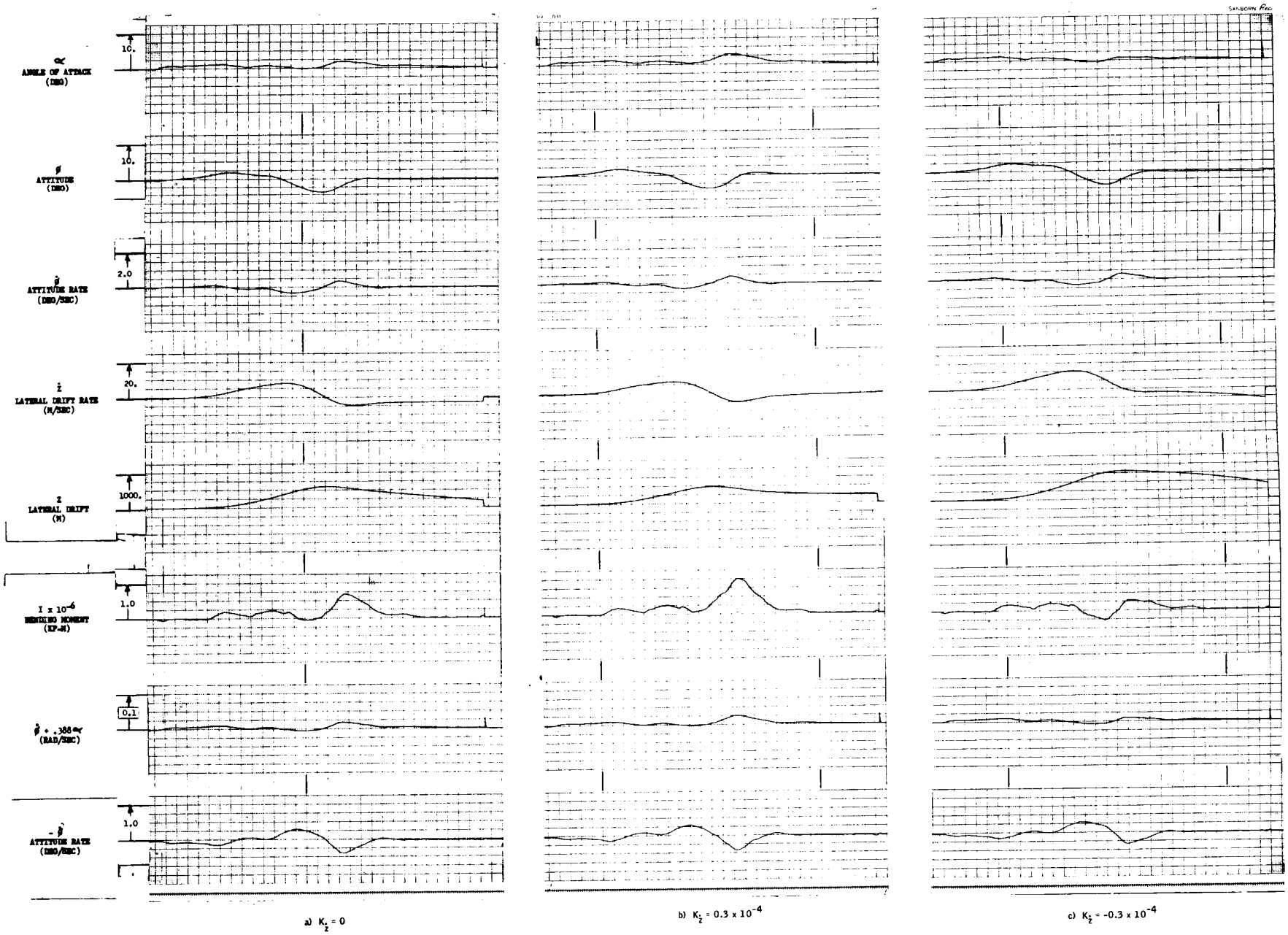

Figure N-27. Load-Relief System, System Simplifications - Mean-Wind Response

$$U = 10 \quad \frac{0.0685\ S+1}{\quad} \quad f(t) + 0.035\phi + 0.12\dot{\phi} + K_z(t)\ \dot{z}$$

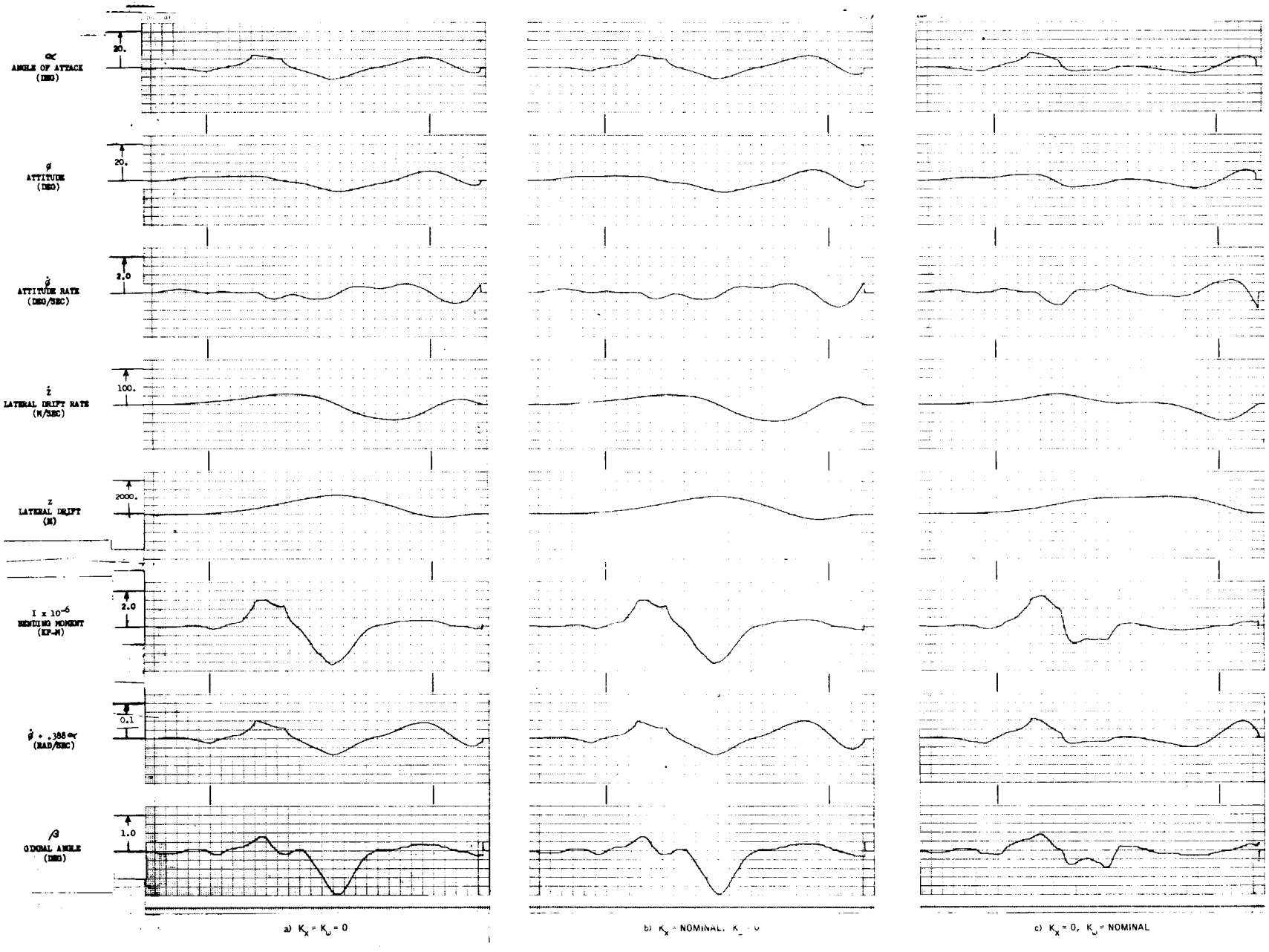

Figure N-28. Load-Relief Controller, Case I Estimator - Evaluation of Estimator Feed Forward Signals (Response to 48-second NASA wind)

Figure N-29. Load-Relief Controller, Case I Estimator - Evaluation of Estimator Feed Forward Signals (Response to 56-second NASA wind)

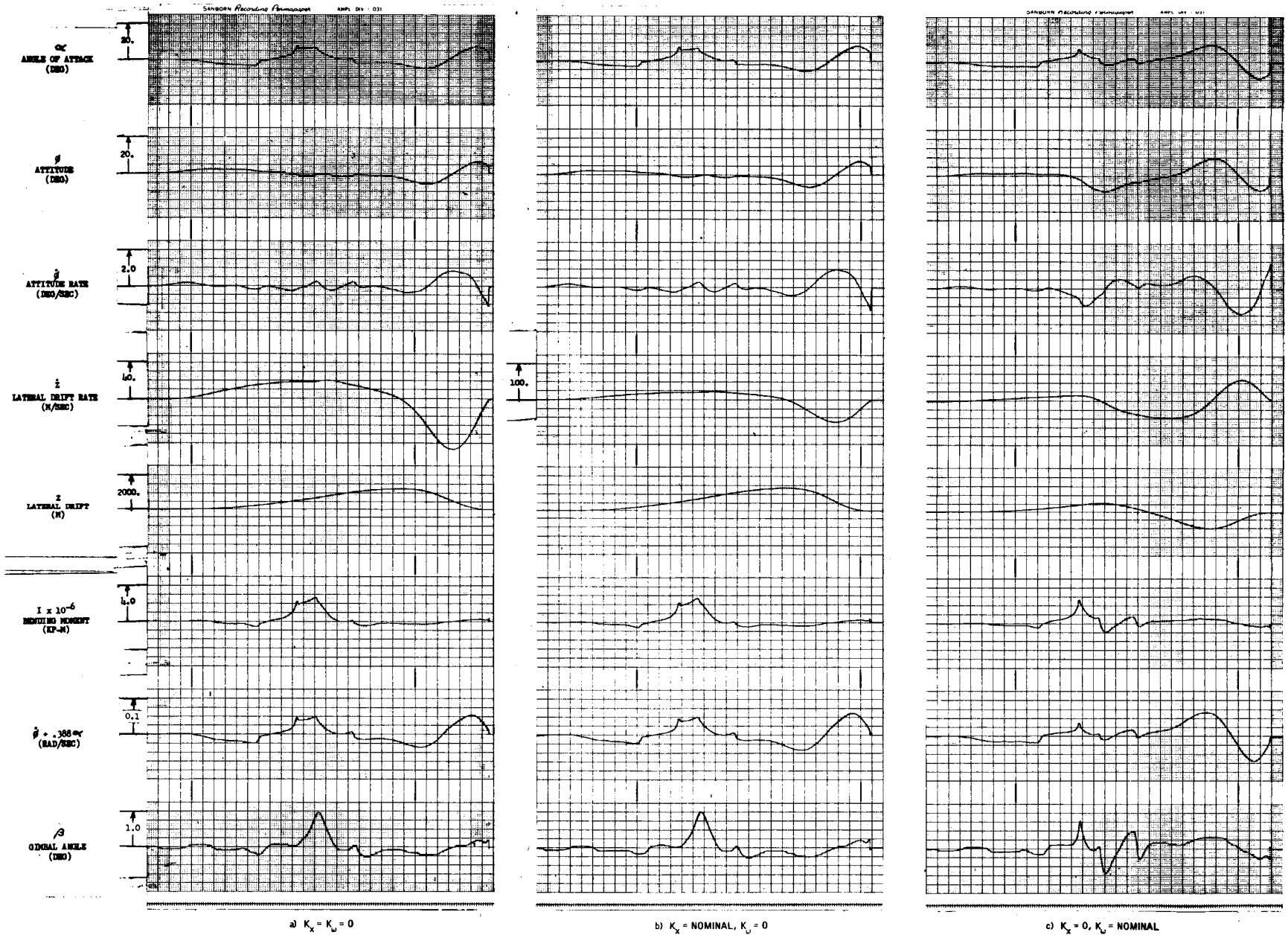

Figure N-30. Load-Relief Controller, Case I Estimator - Evaluation of Estimator Feed Forward Signals (Response to 64-second NASA wind)

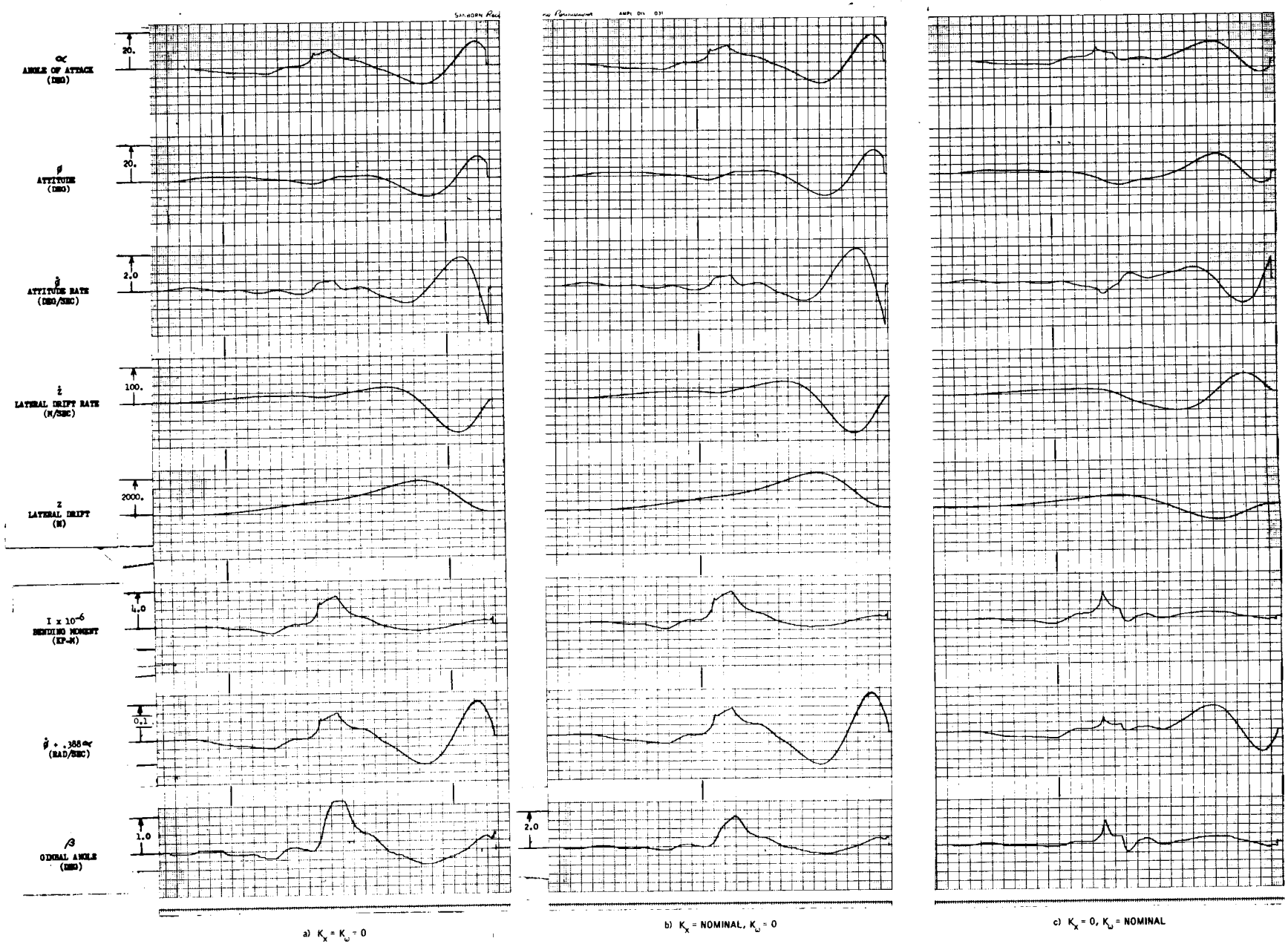

Figure N-31. Load-Relief Controller, Case I Estimator - Evaluation of Estimator Feed Forward Signals (Response to 72-second NASA wind)

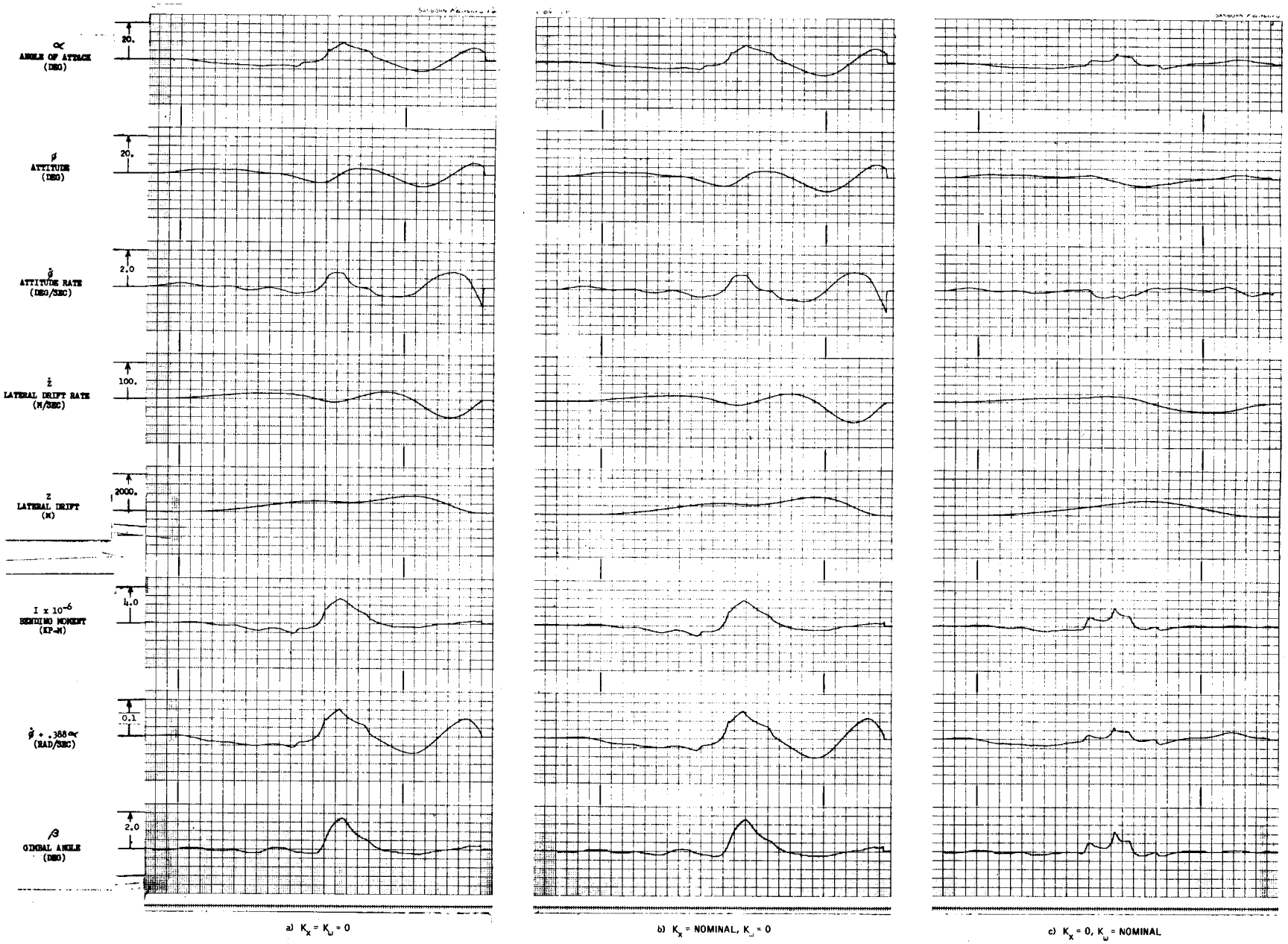

Figure N-32. Load-Relief Controller, Case I Estimator - Evaluation of Estimator Feed Forward Signals (Response to 80-second NASA wind)

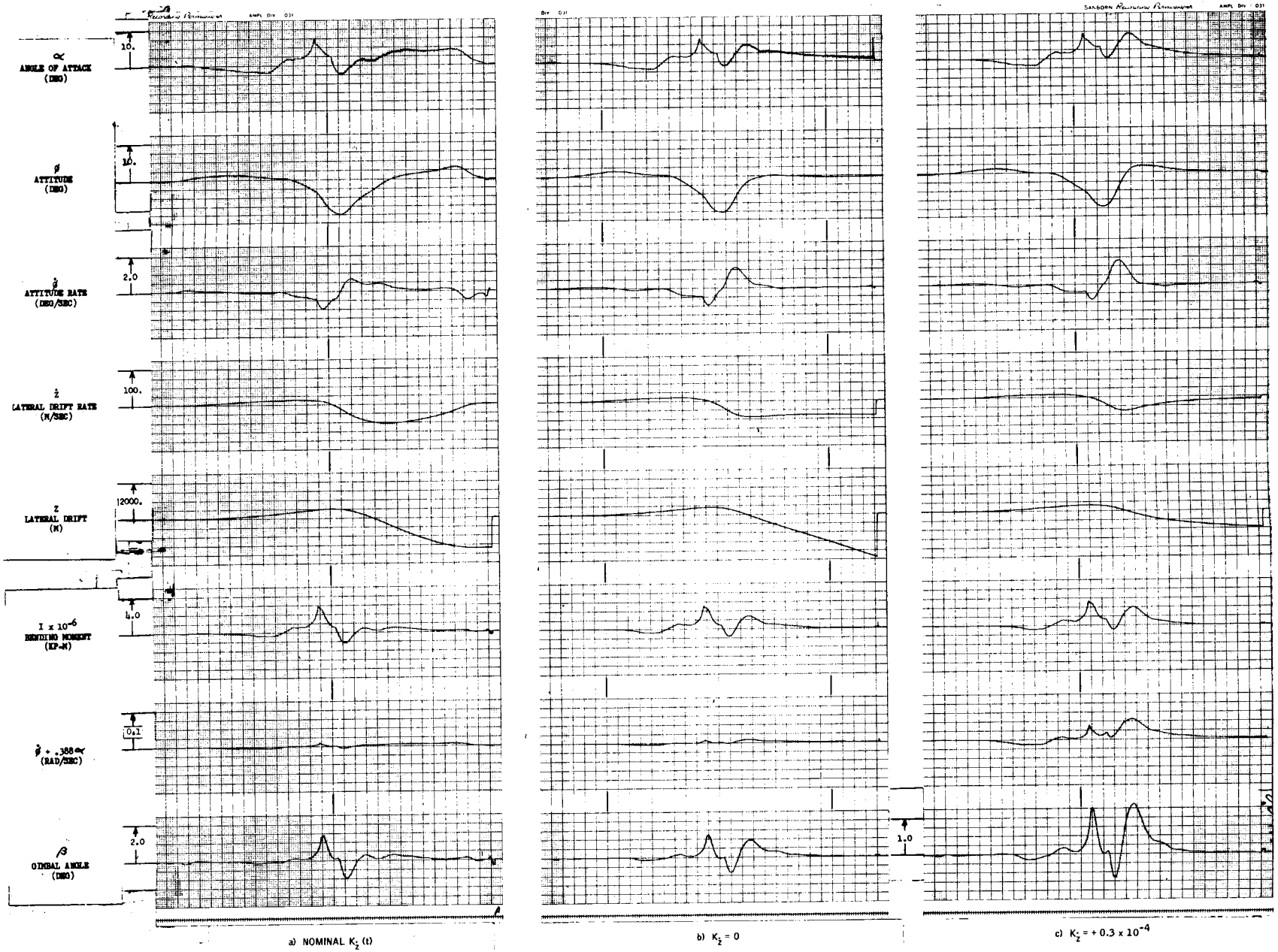

Figure N-33. Load-Relief System, System Simplification - 72-second NASA Wind Responses [(a) Nominal $K_{\dot{z}}(t)$, (b) $K_{\dot{z}} = 0$, (c) $K_{\dot{z}} = +0.3 \times 10^{-4}$]

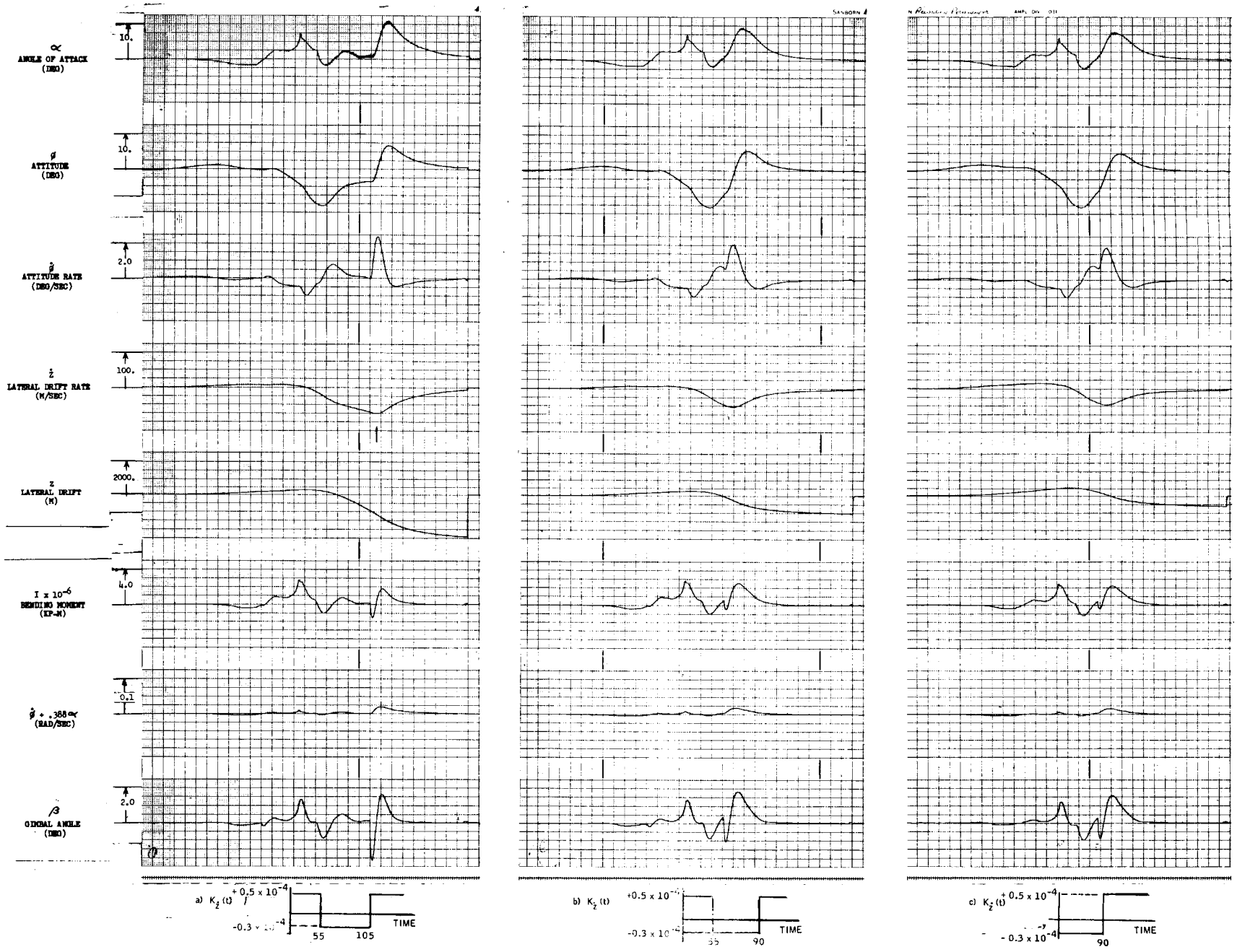

Figure N-34. Load-Relief System, System Simplification, 72-second NASA Wind Response - Step $K_{\dot{z}}$

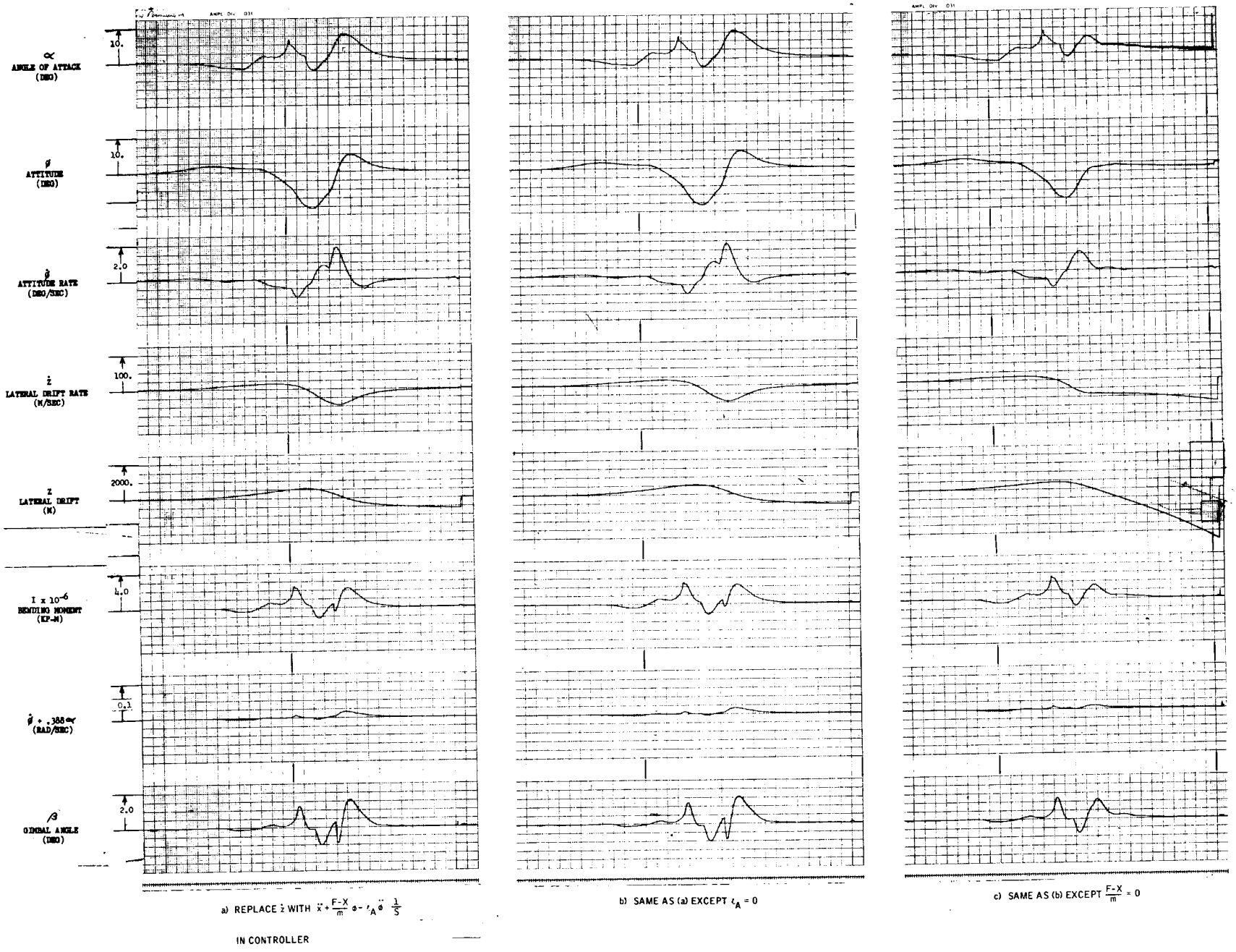

Figure N-35. Load-Relief System, System Simplification, 72-second NASA Wind Response - Modified ż

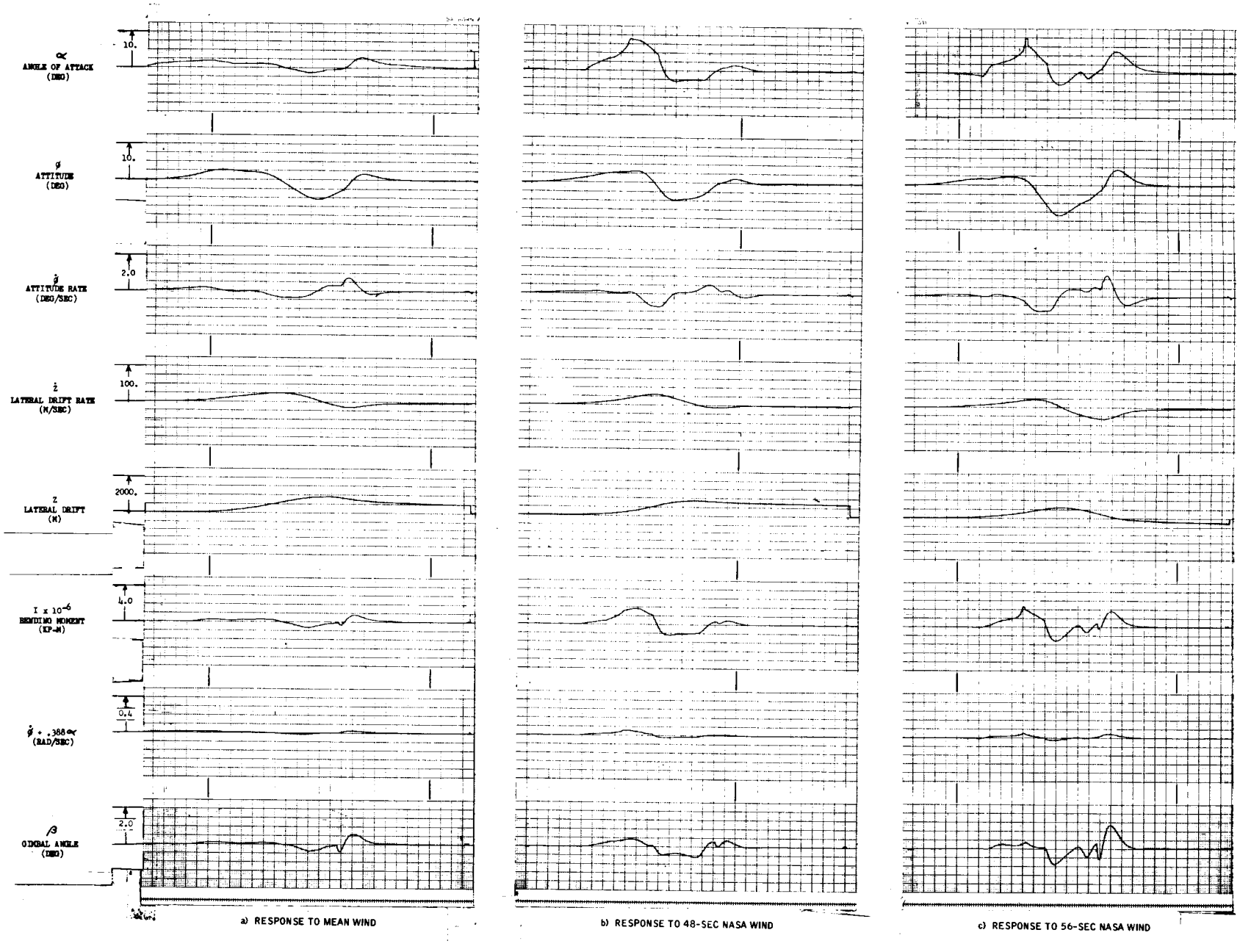

Figure N-36. Simplified Load-Relief Controller - Nominal Responses [(a) Mean Wind, (b) 48-second NASA Wind, (c) 56-second NASA Wind]

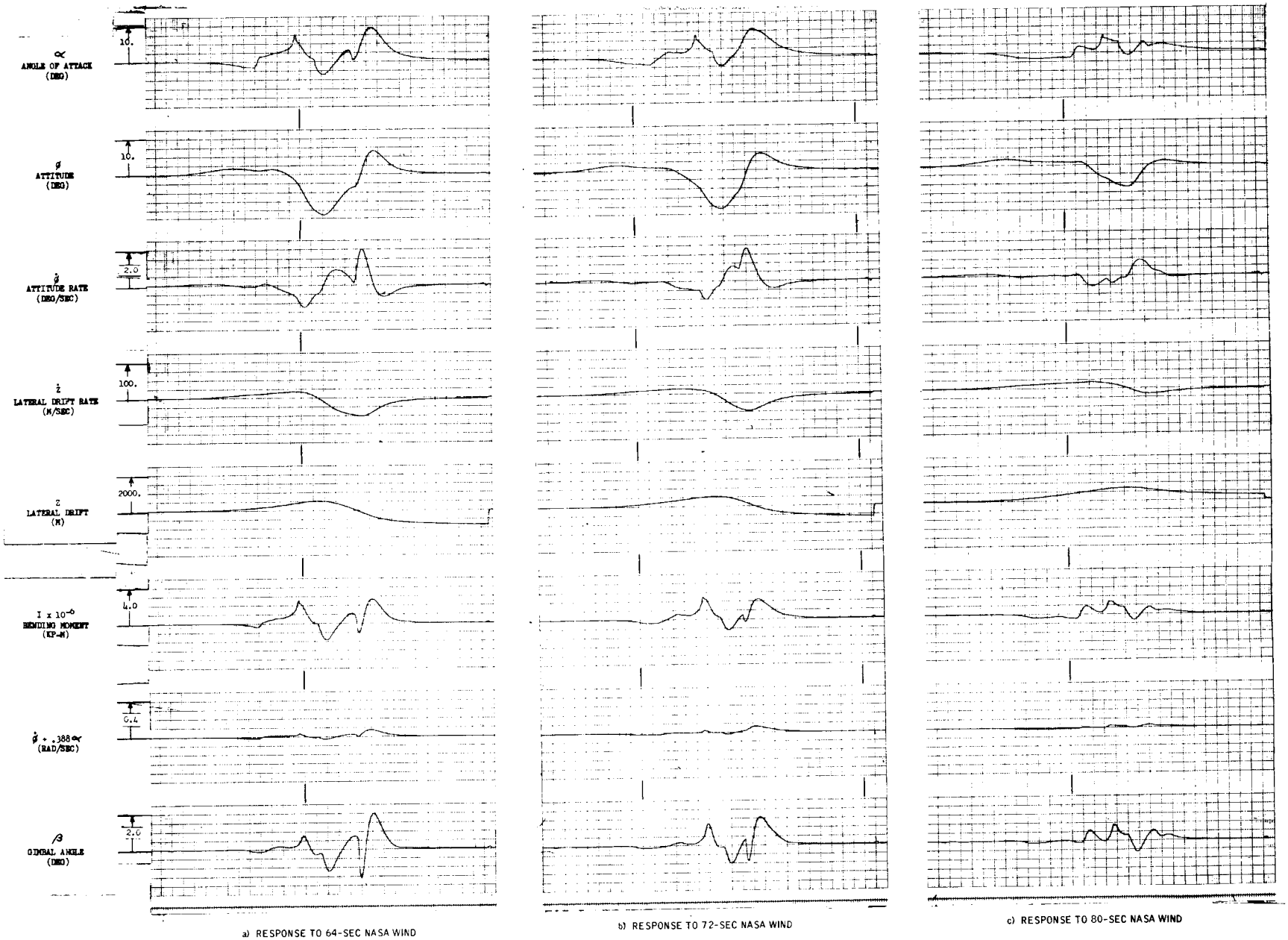

Figure N-37. Simplified Load-Relief Controller - Nominal Responses [(a) 64-second NASA Wind, (b) 72-second NASA Wind, (c) 80-second NASA Wind]

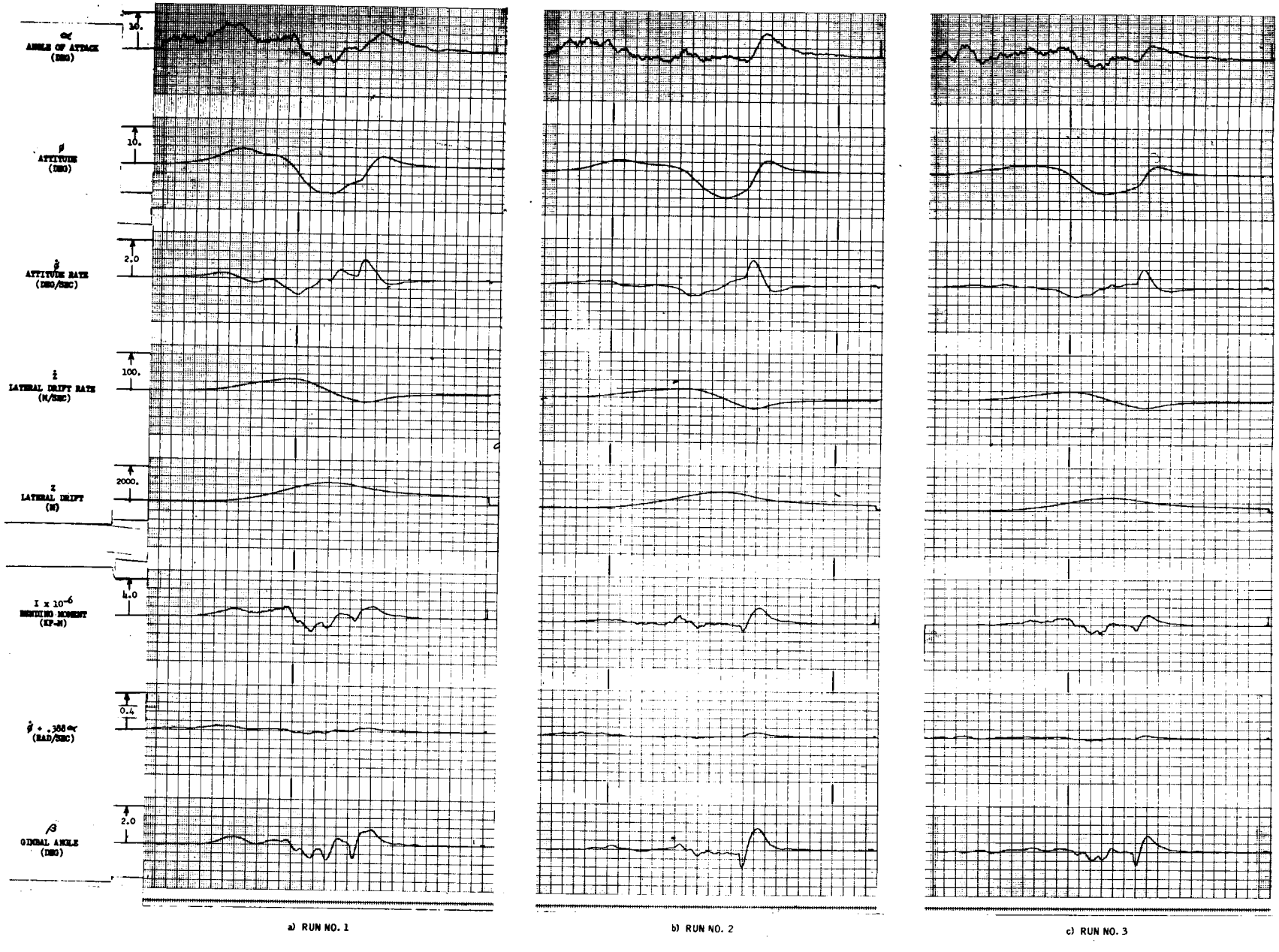

a) RUN NO. 1

b) RUN NO. 2

c) RUN NO. 3

Figure N-38. Simplified Load-Relief Controller - Response to Random Wind

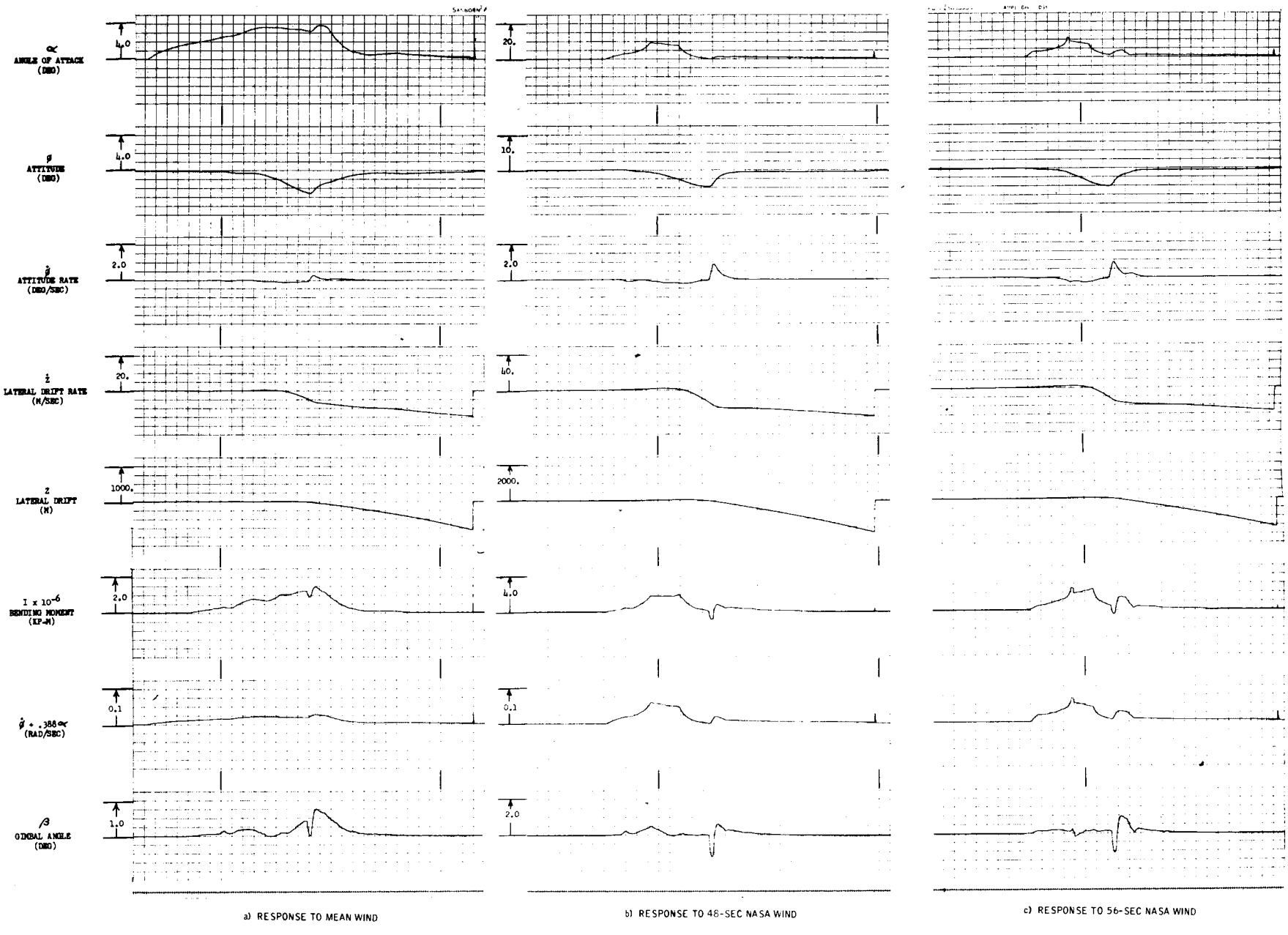

Figure N-39. Minimax Controller, Nominal System [(a) Mean Wind, (b) 48-second NASA Wind, (c) 56-second NASA Wind]

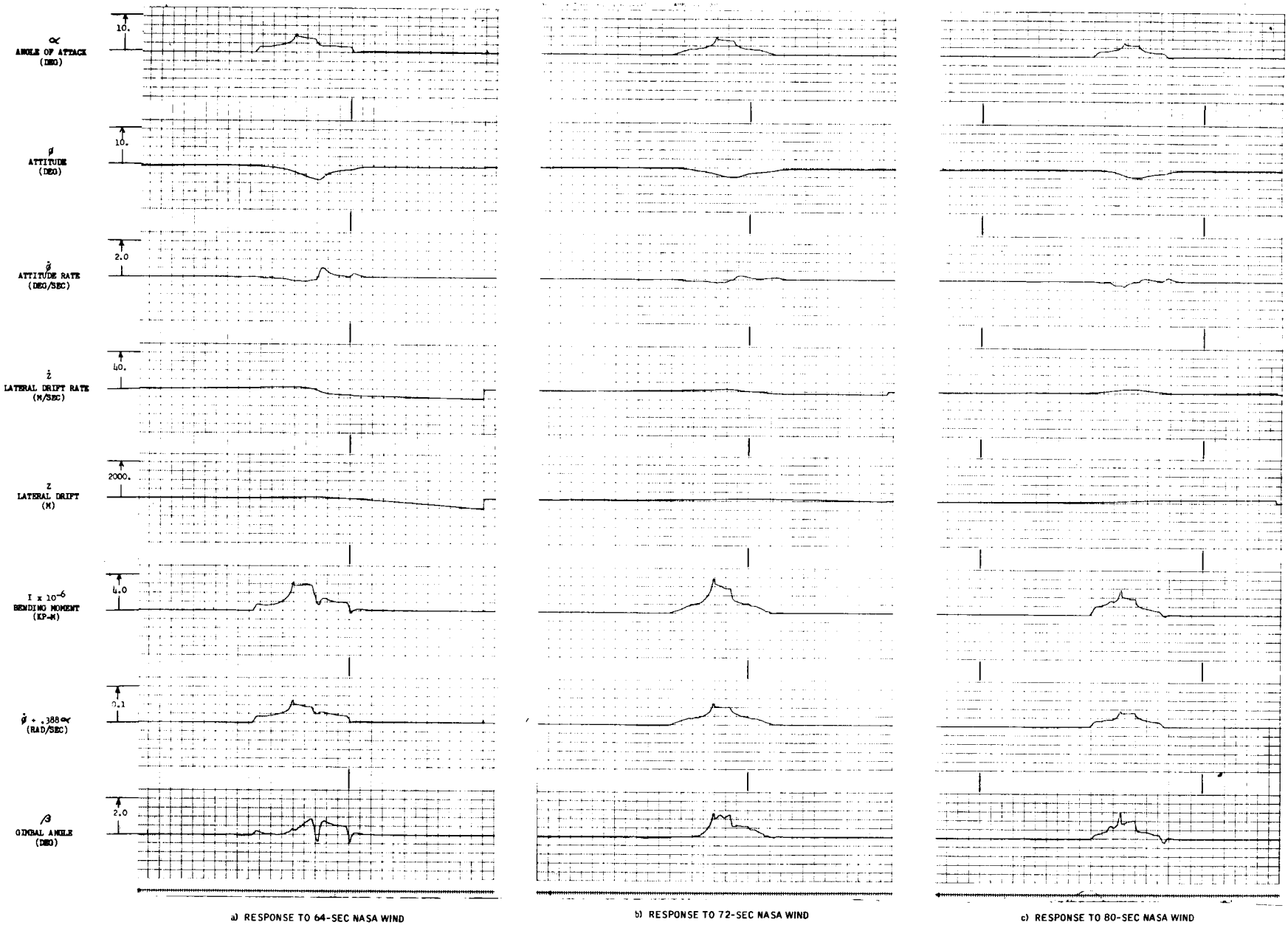

Figure N-40. Minimax Controller, Nominal System [(a) 64-second NASA Wind, (b) 72-second NASA Wind, (c) 80-second NASA Wind]

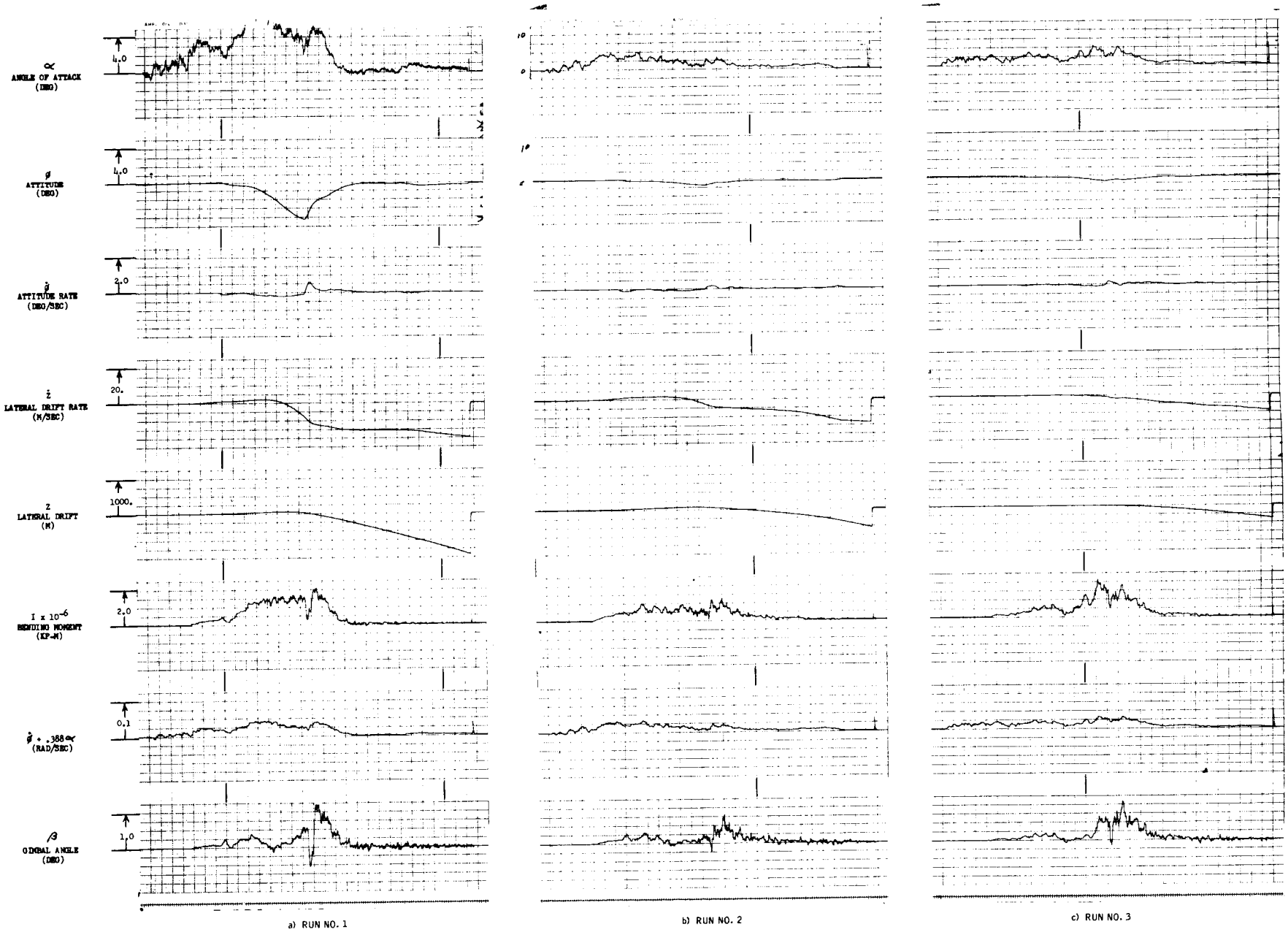

Figure N-41. Minimax Controller, Nominal System - Response to Random Wind

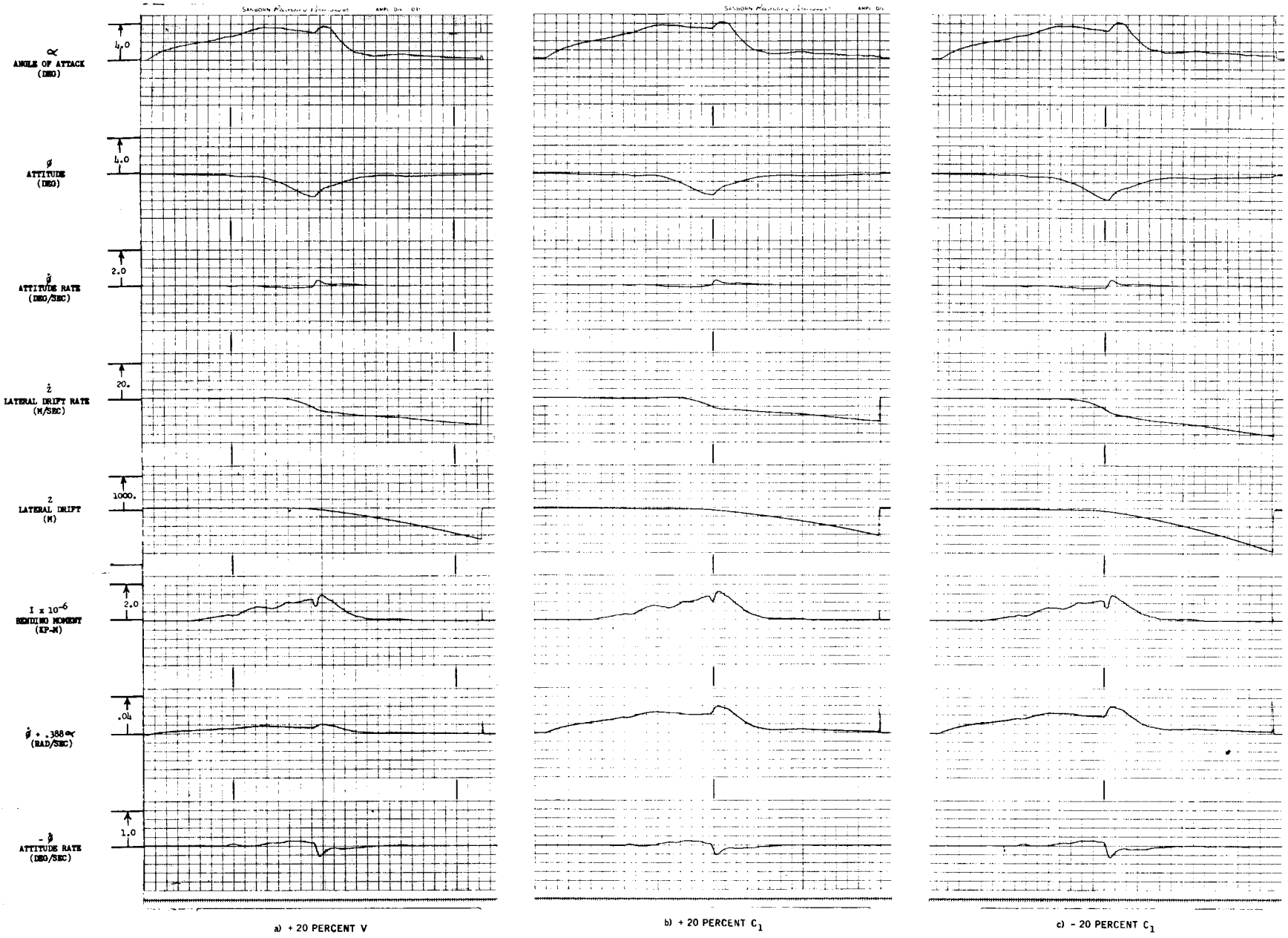

Figure N-42. Minimax Controller, Vehicle Parameter Variations - Response to a Mean Wind [(a) + 20% v, (b) +20% c_1, (c) -20% c_1]

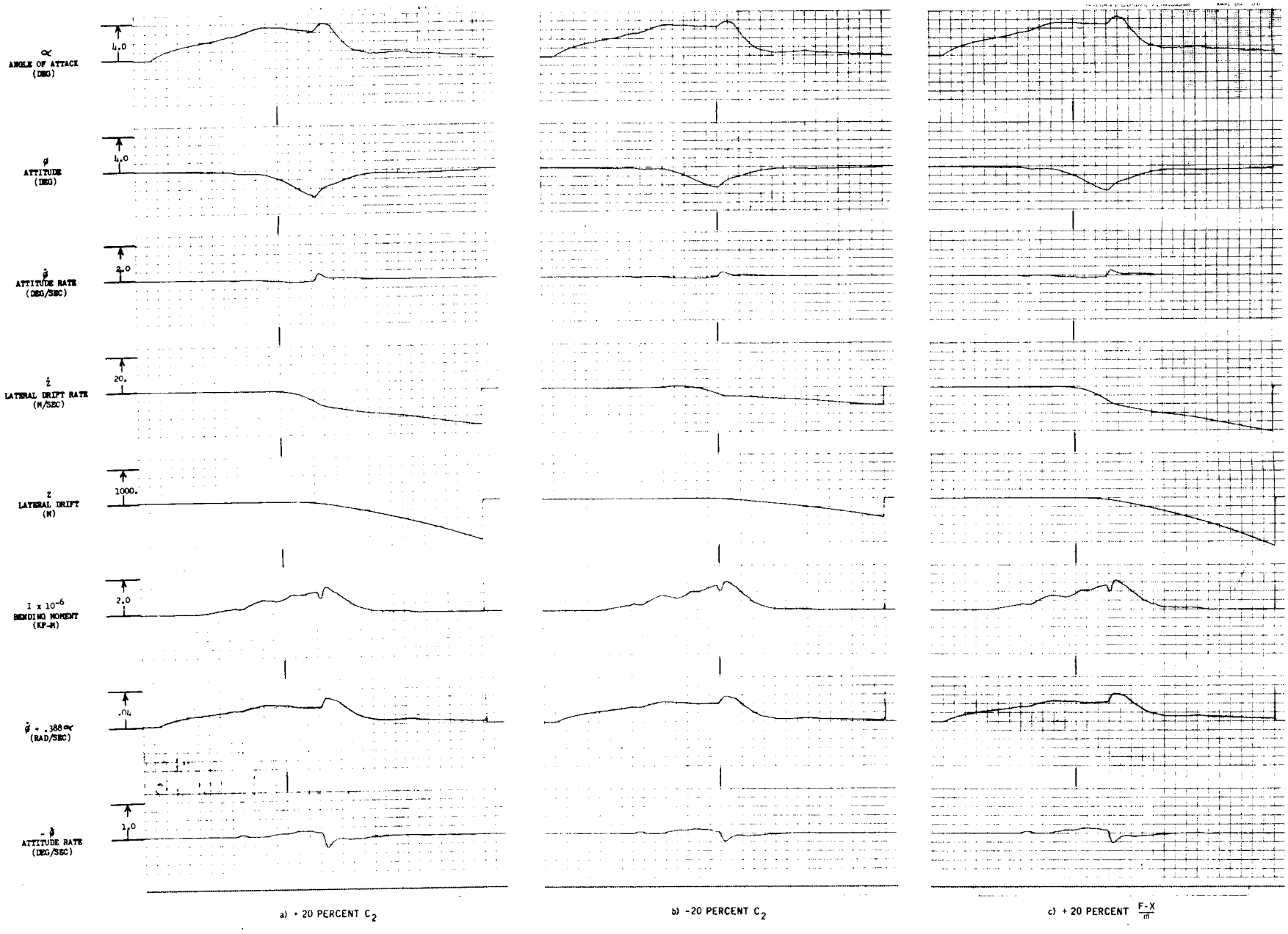

Figure N-43. Minimax Controller, Vehicle Parameter Variations - Response to a Mean Wind [(a) +20% c_2, (b) -20% c_2, (c) +20% $\left(\frac{F-X}{m}\right)$]

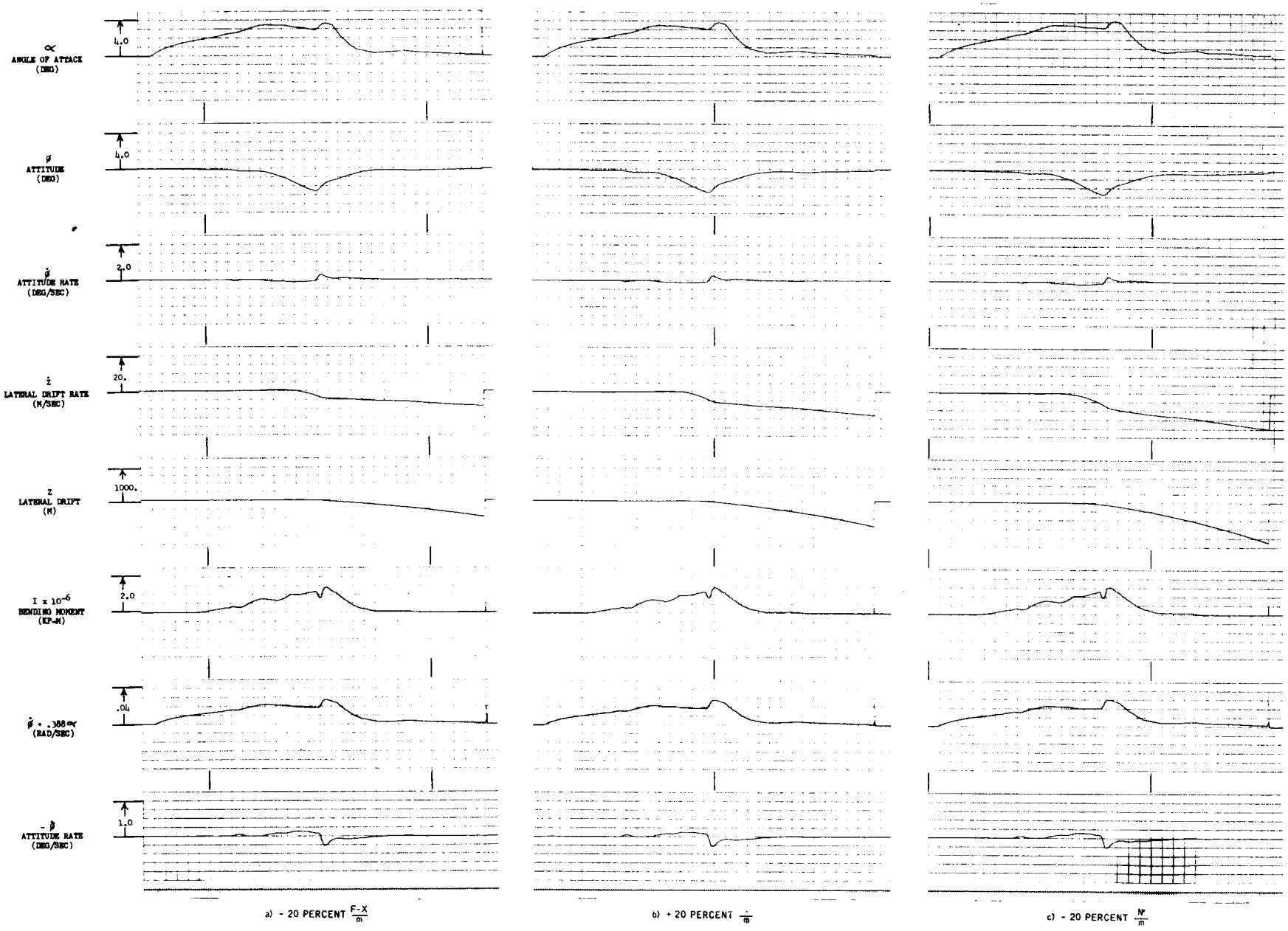

Figure N-44. Minimax Controller, Vehicle Parameter Variations - Response to a Mean Wind [(a) $-20\%\left(\frac{F-X}{m}\right)$, (b) $+20\%\ \frac{N'}{m}$, (c) $-20\%\ \frac{N'}{m}$]

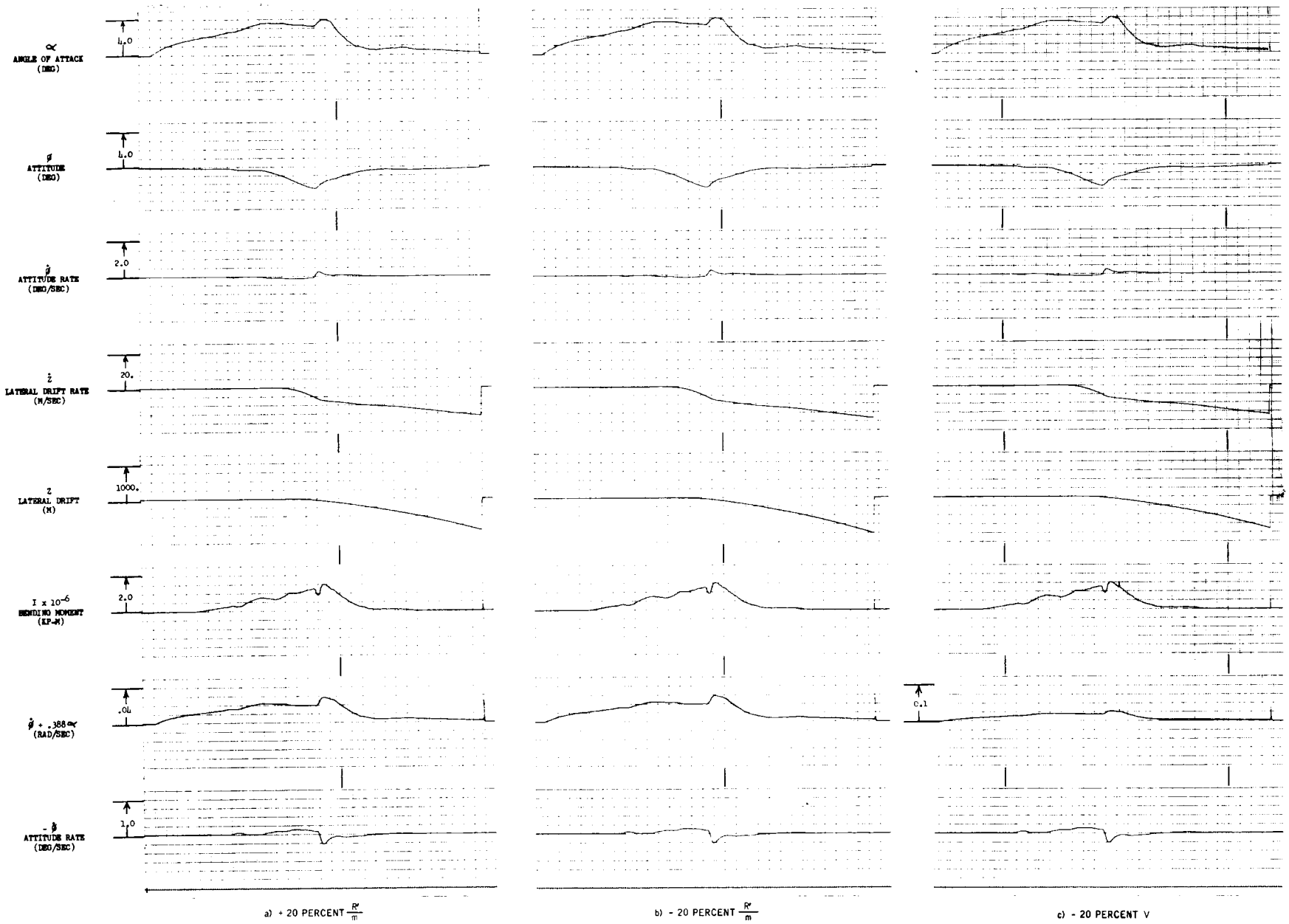

Figure N-45. Minimax Controller, Vehicle Parameter Variations - Response to a Mean Wind [(a) +20% $\frac{R'}{m}$, (b) -20% $\frac{R'}{m}$, (c) -20% V]

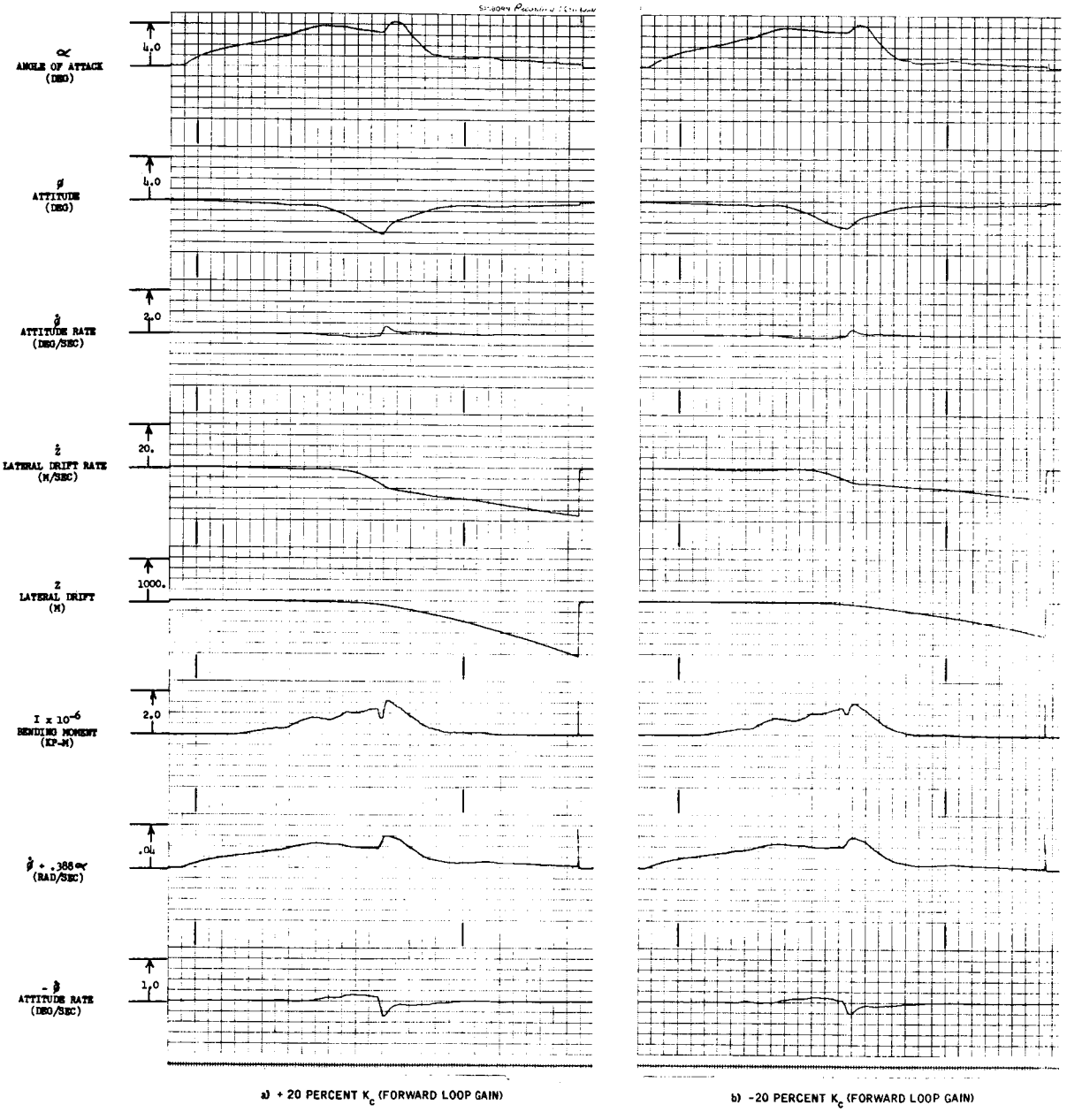

Figure N-46. Minimax Controller, Controller Parameter Variations - Response to Mean Wind [(a) +20% K_c, (b) -20% K_c]

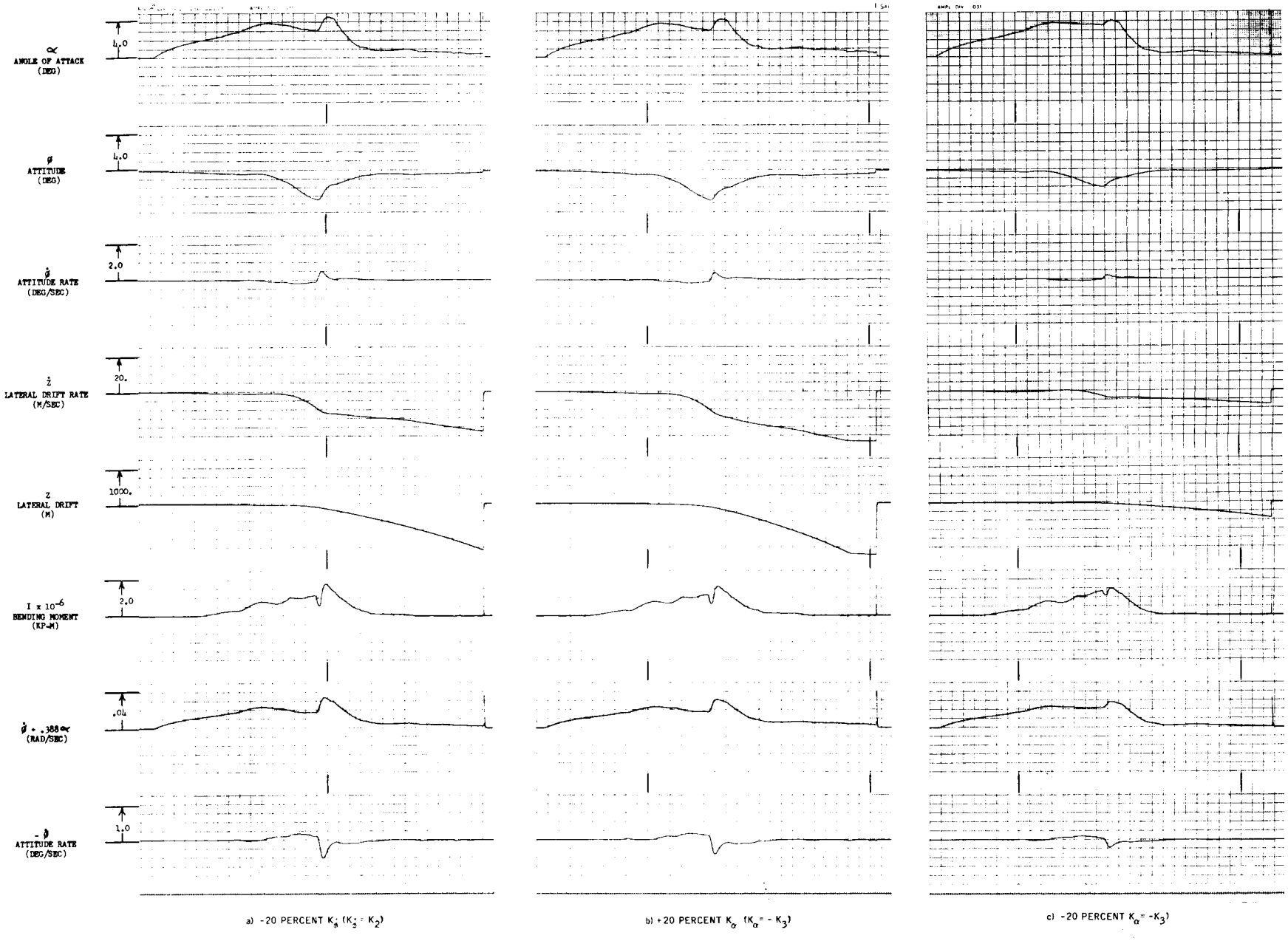

Figure N-47. Minimax Controller, Controller Parameter Variations - Response to Mean Wind [(a) -20% $K_{\dot{\phi}}$, (b) +20% K_{α}, (c) -20% K_{α}]

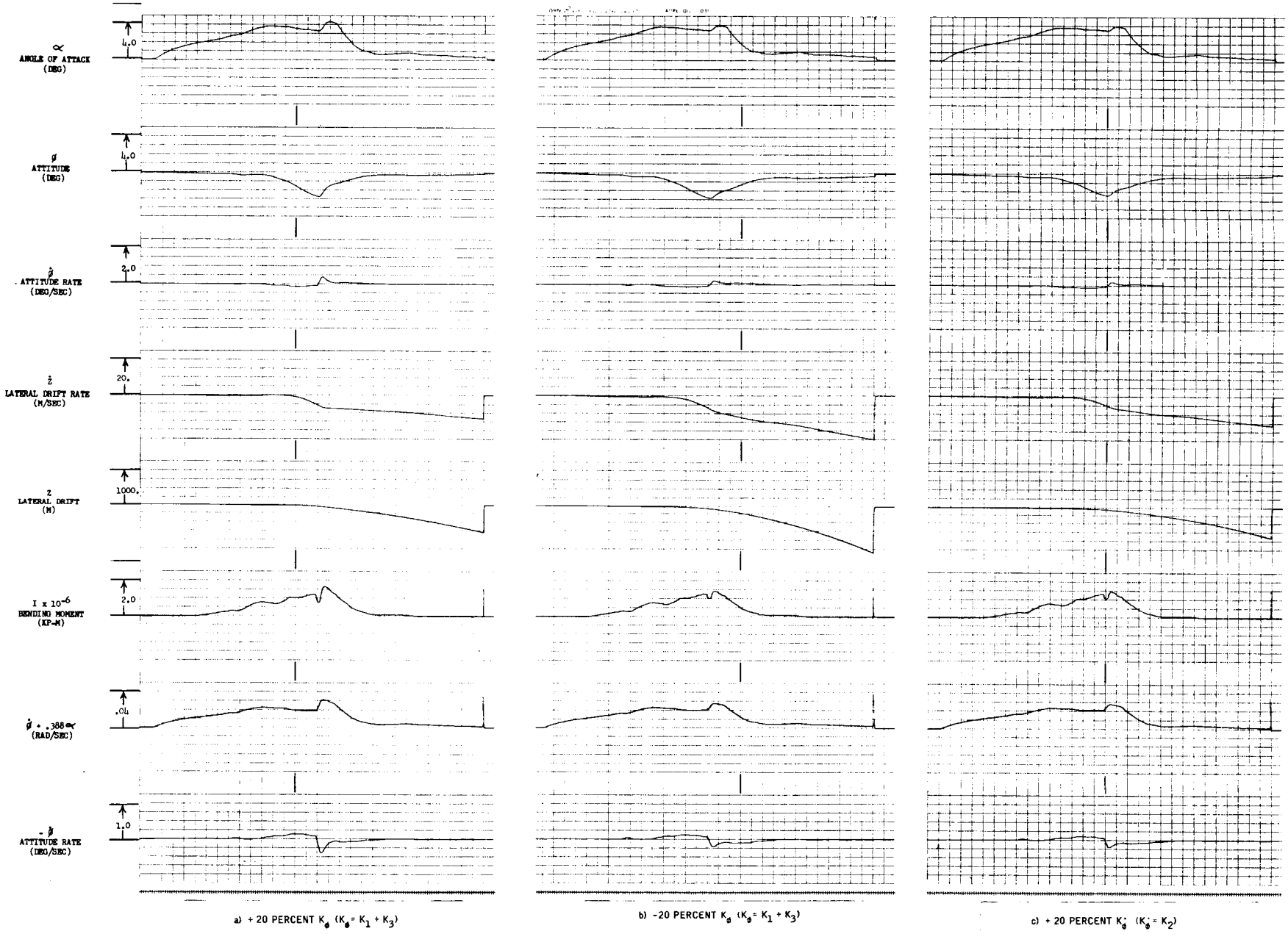

Figure N-48. Minimax Controller, Controller Parameter Variations - Response to Mean Wind [(a) +20% K_ϕ, (b) -20% K_ϕ, (c) +20% $K_{\dot\phi}$]

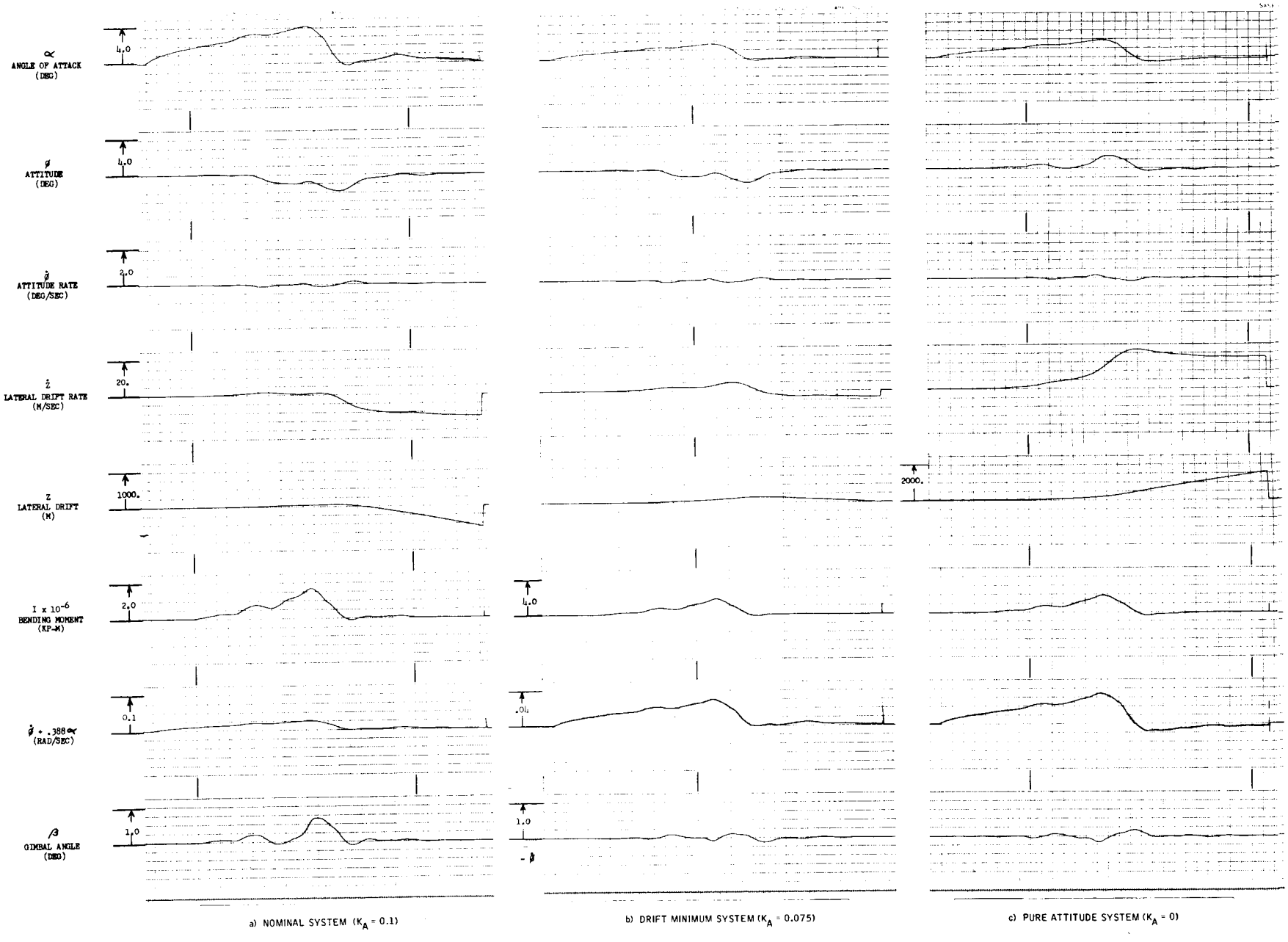

Figure N-49. Conventional Controller - Response to Mean Wind

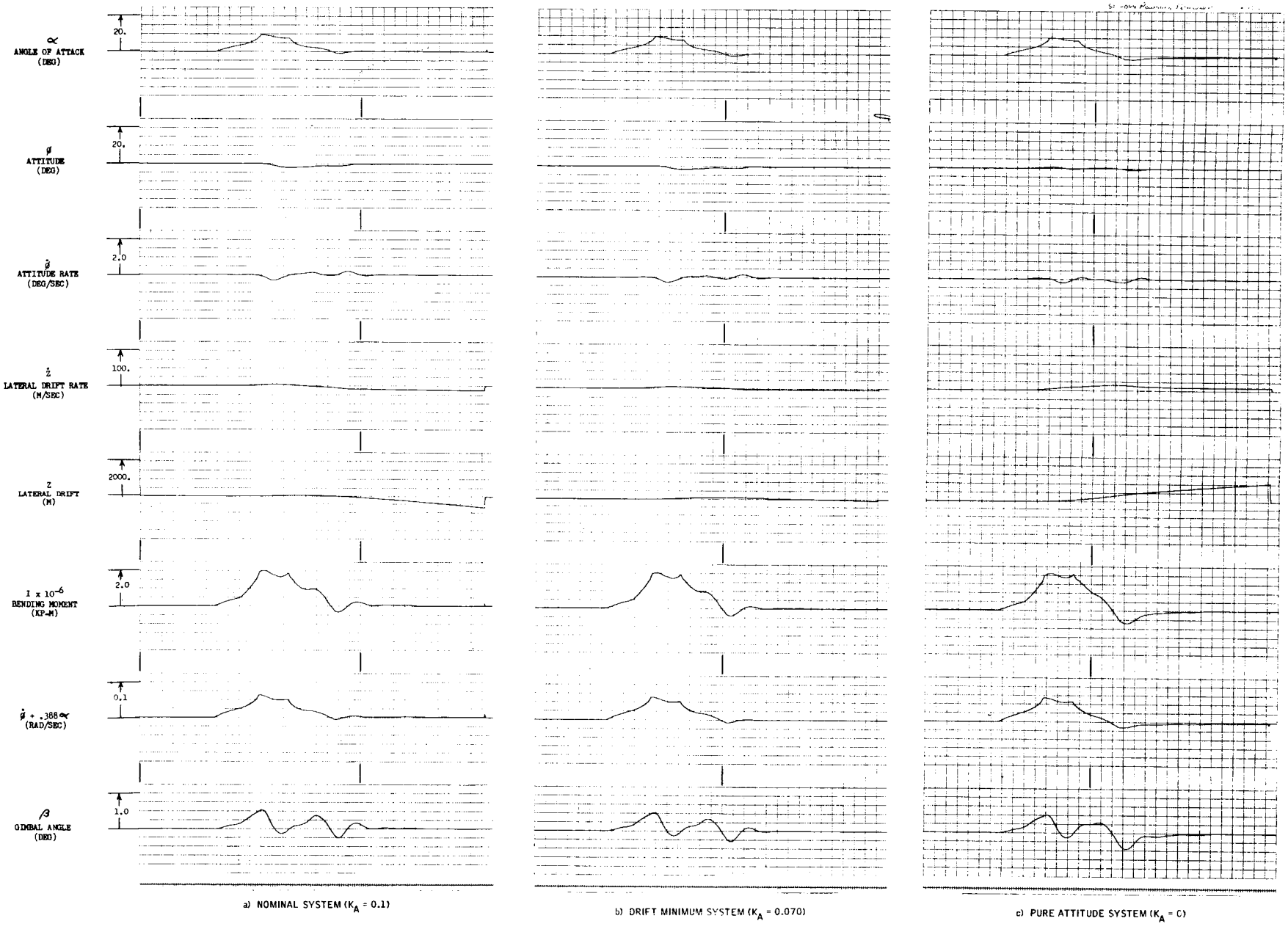

a) NOMINAL SYSTEM (K_A = 0.1)

b) DRIFT MINIMUM SYSTEM (K_A = 0.070)

c) PURE ATTITUDE SYSTEM (K_A = 0)

Figure N-50. Conventional Controller - Response to 48-second NASA Wind

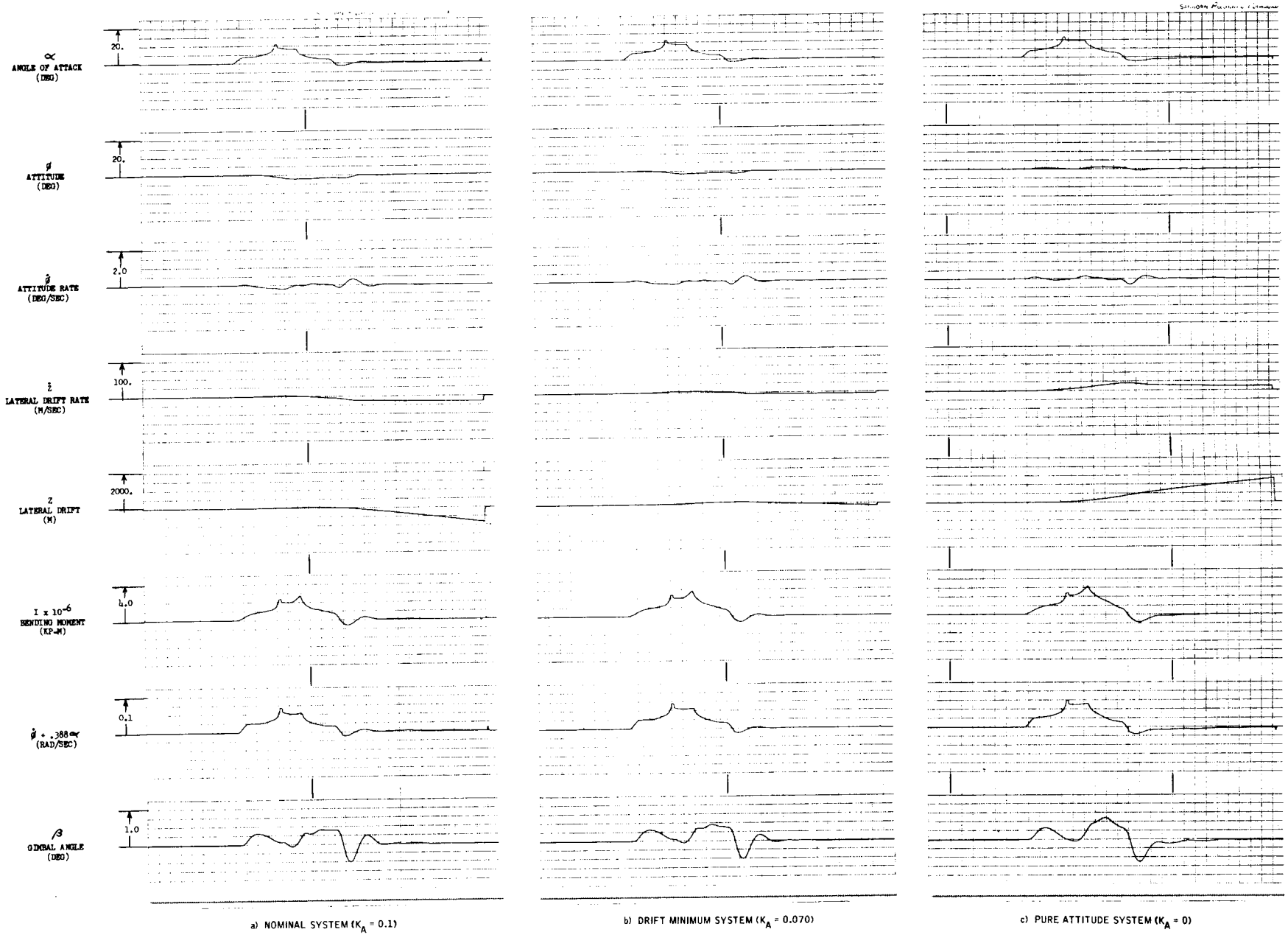

Figure N-51. Conventional Controller - Response to 56-second NASA Wind

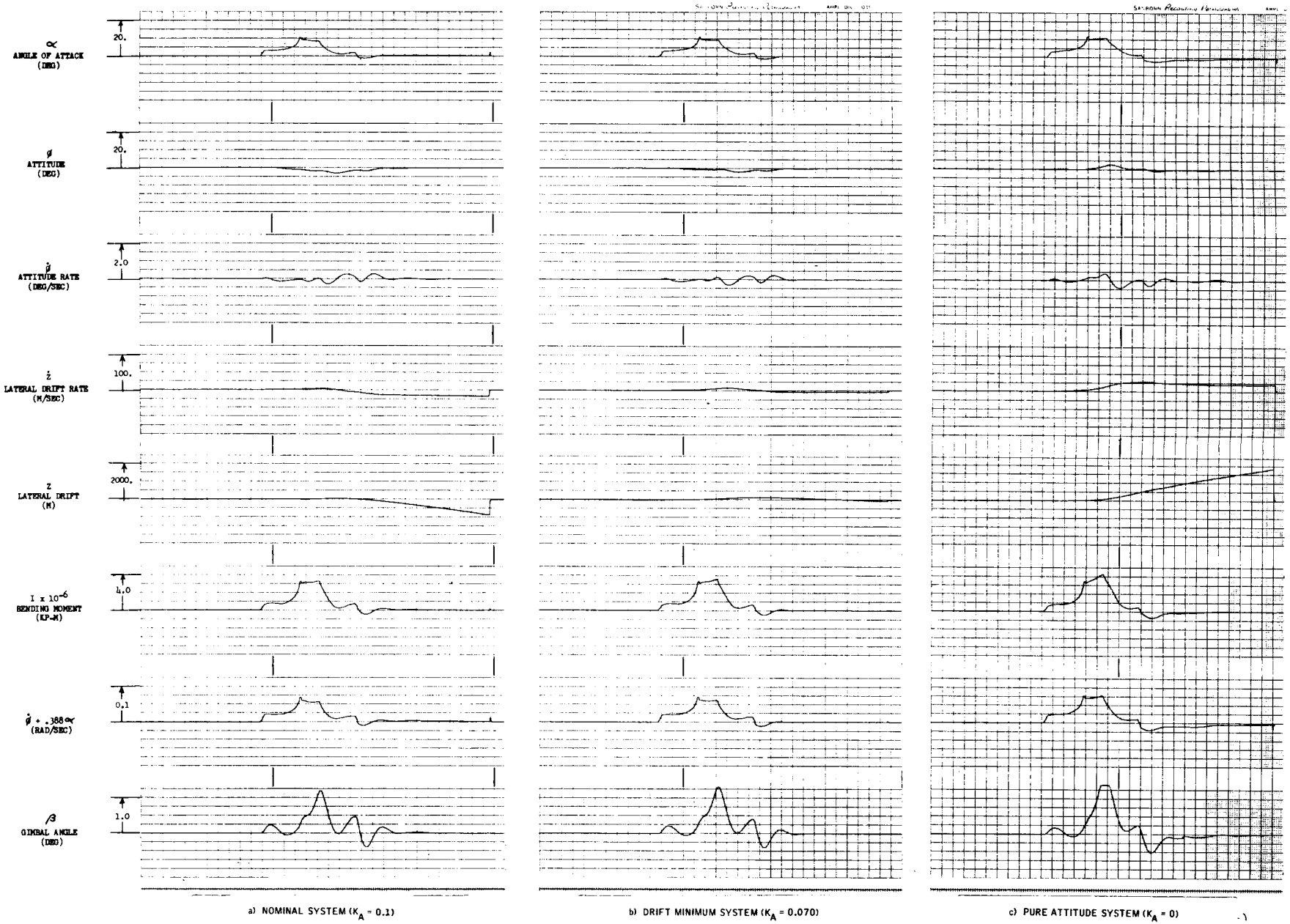

a) NOMINAL SYSTEM (K_A = 0.1)

b) DRIFT MINIMUM SYSTEM (K_A = 0.070)

c) PURE ATTITUDE SYSTEM (K_A = 0)

Figure N-52. Conventional Controller - Response to 64-second NASA Wind

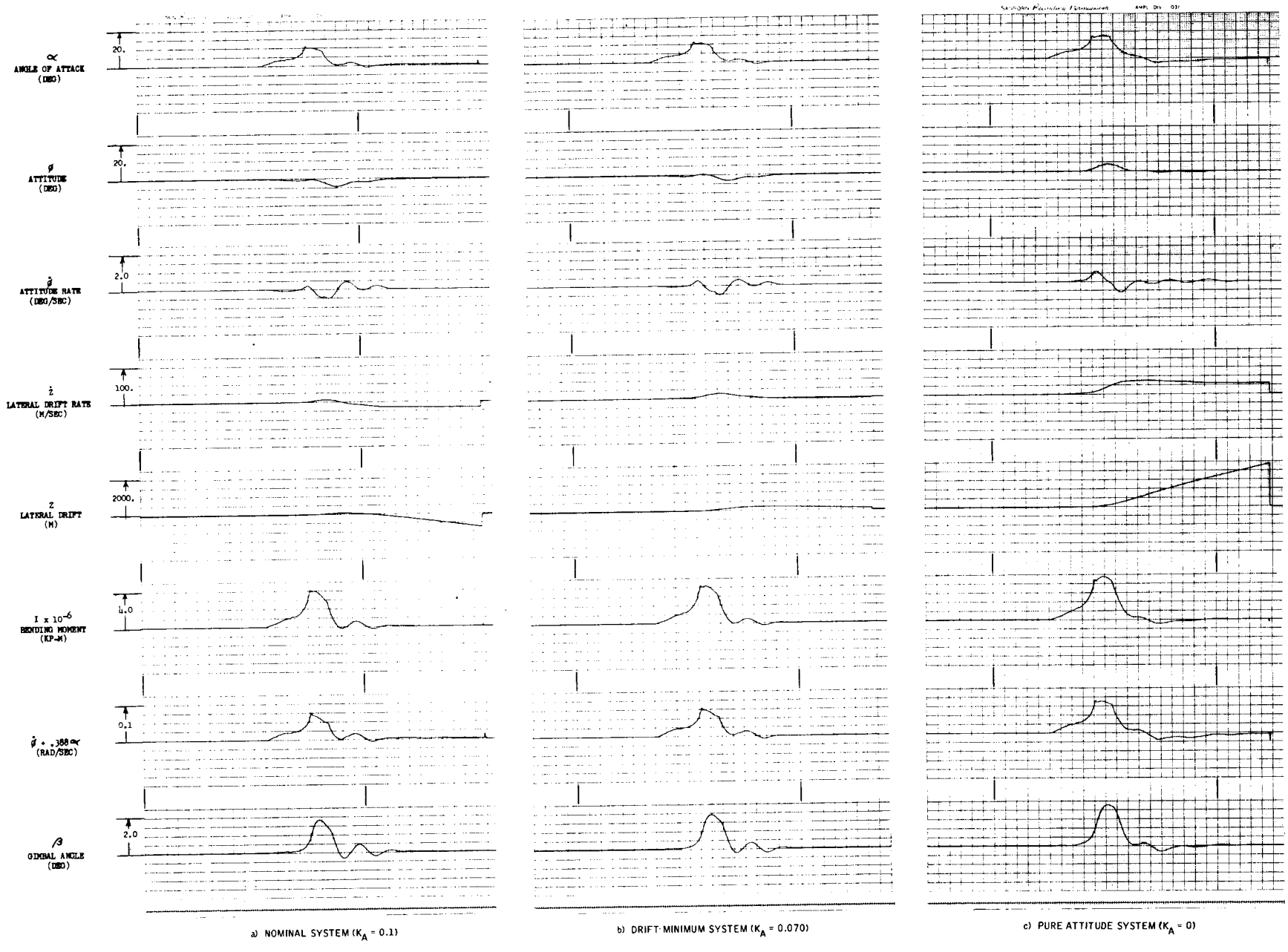

Figure N-53. Conventional Controller - Response to 72-second NASA Wind

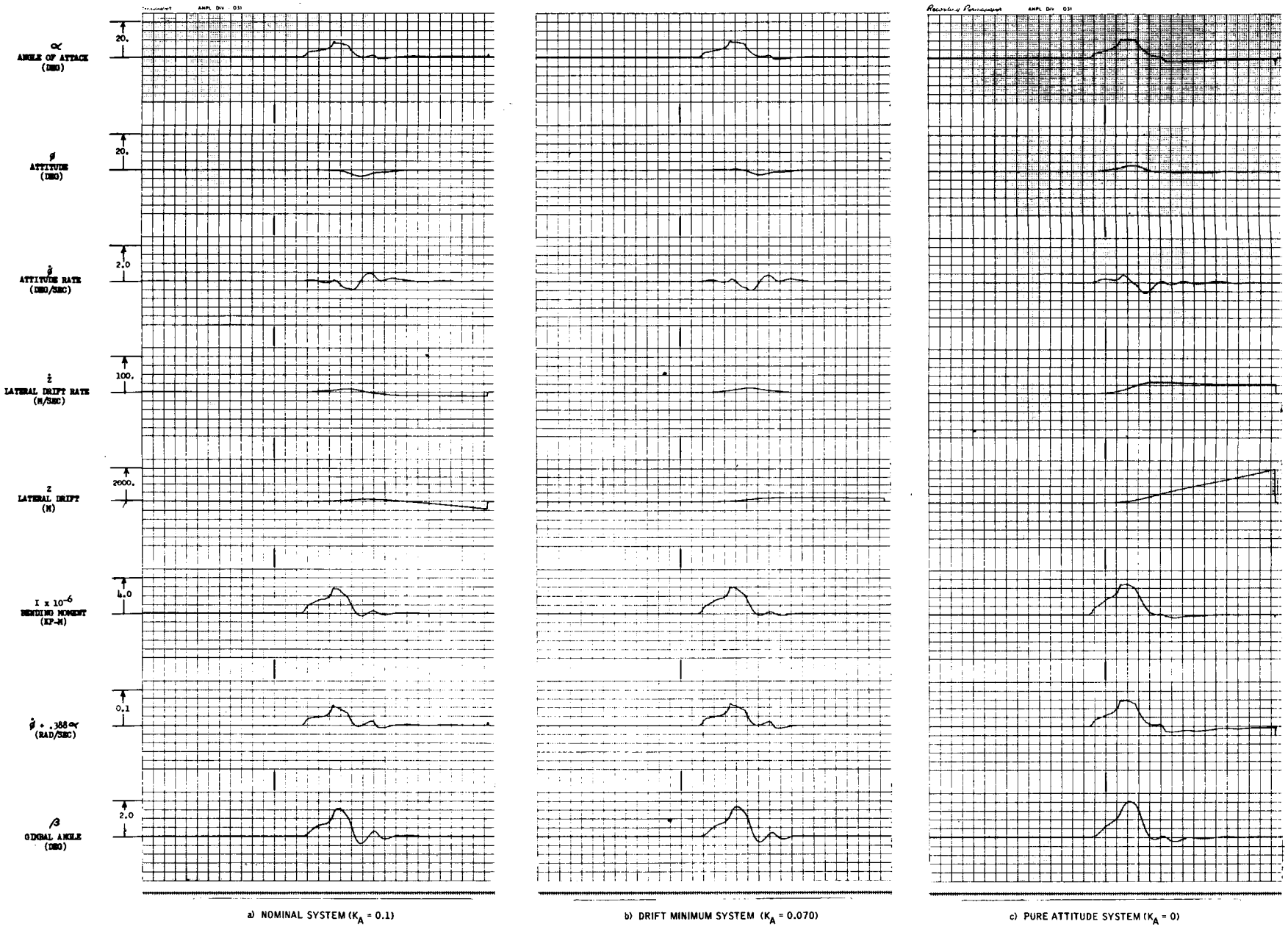

Figure N-54. Conventional Controller - Response to 80-second NASA Wind

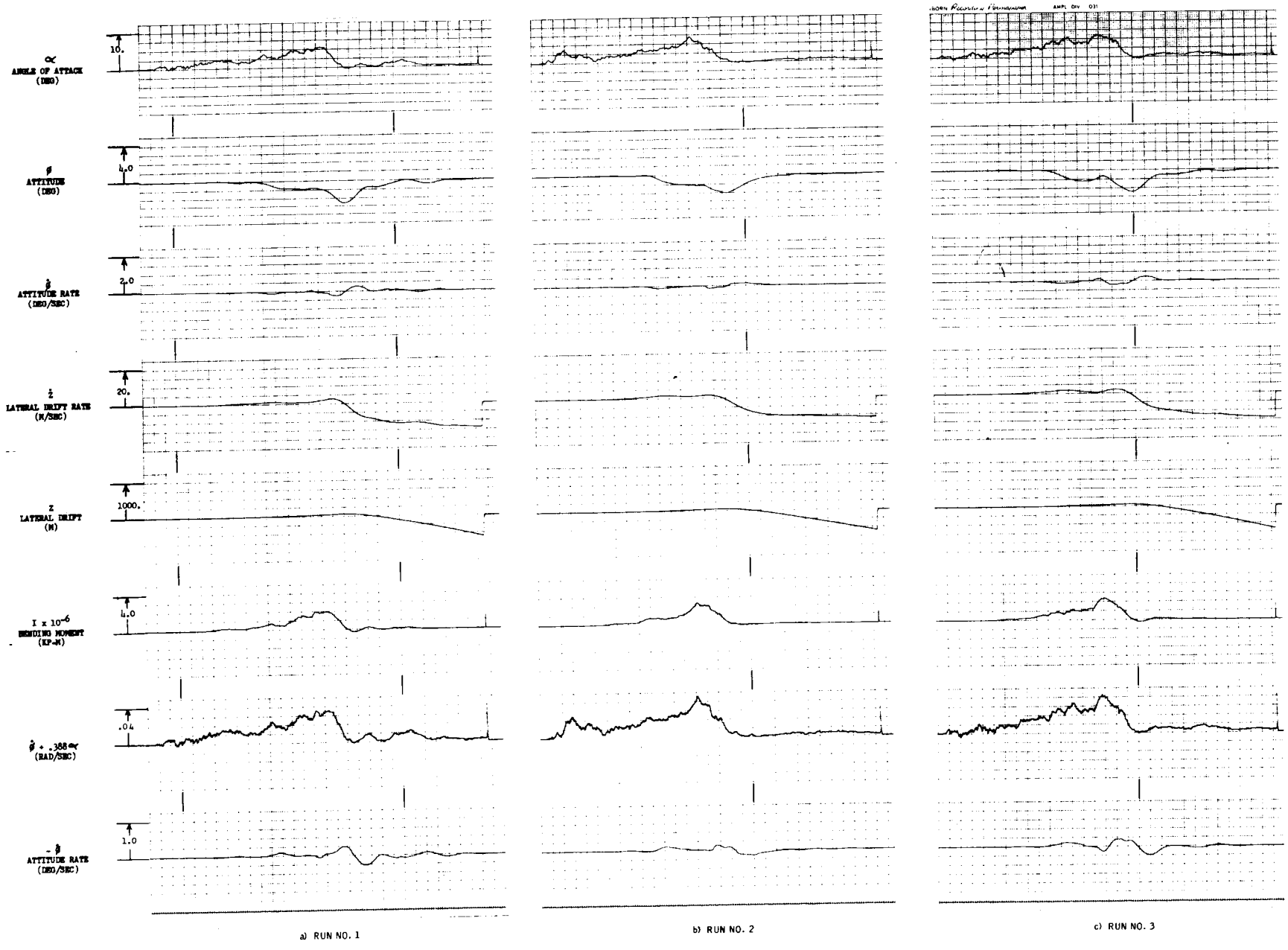

Figure N-55. Conventional Controller - Response to Random Wind

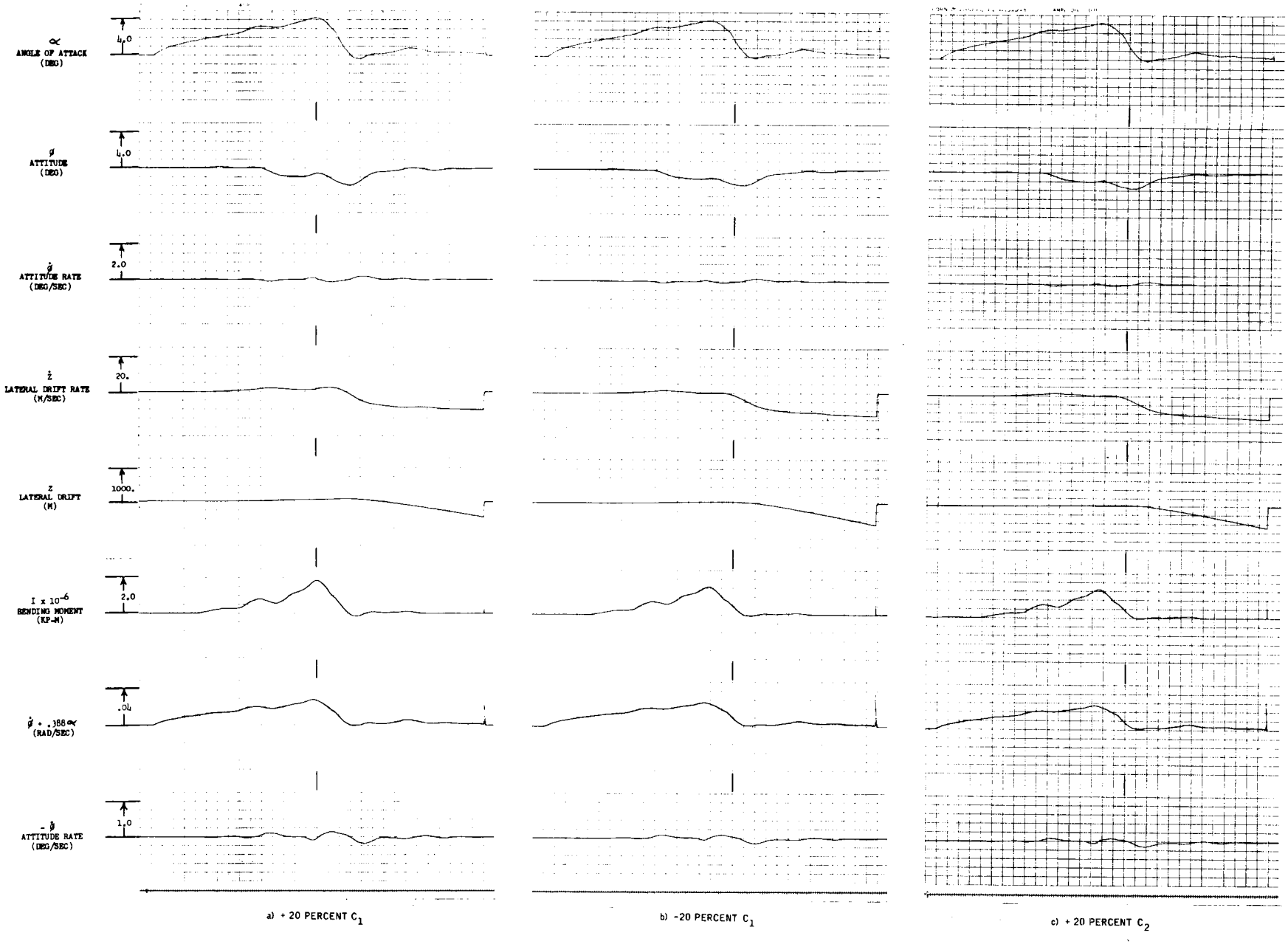

Figure N-56. Conventional Controller, Vehicle Parameter Variations - Response to Mean Wind [(a) +20% c_1, (b) -20% c_1, (c) +20% c_2]

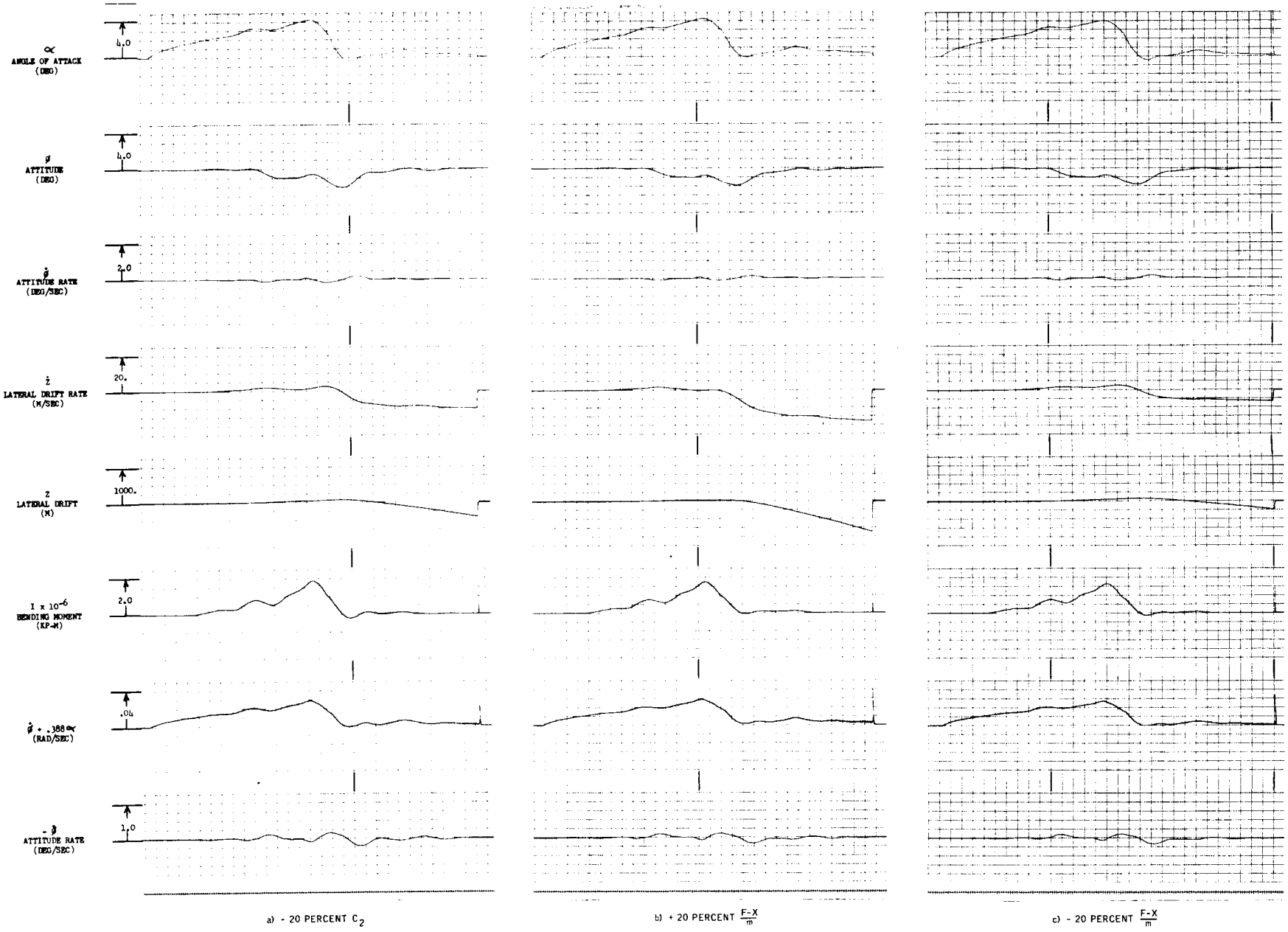

Figure N-57. Conventional Controller, Vehicle Parameter Variations - Response to Mean Wind [(a) -20% c_2, (b) +20% $\left(\frac{F-X}{m}\right)$, (c) -20% $\left(\frac{F-X}{m}\right)$]

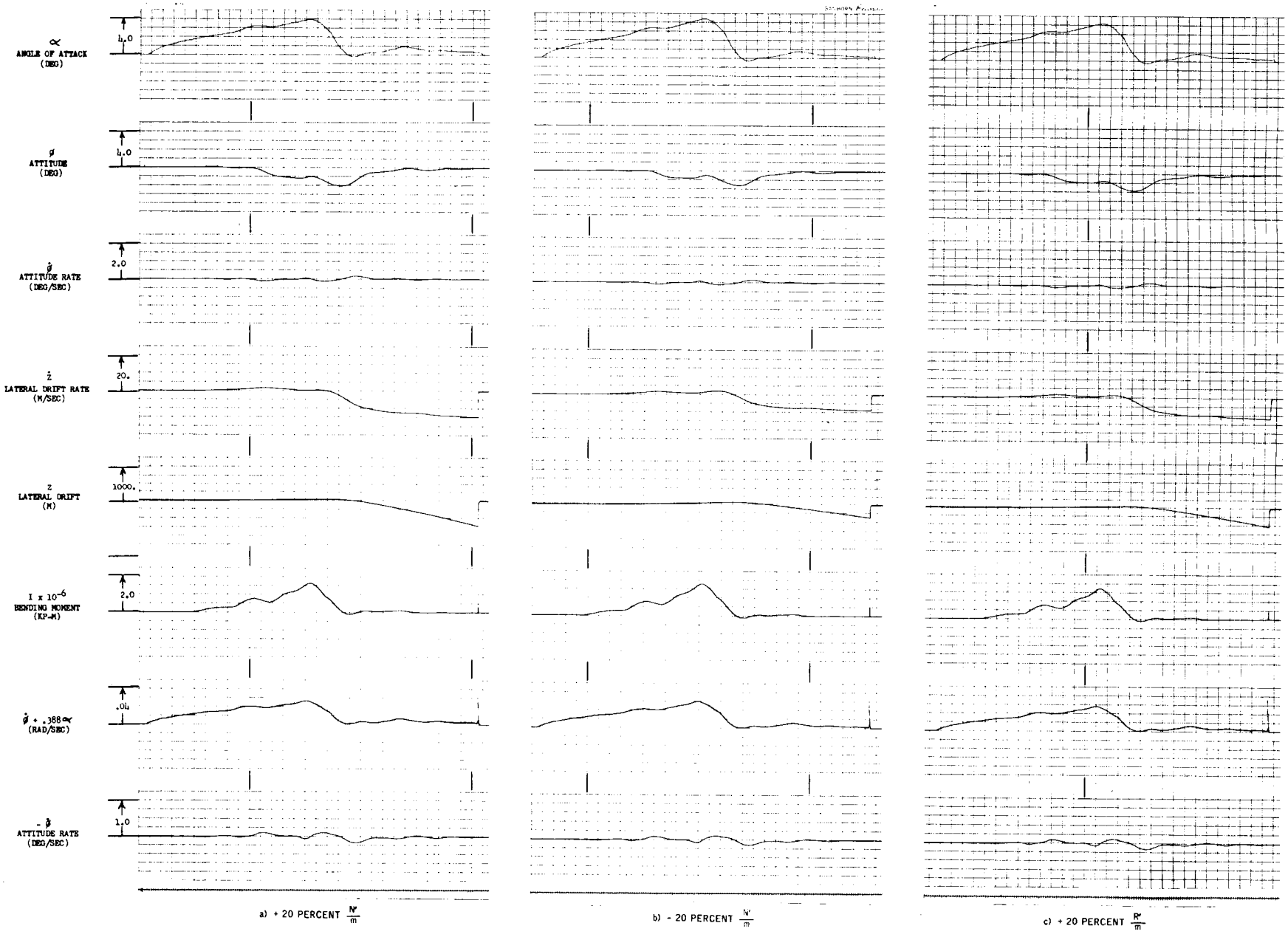

Figure N-58. Conventional Controller, Vehicle Parameter Variations - Response to Mean Wind [(a) +20% $\frac{N'}{m}$, (b) -20% $\frac{N'}{m}$, (c) +20% $\frac{R'}{m}$]

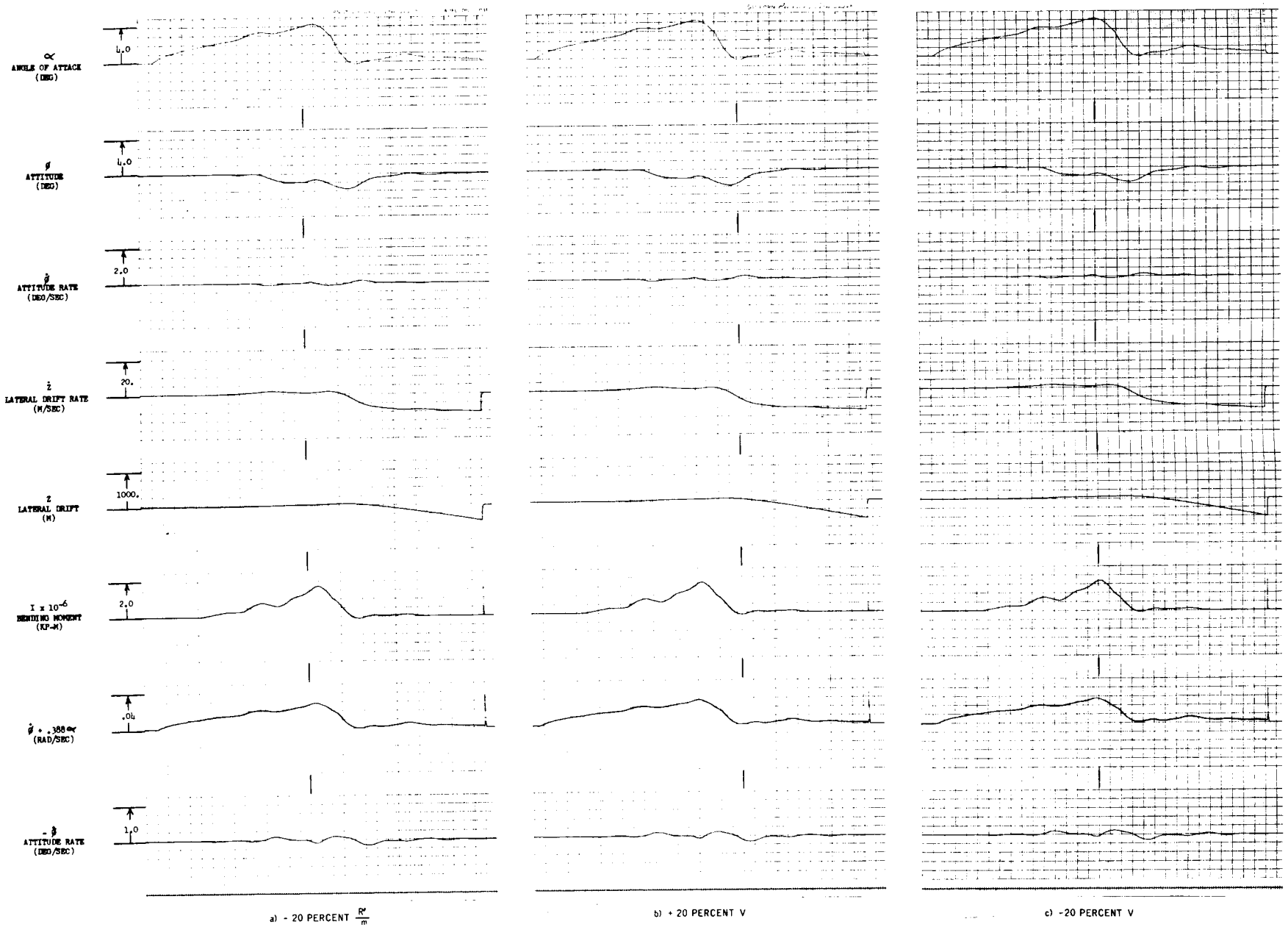

Figure N-59. Conventional Controller, Vehicle Parameter Variations - Response to Mean Wind [(a) -20% $\frac{R'}{m}$, (b) +20% v, (c) -20% v]

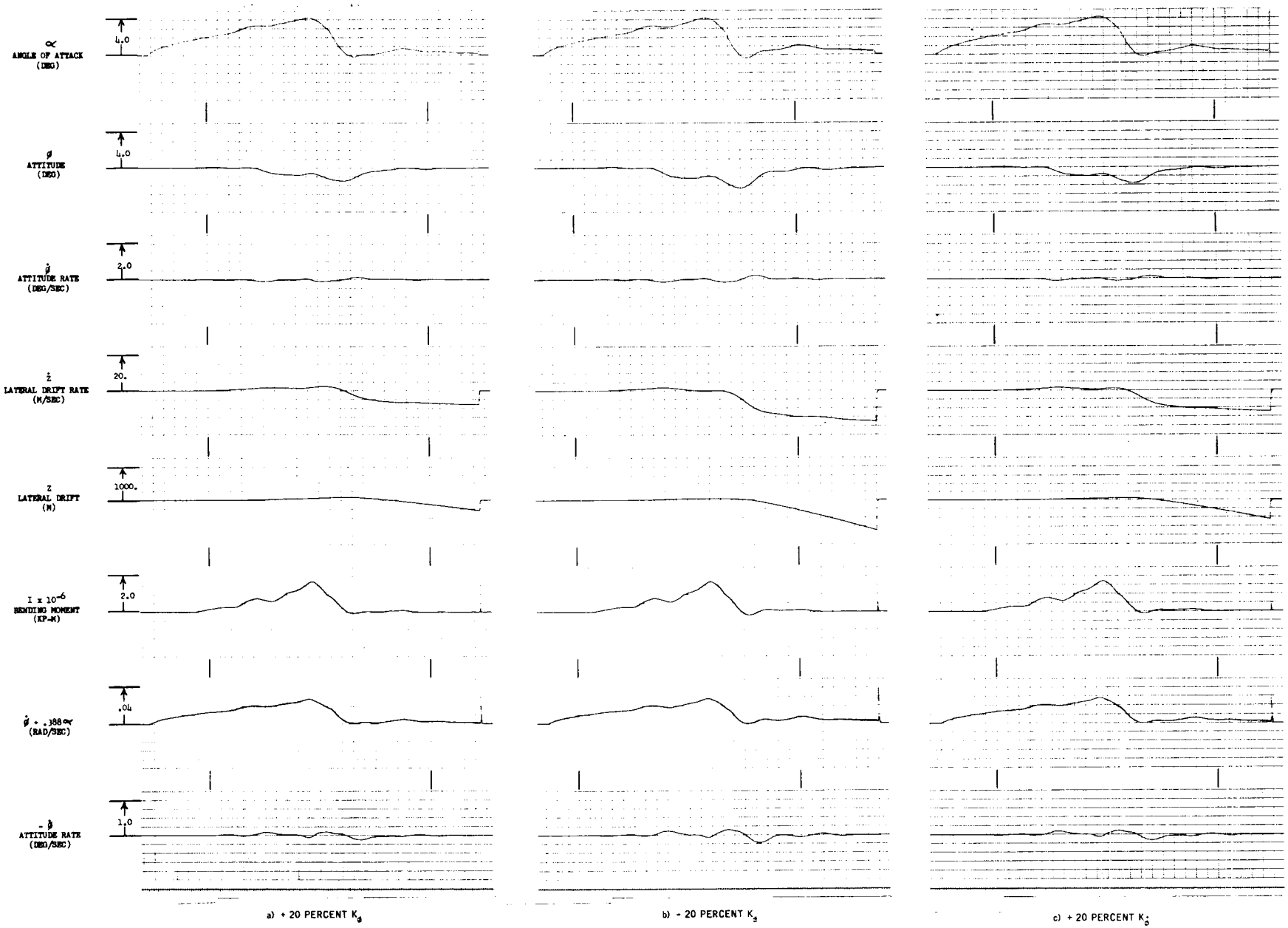

Figure N-60. Conventional Controller, Controller Parameter Variations - Response to Mean Wind [(a) +20% K_ϕ, (b) -20% K_ϕ, (c) +20% $K_{\dot\phi}$]

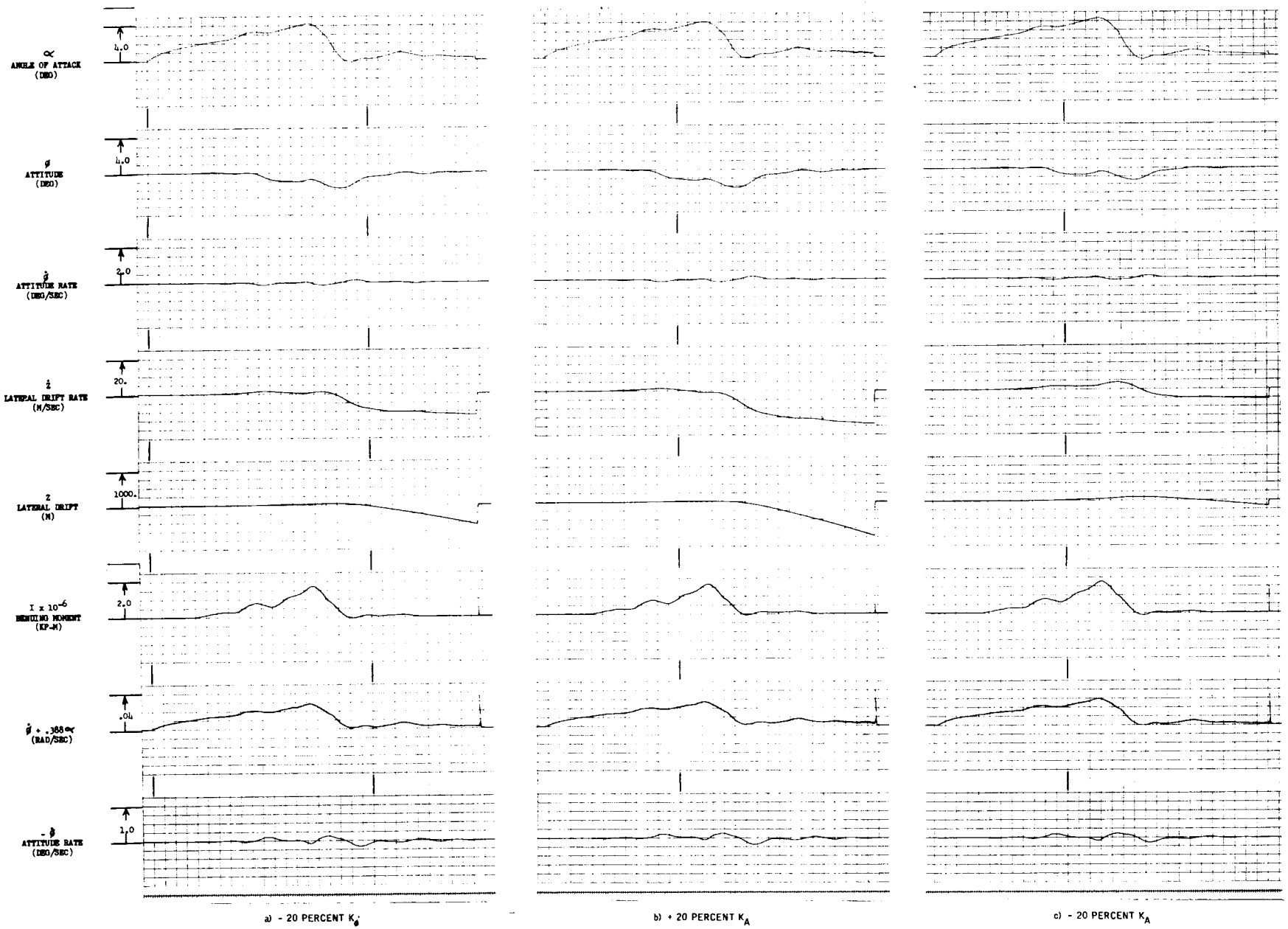

Figure N-61. Conventional Controller, Controller Parameter Variations - Response to Mean Wind [(a) -20% K_ϕ, (b) +20% K_A, (c) -20% K_A]

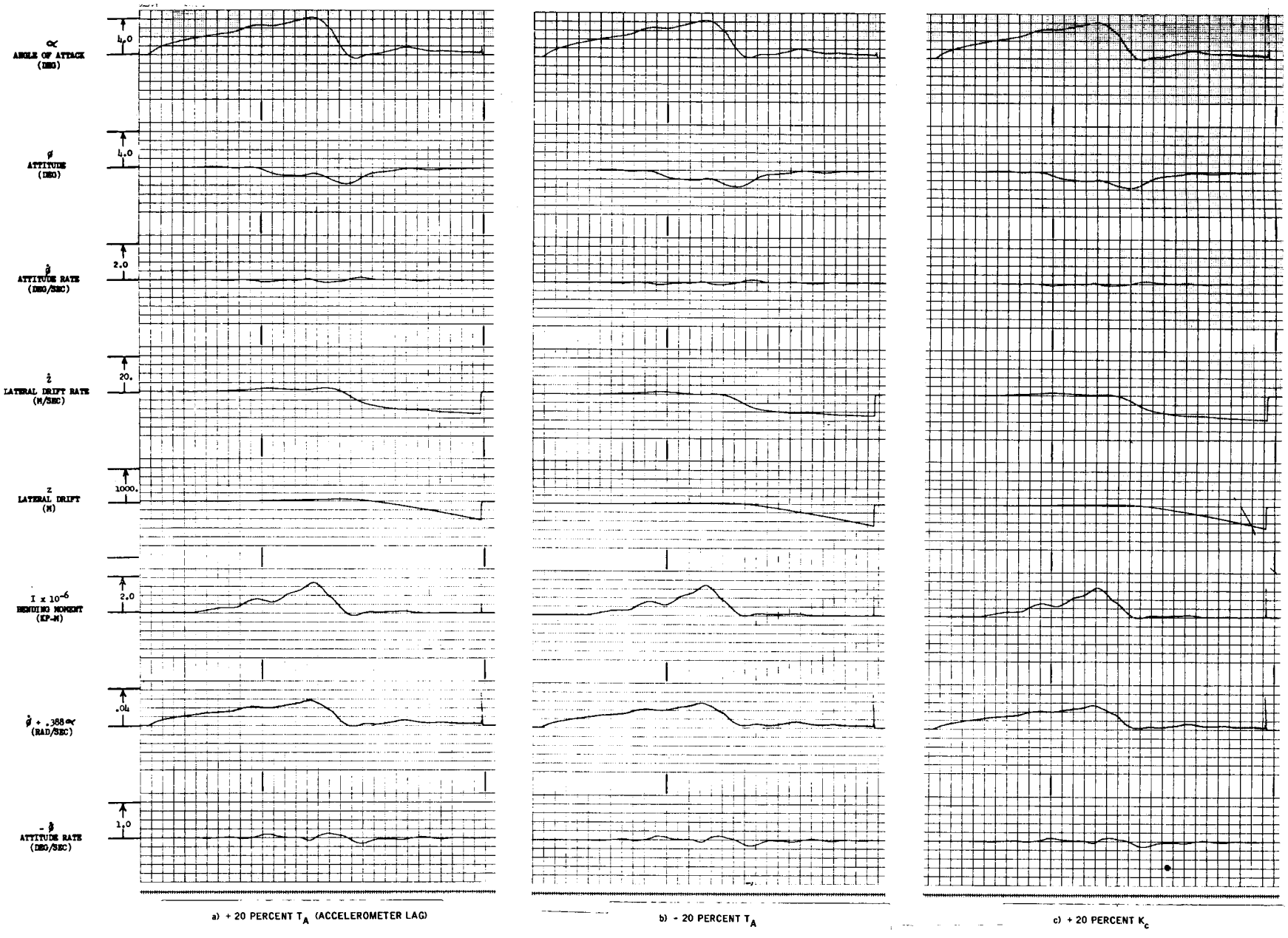

Figure N-62. Conventional Controller, Controller Parameter Variations - Response to Mean Wind [(a) +20% T_A (accelerometer lag), (b) -20% T_A, (c) +20% K_c]

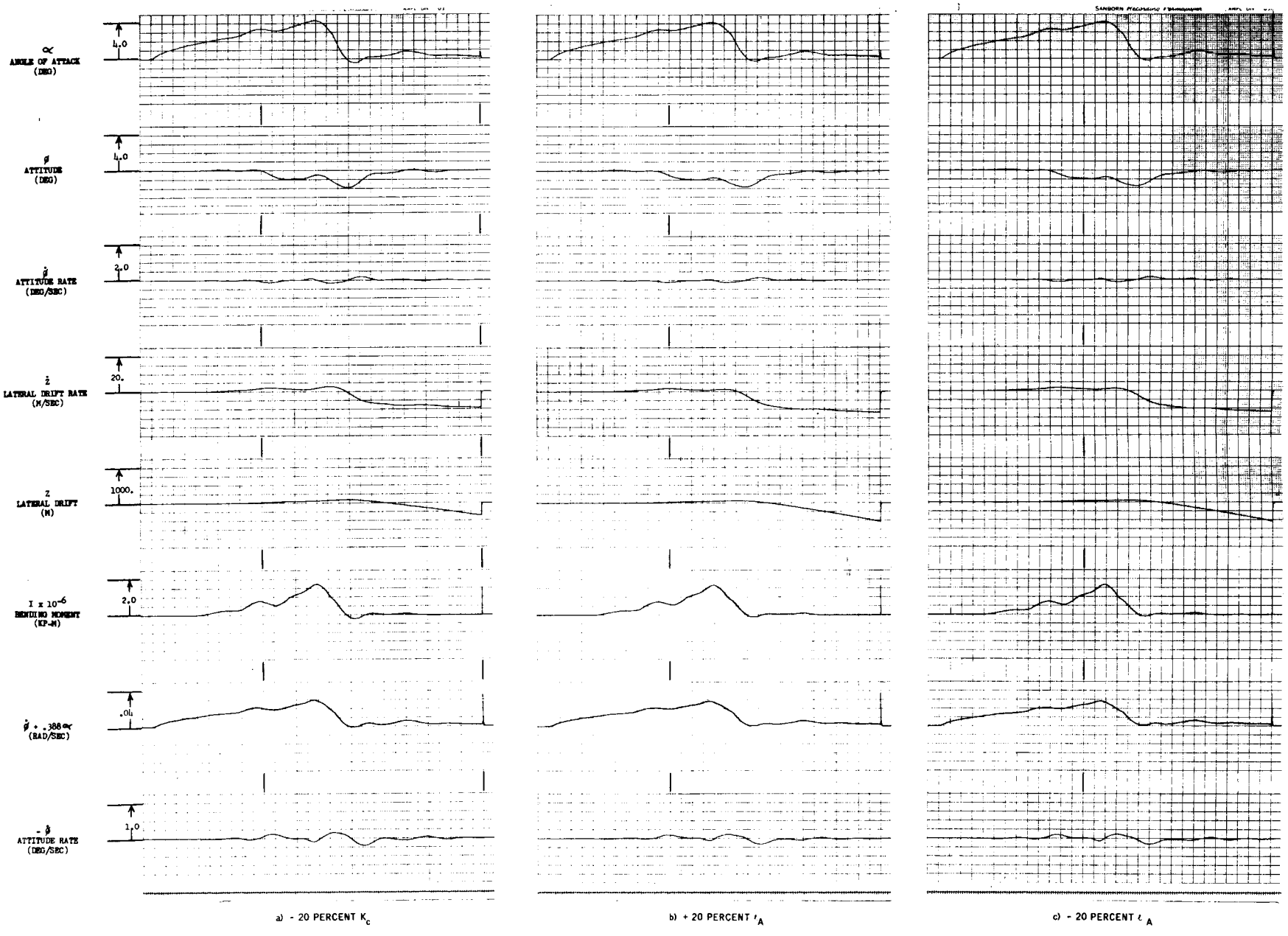

Figure N-63. Conventional Controller, Controller Parameter Variations - Response to Mean Wind [(a) -20% K_c, (b) +20% ℓ_A (c) -20% ℓ_A]

APPENDIX O
ROOT LOCI PLOTS

Root loci diagrams for Model Vehicle No. 2 with load-relief and minimax control are presented in this appendix for various flight times in Figures 0-1 through 0-23.

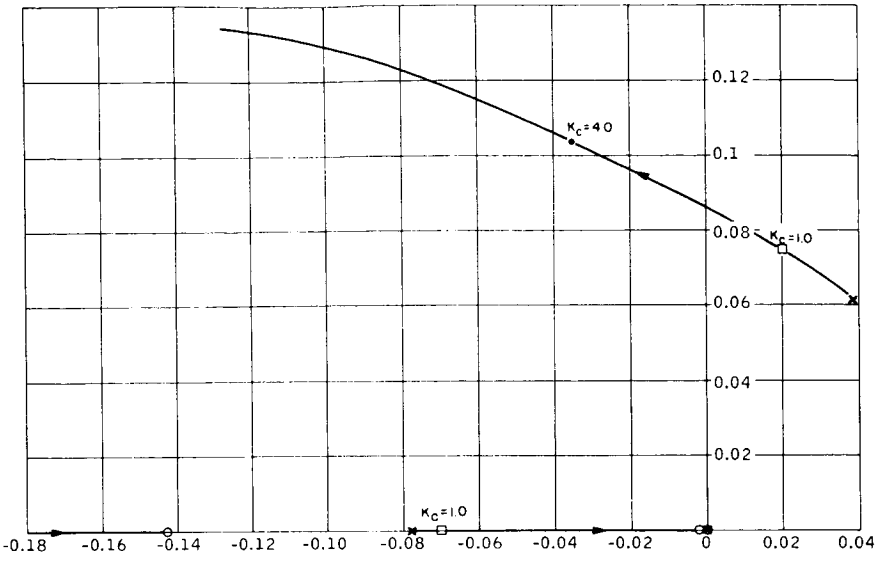

Figure O-1

Vehicle plus Load-Relief Controller-
t = 8 seconds, $u = K_c(K_\phi \phi + K_{\dot\phi} \dot\phi)$

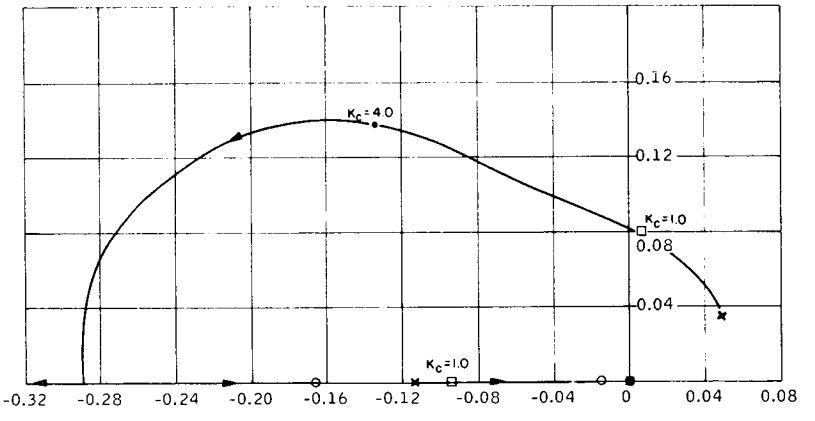

Figure O-2

Vehicle plus Load-Relief Controller-
t = 64 seconds, $u = K_c(K_\phi \phi + K_{\dot\phi} \dot\phi)$

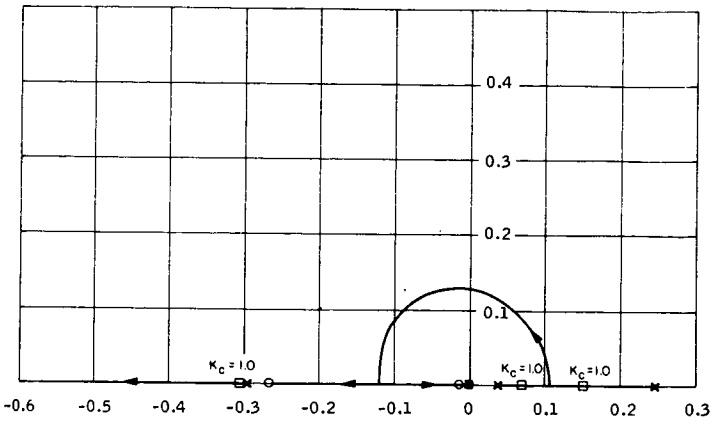

Figure O-3

Vehicle Plus Load-Relief Controller-
t = 80 seconds, $u = K_c(K_\phi \phi + K_{\dot\phi}\dot\phi)$

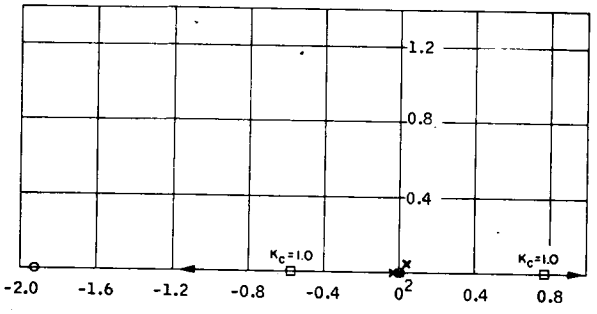

Figure O-4

Vehicle Plus Load-Relief Controller-
t = 149 seconds, $u = K_c(K_\phi \phi + K_{\dot\phi}\dot\phi)$

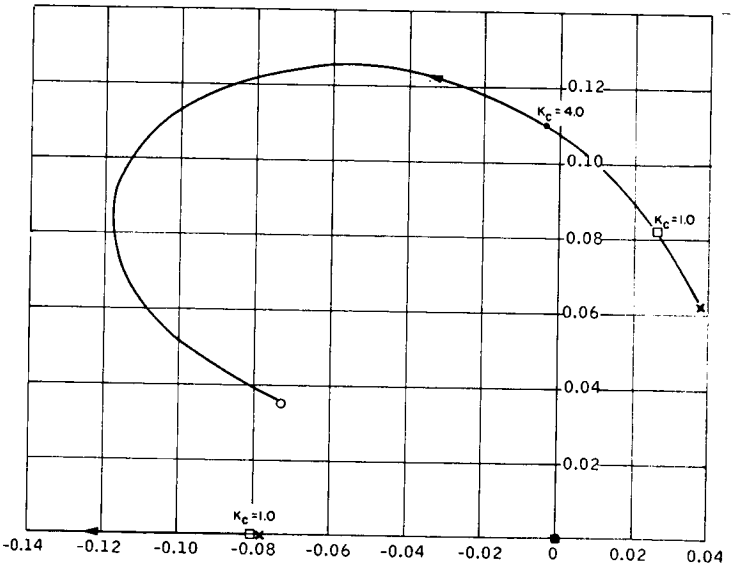

Figure O-5

Vehicle Plus Load-Relief Controller-
t = 8 seconds, $u = K_c(K_\phi \phi + K_{\dot\phi}\dot\phi + K_z \dot z)$

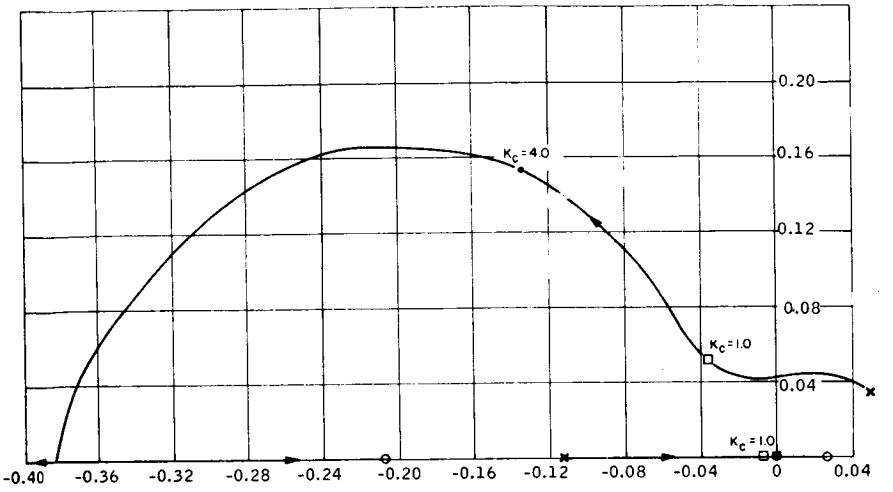

Figure O-6

Vehicle Plus Load-Relief Controller-
t = 64 seconds, $u = K_c(K_\phi \phi + K_{\dot\phi}\dot\phi + K_z \dot z)$

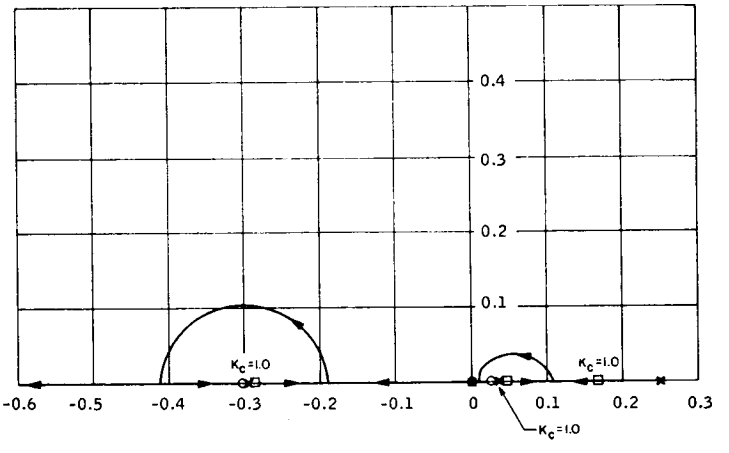

Figure O-7

Vehicle Plus Load-Relief Controller-
t = 80 seconds, $u = K_c(K_\phi \phi + K_{\dot\phi}\dot\phi + K_z \dot z)$

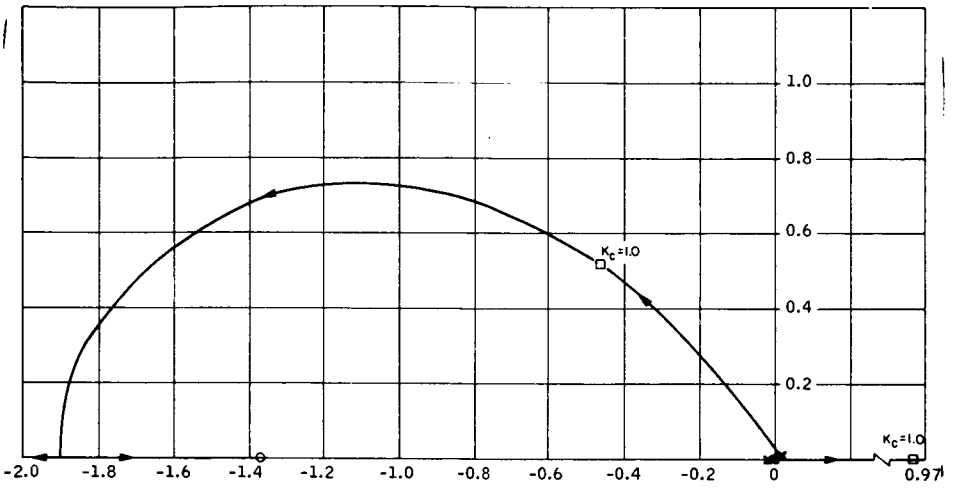

Figure O-8

Vehicle Plus Load-Relief Controller-
t = 149 seconds, $u = K_c(K_\phi \phi + K_{\dot\phi}\dot\phi + K_{\dot z}\dot z)$

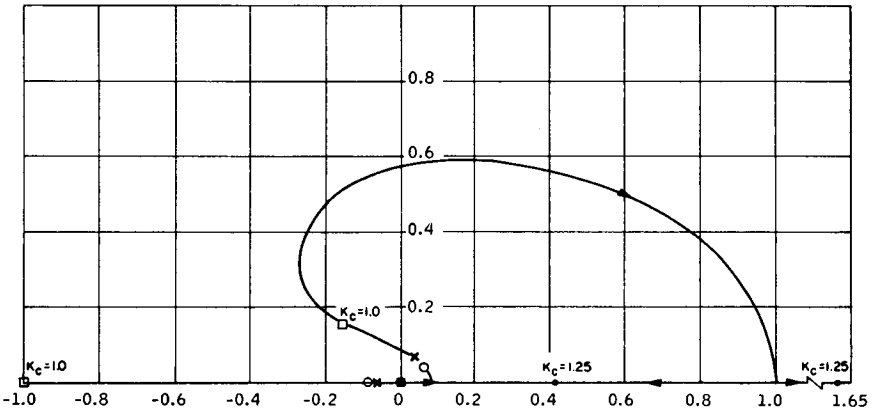

Figure O-9

Vehicle Plus Load-Relief Controller-
t = 8 seconds, $u = K_c(K_\phi \phi + K_{\dot\phi}\dot\phi + K_\beta \beta)$

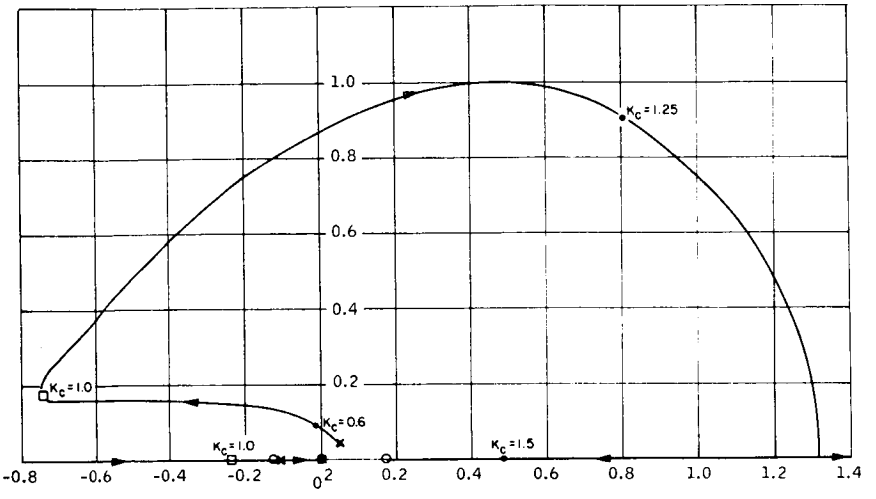

Figure O-10

Vehicle Plus Load-Relief Controller-

t = 64 seconds, $u = K_c(K_\phi \phi + K_{\dot\phi} \dot\phi + K_\beta \beta)$

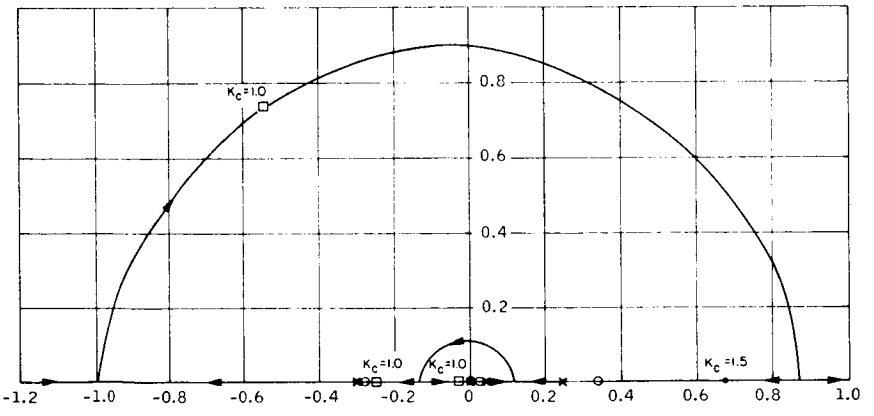

Figure O-11

Vehicle Plus Load-Relief Controller-

t = 80 seconds, $u = K_c(K_\phi \phi + K_{\dot\phi} \dot\phi + K_\beta \beta)$

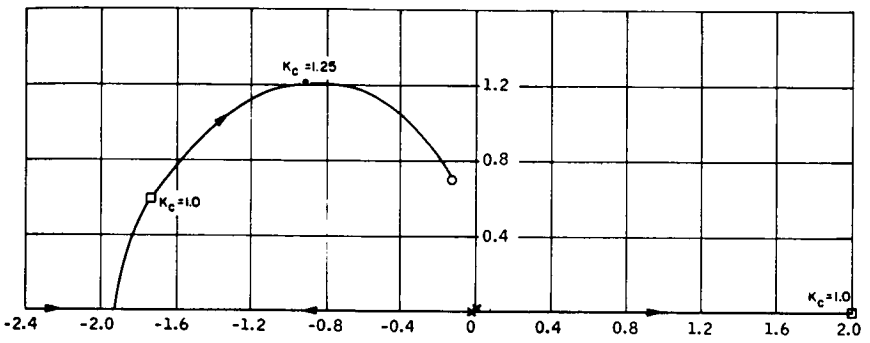

Figure O-12

Vehicle Plus Load-Relief Controller-
t = 149 seconds, $u = K_c(K_\phi \phi + K_{\dot\phi} \dot\phi + K_\beta \beta)$

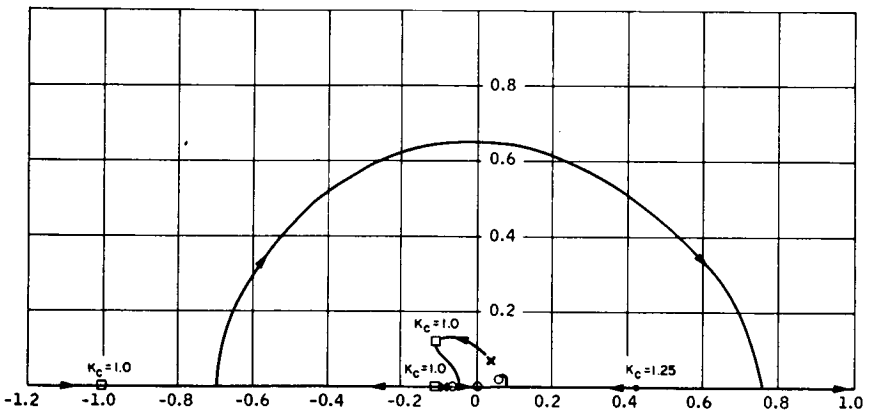

Figure O-13

Vehicle Plus Load-Relief Controller-
t = 8 seconds, $u = K_c(K_\phi \phi + K_{\dot\phi} \dot\phi + K_\beta \beta + K_{\dot z} \dot z)$

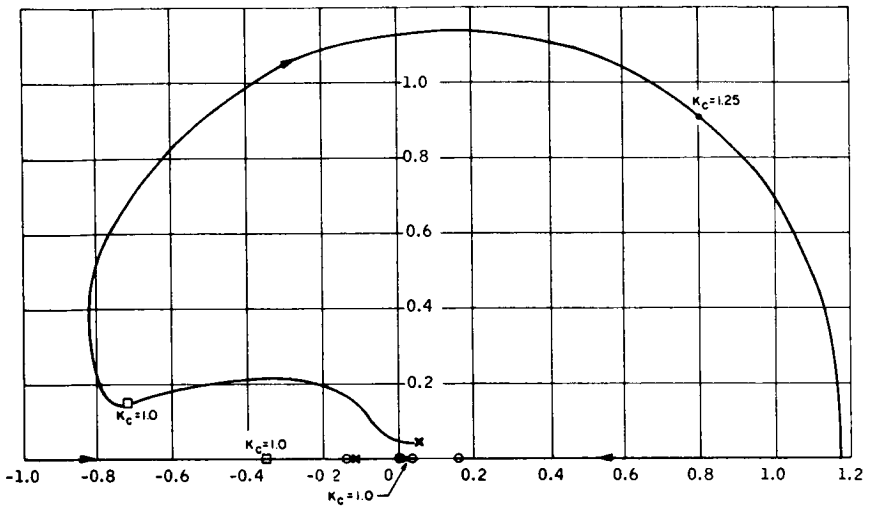

Figure O-14

Vehicle Plus Load-Relief Controller - t = 64 seconds, $u = K_c(K_\phi \phi + K_{\dot\phi}\dot\phi + K_\beta \beta + K_{\dot z}\dot z$

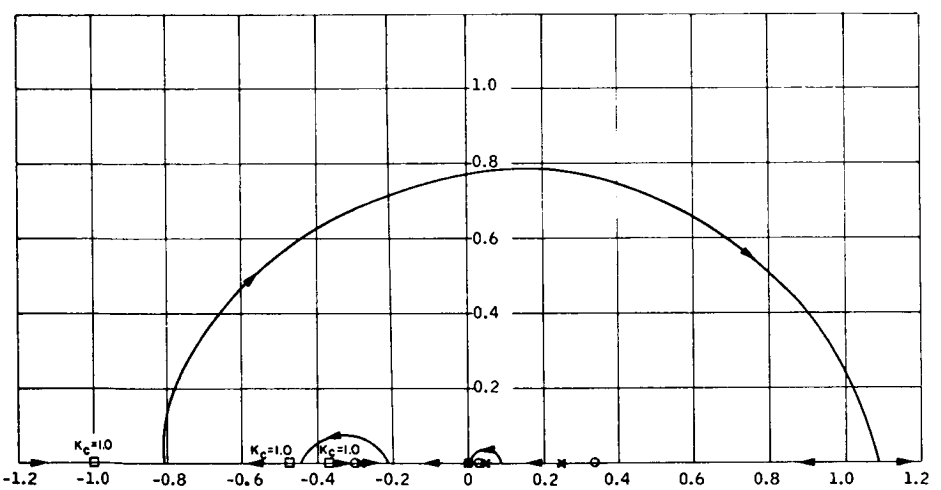

Figure O-15

Vehicle Plus Load-Relief Controller - t = 80 seconds, $u = K_c(K_\phi \phi + K_{\dot\phi}\dot\phi + K_\beta \beta + K_{\dot z}\dot z)$

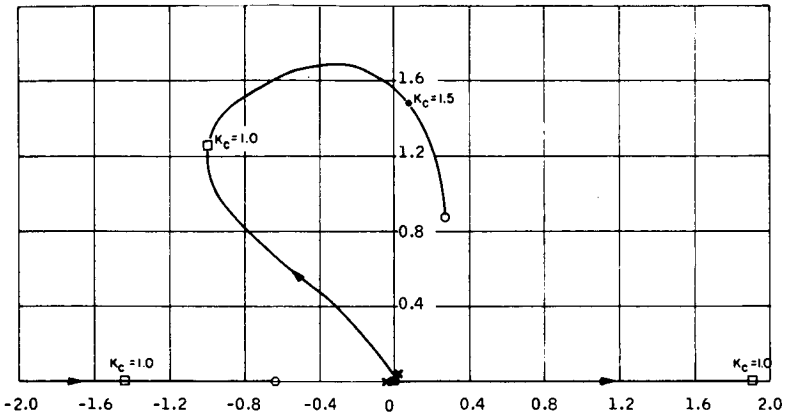

Figure O-16

Vehicle Plus Load-Relief Controller - t = 149 seconds, $u = K_c(K_\phi \phi + K_{\dot\phi}\dot\phi + K_\beta \beta + K_{\dot z}\dot z)$

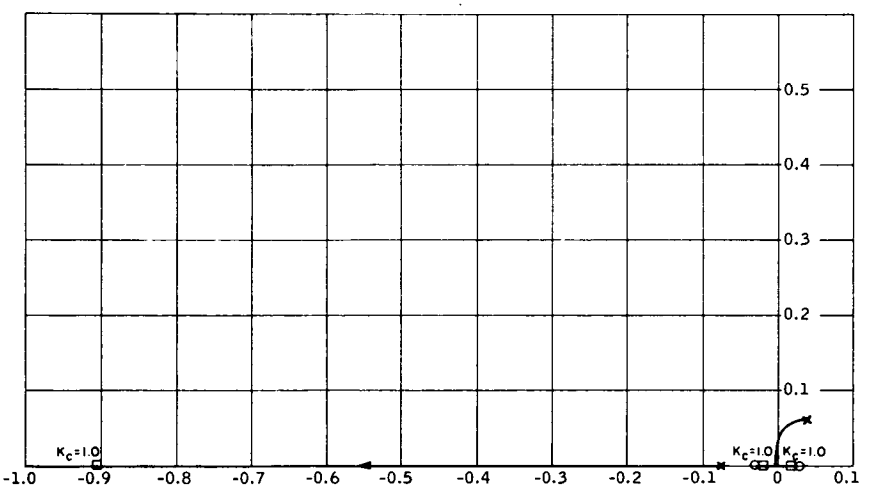

Figure O-17

Model Vehicle No. 2 with Minimax Controller - Interval 1, $u = K_c [(0.0006-0.0044)\phi + 2.6\dot\phi + 0.0044\alpha]$

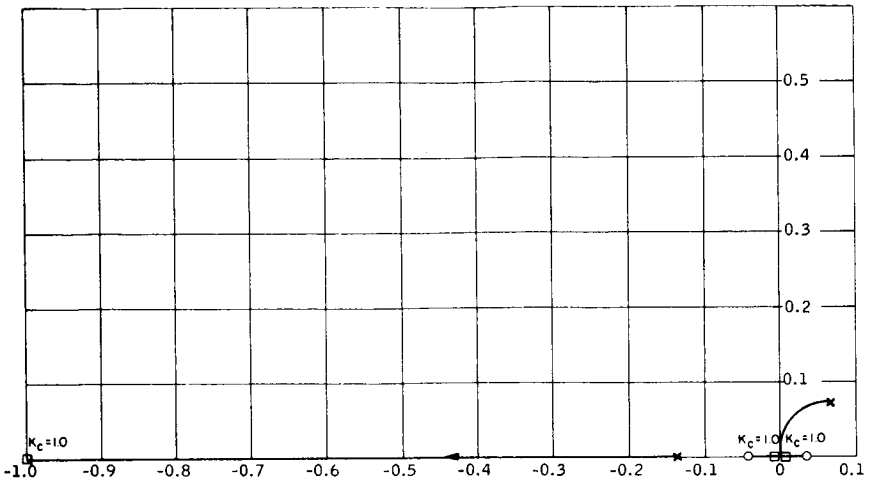

Figure O-18

Model Vehicle No. 2 with Minimax Controller - Interval 2, $u = K_c$ $[(0-0.025\,\phi + 2.7\,\phi + 0.025\,\alpha]$

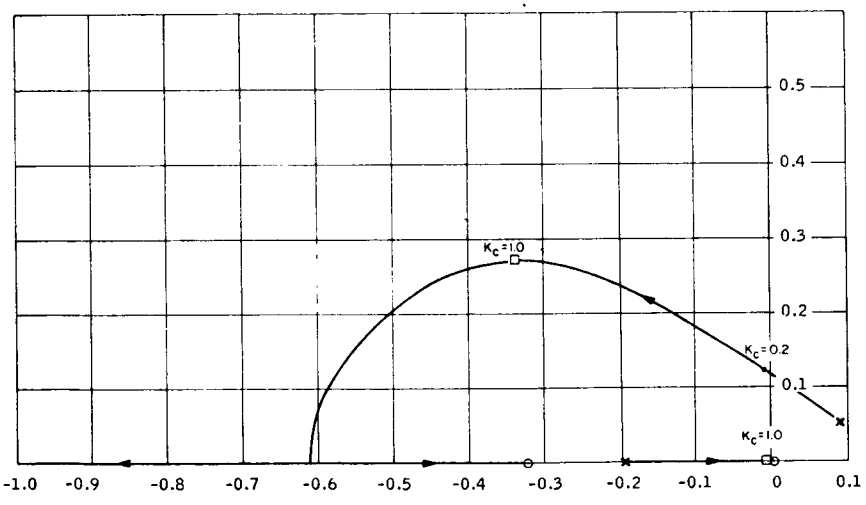

Figure O-19

Model Vehicle No. 2 with Minimax Controller - Interval 3, $u = K_c$ $[(0.55 - 0.10)\,\phi + 1.8\phi + 0.10\,\alpha]$

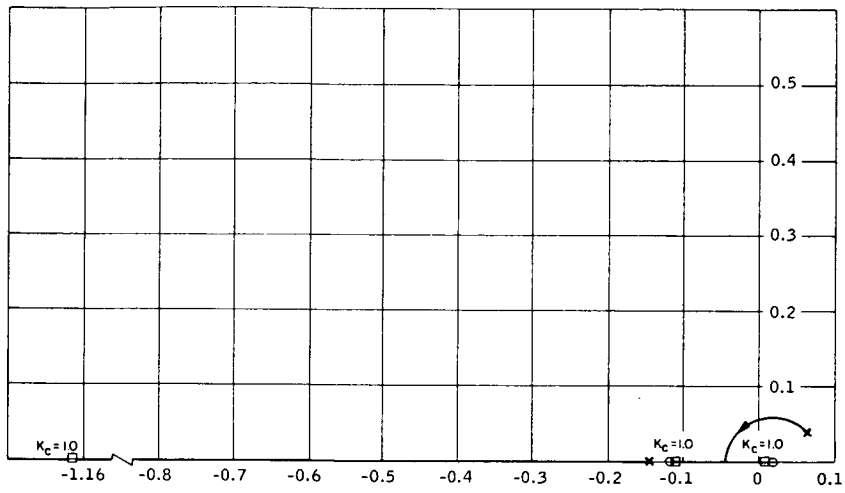

Figure O-20

Model Vehicle No. 2 with Minimax Controller - Interval 4, $u = K_c [(0.28 - 0.11) \phi + 3.0 \phi + 0.11 \alpha]$

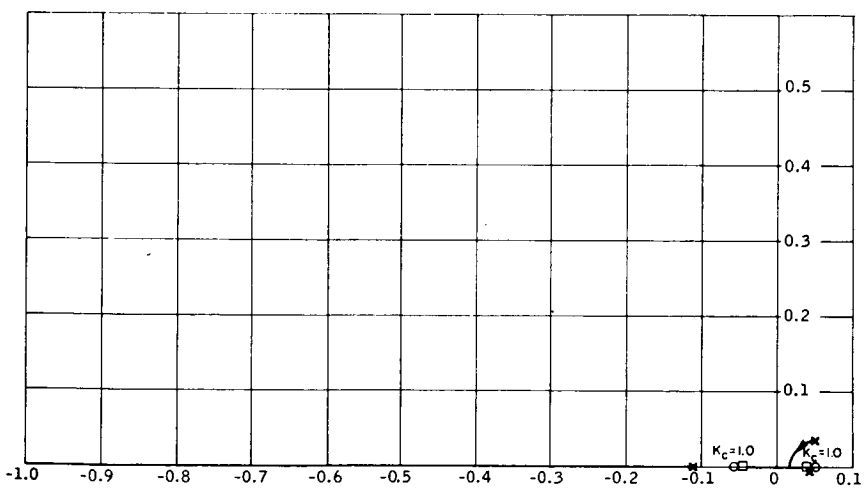

Figure O-21

Model Vehicle No. 2 with Minimax Controller - Interval 5, $u = K_c [(0 - 0.065) \phi + 1.7 \phi + 0.065 \alpha]$

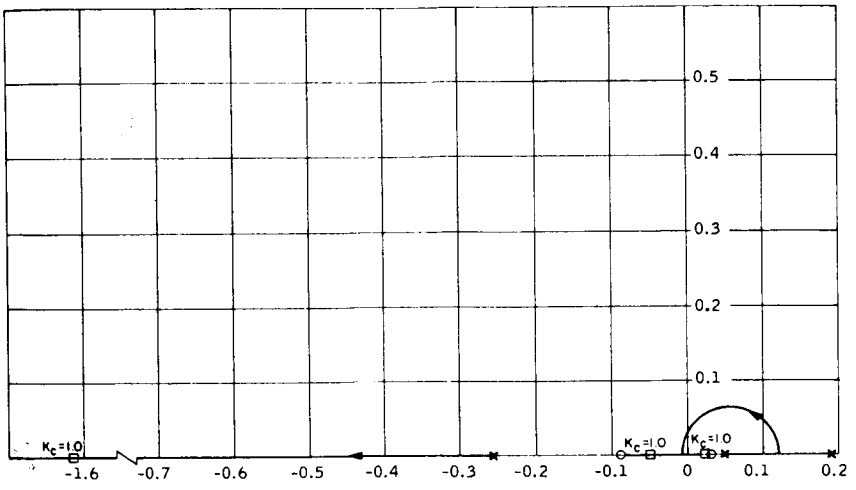

Figure O-22

Model Vehicle No. 2 with Minimax Controller - Interval 6, $u = K_c [(0.15 - 0.19)\phi + 3.4\phi + 0.19\alpha]$

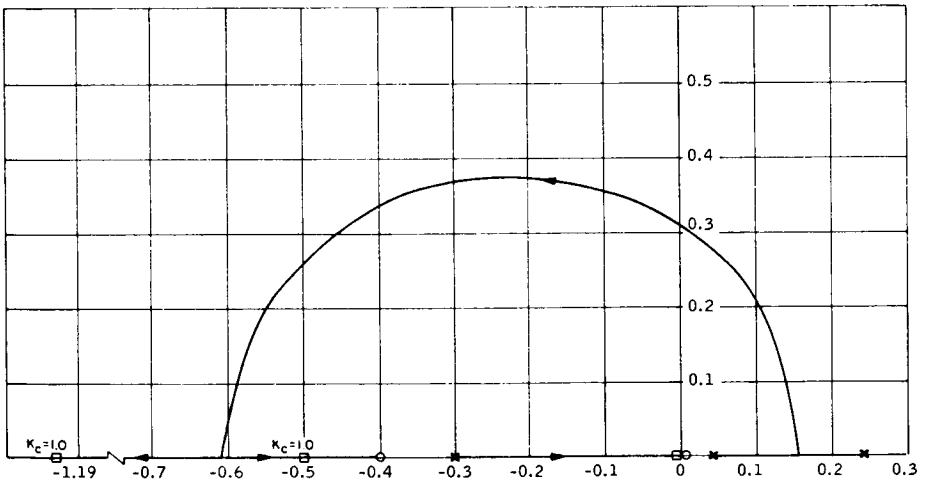

Figure O-23

Model Vehicle No. 2 with Minimax Controller - Interval 7, $u = K_c [(1.3 - 0.45)\phi + 3.4\phi + 0.45\alpha]$